School of
Civil Engineering and Geosciences

Newcastle University

SEISMIC BEHAVIOUR OF GRAVITY QUAY WALLS BUILT ON LIQUEFIABLE SOILS

By

Mahdi Alyami

Supervisors

Dr M. Rouainia & Dr S. M. Wilkinson

A thesis submitted to the university of Newcastle upon Tyne in partial fulfilment of the requirements for the degree of Doctor of Philosophy

DECLARATION

I hereby certify that this work is my own, except where otherwise acknowledged, and that this work has not been submitted previously for a degree at this, or any other university.

Signed:

Mahdi Ali Alyami

Submitted in full: 15th of February 2008

ACKNOWLEDGEMENTS

I am grateful to **God** almighty, the giver of life, hope and destiny for His unfailing love and grace over my life. For God has made my ordinary hands and eyes to behold the extraordinary.

I am most grateful to my supervisors, **Dr. M. Rouainia** and **Dr. S. M. Wilkinson** for their guidance, effort and valuable contributions towards the success of this thesis.

I would also like to thank **Professor. B. Elsharoby** (University of Alexandria, Egypt), **Professor K. Ishihara** (Tokyo University, Japan), **Professor S. Iai** (Tokyo University, Japan) and **Professor A. H. C. Chan** (Birmingham University, UK) for advice, helpful discussions and encouragement. **Dr. K. Ichii** (Hiroshima University, Japan) is thanked for the helpful discussions, advice, and valuable data for the Kobe earthquake while the author visited the Port and Harbour Research Institute, Ministry of Transport, Japan in 2005.

My unreserved gratitude goes to the **Saudi Arabia Interior Ministry** represented by the **Navy Border Guard** for providing the funds for this research. I would also like to thank the **Saudi Port Authority** for the valuable data, and collected samples from Jeddah Port.

I am grateful to the director of the FORUM 8 Co., **Mr. Y. Ito,** for inviting me to visit Tokyo in 2006 to have a training course at their company to use UWLC software used for the analysis in this thesis as the first user for the English version. My thanks are extended to all the staff of the FORUM 8 Co. In addition, I would like to acknowledge **Dr. H. Nakamura** for his technical support.

Some of the ideas in this research were obtained during my visit to Gunma University, Gunma, Japan. Therefore, I greatly appreciate the lecture and advice given by **Professor K. Ugai** and **Dr. F. Cai,** which are implemented in the methodology of this thesis.

I wish to express my thanks to **Mr. A. Morisson**, an MSc student at the University of Newcastle upon Tyne and to whom I was a co-supervisor, for his assistance while we were working together to conduct the triaxial tests of Jeddah Port sand. Also I would like to acknowledge **Mr. S. Patterson** for his technical support during this project.

Finally, I am highly indebted to my parents, **Mr. Ali Alyami** and **Mrs. Sharefah Albabtain**, my siblings, and my wife **Mrs. Reem Alharthi** for their enduring moral support. My gratitude goes to my friends and colleagues **Mr. H. Shaman** (Heriott Watt University, UK), **Mr. H. Albisher** and **Mr. S. Hamodah** (Newcastle University, UK) for their support and assistance.

DEDICATION

I dedicated this thesis to my Parents Mr. Ali Alyami and Mrs. Sharefah Albabtain, my siblings and my wife Mrs Reem Alharthi.

ABSTRACT

In the last 50 years there have been many documented failures of gravity retaining quay walls due to earthquake events. These failures are often associated with significant deformation of liquefiable soil deposits (e.g. major damage occurred at Kobe Port during the 1995 Hyogoken-Nanbu earthquake). Saudi Arabia has similar types of quay walls located in regions that have the potential to experience significant seismic events. These walls have not been designed for seismic resistance and therefore have the potential to suffer serious damage from seismic activity. For many years the design of seismic gravity quay walls has been studied and design codes for engineering practice established; however, the widespread failures of these structures during recent earthquakes demonstrates that these design methods may be insufficient. Such gravity quay wall failures have stimulated progress in the development of a performance-based seismic design method using non-linear inelastic dynamic analysis for quay wall structures.

The aim of this study was to develop a methodology for the seismic design of gravity quay walls using a non-linear elasto-plastic dynamic analysis. The final method adopted in this work is based on the generalised elasto-plasiticity constitutive model developed by Pastor *et al.* (1990), with some minor modifications, which has been incorporated into a finite element procedure. The proposed P-Z sand model was first validated by simulating published monotonic and cyclic test results. Secondly, an effective stress analysis was established by developing a finite element model for Kobe Port Island quay walls using the P-Z sand model. This model was validated by comparing the predicted deformations with those experienced at Kobe. The computed residual deformations from the analysis were in good agreement with published field observations.

To develop mitigation strategies, a parametric study of the seismic performance of gravity quay walls, using the effective stress analysis, was conducted. This study assessed the effect of various structural and geotechnical parameters on the seismic performance of quay walls. Twenty-six cases of effective stress analysis with variation in tidal range, soil permeability, soil relative densities, and wall widths were conducted as well as analyses to test the importance of considering multi-directional seismic excitations as opposed to uni-directional.

In order to assess the safety of existing quay walls in Jeddah Port, an experimental programme was conducted. This programme consisted of a site investigation (using a standard penetration test (SPT)) to determine the *in situ* relative density of the existing backfill, a series of laboratory based, monotonic and cyclic triaxial tests (to define the soil properties of Jeddah Port sand) and a two-dimensional effective stress finite element analysis of a typical Jeddah quay wall.

The monotonic and cyclic triaxial tests were conducted for three different relative densities of D_r = 35 %, 55% and 75%. These represent loose (equal to *in situ* conditions as established by the site investigation), medium dense and dense sand. The experimental results are discussed and then used to identify the P-Z sand model parameters. These parameters were used in conjunction with a finite element analysis of Jeddah Port quay walls to predict the seismic deformations. In this analysis the finite element model was subjected to a number of different ground motions, which represented two different levels of earthquake intensity; namely moderate and strong ground shaking. The effect of improvement strategies such as increasing the relative density of the backfill and foundation materials was then assessed

The results of the simulations showed that existing Jeddah Port quay walls are not satisfactory to resist either moderate or strong earthquake excitations. However, if the relative density is increased to 55% then satisfactory performance can be achieved for a moderate intensity earthquake. For the case of strong shaking, the analysis showed that the quay walls did not demonstrate the required performance levels; however, they were only under specification by 10%.

Finally, a flowchart illustrating a seismic design procedure for gravity quay walls has been proposed, which is applicable to both existing and new gravity quay walls.

Key-words: quay wall, liquefaction, earthquake, port, effective stress, constitutive model

TABLE OF CONTENTS

LIST OF FIGURES

LIST OF TABLES

LIST OF SYMBOLS AND ABBREVIATIONS

The use of a symbol to denote more than one quantity has been avoided as much as possible and every effort has been made to define symbols and abbreviations used where they appear in the text.

A	Specimen cross sectional area
a	Acceleration
a_h	Horizontal acceleration
a_v	Vertical acceleration
B	Skempton's B value for saturation
C	Ratio of the critical state line (CSL)
C	Cohesion (see Table 3.8)
C_u	Coefficient of uniformity
c_v	Coefficient of consolidation
C_z	Coefficient of curvature
D	Specimen diameter
D	Damping ratio
D_{50}	Median formatting sand diameter
D_{50}	Median formation sand diameter
D_{max}	Maximum density
D_{min}	Minimum density
D_r	Relative density
$D_{r\ (con.)}$	Relative density after consolidation stage
$d\varepsilon_v$	Increments of volumetric strain
$d\varepsilon_{kk}$	Principal strain
$d\varepsilon_{ij}$	Shear strain
de_{ij}	Deviatoric strain
$d\varepsilon_s$	Strain tensor
Δu	Change in pore water pressure
ΔV_c	Volume change due to consolidation
e	Void ratio
E	Young's modulus
$e_{(con.)}$	Void ratio after consolidation stage
ε_a	Axial strain

e_{max}	Maximum void ratio
e_{min}	Minimum void ratio
ϕ	Internal friction angle for soil
ϕ'	The effective internal friction angle of the soil
$\boldsymbol{f}^p$	Force vector for fluid
$\boldsymbol{f}^u$	Force vector for mixture
G	Shear modulus
G_0	The value at the reference confining pressure
G_{es0}	Initial constant of shear modulus
G_{max}	Maximum shear modulus
G_s	Particle density/specific gravity
H	Height of wall
h	Total head
$\boldsymbol{H}$	Permeability matrix (see Equation 3.1)
H_0	Plastic modulus on loading
H_{U0}	Plastic modulus on unloading
I_L	Liquidity index
J_2	Second invariant of the deviatoric stress tensor
J_3	Third invariant of the deviatoric stress tensor
k	Permeability
K	Stiffness matrix
K_A	Static active earth pressure coefficient
K_{AE}	Dynamic active earth pressure coefficient
K_{ev0}	Initial constant of bulk modulus
k_h	Horizontal seismic coefficient
k_{he}	Horizontal seismic coefficient for restrained water case
k_v	Vertical seismic coefficient
L	Length of specimen
$\boldsymbol{M}$	Mass matrix
m	Material constant (see Table 3.8)
M	Slope line of (SSL)
m_b	Short-period body wave magnitude
M_f	Slope of the critical state line (CSL) for loading vector
M_g	Slope of the critical state line (CSL) for plastic strain vector

M_J	Japan meteorological agency magnitude
M_L	Richter local magnitude
M_S	Surface wave magnitude
m_s	Long-period body wave magnitude
m_s	Bulk modulus exponent
m_v	Coefficient of volume compressibility
m_v	Shear modulus exponent
M_w	Moment magnitude
OCR	Over consolidation ratio
$\boldsymbol{P}$	Pore pressure vector
p'	Effective confining pressure (Interchangeable with σ_3)
p'_0	The initial mean effective stress of the undrained triaxial test
P_A	Active earth pressure acting in a wall for static loading
p_a	Atmospheric pressure
P_{AE}	Active earth pressure acting in a wall for pseudo-static loading
p_{wd}	Westergaard hydrodynamic water pressure force
q	Deviator stress
$\boldsymbol{Q}$	Coupling matrix
ρ	Bulk density
R_f	Material constant
ρ_s	Particle density
r_u	Exess pore water pressure ratio
r_u	Pore pressure ratio
$\boldsymbol{S}$	Coupling matrix
S	Compressibility
S_{ij}	Deviatoric stress tensor
Sr	Degree of saturation
τ_{cyc}	Cyclic shear stress
τ_{static}	Static shear stress
u	Pore water pressure
$\boldsymbol{U}$	Displacement vector
V	Specimen volume
v	Poisson's ratio
w	Moisture content

w_L	Liquid limit
α_f	Dilatancy parameter for plastic strain vector
α_g	Dilatancy parameter
β	Inclination of the backfill from horizontal
β_0	Shear hardening parameter 1
β_1	Shear hardening parameter 2
γ	Unit weight
γ	Plastic deformation during reloading (see Table 3.1)
γ	Shear strain (see Figure 2.14)
γ_d	Dry unit weight
γ_{sub}	Submerged unit weight
γ_t	Total unit weight
γ_U	Plastic deformation during unloading
γ_w	Unit weight of water
γ_w	Unit weight of water
δ_{ij}	Kronecker delta
θ	Inclination of the back of wall to soil interface from vertical
θ	Lode's angle
σ'	Effective stress tensor
σ_{ij}	Stress tensor
σ_{kk}	Principal stresses
σ'_v	Effective vertical stress
σ'_{v0}	Initial vertical effective stress
τ	Shear stress
τ_f	Maximum shear stress
ψ	Seismic inertia angle
ψ_{he}	Seismic inertia angle for restrained water case
δ	Effective angle of interface friction between the soil and the structure

ABBREVIATIONS

UWLC: Dynamic effective stress analysis for ground (Software)

FEM: Finite Element Method

PZ-sand: The constitutive model for sand developed by Pastor *et al.* (1990)

CU: Consolidated-undrained monotonic triaxial test

CD: Consolidated-drained monotonic triaxial test

CSR: Cyclic Stress Ratios

HWL: High water table level

LWL: Low water table level

JPS: Jeddah Port Sand

LIST OF PUBLICATIONS

Elsharnoby, B., Elkamhawy, H., Elnaggar, E. & Alyami, M., (2004). "Enhancing load capacity performance of Harbour berths". *In: The 20th International Port Conference*, Alexandria, Egypt, No. 4, 1-11.

Elsharnoby, B., Elkamhawy, H., Elnaggar, E. & Alyami, M., (2004). "Effect of seismic forces on Harbour walls". *In: The 20th International Port Conference*, Alexandria, Egypt, No. 7, 1-21.

Alyami, M., Wilkinson, S. M., & Rouainia M., (2007). "Influence of Density of Gravity Quay Walls under Earthquake Loading". *In: Newcastle University, Proceedings of the Saudi Innovation Conference (SIC)*, Newcastle, UK.

Alyami, M., Rouainia, M. & Wilkinson, S. M., (2007). "Effective stress analysis of gravity quay walls under earthquake loading". *Proceedings of the 15th UK conference of the Association of Computational Mechanics in Engineering (ACME)*. Glasgow, UK, Paper 72.

Alyami, M., Wilkinson, S. M., Rouainia, M. & Cai, F., (2007). "Simulation of seismic behaviour of gravity quay wall using modified PZ sand model". *Proceedings of the 4th International Conference of Earthquake Geotechnical Engineering*. Thessaloniki, Greece, Paper 1734.

Alyami, M., Rouainia, M. & Wilkinson, S. M., (2008). "Numerical analysis of deformation behaviour of quay walls under earthquake loading". *Soil Dynamic and Earthquake Engineering.*

Alyami, M., Rouainia, M. & Wilkinson, S. M., (2008). "Modelling the cyclic behaviour of Jeddah Port sand using a generalized plasticity model". *Proceedings of the 16th UK conference of the Association of Computational Mechanics in Engineering (ACME).* Newcastle, UK, Paper 01.

Alyami, M., Rouainia M., & Wilkinson, S. M., (2008). "Deformation behaviour of Jeddah Port quay walls subjected to earthquake loading". *In: Leeds University, Proceedings of the Saudi Innovation Conference (SIIC)*, Leeds, UK. Paper No.37. Paper accepted.

CHAPTER ONE

1. INTRODUCTION

1.1 Background

Gravity quay walls are the most common type of construction for docks because of their durability; ease of construction and the capacity to reach deep seabed levels. The design of gravity quay walls requires sufficient capacity for three design criteria; sliding, overturning and allowable bearing stress under the base of the wall. Although the design of gravity quay walls is reasonably well understood for static loads, analysis under seismic loads is still being developed. During strong ground shaking, the pore water pressure of cohesionless saturated soils builds up leading to a reduction in the effective stress of the soil foundation and backfill of the wall; hence settlement and/or failure can occur in the foundation and in the backfill (which may make the wall fail). This phenomenon is known as "liquefaction".

The occurrence of liquefaction in both the saturated backfill and the foundation was the main reason for the damage from earthquakes to gravity quay walls in 1993 at Kushiro-oki and in 1994 at Hokkaido Toho-oki (Sasajima *et al.*, 2003) . In addition, liquefaction caused major damage to port facilities in Kobe, Japan, in the 1995 Hyogo-ken Nanbu earthquake as shown in Figure 1.1. The typical types of damage observed after the Kobe earthquake were: seaward displacement, approximately 5 m maximum and approximately 3 m average; the walls also settled approximately 1 to 2 m and tilted approximately 4 degrees (Ichii, 2004). Moreover, observations of 24 marine structures in the earthquake in 1999 at Kocaeli, Turkey, showed the backfill of quay walls also liquefied resulting in seaward displacements of the quay walls (Sumer, *et al.*, 2002) . The same observations were reported in 1999 during the Chi Chi earthquake in Taiwan, (Chen & Hwang, 1999). The seismic coefficient method consisting of the Mononobe-Okabe's formula based pseudo-static limit equilibrium approach is usually adopted in the structural design of gravity type quay walls to resist earthquake damage. However, this design method does not take into account the liquefaction of the backfill or the foundation soils.

Figure 1.1. Effects of liquefaction of backfill behind quay wall following the Kobe earthquake

For many years the design of seismic gravity quay walls has been studied and design codes for engineering practice are established. However, the widespread failures of these structures during recent earthquakes demonstrates that these design methods can be insufficient for loose cohesionless soils. Such gravity quay wall failures have stimulated progress in the development of a performance-based seismic design method for quay wall structures. Performance-based seismic design concepts using inelastic dynamic analysis for port structures has been proposed by Iai & Ichii (1998) then introduced by PIANC (International Navigation Association) in its seismic design guidelines (PIANC, 2001). This method permits a significant reduction in the high cost associated with repair and loss of use of quay wall structures; however, to adopt this methodology, it is necessary to define both, relevant design earthquakes and associated performance objectives that need to be met.

Although this method has great merit in mitigating seismic disaster, relatively little research has been conducted on performance-based seismic design for gravity quay walls. This may be explained by the fact that this approach is still being developed and therefore has been applied only to a limited number of case histories.

1.2 Aims and scope of project

1.2.1 Aim

The aim of this study is to develop a methodology for the seismic design of gravity quay walls and to use this to assess the safety of existing gravity quay walls in Jeddah Port.

1.2.2 Objectives

1) Review previous studies on seismic behaviour of gravity quay walls and examine the validity of simplified analysis methods.
2) Review liquefaction phenomena and the procedure for determining soil properties relevant to liquefaction potential.
3) Review the available constitutive soil models that describe soil behaviour under earthquake loading and identify the most suitable.
4) Validate the selected constitutive model by comparing results to existing triaxial tests.
5) Incorporate the constitutive model into a fully coupled finite element procedure and demonstrate the validity of this method by analysing the performance of existing quay walls that have experienced significant seismic events.
6) Perform a parametric study on gravity quay walls constructed on liquefiable soils and hence quantify the influence of various soil and quay wall parameters on liquefaction behaviour and hence develop mitigation strategies.
7) Determine the soil parameters of Jeddah Port sand (JPS) necessary to perform an appropriate seismic assessment.
8) Apply the finite element procedure to Jeddah Port quay walls and assess the success of mitigation strategies.
9) Make recommendations for the performance-based seismic design of gravity quay walls in seismic regions.

1.2.3 Thesis outline

Chapter 2 presents a review of the important aspects of the seismic design of port structures. Initially, previous studies on the seismic behaviour of gravity quay

walls are reviewed and the validity of simplified methods is examined. Liquefaction phenomena have also been reviewed, as have how to determine the soil properties relevant to liquefaction potential. Finally existing constitutive soil models are reviewed and the most suitable for simulating cyclic behaviour of sand identified.

Chapter 3 assesses the validity of using an effective stress method of analysis. In this chapter the elasto-plastic constitutive model of Pastor *et al.* (1990) with slight modifications has been used to analyse Port Island quay walls. The proposed P-Z sand model was first validated by simulating published monotonic and cyclic test results. Then the validity of the finite element procedure was demonstrated, by analysing a model of Port Island quay walls. The computed residual deformation results were then compared to field observations.

In Chapter 4, mitigation strategies for the seismic performance of gravity quay walls are investigated. This was achieved by conducting effective stress analysis and varying structural and geotechnical parameters. Twenty-six cases of effective stress analysis with variation of tidal range, soil permeability, soil relative densities, wall width size and level of seismic excitation were performed and conclusions made on possible mitigation strategies.

In chapter 5, the soil properties of Jeddah Port were measured. This was achieved by conducting Standard Penetration Test (SPT) at Jeddah Port, Saudi Arabia, and then the measured N-value is correlated with empirical relationships to give the relative density. The index and classification tests for samples were obtained from the North Container Terminal at Jeddah Port.

In order to characterize the liquefaction characteristics of Jeddah Port sand, a previously untested material, and to provide a framework for calibration and validating numerical models, a series of monotonic and cyclic triaxial tests were conducted under undrained conditions for Jeddah Port sand for three different relative densities; D_r = 35%, 55% and 75%. These represent loose (equal to *in situ* conditions), medium dense and dense Jeddah Port sand.

The consolidated undrained monotonic and cyclic triaxial test results of Jeddah Port sand presented in Chapter 5 for three different relative densities were

used to identify the P-Z sand model parameters. A two-dimensional effective stress method of analysis has been carried out for the Jeddah quay wall Berth 4.

To predict the expected deformation due to an earthquake, two levels of earthquake motion were implemented using different earthquake acceleration records and then the effect of improving the backfill on the final deformation was investigated using the soil model parameters for sands of relative densities of D_r = 35%, 55% and 75%. Finally, a flowchart illustrating a proposed seismic design procedure for gravity quay walls is suggested. These proposed seismic design stages can be applied for both existing and new gravity quay walls.

Chapter 7 contains a summary, conclusions and recommendations for future research.

CHAPTER TWO

2. LITERATURE REVIEW ON SEISMIC BEHAVIOUR OF GRAVITY QUAY WALLS

2.1 Introduction

This chapter presents a review of the important aspects of the seismic design of port structures. The information collected in this chapter will inform the experimental programme contained in Chapters 3, 4, 5 and 6.

Initially, previous studies on the seismic behaviour of gravity quay walls are reviewed and the validity of simplified methods is examined. Secondly, to determine what soil behaviour any model appropriate for seismic design must be able to incorporate, liquefaction phenomena has been reviewed, as has how to determine the soil properties relevant to liquefaction potential. Finally, existing constitutive soil models are reviewed and the most suitable for simulating cyclic behaviour of sand identified. This model will then be used in subsequent chapters to simulate the seismic behaviour of sand.

2.1.1 Performance based design of seismic resistant structures

Moderrn seismic design is starting to adopt a performance based approach. This design philosophy is an extension of the limit states design method and it is particularly useful for seismic design as it enables the wide range of seismic intensities that may be experienced at a site to be accommodated.

In performance based design a number of earthquake intensities with different probabilities of occurrence are specified, the performance of the structure to these different intensities is then assessed and compared to a number of damage criteria. As the high intensity earthquakes have a very low probability of occurrence the designer can accept greater levels of damage for these, while still requiring higher performance levels for earthquakes that are less likely to occur during the service life of the

structure. One of the reasons why this philosophy has not yet been universally adopted is that it requires models that can accurately simulate the behaviour of the structure.

Performance-based seismic design was first introduced, for buildings, by SEAOC (Structural Engineering Association of California (SEAOC, 1995) and later for port structures by Iai & Ichii (1998). It has now been introduced by PIANC (International Navigation Association) in its seismic design guidelines (PIANC, 2001). Although performance based design is starting to be adopted, in the case of geotechnical problems, it is still not widely used because of the lack of accurate soil models.

To determine how best to develop a performance based design approach for quay wall, some of the traditional design approaches as well as modern soil models are now reviewed and their applicability for incorporation into performance based design assessed.

2.2 Review of previous studies

Gravity quay walls, including caisson and block types, are simple structures made of concrete that are placed on a foundation and retain earth pressure from the backfill soil behind the wall. The practical current standard seismic design for quay walls is based on a seismic pressure based pseudo-static limit equilibrium approach; see Ebeling & Morrison (1993) ; Waerner (1998) and PIANC (2001) . The design of quay walls requires sufficient capacity for the three design criteria. These are sliding, overturning and allowable bearing stress under the base of the wall. The seismic loading is simulated with seismic coefficients. The seismic coefficients are accelerations and are specified in two directions; they are horizontal seismic coefficient (k_h) and vertical seismic coefficient (k_v). These coefficients are normalized by dividing by the acceleration due to gravity; both seismic inertia and seismic earth pressure acting on the wall are calculated by seismic coefficients, e.g. Okabe (1924); Mononobe & Matsuo (1929); Seed & Whitman (1970); Ebeling & Morrison (1993); Zeng & Steedman (2000); Nadim & Whitman (1983), among others.

Simple straightforward methods have been developed for evaluating the residual deformation of gravity walls based on a similar assumption to the pseudo-static approach; e.g. Newmark (1965); Franklin & Chang (1977); Richards & Elms (1979); Zhang *et al.* (1998); Mohajeri *et al.* (2002), among others. These procedures are based on the sliding block model and developed as a more useful tool for a performance-based design of gravity quay walls to predict residual deformation during earthquake loading. Furthermore, Zeng & Steedman (2000) proposed a method called a rotating block method, which is similar to the pseudo-static sliding block method of Newmark, to calculate the rotational displacement of gravity retaining walls based on rigid foundation under seismic loading.

2.2.1 Validity of simplified methods

Okabe (1924) and Mononobe & Matsuo (1929) developed the basis of a pseudo-static analysis of seismic earth pressures on retaining structures. Presently, this method has become one of the most widely used procedures in the design of quay walls by practical engineers and is popularly known as the Mononobe-Okabe (M-O) method. The M-O method is a direct extension of the static Coulomb theory to pseudo-static conditions. In an M-O analysis, pseudo-static accelerations are applied to a Coulomb active wedge. The pseudo-static soil thrust is then obtained from the force equilibrium of the wedge.

The forces acting on an active wedge in a dry, cohesionless backfill are shown in Figure 2.2. In addition to the forces that exist under static conditions shown in Figure 2.1, the wedge is also acted upon by horizontal and vertical pseudo-static forces whose magnitudes are related to the mass of the wedge by the pseudo-static accelerations $a_h=k_h\ g$ and $a_v=k_v\ g$, where k_h and k_v are seismic coefficients and g is gravity acceleration.

The total active pressure can be expressed in a form similar to that developed for static conditions, that is,

$$P_{AE} = \frac{1}{2} K_{AE} \gamma H^2 (1 - k_V) \qquad (2.1)$$

where P_{AE} is the active earth pressure acting in a wall for pseudo-static loadingm, H is the wall height and the dynamic active earth pressure coefficient, $K_{AE,}$ is given by:

$$K_{AE} = \frac{\cos^2(\phi - \theta - \psi)}{\cos\psi \cos^2\theta \cos(\delta + \theta + \psi)\left[1 + \sqrt{\frac{\sin(\delta + \phi)\sin(\phi - \beta - \psi)}{\cos(\delta + \theta + \psi)\cos(\beta - \theta)}}\right]^2} \qquad (2.2)$$

Where $\phi - \beta \geq \psi$, $\gamma = \gamma_d$ and $\psi = \tan^{-1}\left[k_h / (1 - k_v)\right]$. where ϕ is the internal friction angle for soil, ψ is the seismic inertia angle, β is the inclination of the backfill from horizontal, δ is the effective angle of interface friction between the soil and the structure and θ is the inclination of the back of wall to soil interface from vertical.

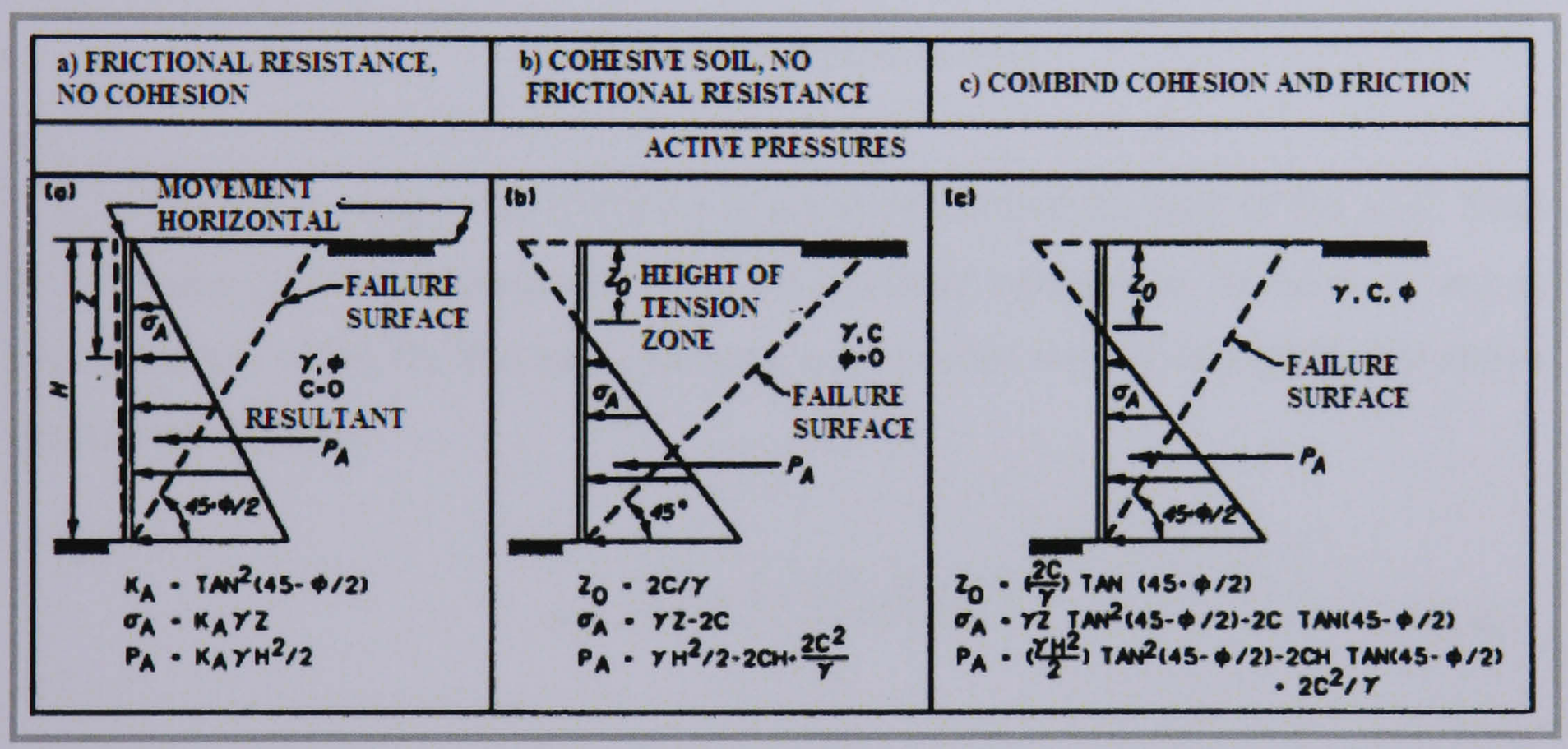

Figure 2.1. Computation of Rankine active and passive earth pressures for level backfills, after NAVFAC DM-7.2 reported by Ebeling & Morrison (1993)

Although the M-O analysis implies that the total active thrust should act at a point *H/3* above the base of a wall of height *H,* experimental results suggest that it actually acts at a higher point under dynamic loading conditions (Ebeling & Morrison, 1993). The total active force, P_{AE} in Equation 2.1, can be divided into a static component, $P_A = \frac{1}{2} K_A . \gamma . H^2$ and a dynamic component, ΔP_{AE} :

$$P_{AE} = P_A + \Delta P_{AE} \qquad (2.3)$$

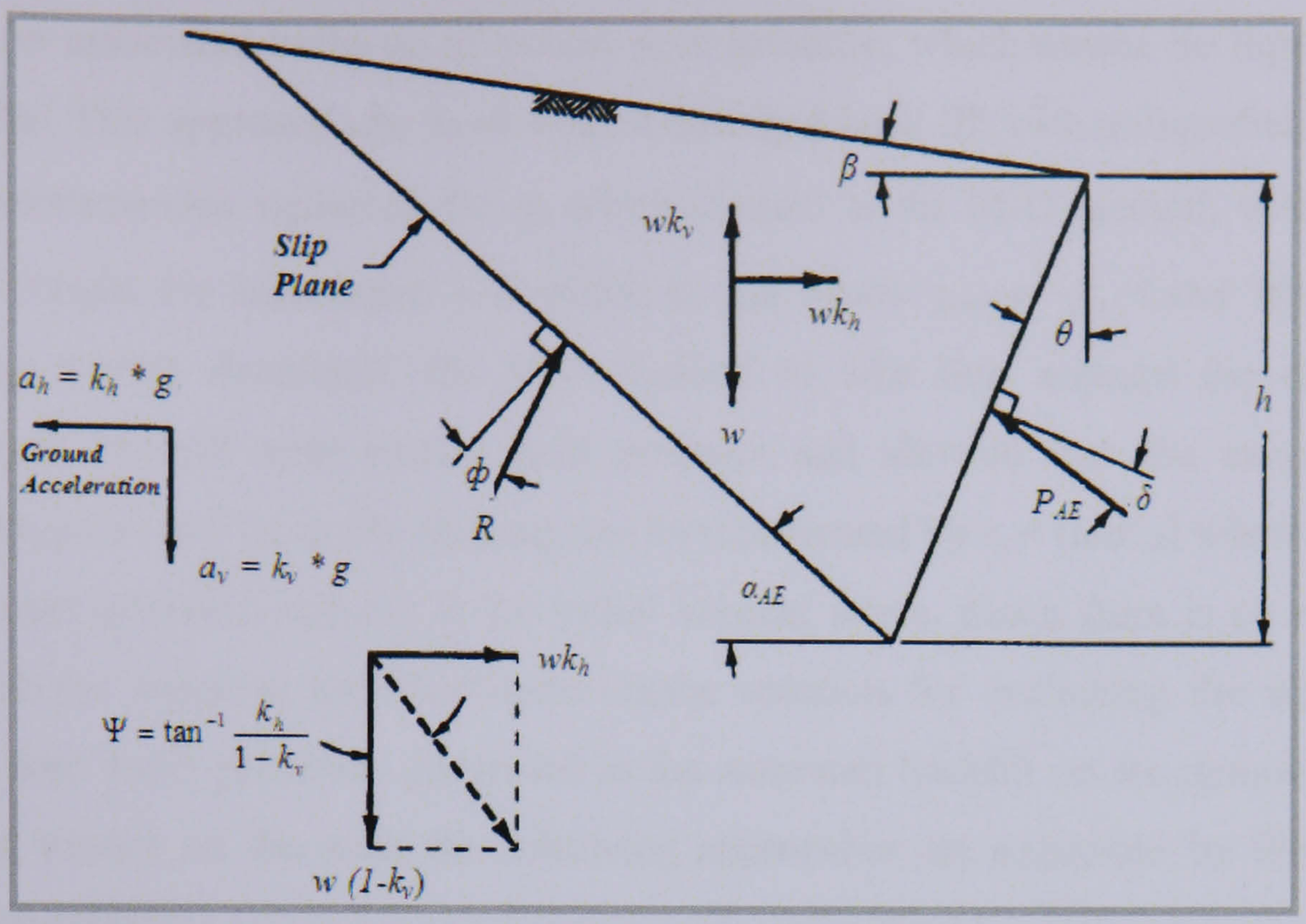

Figure 2.2. Mononobe-Okabe (active) wedge, after EM 1110-2-2502 reported by Ebeling & Morrison (1993)

The static component is known to act at *H/3* above the base of the wall. Seed & Whitman (1970) recommended that the dynamic component be taken to act at approximately 0.6*H*. On this basis, the total active thrust will act at a height (*h*) above the base of the wall.

$$h = \frac{P_A H/3 + \Delta P_{AE}(0.6H)}{P_{AE}} \qquad (2.4)$$

The value of *h* depends on the relative magnitudes of P_A and P_{AE}. It often ends up near the mid height of the wall. M-O analyses show that k_v, when taken as one-half to two-thirds the value of k_h affects P_{AE} by less than 10%. Seed & Whitman (1970) concluded that vertical acce1erations can be ignored when the M-O method is used to estimate P_{AE} for typical wall designs.

2.2.1.1 Effects of excess pore water pressure

The Mononobe-Okabe equation was derived for dry yielding backfill retained by a rigid wall. However, it is known that the quay walls have a submerged backfill because they are constructed on the coastline and the ground water table is close to ground level. Matsuzawa *et al.* (1985) studied this case and assumed that shaking

causes no associated build-up of excess pore pressure, which means no liquefaction can occur. This approach can work with submerged back fill with unliquefiable soils. They recommended replacing the γ_d which is used in the M-O method, with a new unit of weight for submerged soil which is γ_{sub}, where $\gamma_{sub}=\gamma_t - \gamma_w$. Later Ebeling & Morrison (1993) developed the M-O method to take into account the effect of submerged backfill with excess pore pressure and showed that the excess pore pressures generated by cyclic shaking can be represented by $r_u = (u/\sigma'_{v0})$ where u is the excess pore pressure and σ'_{v0} is the initial vertical stress. Since there is no rigorous approach for adapting the Mononobe-Okabe solution for evaluating the effects of excess pore water pressures generated in the saturated backfill on the dynamic earth pressure extract on the wall, the following approaches are suggested by Ebeling & Morrison (1993).

Assuming that the permeability of soil is low, say $k<1*10^{-3}$ (m/s^2) where pore water moves with the mineral skeleton, this case is called the "*restrained water case*". Ignoring vertical accelerations, the effective unit weight of soil becomes:

$$\gamma_{sub1} = \gamma_{sub}\,(1 - r_u) \tag{2.5}$$

The thrust from the soil skeleton, P_{AE}, is computed using

$$k_{he} = \frac{\gamma_t}{\gamma_{sub1}} k_h \tag{2.6}$$

and

$$\psi_{he} = \tan^{-1}(k_{he}) \tag{2.7}$$

Where k_{he} is the horizontal seismic coefficient for restrained water case.

However, Alyami (2003) wrote a computer program using an M-O method and Ebeling & Morrison's (1993) suggestion for Submerged Backfill with Excess Pore Pressure as presented, which used visual basic.net and .net framework technology to analyse the plain concrete block gravity quay wall under dynamic effects. These forces are idealized in Figure 2.3. Hundreds of runs were conducted

and they showed that increasing pore water pressure had a corresponding effect on the lateral pressure for a wide range of water pressures, but a large magnitude of excess pore water pressure caused a dramatic rise in lateral pressure acting on the wall as shown in Figure 2.4. That clearly means that there is a limitation for the applicability of these practical methods of design based on the pseudo-static approach.

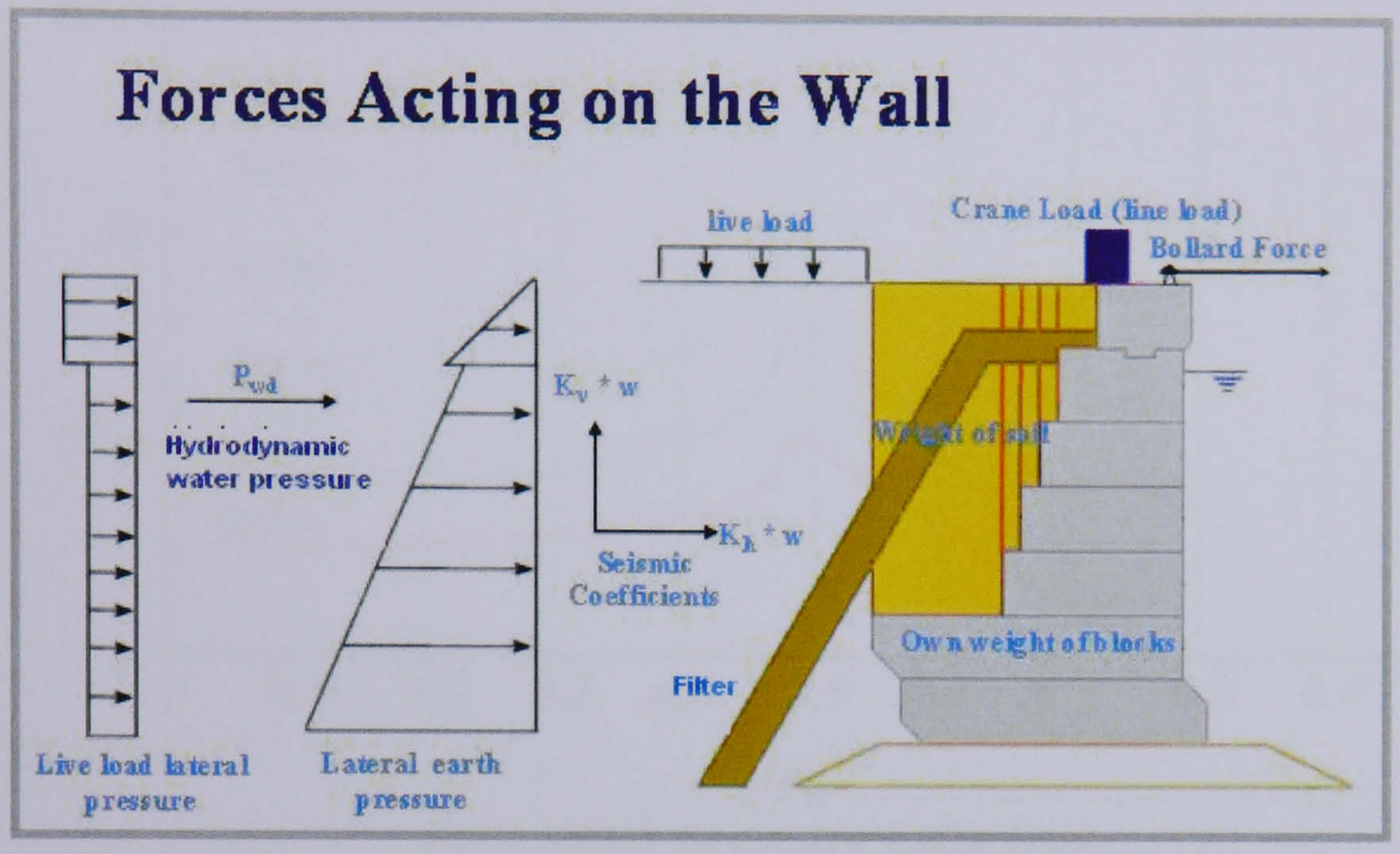

Figure 2.3. Forces acting on the wall, after Alyami (2003)

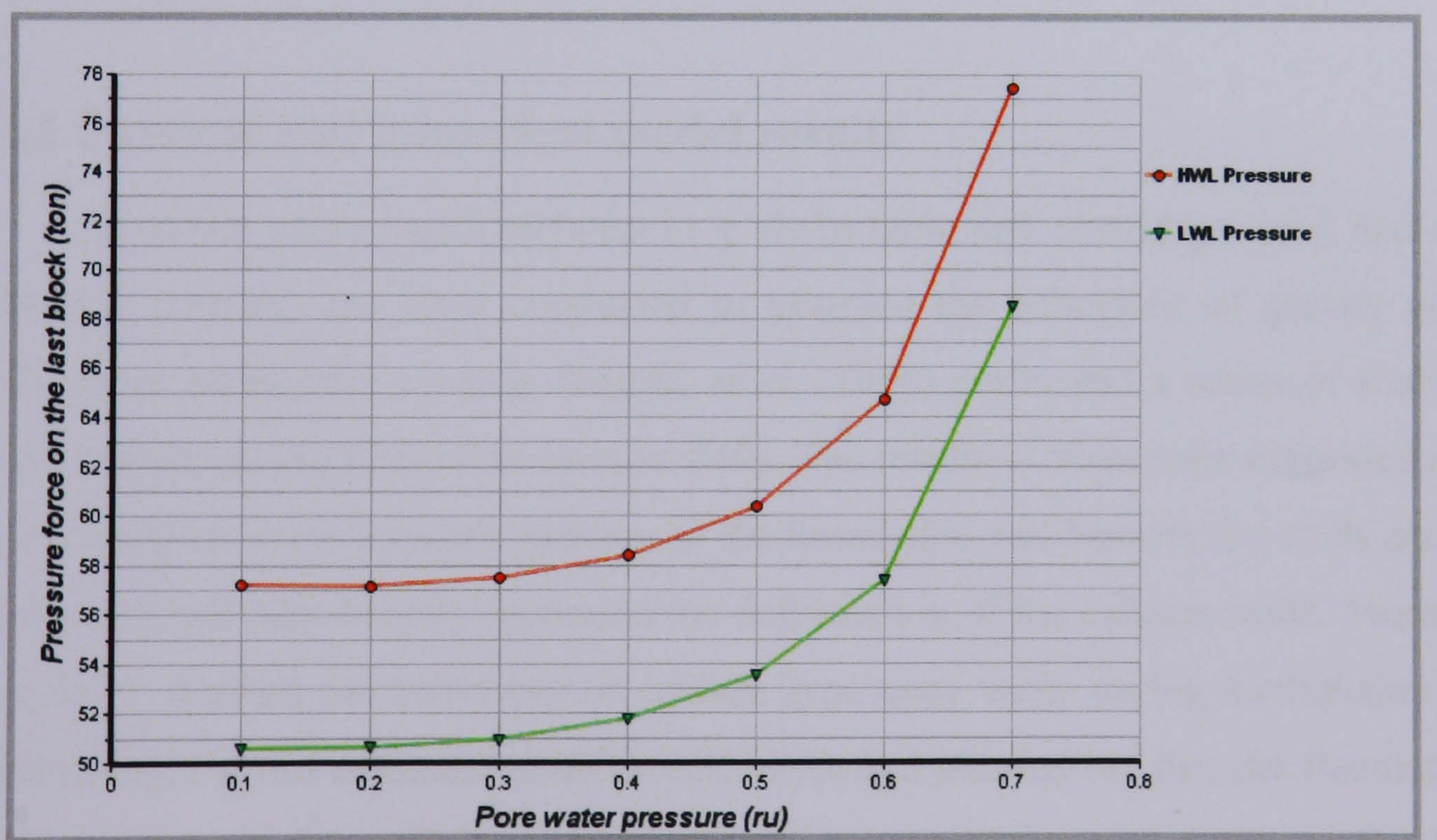

Figure 2.4. Effect of pore water pressure on lateral pressure, after Alyami (2003)

Furthermore, in this study Ebeling & Morrison's (1993) suggestion has been examined for various values of wall height (H=8-16 m) using MathCAD. The results are shown in Figure 2.5. In the figure for values of the exess pore water pressure ratio

(r_u) > 0.5 the active earth pressure starts to reduce, reaching zero at approximate r_u = 0.75. This indicates that the method is not applicable for $\phi - \beta \geq \psi$.

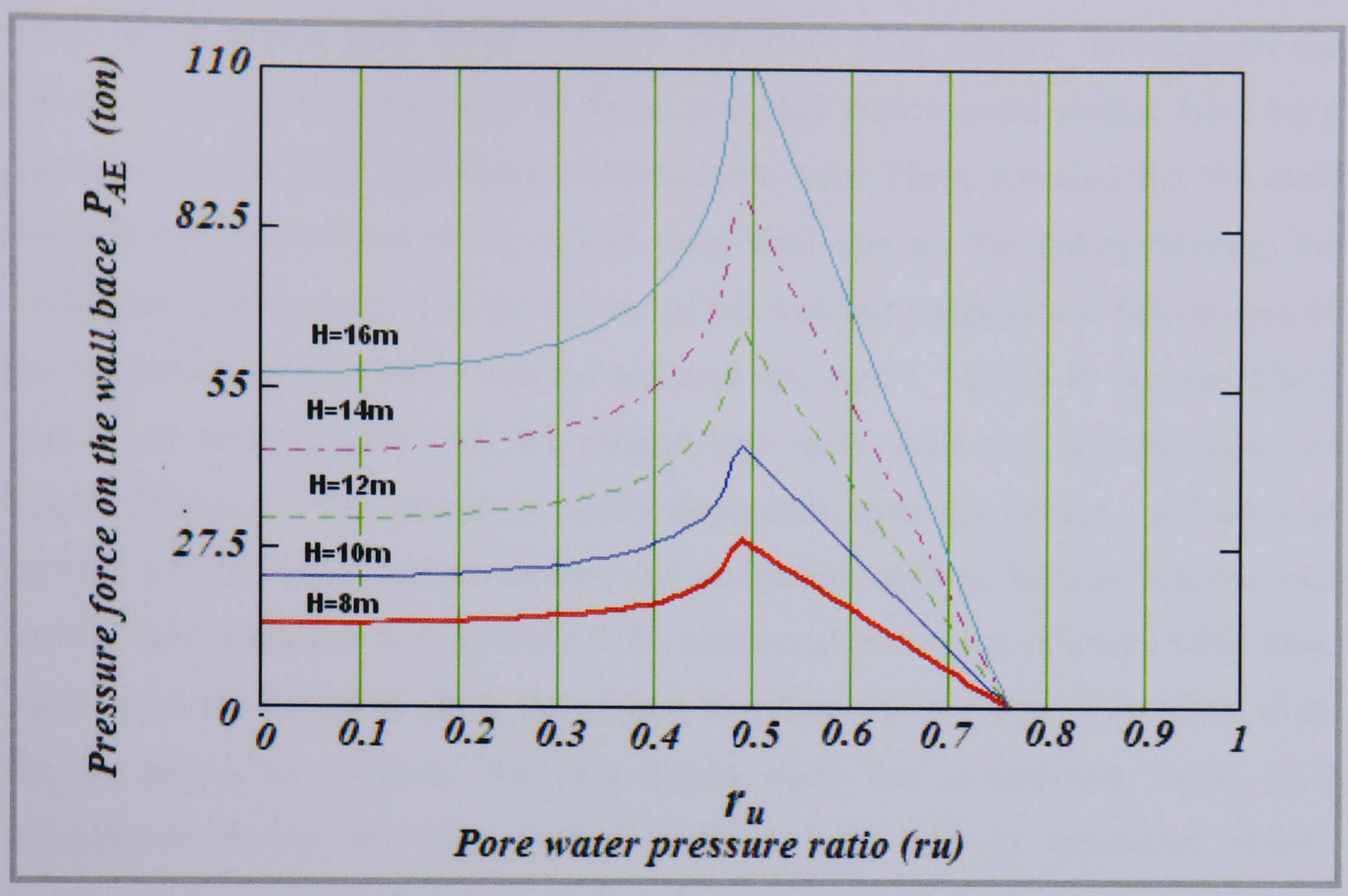

Figure 2.5. Effect of pore water pressure ratio on lateral pressure

2.2.2 Physical and numerical model results

In recent years, much physical (1 g shake table and centrifuge tests) and / or numerical research has been conducted to examine the behaviour of gravity quay walls under earthquake loading. Inagaki *et al.* (1996) performed a series of shaking table tests simulating Kobe Port caisson walls. The results of these tests suggested that the excess pore water pressure increase in the foundation soil beneath the walls and in the backfill soil significantly increased the deformation of the caisson walls. Miura *et al.* (1997) derived the behaviour of caisson type quay walls during earthquakes by undertaking a series of model shaking table tests and pointed out that the fluctuating earth pressure on the wall has a tendency to suppress movement of the wall when liquefaction does not occur in the backfill. Ghalandarzadeh *et al.* (1998) conducted a series of shaking table tests in order to study the mechanism of deformation of a gravity quay wall during a strong earthquake. It was found that the significant distortion of a wall was induced by combined effects of dynamic earth pressure exerted upon the wall by the softened backfill soil and the decrease of rigidity in the

foundation sand. Iai & Sugano (2000) also conducted a series of shake table tests and reported that the effects of the excess pore water pressures in the backfill and foundation soils increases the deformation about twice as much as that without the effect of the excess pore water pressure. Nakahara *et al.* (2000) investigated the damage mechanism of the piers of Kobe port and experimental studies have been carried out using large underwater shaking table tests. These revealed that the main cause of the deformation of the caisson quay wall was not the sliding between the foundation rubble mound and the bottom of the wall but a significant deformation of the foundation rubble mound and the replaced soil region. Miyata & Sugano (2000) carried out shaking table tests for caisson type quay walls and demonstrated that bottom friction of the caisson is highly dependent upon the natural oscillation of backfill soil, the input seismic motion and interaction stiffness between caisson and backfill soil. Mohajeri & Towhata (2003) conducted two series of shake table tests, which were performed to study the sliding displacement of caisson type quay walls due to earthquake motions. The test results show that considering single yield acceleration during the displacement analysis may lead to erroneous results. Moreover, Zeng (1992 & 1998), studied the behaviour of gravity quay walls under seismic loading using data from three centrifuge tests and pointed out that the current design practice can achieve satisfactory results for a gravity retaining wall with dry backfill but may not do so for saturated backfill because the excess pore pressure generated in the soil increases the horizontal thrust on a wall and degrades the stiffness and strength of soil. Therefore, limiting the magnitude of excess pore pressure is very important. Lee (2005) carried out a series of 2-D centrifuge modelling test with an in-flight shaker in order to model both the deformation characteristics of backfill and the seismic responses of caisson-type walls embedded in soils with various levels of permeability and found that the rotational mode made changes in excess pore water pressure and increased the earth pressure in the deep layer but the translation mode changed these pressures in the shallow layers.

The above discussion demonstrates that the pseudo-static approach is a simplified method used only for design and cannot express the real behaviour of quay walls under seismic loading. As the pore water pressure can build up in the foundation not only in the backfill of the wall; hence damage can occur in the foundation and in the backfill. Since the pseudo-static limit equilibrium approach does not include the

effect of foundations during the earthquake loading, other approaches are required to evaluate the overall deformation including the foundations.

The finite element method is generally considered to be one of the most advanced approaches; Zienkiewicz *et al.* (2005) discussed and summarized the details of adapting finite element analysis to a dynamic problem. Recently the finite element method has been used by researchers to simulate the seismic response of gravity retaining walls.

Pitilakis & Moutsakis (1989) simulated the case of the seismic behaviour of Kalamata harbour quay wall during the large Kalamata earthquake using a simple equivalent non-linear model with variable damping proposed by Idriss & Seed (1974) which was incorporated into the two-dimensional finite element code QUAD-4. Later, Madabhushi & Zeng (1998) compared the centrifuge test data of gravity retaining walls carried out by Zeng (1992 & 1998) with the non-linear finite element method by using the constitutive model described by Pastor *et al.* (1985). That model is P-Z Mark II, which incorporates the numerical code dubbed SWANDYNE (Chan, 1989) and shows that the numerical finite element method incorporating the special numerical techniques is capable of simulating the behaviour of gravity quay walls under dynamic loads. A similar outcome is reported by Kohama *et al.* (1998) by comparing the centrifuge test data of a gravity retaining wall with the non-linear finite element method (FLIP). To apply this numerical method to a structure with foundations, it is necessary to model the behaviour of the foundations, which has led to many constitutive models being developed to express the behaviour of soil, since most of the damaged quay walls have suffered from liquefaction in their backfill and foundations. However, Iai *et al.* (1998) and Dakoulas & Gazetas (2005), demonstrated that the cyclic behaviour of soil, idealized through the finite element method, can reasonably explain the variety of seismic responses of the port structures analysed, including the modes and extent of the deformation. Thus, this finite element method is one of the most useful tools to simulate the seismic response of gravity quay walls and ideal for performance based design.

2.2.3 Performance-based seismic design for Port structures

Figure 2.6 shows the Flowchart for Performance Based Seismic Design for Port structures suggested by Iai & Ichii (1998). The main aspects in the proposed approach are;

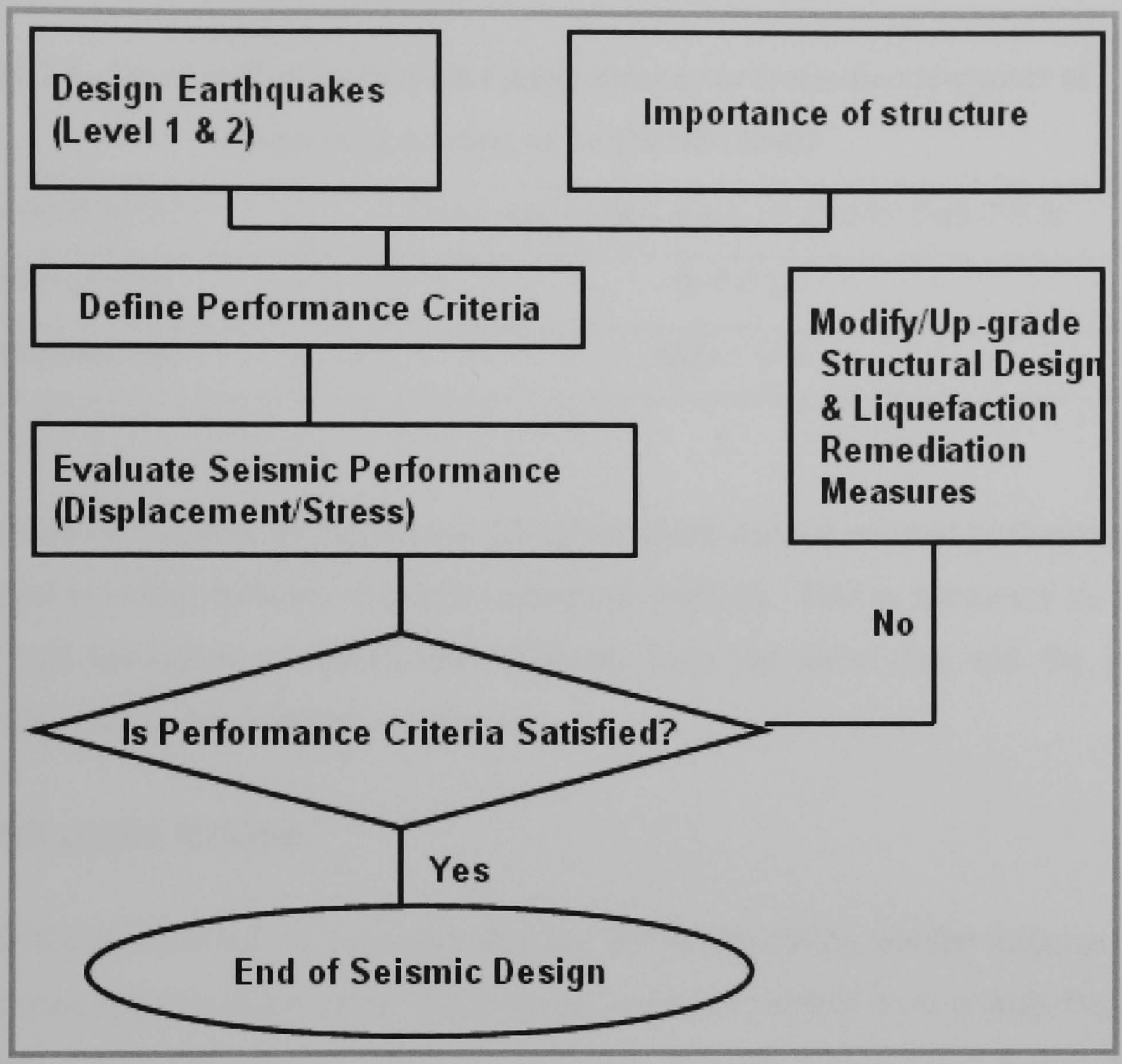

Figure 2.6. Flowchart for Performance Based Seismic Design for Port structures, after (Iai & Ichii, 1998)

Design Earthquake (Level 1 and Level 2) Firstly, two levels of design earthquake intensity, namely Level 1 and Level 2, should be considered in the design of earthquake motions for Port structures. Level 1, where the earthquake motion is expected to have a return period of 75 years, is used as a motion input to design all facilities except those classified as Level 2. The latter is utilised to construct high seismic resistant structures, based on an earthquake motion having a return period of 475 years, such as Maya Wharf, which survived after the 1995 Hyogoken-nambu earthquake (Ichii *et al.* 2000). These two levels are adopted in the Japanese standard (OCDI, 2002).

Define Performance Criteria: the performance criteria should be defined. In case of gravity quay walls and based on the experience of Kobe disaster in 1995, a damage level index has been proposed from the viewpoint of temporally service and listed in Table 2.1 (OCDI, 2002). These level indexes are indicating that the seaward displacement is main factor to evaluate the quay wall performance.

Table 2.1. Quay wall deformation rough standards from the viewpoint of temporally service, after OCDI (2002)

Function of use	Quay wall height equal or greater than 7.5 m
Normal use	0~0.3 m
Restricted use	0.3~1.0 m

Evaluate Seismic Performance (Displacement/ stress) seismic performance is evaluated by using inelastic dynamic numerical analysis. This is necessary as the dynamic soil behaviour is significantly different from the static case and the soil stress/strain relationship is highly nonlinear

2.3 Earthquake motion

Earthquake motion is a ground shaking and is caused by sudden slippage in the earth crust. The interface where the slippage occurs is referred to as a fault. Faults are classified into three classes: Dip-slip (normal), Dip-slip (thrust) and Strike-slip. Each class depends on a different force mechanism causing the slippage as illustrated in Figure 2.7.

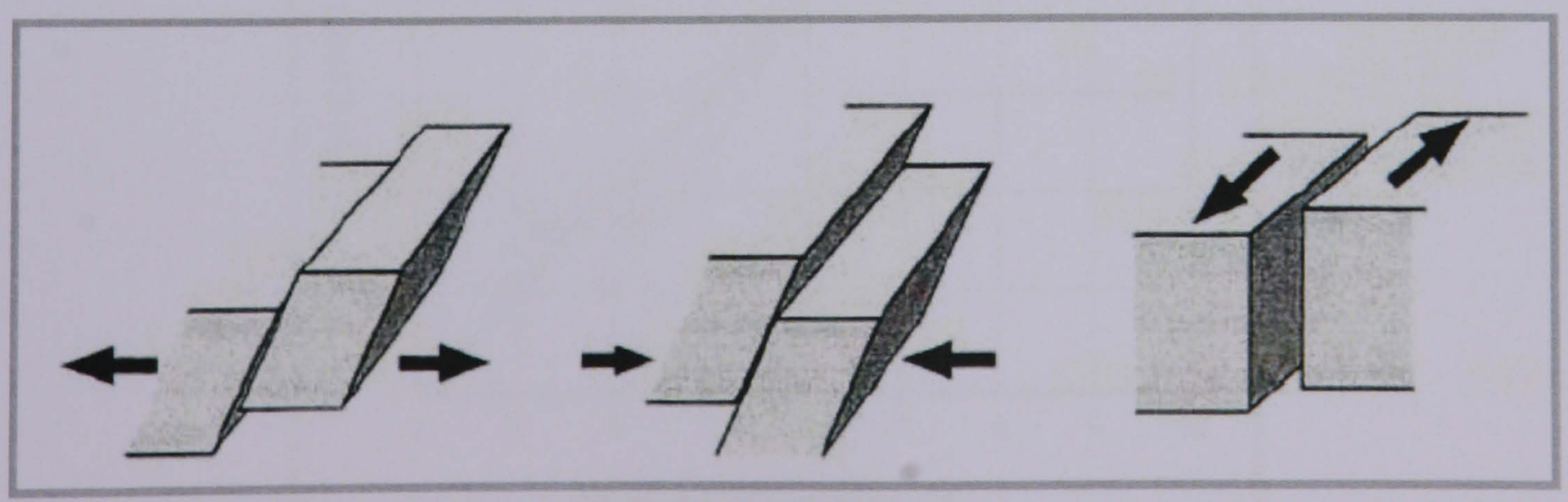

Figure 2.7. A simple explanation of the earthquake mechanism and a fault, after Ichii (2006)

2.3.1 Size of earthquake

There are two basic parameters to describe the size of an earthquake; magnitude and intensity.

2.3.1.1 Earthquake Magnitude

Earthquake magnitude is a physical measure of the size of earthquake, which is evaluated from the recorded data. There are six different magnitude scales used by seismologists, namely:

1) The Richter local magnitude (M_L)
2) The Surface wave magnitude (M_S)
3) The Short-period body wave magnitude (m_b)
4) The Long-period body wave magnitude (m_B)
5) The Moment magnitude (M_w)
6) The Japan meteorological agency magnitude (M_J)

The Moment magnitude (M_w) is the scale preferred by seismologists and by engineers for engineering applications (Youd & Idriss, 2001). The relationship between the various magnitude scales is shown in Figure 2.8.

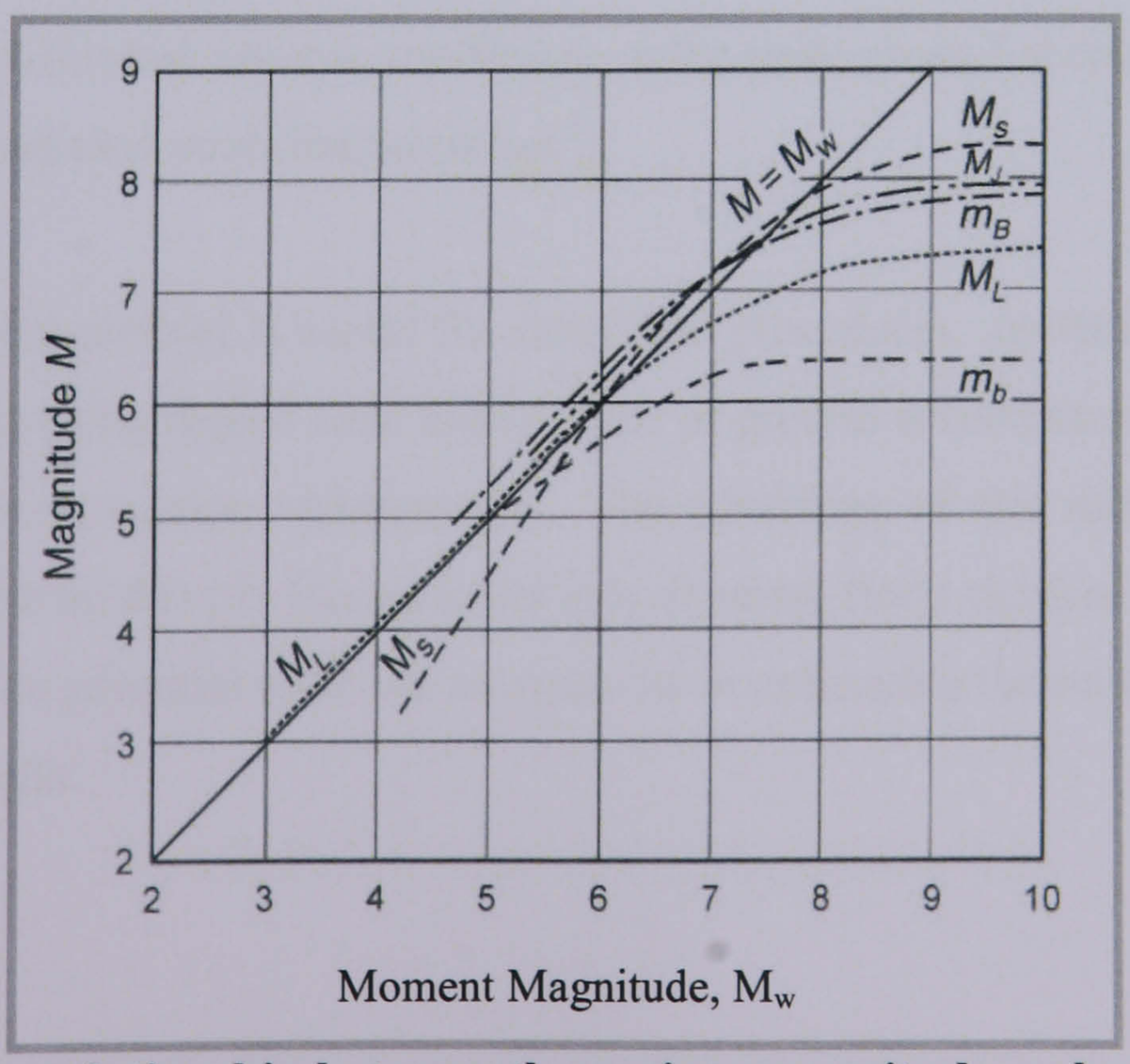

Figure 2.8. The relationship between the various magnitude scales, after Heaton *et al*; as reported by Youd & Idriss (2001)

2.3.1.2 Seismic Intensity

Seismic Intensity is a theoretical measure of the destructiveness of the earthquake, which evidenced by human reaction and observed damage. Earthquake intensity may also vary from one site or location to another. Several local and international scales are used to express seismic intensity such as gal, g, m/s^2 and cm/s^2. Since different earthquakes of similar magnitude may cause very different levels of damage, measuring earthquake intensities at various locations for each earthquake is a very useful method of estimating seismic risk; however, as this is subjective, peak horizontal acceleration a_{max} or peak ground acceleration (PGA) is generally used to characterize the intensity of ground shaking.

The effect of earthquakes should be carefully examined in the design of port facilities. Japanese code (Ministry of Transport, 2002) proposed that a modified seismic coefficient can be used in the simplified procedures, which was mentioned earlier. The proposed seismic coefficient can be calculated as follows:

$$\text{a)}\quad k_h = \frac{a}{g} \quad \text{, for } a \le 2(m/\sec^2) \tag{2.8}$$

$$\text{b)}\quad k_h = 1/3\left(\frac{a}{g}\right)^{1/3} \quad \text{, for } a > 2(m/\sec^2) \tag{2.9}$$

where, k_h the horizontal seismic coefficient, a the peak ground acceleration (m/sec^2) and g the gravitational acceleration (m/sec^2).

While this method is useful for simplified procedures, modern procedures are moving towards using digital time history files of ground acceleration measured by a SMAC-type strong motion seismograph. The advantage of this method is that the accelerations can be directly incorporated into dynamic finite element method. These methods have the potential to be the most useful in estimating the seismic response of gravity quay walls.

2.4 Case histories

There are nine case histories of damage to port structures made of gravity retaining walls that were well-documented during the period 1964–1999. These events are listed in Table 2.2; more details and a cross section of each case are presented in Table 2.3 – Table 2.11.

Table 2.2. Selected case histories of damage to port structures (1964–1999)

No.	Type	Earthquake Year (magnitude)	Port	Country
1	Block	1964(Ms-7.5)	Niigata port	Japan
2	Block	1985(Ms=7.8)	San Antonio port	Chile
3	Block	1986(Ms=6.2)	Kalamata port	Greece
4	Block	1989(M=6.0)	Port of Algiers	Algeria
5	Caisson	1993(Mj=7.8)	Kushiro port	Japan
6	Caisson	1993(Mj=7.8)	Kushiro port	Japan
7	Caisson	1995(Mj=7.2)	Kobe port	Japan
8	Block	1999(Mw=7.4)	Derince port	Turkey
9	Caisson	1999(Ms=7.7)	Taichung port	Taiwan

Table 2.3. Niigata quay wall damaged during 1964 earthquake, after Hayashi *et al.* (1966)

Port & location	Niigata port, Japan, Berths Rinko Wharves
Type	Block quay wall
Height	+2.4 m
Water depth	-11.6 m
Earthquake & Magnitude	June, 16, 1964, M_s =7.5
Design seismic coefficient (Kh)	0.1
Peak ground surface acceleration (PGA)	0.155 to 0.180g, PGA evaluated based on strong motion seismograph in an apartment in Kawagishi Cho.
Horizontal displacement	1.0 m
Vertical displacement	As shown in the figure
Tilt	As shown in the figure
Comments	A tremendous settlement occurred. In some parts it was observed that four blocks in the upper part fell down and the next block slid by about one metre toward the sea. The liquefaction of sand has been pointed out as the characteristic factor on the earthquake damage in Niigata port.
Reference	Hayashi *et al.* (1966)

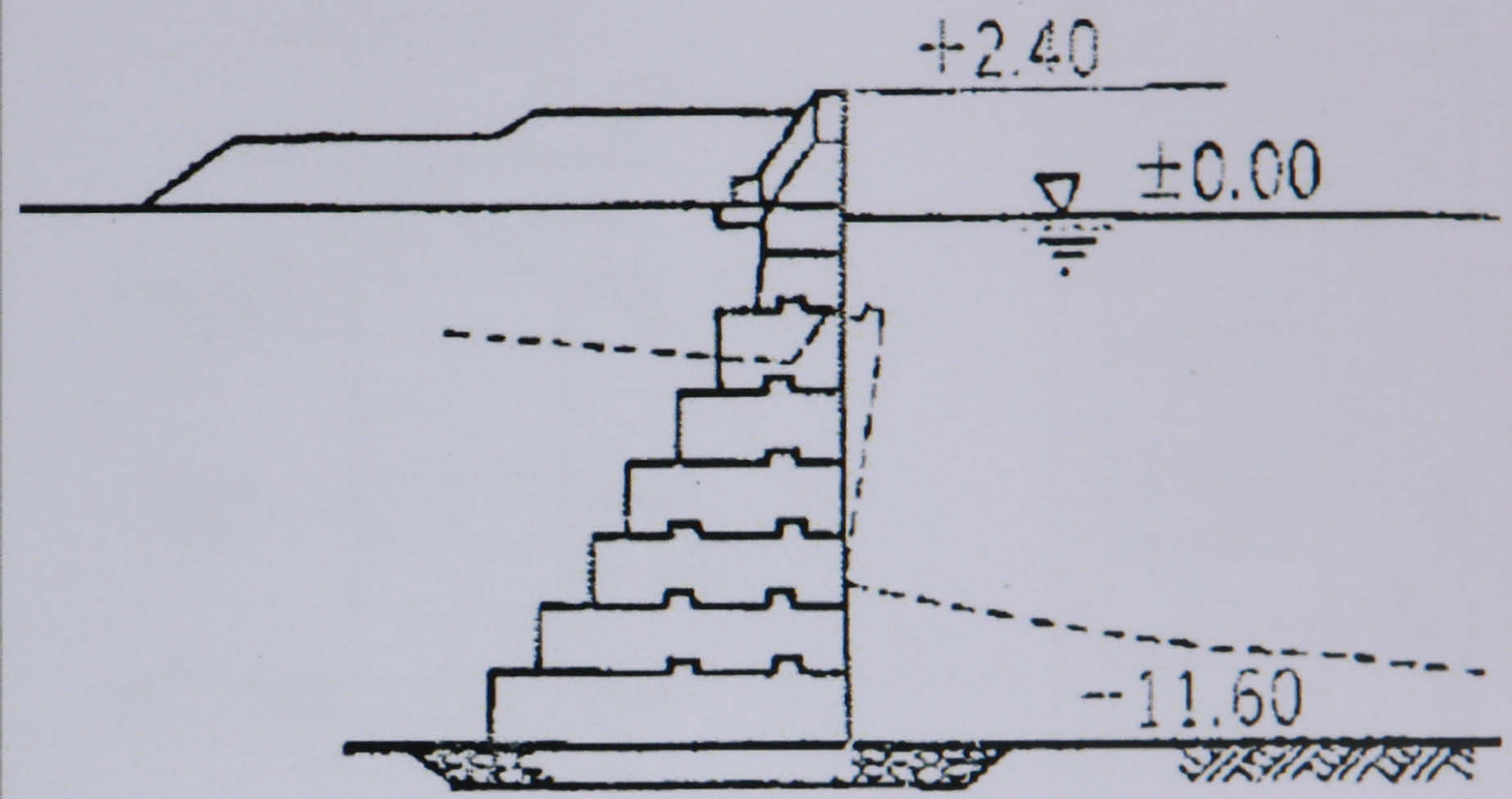

Table 2.4. San Antonio quay wall damaged during 1985 earthquake, after Tsuchida *et al.* (1986) & Wyllie *et al.* (1986) as reported by PIANC (2001)

Port & location	San Antonio Port, Chile, Berths 1& 2
Type	Block quay wall
Height	+4.9
Water depth	-9.6 m
Earthquake & Magnitude	March 3. 1985 Chile earthquake, M_s =7.8
Design seismic coefficient (Kh)	Not reported
Peak ground surface acceleration (PGA)	0.67g, PGA evaluated based on strong motion earthquake records.
Horizontal displacement	Not reported
Vertical displacement	Not reported
Tilt	Not reported
Comments	Collapse of block type quay wall over 60% of wharf length (452 m) due to strong earthquake motion and backfill liquefaction.
Reference	Tsuchida *et al.* (1986) & Wyllie *et al.* (1986) as reported by PIANC (2001)

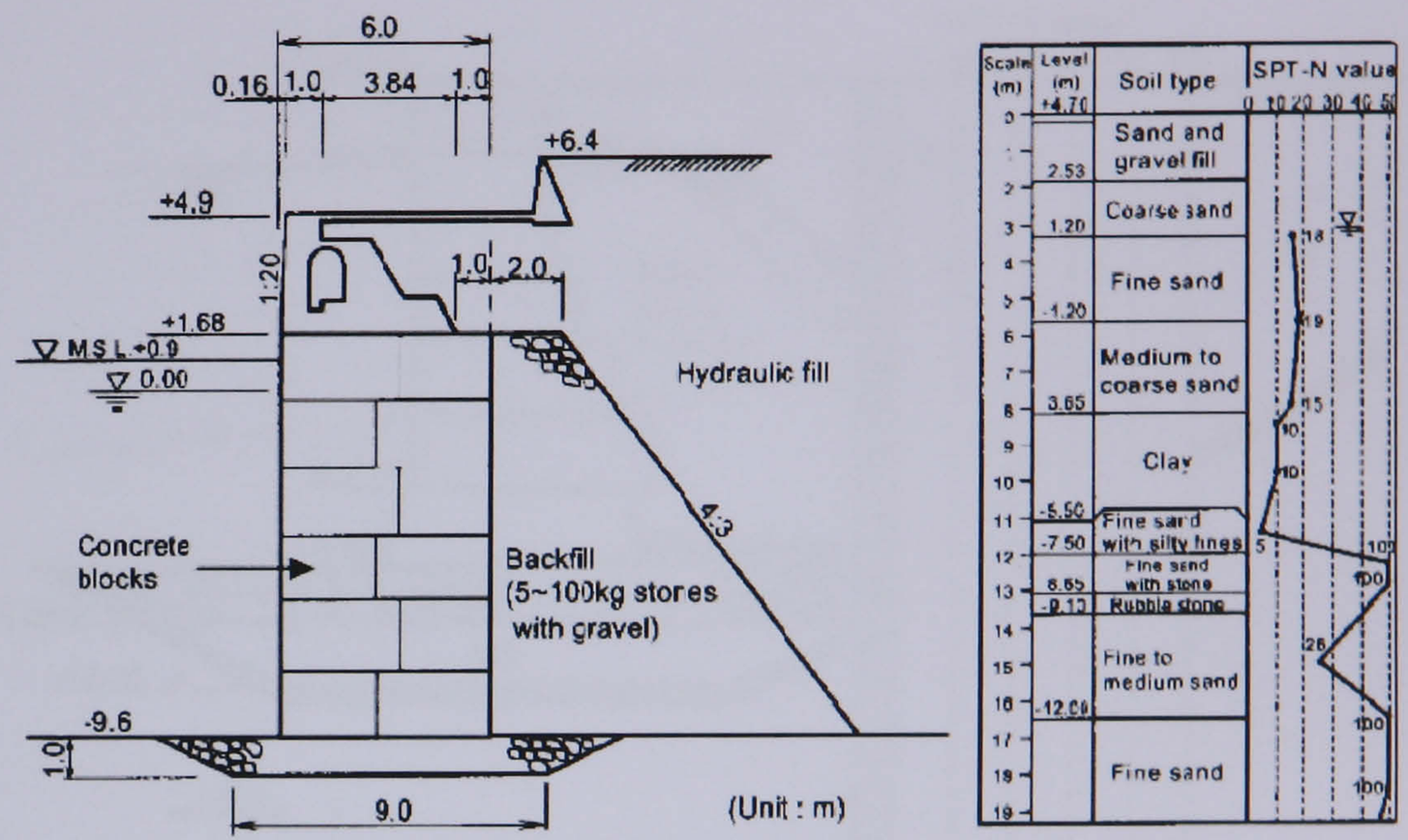

Table 2.5. Kalamata quay wall damaged during 1986 earthquake, after Pitilakis & Moutsakis (1989)

Port & location	Kalamata Port, Greece.
Type	Block quay wall
Height	+2.1 m
Water depth	-9.5 m
Earthquake & Magnitude	September 13. 1986 Kalamata earthquake, M_s =6.2
Design seismic coefficient (Kh)	Not reported
Peak ground surface acceleration (PGA)	0.2 to 0.3 g , PGA/PAV evaluated based on ID & 2D equivalent linear analysis
Horizontal displacement	0.15 $\pm$ 0.05 m
Vertical displacement	Not reported
Tilt	4 to 5 degree
Comments	Seaward displacement with tilt of block type quay wall constructed on firm foundation. The backfill settled 20 cm behind the wall with no settlement at a distance of 30 to 40 metres away. The quay wall remained serviceable.
Reference	Pitilakis & Moutsakis (1989)

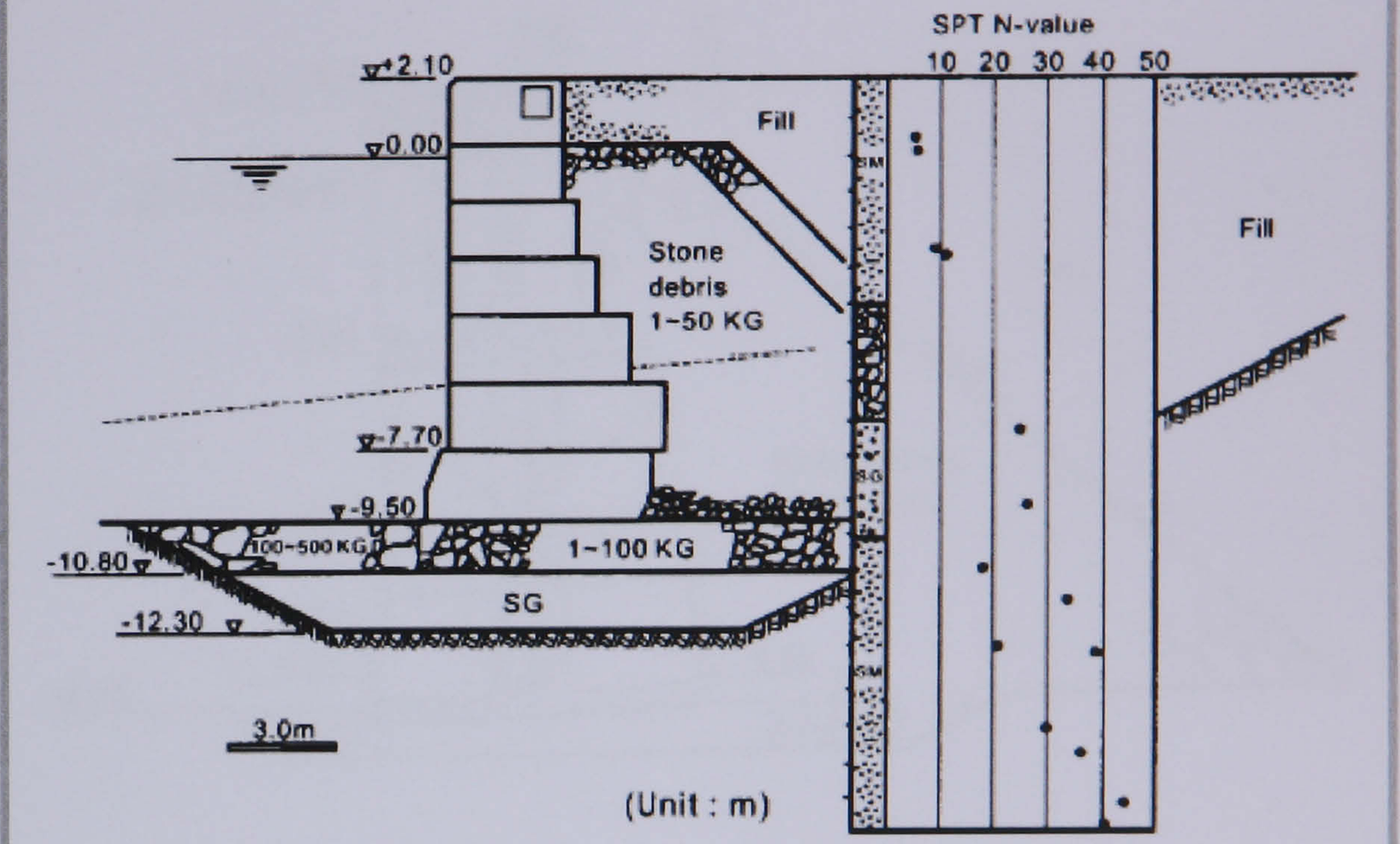

Table 2.6. Algiers quay wall damaged during 1989 earthquake, after Manja (1999) as reported by PIANC (2001)

Port & location	Port of Algiers, Algeria, Quay No. 34.
Type	Block quay wall
Height	+ 2.2 m
Water depth	- 10.0 m
Earthquake & Magnitude	October 29. 1989 Chenoua earthquake , M = 6.0
Design seismic coefficient (Kh)	Not reported
Peak ground surface acceleration (PGA)	0.2 to 0.3 g , PGA/PAV evaluated based on ID & 2D equivalent linear analysis
Horizontal displacement	0.5 m
Vertical displacement	0.3 m
Tilt	Not reported
Comments	During this earthquake. 8,000 buildings were destroyed: there were ground ruptures, landslides, and the coastal road was closed by falling rock. No additional detailed information is available on the earthquake.
Reference	Manja (1999) as reported by PIANC (2001)

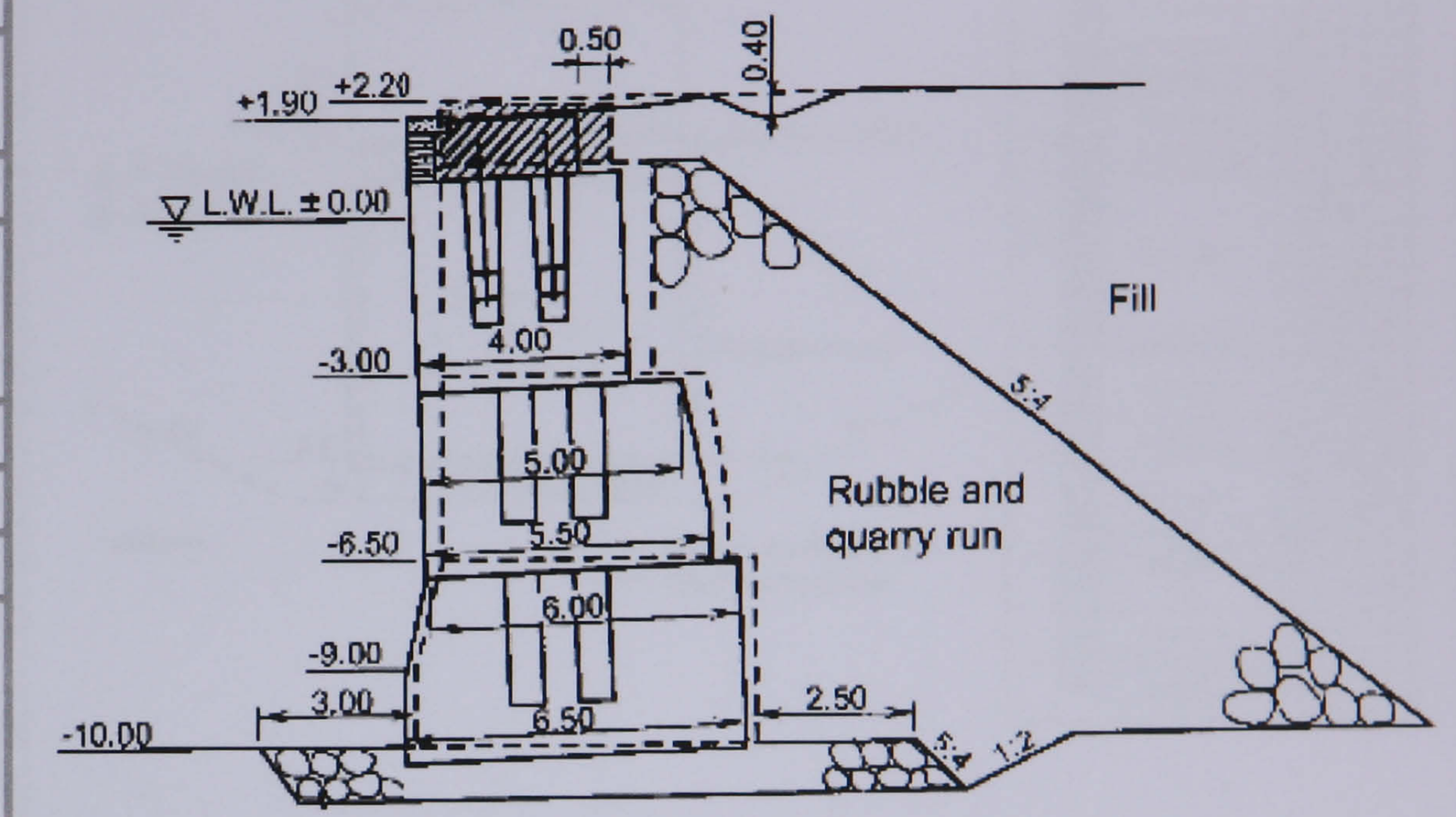

Table 2.7. Kushiro west quay wall damaged during 1993 earthquake, after Iai *et al.* (1994) as reported by PIANC (2001)

Port & location	Kushiro Port, Japan, West No. 1
Type	Caisson quay wall
Height	+ 3.0 m
Water depth	- 9.0 m
Earthquake & Magnitude	January 15. 1993 Kushiro-Oki earthquake, M_s =7.8
Design seismic coefficient (Kh)	0.2
Peak ground surface acceleration (PGA)	0.47g, PGA evaluated based on strong motion earthquake records.
Horizontal displacement	0.75 m
Vertical displacement	0.2 m
Tilt	2 %
Comments	Seaward displacement of caisson type quay wall constructed on firm foundation. Liquefaction of backfill.
Reference	Iai *et al.* (1994) as reported by PIANC (2001)

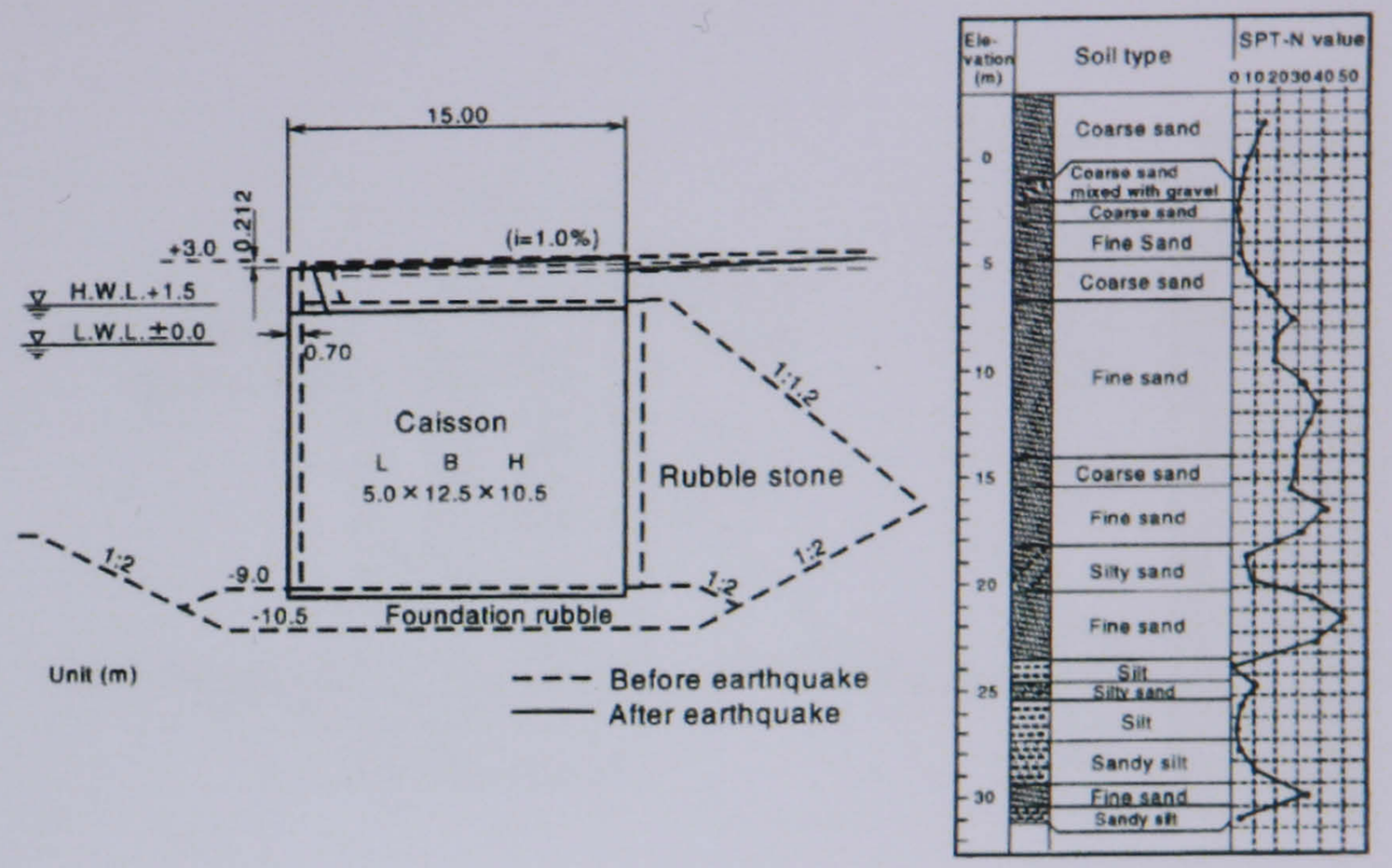

Table 2.8. Kushiro east quay wall damaged during 1993 earthquake, after Iai *et al.* (1994) as reported by PIANC (2001)

Port & location	Kushiro Port, Japan, East Quay, Kita Wharf
Type	Caisson quay wall
Height	+ 2.5 m
Water depth	- 8.5 m
Earthquake & Magnitude	January 15. 1993 Kushiro-Oki earthquake, M_s =7.8
Design seismic coefficient (Kh)	0.15
Peak ground surface acceleration (PGA)	0.47g, PGA evaluated based on strong motion earthquake records.
Horizontal displacement	1.9 m
Vertical displacement	0.2 to 0.5 m
Tilt	Not reported
Comments	Seaward displacement of caisson type quay wall constructed on firm foundation. Liquefaction of backfill.
Reference	Iai *et al.* (1994) as reported by PIANC (2001)

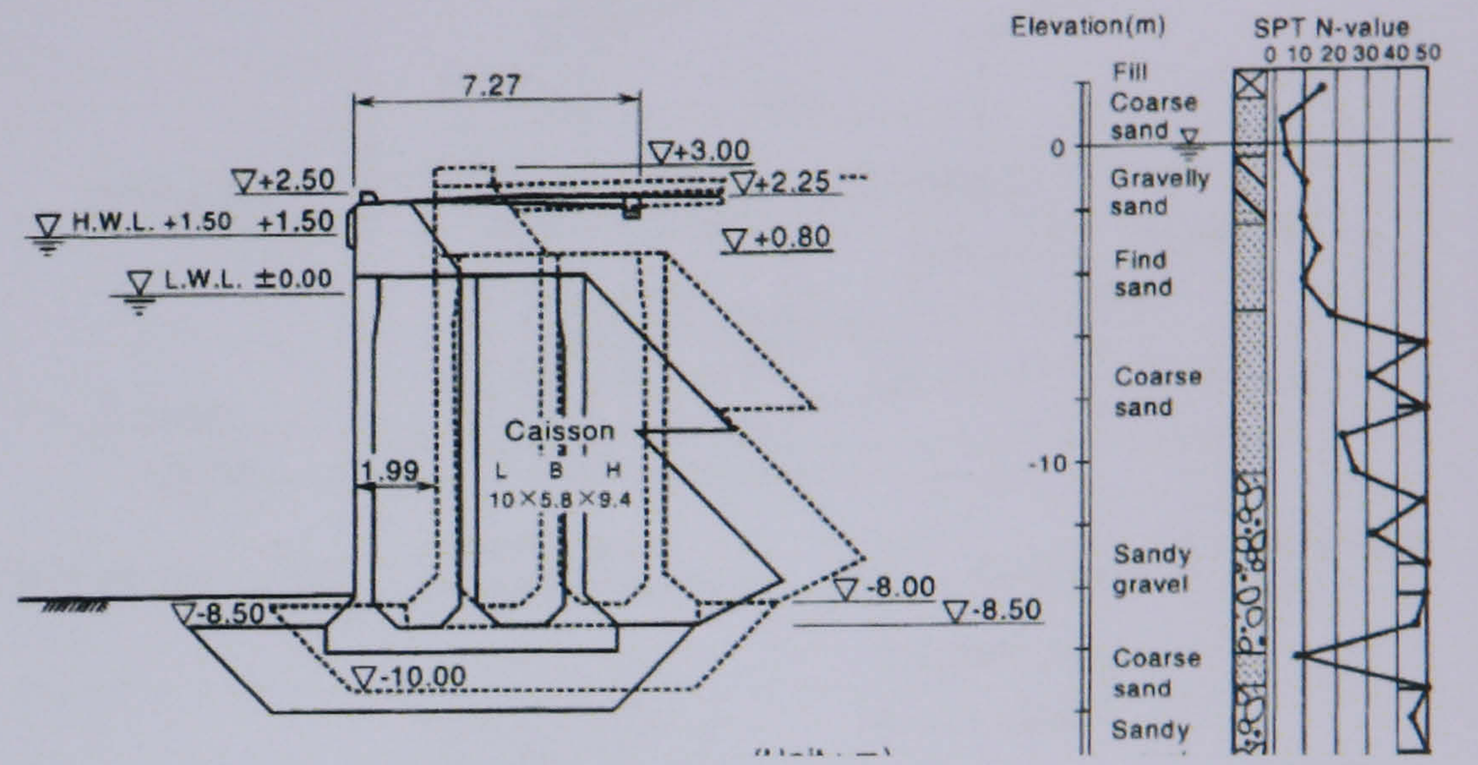

Table 2.9. Kobe quay wall damaged during 1995 earthquake, after Inagaki *et al.* (1996)

Port & location	Kobe Port, Japan, Rokko Island RC5
Type	Caisson quay wall
Height	+ 4.0 m
Water depth	- 14.0 m
Earthquake & Magnitude	January 17. 1995 Hyogoken-Nambu earthquake, M_s =7.2
Design seismic coefficient (Kh)	0.15
Peak ground surface acceleration (PGA)	0.53g, PGA evaluated based on strong motion earthquake records.
Horizontal displacement	4.2 to 5.2 m
Vertical displacement	1.5 to 2.2 m
Tilt	4 to 5 degree
Comments	Loose foundation soil below the wall induced significant seaward displacement and tilting, associated with the deformation in the foundation soil.
Reference	Inagaki *et al.* (1996)

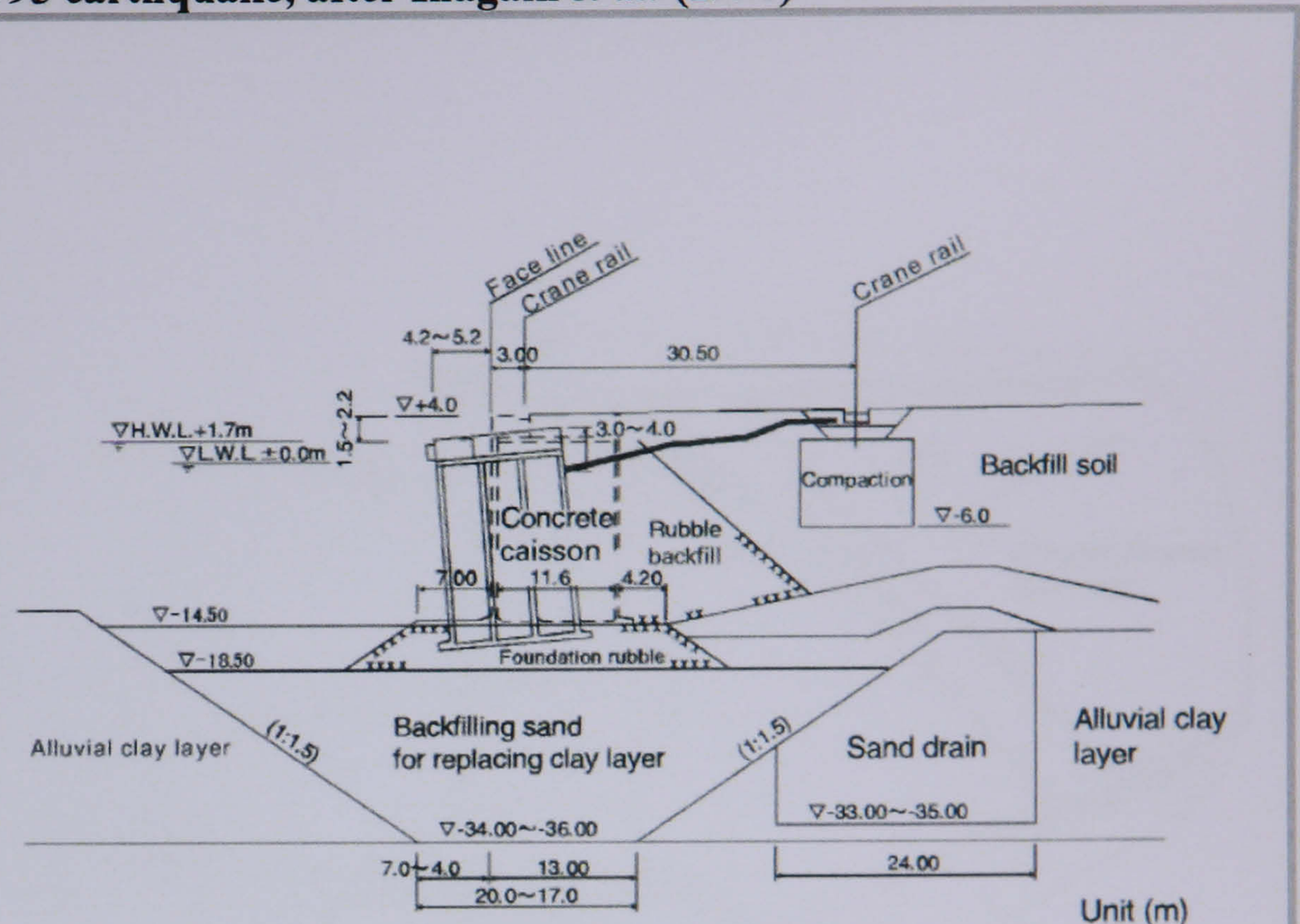

Table 2.10. Derince quay wall damaged during 1999 earthquake, after Sugano & Iai (1999) as reported by PIANC (2001)

Port & location	Derince Port, Turkey. No. 6 quay wall
Type	Block quay wall
Height	+ 2.25 m
Water depth	- 12.0 m
Earthquake & Magnitude	August 17. 1999 Kocaeli earthquake, M_w =7.4
Design seismic coefficient (Kh)	Not reported
Peak ground surface acceleration (PGA)	0.2 to 0.25g, PGA evaluated based on strong motion earthquake records.
Horizontal displacement	0.7 m
Vertical displacement	Not reported
Tilt	Not reported
Comments	Loose foundation soil below the wall induced significant seaward displacement and tilting, associated with the deformation in the foundation soil.
Reference	Sugano & Iai (1999) as reported by PIANC (2001)

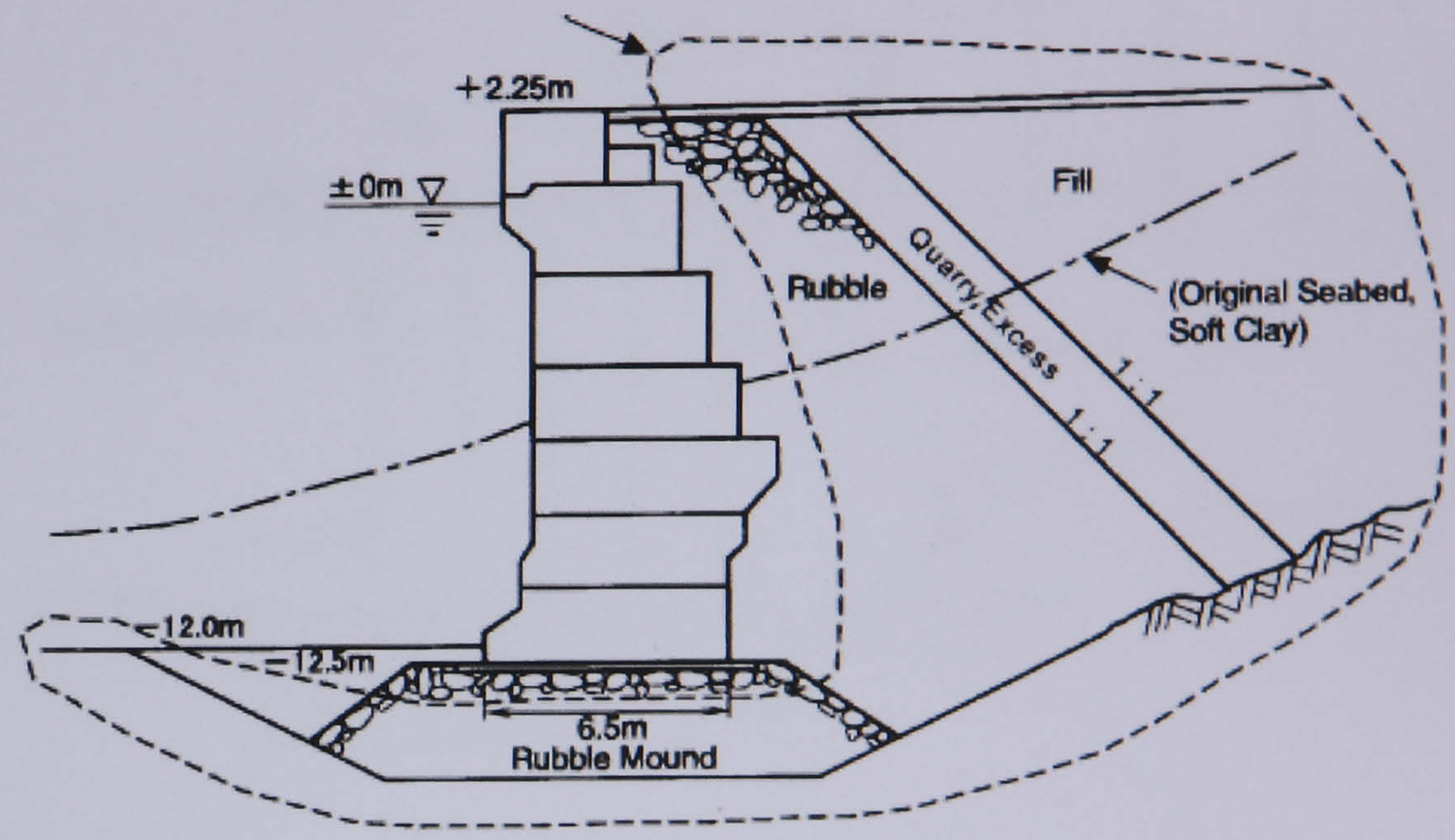

Table 2.11. Taichung quay wall damaged during 1999 earthquake, after Lee (2005)

Port & location	Taichung Port, Taiwan, No.1
Type	Caisson quay wall
Height	+ 6.2 m
Water depth	- 13.0 m
Earthquake & Magnitude	September 21, 1999 Ji-Ji earthquake, M_s =7.7
Design seismic coefficient (Kh)	0.15
Peak ground surface acceleration (PGA)	0.16g, PGA evaluated based on strong motion earthquake records.
Horizontal displacement	1.5 m
Vertical displacement	0.1 m
Tilt	Not reported
Comments	Displacement of caisson quay wall constructed on firm foundation. Liquefaction of backfill. Settlement at backfill was 1 m maximum.
Reference	Lee (2005)

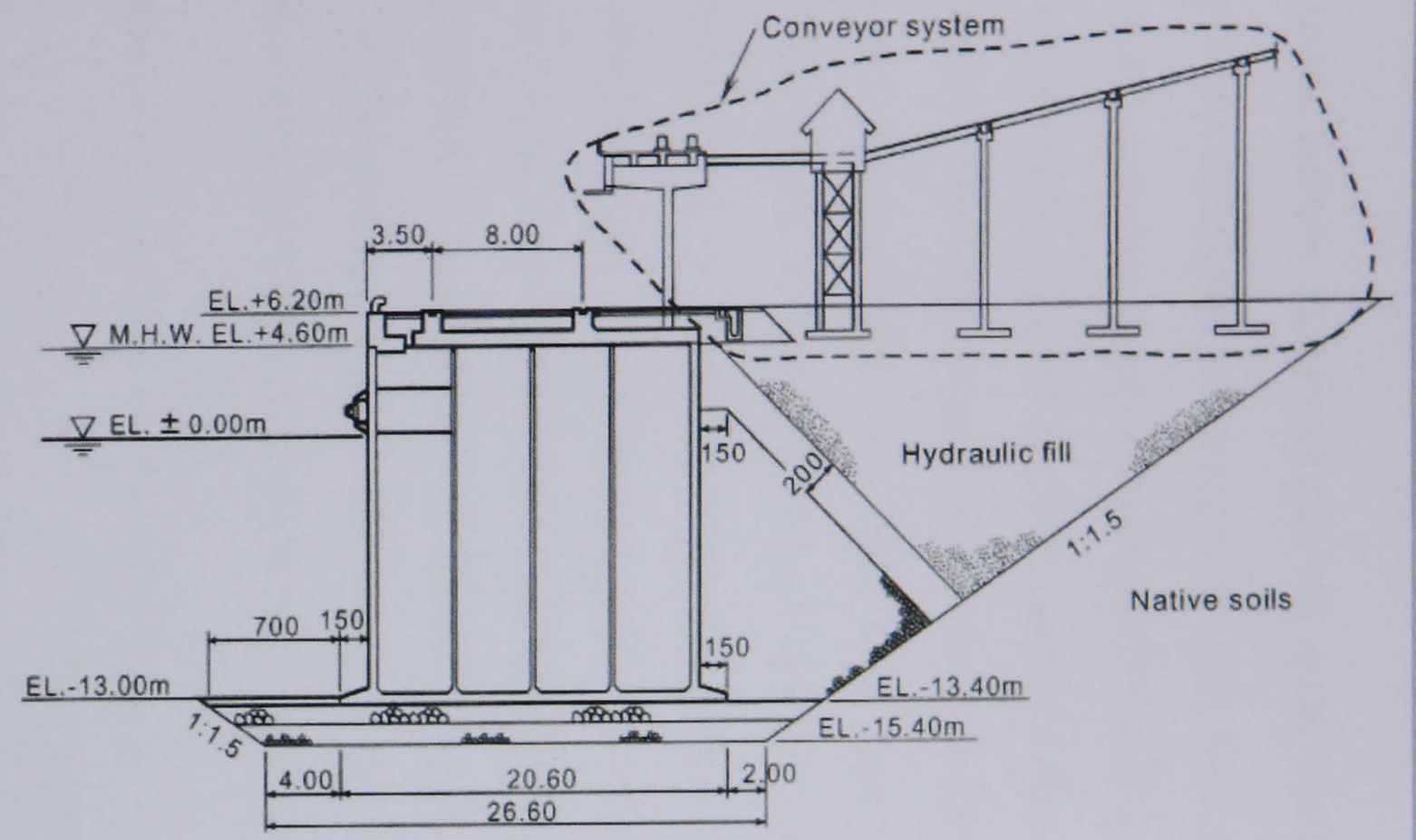

2.4.1 Earthquake failure modes of gravity quay walls

Gravity quay walls are made of concrete placed on a foundation. The stability of the wall against earth pressure applied by backfill soil is maintained by the wall's own weight and the resistance due to friction between the wall and the foundation. If the foundation beneath the wall is rigid, the failure modes after the shaking are seaward displacement and tilting of the quay wall. This type of failure has been observed in cases 8 and 9 as shown in Table 2.10 and Table 2.11, respectively. However, if the foundation is made out of loose material, the failure modes that result after shaking are seaward displacement and tilting, as well as settlement of the wall. These modes of failures have been observed for the remaining cases 1, 2, 3, 4, 5, 6 and 7 presented in Table 2.3 to Table 2.9, respectively. These types of damage depend on the strength and duration of the shaking and the efficiency of soil treatment behind the quay wall. Figure 2.9 illustrates the typical failure modes of gravity quay walls.

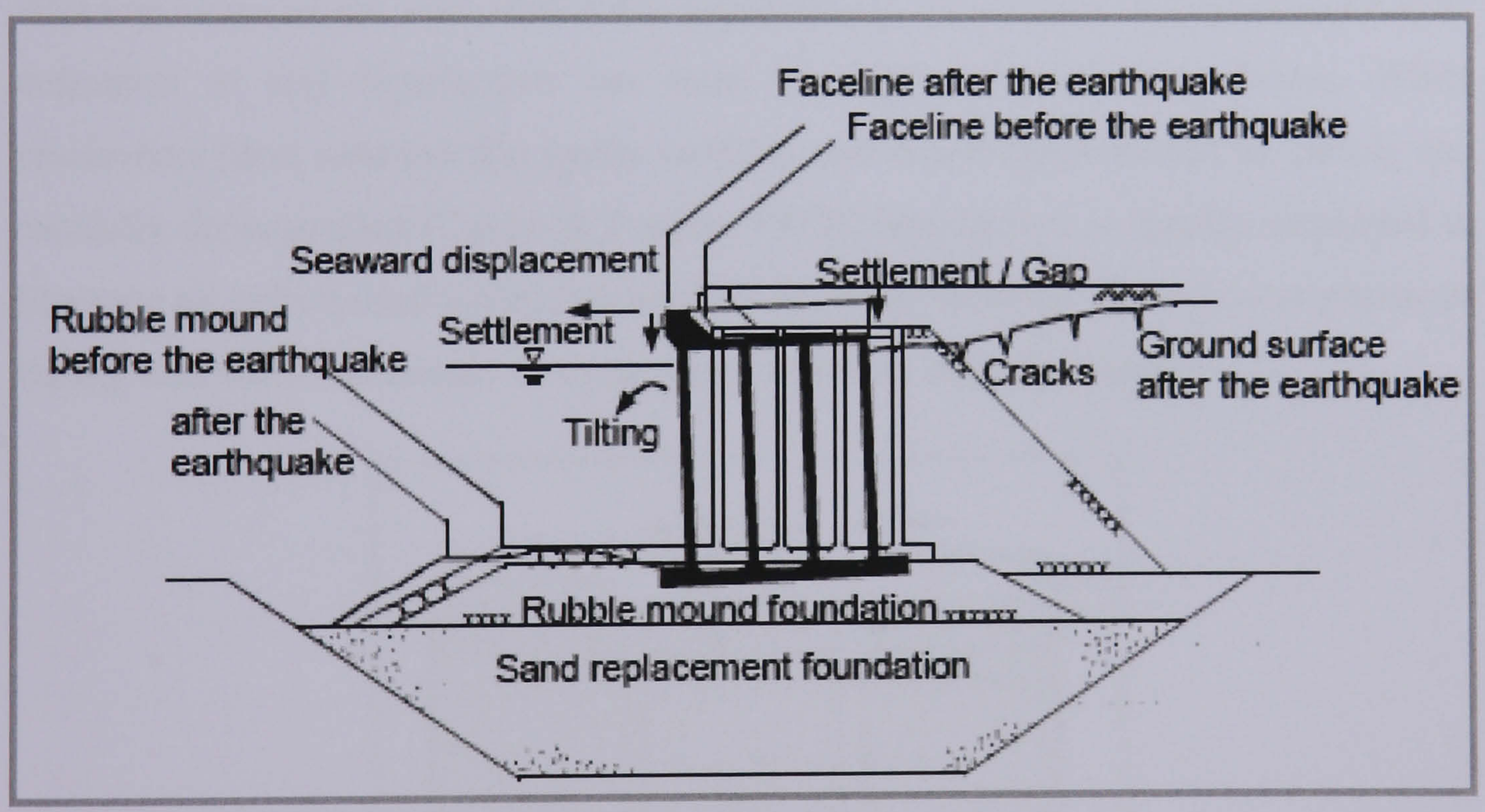

Figure 2.9. A typical failure mode of a caisson-type quay wall due to earthquake, after Ichii (2004)

The cases that have been presented through case histories suggest that the damage to gravity quay walls is often associated with significant deformation of liquefiable soil deposits. Therefore, better seismic performance can be obtained by using appropriate design methods such as performance-based designs and prevention measures against liquefaction.

2.5 The Liquefaction Phenomenon

During a shaking motion, a saturated soil's deposits are sheared rapidly back and forth, which results in a rise of pore water pressure. The strength and stiffness of loose saturated soils is temporarily lost completely due to this rise in pore water pressure, which causes the particles to float apart. This phenomenon is called soil liquefaction, and it is shown schematically in Figure 2.10. A more precise definition of soil liquefaction is given by Castro & Poulos (1977):

"liquefaction is a phenomenon wherein a saturated sand loses a large percentage of its shear resistance (due to monotonic or to cyclic loading) and flows in a manner resembling a liquid until the shear stresses acting on the mass is as low as its reduced shear resistance".

However, liquefaction can be defined in general as the transformation from a solid state to a liquid state as a result of increased pore water pressure and reduced effective stress of the soil. Within the geotechnical community, the appropriate brief definition of soil liquefaction has been the topic of continuing debate. While researchers have asserted that cyclic mobility and liquefaction should be clearly and carefully distinguished (Castro & Poulos, 1977), liquefaction is usually employed to illustrate all failure mechanisms consequent upon the build-up of pore water pressures during undrained monotonic or cyclic loads of loose, saturated sands.

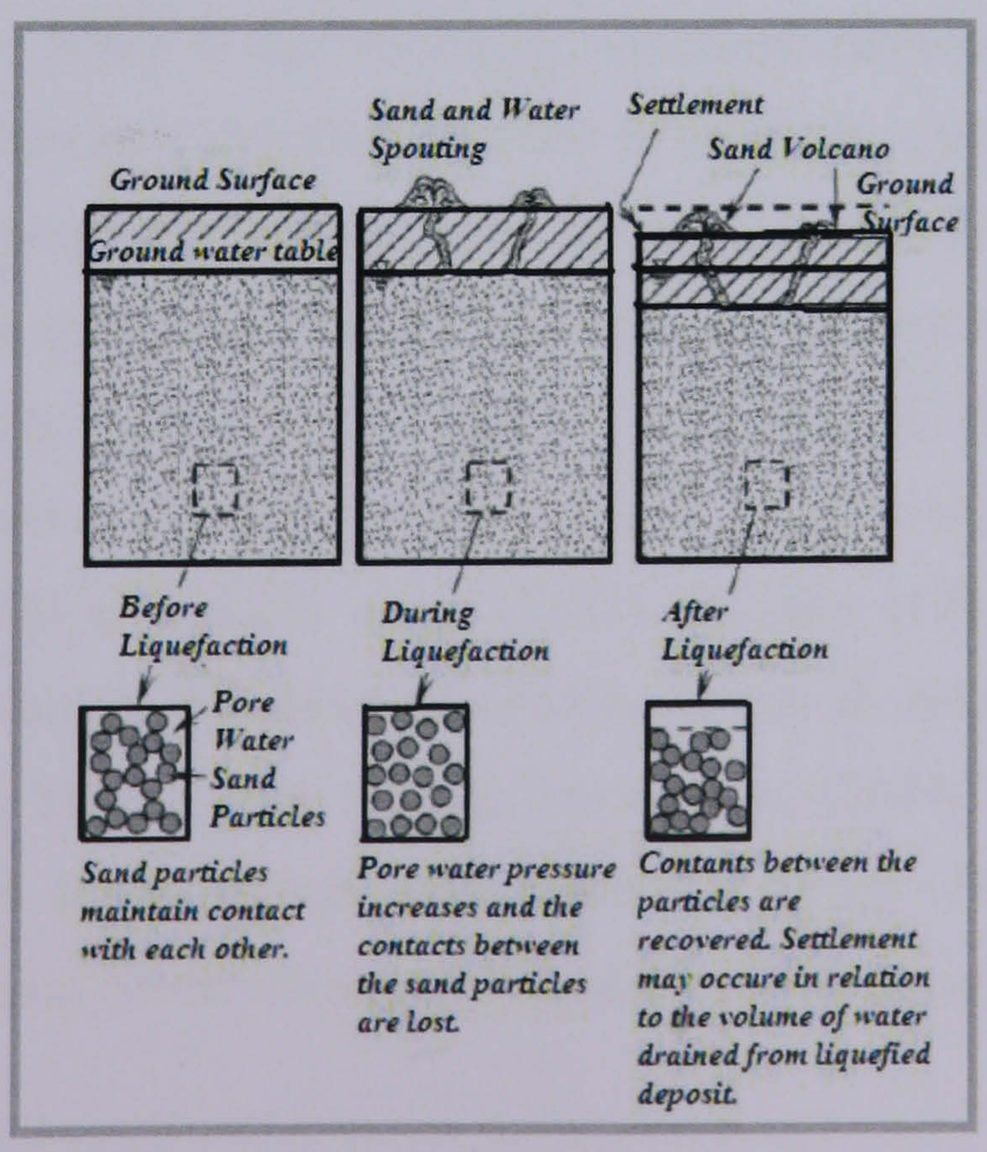

Figure 2.10. Illustration of liquefaction, after PIANC (2001)

Subjected to strong ground shaking in large-magnitude earthquakes, liquefaction is most commonly observed in shallow, loose and saturated soil deposits. However, it has been observed that liquefaction can even occur in unsaturated soil for which the compressibility, suction, degree of saturation and confining pressure play key roles (Yoshimi *et al.,* 1989; Sawada *et al.,* 2006; Okamura *et al.,* 2006). This aspect will not be addressed in the present study.

Liquefaction has been classified into two distinct definitions described by Castro (1975), Castro & Poulos (1977), Kramer (1996), and PIANC (2001), among others, as follows:

"Cyclic liquefaction" refers to the undrained flow of a saturated soil when the shear stress is greater than the shear strength of the soil in its liquefied state.

"*Cyclic mobility*" is used for the undrained flow of a saturated soil when the shear stress is less than the shear strength of liquefied soil.

These two definitions of liquefaction will be discussed in detail in the next sections.

2.5.1 Behaviour of saturated, cohesionless soils in undrained shear

Liquefaction susceptibility depends on the initial state of the soil. The tendency to generate excess pore pressure of a deposit soil is greatly influenced by both initial stress and density; the liquefaction susceptibility of the soil depends on its initial state (Kramer, 1996). In the laboratory, undrained monotonic and cyclic shear tests offer important insights into the behaviour of saturated, cohesionless soil during seismic shaking. Significant studies have been published on the behaviour of liquefiable soils and such tests and their descriptions are reported by Seed & Lee (1966), Castro (1969), Castro (1975), Ishihara *et al.* (1975), Martin *et al.* (1975), Poulos (1981), Poulos *et al.* (1985), Castro (1987), Alarcon-Guzman *et al.* (1988), Kramer & Seed (1988), Yoshimi *et al.* (1989), Ishihara (1993), Ishihara (1994), Robertson (1994), Vaid & Sivathayalan (2000), Xenaki & Athanasopoulos (2003), Huang *et al.* (2004), Yilmaz *et al.* (2004), Toyota *et al.* (2004), Ghionna & Porcino (2006), among others. In this section, a brief historical review of some basic concepts helpful in understanding cohesionless soil behaviour will be presented.

In the 1960s, Castro (1969) performed undrained, stress-controlled triaxial tests on anisotropically consolidated specimens. He observed three different types of stress:strain behaviour depending on the relative density of the specimen that are shown in Figure 2.11. The very loose specimens (A) collapsed at low shear strain levels and dropped dramatically to low effective confining pressures and large strain. Castro called this behaviour "liquefaction", which is now recognized as "Cyclic liquefaction". The undrained triaxial tests on medium dense sand (C) showed initially similar contractive behaviour as sample (A) then dilated at the "phase transformation point" (Ishihara *et al.*, 1975) until large strain strength was reached. This type of behaviour has been referred to by Castro as "limited liquefaction". For the dense sample (B), a contractive behaviour was initially observed followed directly by a dilation with an increasing effective confining pressure at large strain being reached.

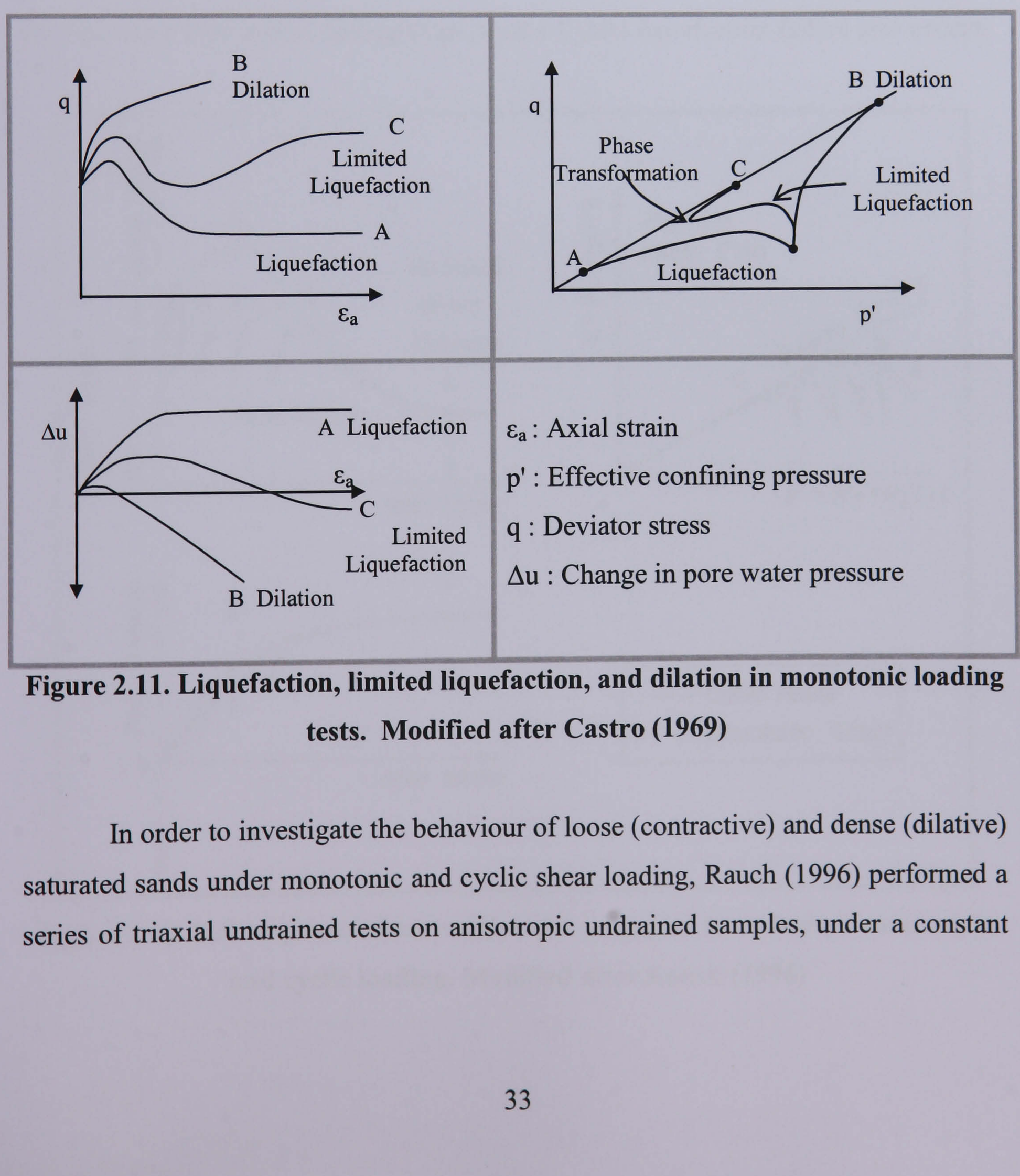

Figure 2.11. Liquefaction, limited liquefaction, and dilation in monotonic loading tests. Modified after Castro (1969)

In order to investigate the behaviour of loose (contractive) and dense (dilative) saturated sands under monotonic and cyclic shear loading, Rauch (1996) performed a series of triaxial undrained tests on anisotropic undrained samples, under a constant

initial effective confining pressure for loose and dense sands. The results are presented in Figure 2.12 and Figure 2.13.

Figure 2.12 shows when an undrained shearing starts from point A, the loose soil generates excess pore pressure to reach at point B. At the same point, the peak shear stress is reached during which the stress path moves to a higher value of deviator stress. Later with increasing strain, excess pore pressure increases dramatically and the shear strength softens rapidly to point C where the specimen is in the steady state deformation or the residual strength resistance. If the static driving shear required for equilibrium at point B were greater than the static shear at point C then a liquefaction flow failure takes place. From the figure it can also be observed that when specimens are sheared cyclically, the effective stress path moves to the left and excess pore pressure accumulates. If the shear strength falls below the static driving stress after cyclic loading stops, then a Cyclic liquefaction failure also occurs.

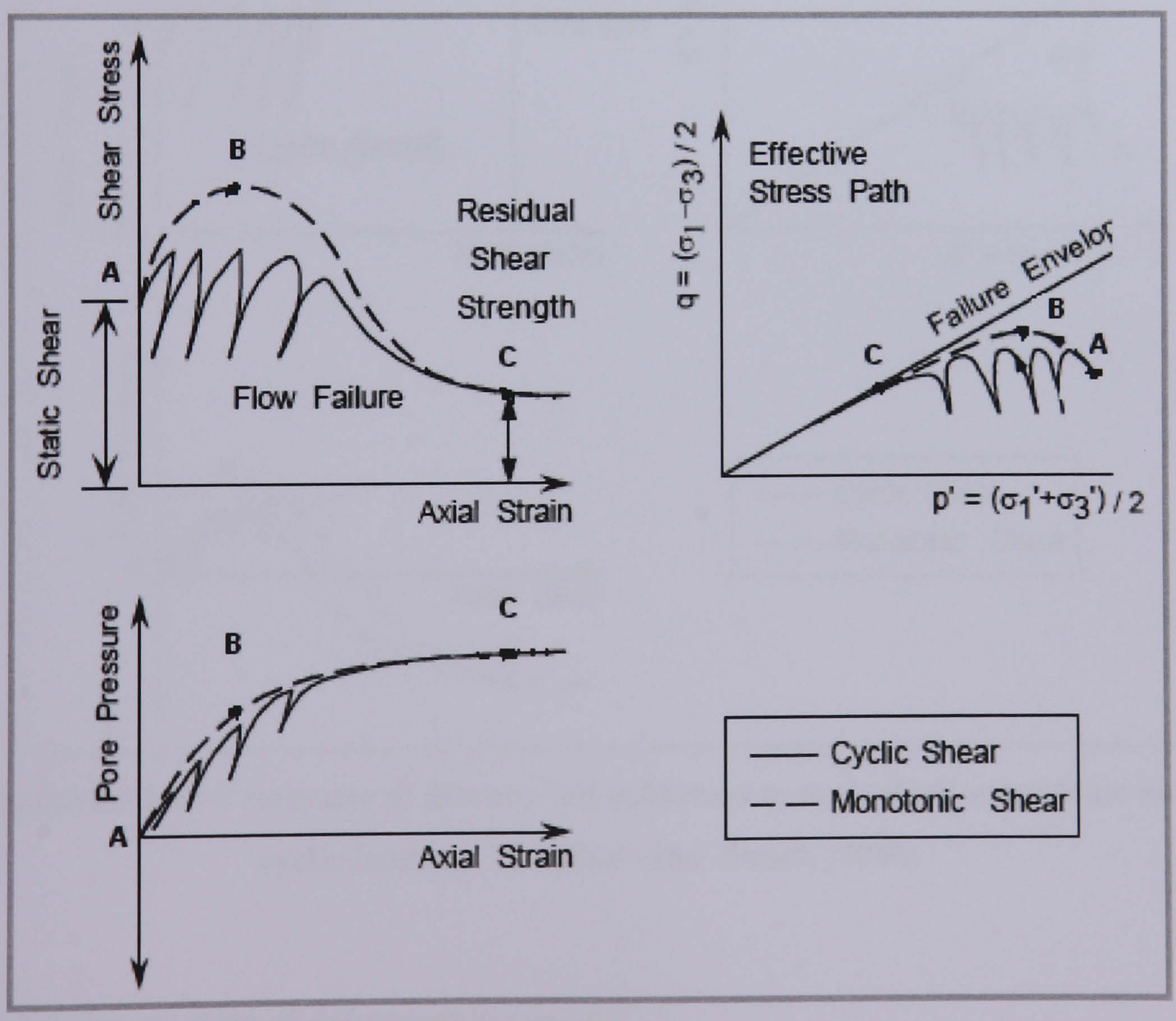

Figure 2.12. Soil response of contractive soil subjected to undrained monotonic and cyclic loading. Modified after Rauch (1996)

In Figure 2.13 it can be observed that dense sand also generates some excess pore pressure at small strains at point B. After applying large strain, the pore pressure decreases, in some cases it can become less than zero, which leads to increased shear resistance and effective stress. If the same soil is sheared cyclically, as illustrated in the figure, excess pore water pressures are generated in each cycle of load resulting in an accumulation of excess pore water pressures and deformation. The upper right graph in Figure 2.13 shows that the effective stress path moves to the left but does not reach the failure level. Consequently, a cyclic liquefaction failure will not occur because the shear strength remains greater than the static driving shear stress in both cases, monotonic and cyclic shear loading, under undrained conditions.

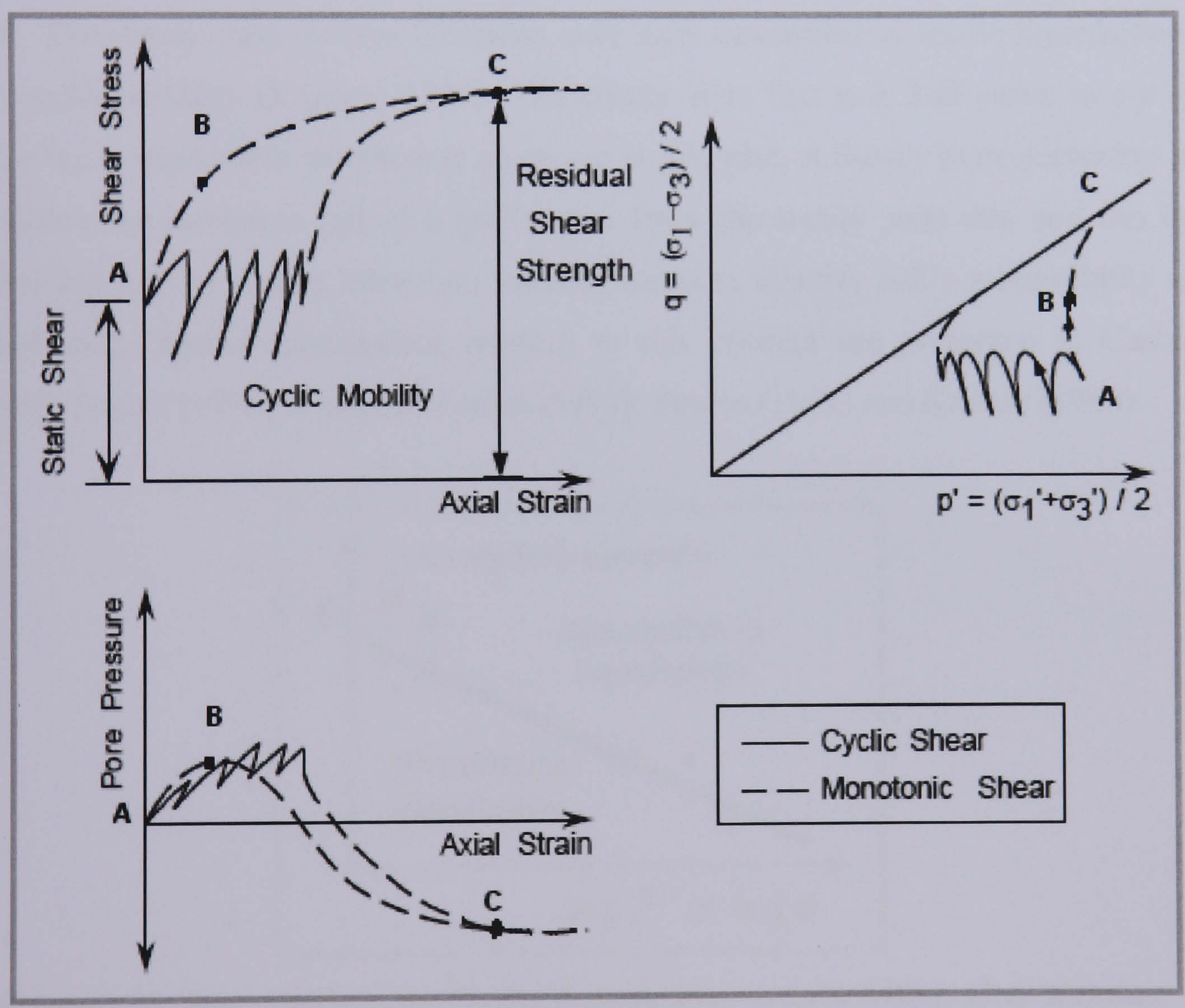

Figure 2.13. Soil response of dilative soil subjected to undrained monotonic and cyclic loading. Modified after Rauch (1996)

2.5.1.1 Steady state of deformation concept

Castro (1969) plotted an exclusive relationship between effective confining pressure and void ratio at high strain as shown in Figure 2.14. This curve was referred

to as "the steady state line (SSL)", which can be used for identifying the susceptibility of soil to liquefy. This relationship has also been studied by Castro (1969), Poulos (1971), Castro & Poulos (1977) and Poulos (1981). The steady state of deformation can be defined as that state in which the mass is continuously deforming at constant volume, effective shear stress and velocity. This state occurs during tests carried out on fully saturated, loose sands after liquefaction has been achieved

The steady state of deformation is a useful concept since it marks the boundary between those soils that are susceptible to cyclic liquefaction from those that are resistant to cyclic liquefaction. Points that plot above the steady state line will be susceptible to liquefaction, but only if the static shear stress exceeds its steady state. The steady state concept identifies only soils susceptible to cyclic liquefaction, not cyclic mobility (Kramer, 1996). The steady state line is a 3-D curve in *e-p'-q* space but is more often represented on an *e-q* or *p'-q* plot. A Steady State parameter is a relative measurement (ψ) of a soil's state from the steady state line and can be correlated with *in situ* or laboratory measurements to identify soil's susceptibility to liquefaction. Further discussions relating to this concept are presented in Castro (1969), Poulos (1971), Castro & Poulos (1977), Poulos (1981) and Kramer (1996).

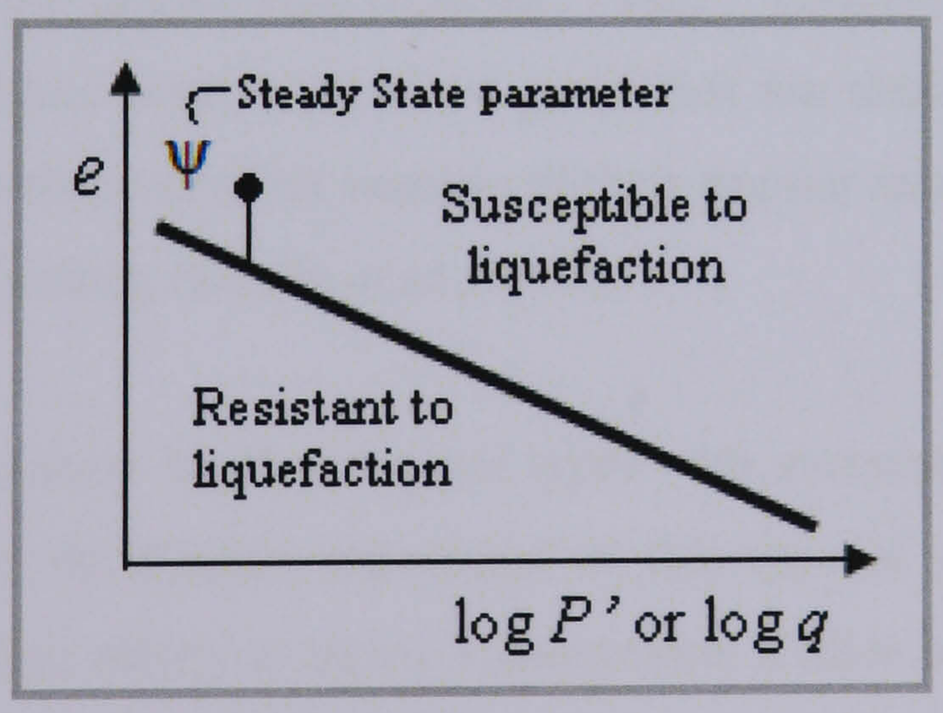

Figure 2.14. State criteria for Cyclic liquefaction susceptibility, after Kramer (1996)

2.5.2 Factors with Significant Effects on Liquefaction Potential

The liquefaction potential of a soil deposit during an earthquake depends on different significant factors that can be classified into three main groups: the characteristics of the soil, the characteristics of the earthquake and the initial stresses acting on the soil (Seed & Idriss, 1971).

2.5.2.1 Characteristics of the soil

The characteristics of soil grains include, among others, shape, distribution of size, and composition; these characteristics influence the susceptibly of the soil to liquefy (Seed & Idriss, 1971) . While liquefaction is commonly associated with silts or sands, gravely soils can also be susceptible to liquefaction (Kramer, 1996) . Poulos *et al.* (1985) reported that rounded soil particles of uniform size are generally the most susceptible to liquefaction because, in soil with many different particle sizes, the smaller particles are liable to fill the voids between the larger particles. This reduces the tendency to increase the pore water pressure during shaking. On the other hand, the particle shape is a significant factor in liquefaction susceptibility. For instance, soil deposits with angular grain shapes generally have a lower susceptibility to liquefaction than poorly graded sand (Kramer, 1996) . However, the crushable soils, when sheared in a dense state, have stress paths that are similar to those for loose sands of a less crushable nature, but because of their angular nature, they do not easily liquefy under cyclic loading (Hyodo *et al.*, 1998).

During cyclic shear loading the soil types with measurable plasticity such as clays are resistant to the relative movement as this type of soil creates sufficient cohesion to restrict their ability to move. Furthermore, studies by Ishihara (1985) and Ishihara (1993) have shown that liquefaction resistance is dependent on the nature of fines. If the mineral composition of the fines has a dry surface texture, they will not exhibit adhesion and are more susceptible to liquefaction. Therefore the most important index property to influence the cyclic strength of a soil has been found to be the Plasticity Index. This parameter is a more useful property to quantify liquefaction in a soil containing fines than relative density when the fines content is greater than

50% (Ishihara, 1993). Wang (1979) lists four indices properties that, if satisfied by a fine grained soil, make it susceptible to the effects of liquefaction:

Fraction finer than 5μm < 15%

Liquid limit, w_L < 35%

Natural water content > $0.9w_L$

Liquidity Index, I_L < 0.75%

Permeability is considered to be an important factor, which can affect the liquefaction characteristics of a soil deposit. Low permeability restricts the pore water movement, which leads to accumulation of pore water pressure. For quay wall structures constructed on liquefying permeable soil, the dissipation of water pressure happens faster than the generation of the dynamically induced pore pressure. This can prevent the soil from liquefying (PIANC, 2001). In addition, Yang *et al.* (2001) conducted computational parametric studies by varying soil permeability for centrifuge models of a quay wall to investigate the spatial extent of liquefaction in the backfill material. It concluded that permeability has a major effect on seismic performance of the quay wall system and for non cohesive materials increasing the permeability can significantly improve the overall system behaviour. The reason for this is that the pore pressure can dissipate in more permeable non cohesive soils.

2.5.2.2 Characteristics of the Earthquake

The characteristics of the earthquake include intensity and duration of ground shaking and have an important effect on liquefaction potential. For example, for a soil under a given confining pressure, the susceptibility to liquefaction during strong ground motion depends on the stress and/or strain induced by the earthquake. The duration of ground shaking is another significant factor in determining liquefaction potential due to the number of stress and/or strain cycles to which a soil is subjected (Seed & Idriss, 1971).

2.5.2.3 Initial stresses acting on the soil

The initial stresses acting on the soil also play an important role in determining the liquefaction resistance of a soil. For example, deposits with an initial static shear stress are usually more resistant to pore pressure generation (Seed, 1979) . Equally, the liquefaction potential of a soil is reduced by an increase in confining pressure. For this reason, soil deposits deeper than 9 ft (2.74 m) during the Niigata earthquake remained stable but similar soils surrounding the fill liquefied extensively (Seed & Idriss, 1967).

2.6 Cyclic Behaviour of soils

PIANC (2001) demonstrates that the complex time history of shear stress, $\tau_{(t)}$, is a key in understanding the effects of earthquake loads on a soil. The shear strain level induced in the soil can vary depending on the level of earthquake motion considered for design. The soil behaviour may be broadly categorised into pre-failure and failure conditions, depending on the strain level. Also the soil behaviour may be characterised with increasing levels of complexity, which will depend on a variety of material parameters and state variables.

2.6.1 Soil behaviour in pre-failure condition

For small and reasonable earthquake motions, the level of shear strain, γ, is usually less than 1% over which the soil exhibits non-linear behaviour. This is typically specified by two parameters which are: equivalent shear modulus, *G,* and equivalent damping ratio, *D* (Richart *et al.,* 1970). These parameters define the characteristics of a shear stress:strain loop as shown in Figure 2.15. When the cyclic strain amplitude, γ, is increased, the equivalent parameters, *G* and *D*, will change as shown in Figure 2.16. The pre-failure soil behaviour is described with respect to three strain levels; small strain, medium strain, and large strain.

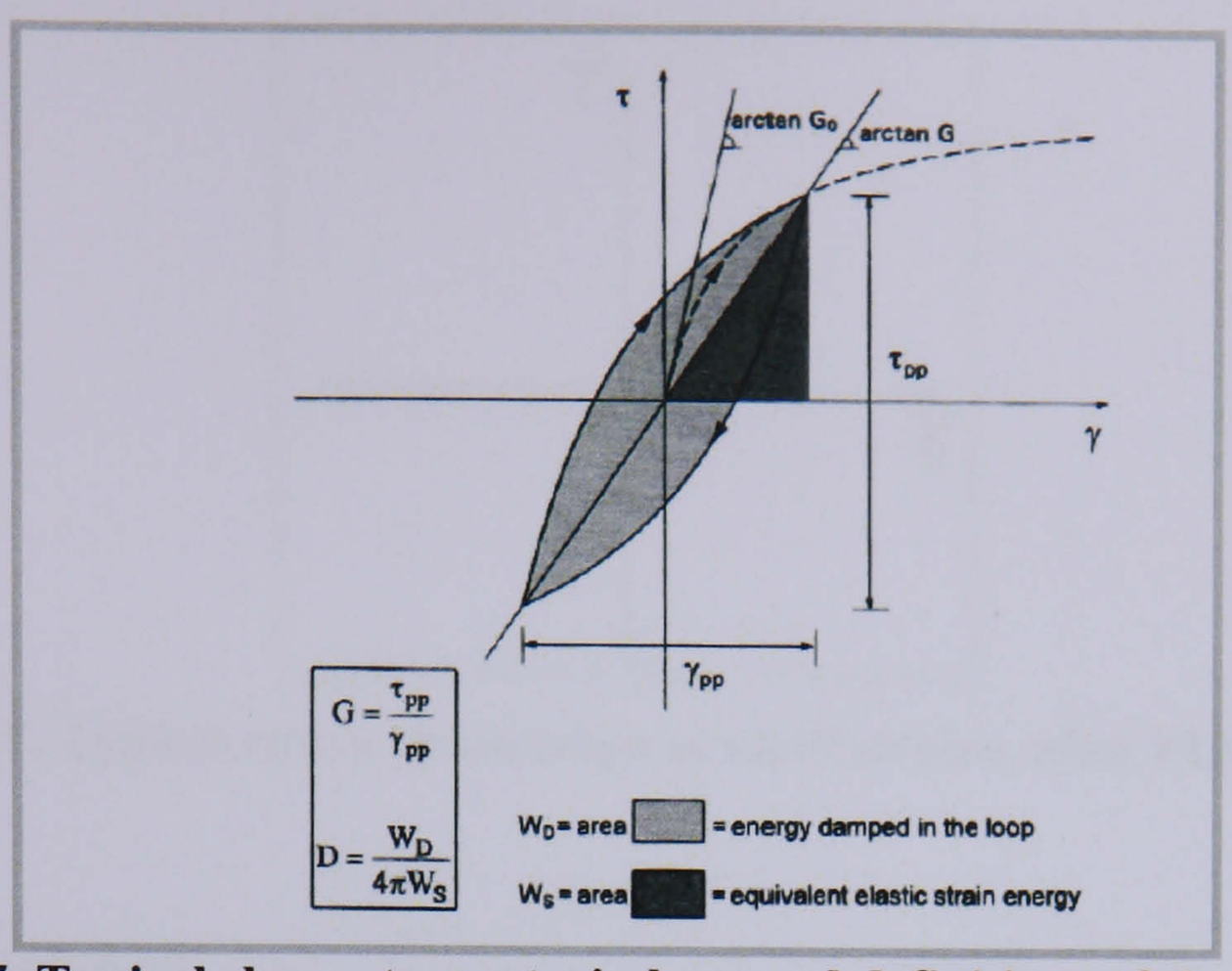

Figure 2.15. Typical shear stress:strain loop and definitions of the equivalent parameters *G* and *D*, after PIANC (2001)

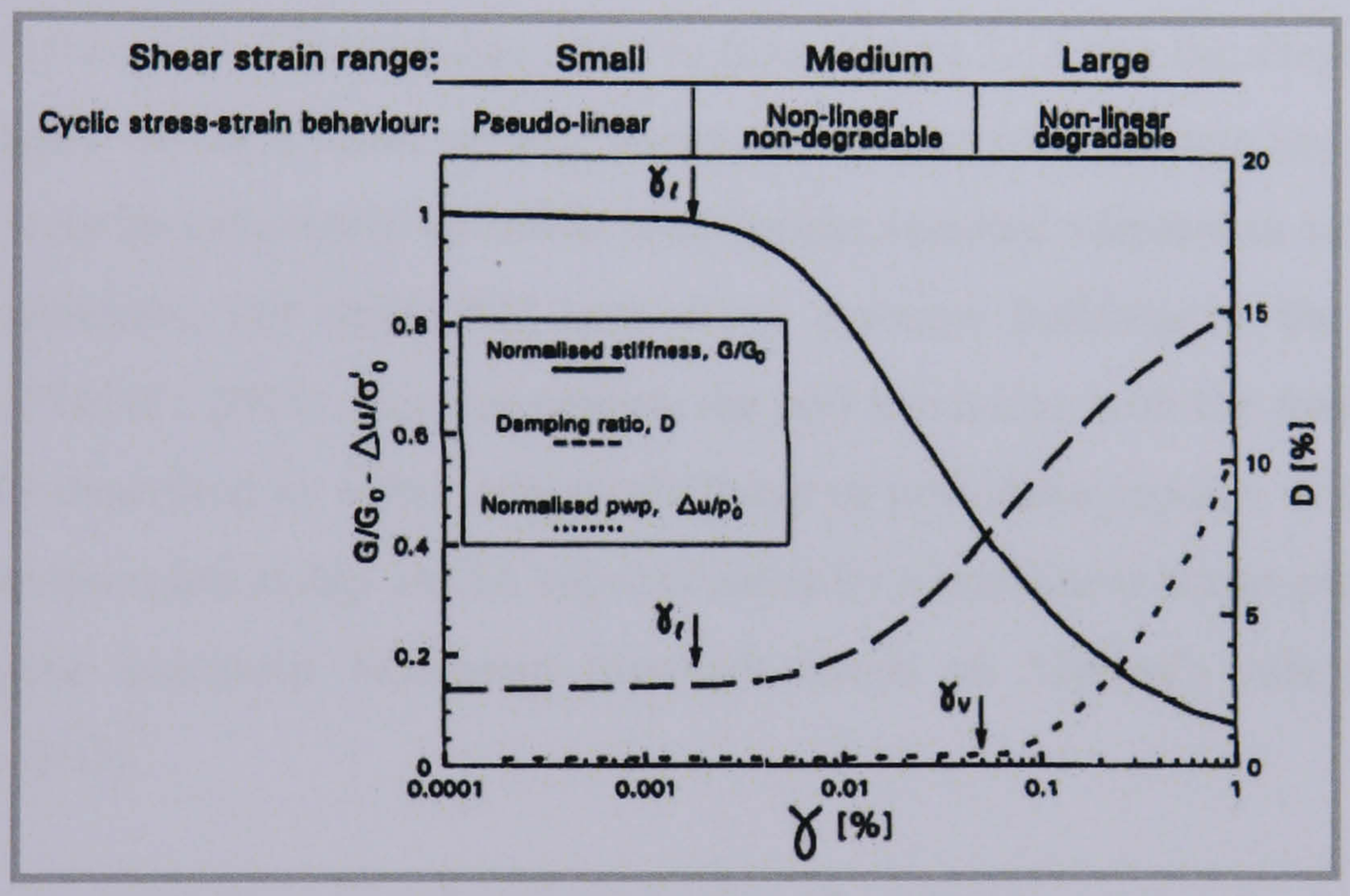

Figure 2.16. Variation of the equivalent shear modulus (*G*) and damping ratio (*D*) with the cyclic shear amplitude, after PIANC (2001)

2.6.1.1 Small strain

It can be seen in Figure 2.16 that the shear modulus, *G,* of a soil initially takes a maximum value (G_0 or G). On the other hand, the equivalent damping ratio, *D*, takes a minimum constant value, D_0, in same strain range. The stress:strain relationship (τ-γ) within this range is practically linear as shown in Figure 2.17. Therefore, the stress:strain relationship can be approximated by a linear model (PIANC, 2001).

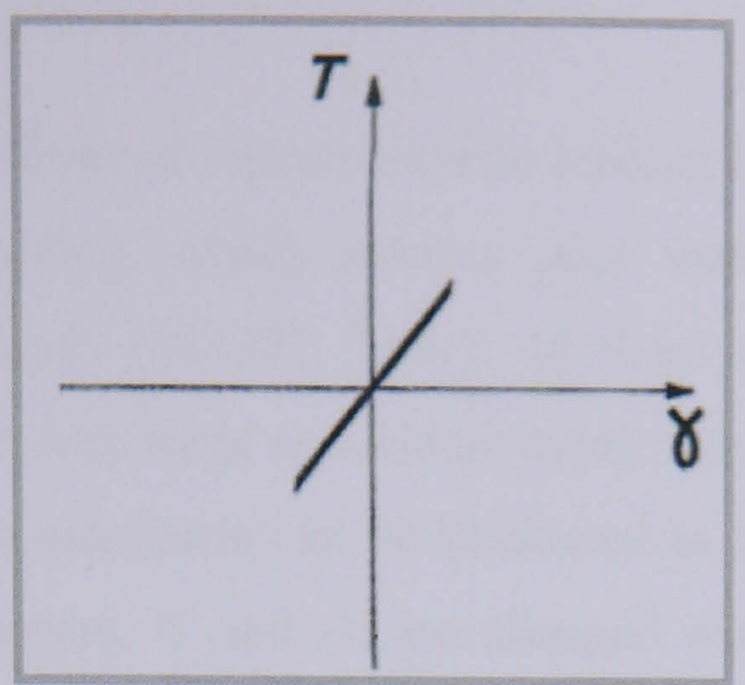

Figure 2.17. Typical stress-strain loops at small strains, after PIANC (2001)

2.6.1.2 Medium strain

Within this range of strain, it can be noted that the equivalent shear modulus, *G*, decreases and the equivalent damping ratio, *D*, increases with increasing γ as shown in Figure 2.16. One can also observe from Figure 2.18 that the shape of the τ-γ loops changes, taking a more spindle shape. Moreover, in this stage the cyclic soil behaviour may be considered as stable with neither residual volumetric strains, ε_v, in drained conditions, nor noticeable pore water pressure build-up in the undrained condition (PIANC, 2001). For this reason, the soil behaviour with the medium strain level can be described by either equivalent linear or non-linear models. Alternatively, the stress:strain relationship can be approximated by a non-linear elasto-plastic model with adequate kinematic hardening functions based on Masing's rule (Hardin & Drnevich, 1972) .

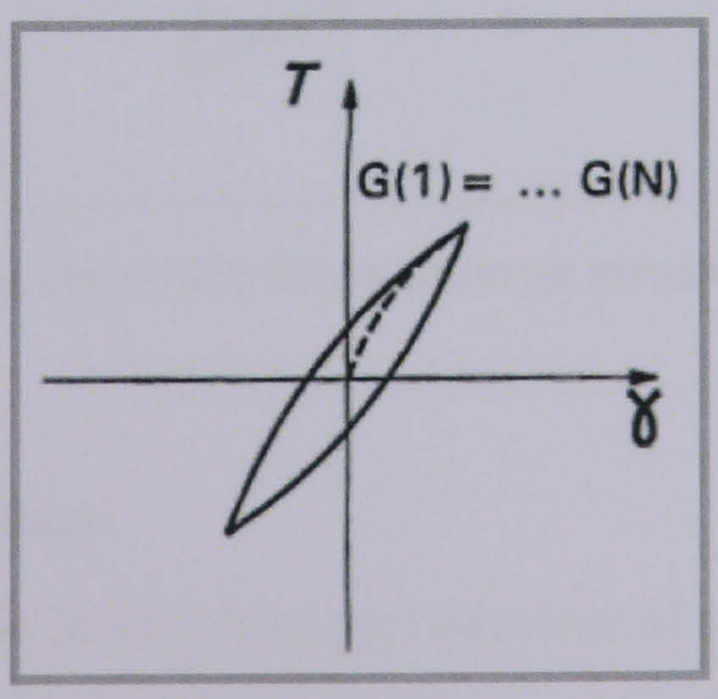

Figure 2.18. Typical stress-strain loops at medium strains, after PIANC (2001)

2.6.1.3 Large strain

At this level the effects of repeated cyclic loading become clear and indicate the shear-volumetric coupling, which induces pore water pressure build-up for undrained cyclic shear loads (PIANC, 2001). In these conditions, a progressive increase in the shear strain amplitude at constant cyclic stress or, equally, a reduction in stress at constant strain amplitude can be illustrated as in Figure 2.19. Therefore, the equivalent soil parameters, G and D, are changed with the number of loading cycles. These changes may be defined by cyclic degradation indexes (δ_G , δ_D):

$$\delta_G = \frac{G(N)}{G(1)} \tag{2-10}$$

$$\delta_D = \frac{D(N)}{D(1)} \tag{2.11}$$

In this stage, constitutive models based on an effective stress approach accounting for shear-volumetric coupling, failure coupling and cyclic degradation may be required (Sagaseta *et al.*, 1991).

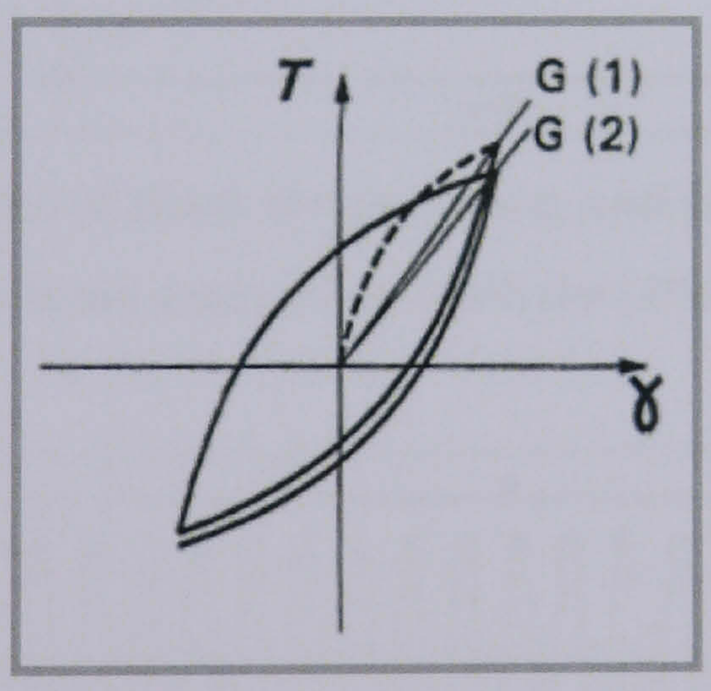

Figure 2.19. Typical stress-strain loops at large strains, after PIANC (2001)

2.6.2 Soil behaviour at failure

After the large strain level, where the behaviour of soil is invariably associated with marked cyclic degradation effects leading to significant irrecoverable strains and/or excess pore water pressure, a significant loss of shear strength of the soil may then occur, resulting in significant damage to geotechnical structures.

The major reason for the failure of saturated soil under large strain is the progressive pore pressure increase. This build-up takes place in all granular soils, either in dense or loose states, with different patterns of behaviour for each state. In loose sand, the pore water pressure becomes equal to the initial effective stress, that is $u = \sigma'_{v0}$. This state is illustrated in Figure 2.20 and this phenomenon is commonly called liquefaction. In contrast, dense sand behaves in a more stable fashion and retains its resistance. This type of behaviour is shown in Figure 2.21, and is referred to as cyclic mobility, which was discussed in Section 2.5 (see Castro (1975), Castro & Poulos (1977), Kramer (1996), PIANC (2001) , among others).

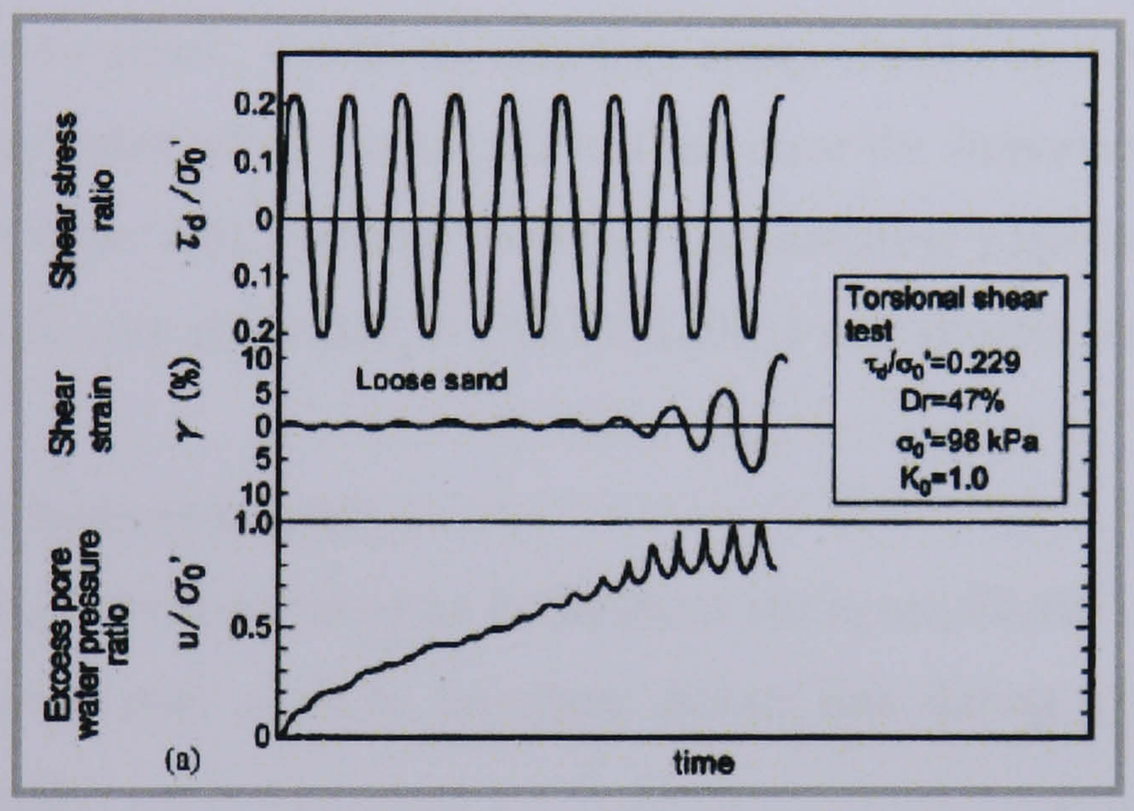

Figure 2.20. Time histories of shear stress, strain, and pore water pressure ratio for loose sand, after Ishihara (1985)

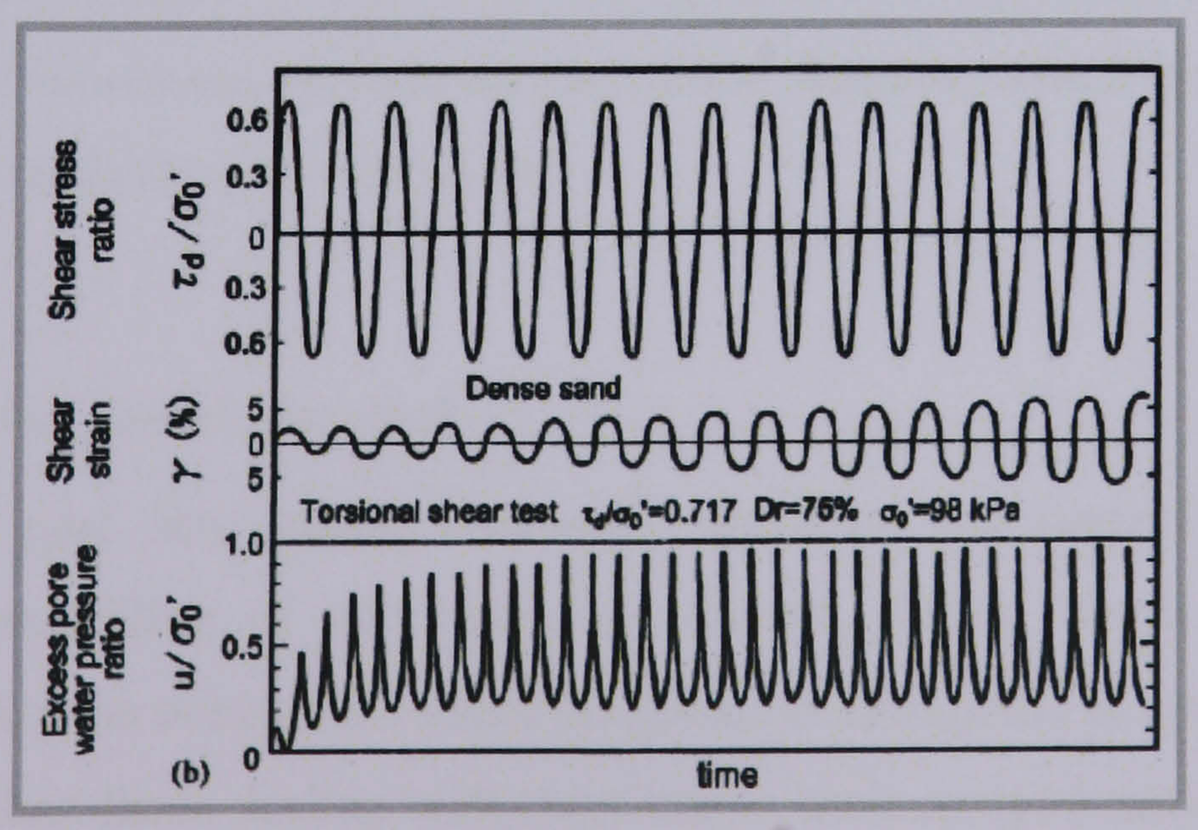

Figure 2.21. Time histories of shear stress, strain, and pore water pressure ratio for dense sand, after Ishihara (1985)

2.7 Soil constitutive models

The finite element method is considered as one of the most advanced methods for seismic performance evaluation. This method has been discussed in detail in textbooks, e.g. Zienkiewicz *et al.* (2005). This method will be briefly described in Chapter 3. In order to apply this numerical method to any geotechnical structure such as gravity quay wall system, it is necessary to model the behaviour of backfill as well as foundation materials. Thus, many constitutive models have been developed to describe the behaviour of such material.

2.7.1 The essential requirements for a constitutive model

A useful elasto-plastic model of effective stress should be simple, numerically robust enough and adequately developed to reproduce the important features of soil behaviour under static and dynamic loading. The essential requirements for such a constitutive model were presented in PIANC (2001) and should, ideally, include the ability to:

1- Reproduce the hysteresis loops.

2- Reproduce the progressive increase in the shear strain amplitude.

3- Follow the stress path close to the shear failure line during cyclic loading of a dense saturated soil.

4- Analyse the cyclic behaviour of anisotropic soils.

To model complex problems involving liquefaction phenomenon, the adopted constitutive model should include all the above features, which enable non-linear effective stress analysis to be carried out.

2.7.2 Constitutive models for sand

In the past few years, increasing attention has been focused on the mathematical modelling of soil behaviour (Wood, 2004). These models, which attempt to predict the behaviour of sand subjected to monotonic or cyclic loading, are less advanced than those dealing with clays due to their complex nature. Schofield & Worth (1968) proposed the 'Critical State Cam-Clay' model. This model is capable of describing the behaviour of soil subjected to monotonic loading under drained and

undrained consolidated conditions. However, the Cam-Clay model is not able to describe cyclic soil behaviour due to the inherent assumption that of the behaviour within the yield surface is purely elastic.

The demand to understand the behaviour of soil subjected to cyclic loading has stimulated progress in the development of the elasto-plastic theory. Martin *et al.* (1975) proposed a model for excess pore water pressure build-up based on the incremental volumetric strain in the drained condition between the shear work and the excess pore water pressure. This approach was referred to as the 'densification law' and was extended later within the framework of 'endochronic theory' by Cuellar *et al.* (1977) and Zienkiewicz *et al.* (1978). Another approach based on 'multi-surface kinematic-hardening' was proposed by Mroz (1967), where a set of loading surfaces within an outer boundary surface was postulated. This approach was improved later by Prevost (1977) and Mroz *et al.* (1981) by considering an unlimited number of nested loading surfaces. This results in the hardening modulus being functions of the ratio of the sizes of loading surfaces. The hardening modulii can still be determined in the situation where the variation of only two surfaces (inner and outer) is considered. This type of model was formulated by Krieg (1975) and Dafalias & Herrmann (1982) and later was known as 'Bounding Surface Theory'. Similar constitutive models have been proposed by Ghaboussi & Momer (1982) and Hirai (1987) and are also able to model liquefaction and other cyclic loading phenomena.

Zienkiewicz *et al.* (1985) proposed a simple model for transient soil loading in earthquake analysis, referred to as Mark I, which gives a reasonable prediction of pore pressure changes occurring during cyclic loading. Pastor *et al.* (1985) extended the bounding surface plasticity, Mark I, to reproduce the behaviour of sand under both static and transient loading, referred to as Mark II. This model was further developed by Pastor & Zienkiewicz (1986) to also capture important features of soil behaviour under cyclic loading, such as the progressive decrease in the stiffness of soil with increasing pore pressure, accumulation of deformation, stress-dilatancy and hysteretic loops in a hierarchical manner. This model was called P-Z Mark III.

Finally, Pastor *et al.* (1990) outlined the theory of *generalised plasticity* in which the yield surface and plastic potential need not be explicitly defined, and

showed how a very effective general model describing the behaviour of sand under monotonic or transient loading can be developed. This model is currently one of the simplest and yet one of the most effective in describing a full range of constitutive behaviour of soil under cyclic loading. In addition, this model satisfies all the essential requirements reported by PIANC (2001) that are given in Section 2.7.1. This model is being used either in its initial form or with slight modifications by many researchers involved in earthquake geotechnical engineering (Chan (1988); Madabhushi & Zeng (1998); Jeyatharan (1991); Liu & Ling (2002); Feng *et al.* (2003); Dakoulas & Gazetas (2005); among others.

In the present work, the constitutive model for sand developed by Pastor *et al.* (1990) is adopted, after minor modifications, which will be described in Chapter 3.

2.8 Summary

The previous studies on seismic behaviour of gravity quay walls were reviewed and the validity of simplified methods was examined. The results showed that that there is a limitation for the applicability of these practical methods of design based on the pseudo-static approach.

In addition, nine case histories of damage to port structures made of gravity retaining walls that were well-documented during the period 1964–1999 have been presented. These case histories suggest that the damage to gravity quay walls is often associated with significant deformation of liquefiable soil deposits. Therefore, better seismic performance can be attained by using appropriate design methods such as performance-based design. These approaches require accurate modelling of seismic behaviour of soil and therefore more sophisticated models that can simulate liquefaction must be adopted.

The liquefaction phenomena and the procedure to determine the soil properties relevant to liquefaction potential were reviewed. The available constitutive soil models, which are able to describe the soil behaviour under earthquake loading, were also reviewed. The P-Z sand model was considered to be the most suitable for use within this study because it satisfies all the essential requirements for a

constitutive model and is therefore most suitable for a performance based design method. In the next chapter, this model will be validated, by comparing the results of finite element analysis, to published monotonic and cyclic triaxial tests.

CHAPTER THREE

3. DEVELOPMENT OF CONSTITUTIVE AND NUMERICAL MODELS FOR GRAVITY QUAY WALLS

3.1 Introduction

In the period from 1964 to 2003, a number of well-documented case histories of damage to port structures made of gravity retaining quay walls show that the damage is often associated with significant deformation of liquefiable soil deposits. Such gravity quay wall failures have stimulated progress in the development of a performance-based design method using non-linear dynamic analysis for waterfront structures. Significant experimental and theoretical research work has been carried out on the subject (Dakoulas & Gazetas (2005); Iai (1998); Iai *et al.* (1998); Iai & Sugano (2000); Ichii *et al.* (2000); Inagaki *et al.* (1996); Inoue *et al.* (2003); Nozu *et al.* (2004); Sugano *et al.* (1996); Madabhushi & Zeng (1998), among others).

On the modelling side, many advanced constitutive models have been formulated to describe liquefaction-induced shear deformation (Martin *et al.* (1975); Finn *et al.* (1977); Zienkiewicz *et al.* (1985); Iai *et al.* (1992)). Recently, more consideration has been given to the role of the progressive decay in soil stiffness with increasing pore pressure, accumulation of deformation, stress-dilatancy and hysteretic loops in formulating constitutive models for liquefiable soils (Prevost (1985); Manazari & Dafalias (1997); Rouainia & Wood (2001); Elgamal *et al.* (2003), among others).

In this chapter, an elasto-plasticity constitutive model proposed by Pastor *et al.* (1990), referred to as P-Z sand model, has been slightly modified and adopted to investigate the liquefaction phenomenon in loose saturated soils. The modified constitutive model has also been incorporated into the FEM code UWLC (Forum8, 2006). The computational scheme of this code follows the methodology of Chan (1988), which is described in great length in Zienkiewicz *et al.* (2001). This fully

coupled non-linear code uses the *u-p* formulation in which *u* is the solid phase displacement and *p* is the fluid phase pore pressure.

In order to assess the predictive capability of the proposed model, numerical results have been compared with published experimental results for monotonic and cyclic tests using different types of sand under different initial densities and different Cyclic Stress Ratios (CSR). In addition, to evaluate the seismic response of gravity quay wall systems constructed on liquefiable soil, the proposed procedure has been validated by back analysis of a typical Port Island caisson type quay wall, PC-1, which was damaged by the 1995 Hyogoken-Nanbu earthquake. The results are compared with observed results, which were obtained from the Ministry of Transport (1997) of Japan and which include seaward displacement, tilting and settlement, known to be typical failure modes of quay walls due to earthquakes.

3.2 Finite element formulation

The finite element method is considered as one of the most advanced methods for static and dynamic analysis of general geotechnical applications including gravity quay walls. This method has been presented at great length in textbooks, e.g. Zienkiewicz *et al.,* (2005) in which a broad range of theoretical issues such as the liquefaction phenomenon has been tackled.

The modelling framework described here is appropriate to saturated porous media, based on the concepts outlined by Biot (1956), and all stress quantities are to be understood as effective stress quantities. In addition, attention is restricted to a small deformation regime and isothermal conditions. In the context of finite element analysis, assuming that the relative velocity of the fluid phase is negligible, and the system of ordinary equations that results from the *u-p* formulation (in which *u* is the displacement of the solid phase and *p* is the pore fluid pressure), can be written as follows:

$$\boldsymbol{M}\,\ddot{\boldsymbol{u}} + \int_{\Omega} \boldsymbol{B}^{T}\,\boldsymbol{\sigma}'\,d\Omega + \boldsymbol{Q}\boldsymbol{p} = \boldsymbol{f}^{s} \tag{3-1}$$

$$\boldsymbol{Q}\dot{\boldsymbol{u}} + \boldsymbol{S}\dot{\boldsymbol{p}} + \boldsymbol{H}\boldsymbol{p} = \boldsymbol{f}^{p} \tag{3-2}$$

where $\boldsymbol{M}$ is mass matrix, B is the strain-displacement matrix, $\boldsymbol{\sigma}'$ is the effective stress tensor, $\boldsymbol{Q}$ is the coupling matrix between the motion and flow equations, $\boldsymbol{H}$ is the permeability matrix, $\boldsymbol{S}$ is the coupling matrix, $\boldsymbol{f}^p$ is the force vector for the fluid phase and $\boldsymbol{f}^s$ is the force vector for the solid phase. The algebraic counterparts of Equations 3.1 and 3.2 are obtained by applying a time-integration scheme. Assuming that the values of displacements, pore pressures and their time derivatives $\{\boldsymbol{u}_n, \dot{\boldsymbol{u}}_n, \ddot{\boldsymbol{u}}_n, p_n, \dot{p}_n\}$ have been obtained at time t_n, the integration consists of updating $\{\boldsymbol{u}_{n+1}, \dot{\boldsymbol{u}}_{n+1}, \ddot{\boldsymbol{u}}_{n+1}, p_{n+1}, \dot{p}_{n+1}\}$ at the next time-step t_{n+1}, according to the Generalised Newmark finite differences scheme as follows:

$$\ddot{\boldsymbol{u}}_{n+1} = \ddot{\boldsymbol{u}}_n + \Delta \ddot{\boldsymbol{u}}_n \tag{3.3}$$

$$\dot{\boldsymbol{u}}_{n+1} = \dot{\boldsymbol{u}}_n + (1+\theta_1)\Delta \ddot{\boldsymbol{u}}_n \, \Delta t \tag{3.4}$$

$$\boldsymbol{u}_{n+1} = \boldsymbol{u}_n + \Delta \dot{\boldsymbol{u}}_n \Delta t + \frac{1}{2}(1+\theta_2)\Delta \ddot{\boldsymbol{u}}_n \, \Delta t^2 \tag{3.5}$$

Similarly, applying the Generalised Newmark scheme to the rate of pore pressure change and pore pressure yields:

$$\dot{\boldsymbol{p}}_{n+1} = \dot{\boldsymbol{p}}_n + \Delta \dot{\boldsymbol{p}}_n \tag{3.6}$$

$$\boldsymbol{p}_{n+1} = \boldsymbol{p}_n + (1+\bar{\theta}_1)\Delta \dot{\boldsymbol{p}}_n \, \Delta t \tag{3.7}$$

where the parameters $\theta_2 \geq \theta_1 \geq \frac{1}{2}$ and $\bar{\theta}_2 \geq \frac{1}{2}$ are typically chosen for unconditional stability of the recurrence scheme. It should be noted that when $\theta_2 = \theta_1 = \bar{\theta}_2 = \frac{1}{2}$, the scheme is second order accurate with zero numerical damping. Inserting the above approximations into Equations 3.1 and 3.2 gives:

$$\begin{bmatrix} \boldsymbol{M} + \frac{1}{2}\boldsymbol{K}\theta_2 \Delta t^2 & -\boldsymbol{Q}\theta_1 \Delta t \\ \boldsymbol{Q}\theta_1 \Delta t & -\bar{\theta}_2/\theta_1 (\boldsymbol{S} + \boldsymbol{H}\theta_1 \Delta t) \end{bmatrix}^i \begin{Bmatrix} \Delta \ddot{\boldsymbol{u}}_n \\ \Delta \dot{\boldsymbol{p}}_n \end{Bmatrix}^{i+1} = -\begin{Bmatrix} \boldsymbol{\Theta}^s_{n+1} \\ -\bar{\theta}_2/\theta_1 \, \boldsymbol{\Theta}^p_{n+1} \end{Bmatrix}^i \tag{3.8}$$

where i is an iteration counter and $\boldsymbol{\Theta}^s_{n+1}$ and $\boldsymbol{\Theta}^p_{n+1}$ are the residuals defined as:

$$\boldsymbol{\Theta}^{s}_{n+1} = \boldsymbol{M}_{n+1}\,\ddot{\boldsymbol{u}}_{n+1} + \int_{\Omega} \boldsymbol{B}^{T}_{n+1}\,\boldsymbol{\sigma}'\,d\Omega - \boldsymbol{Q}_{n+1}\,\boldsymbol{p}_{n+1} - \boldsymbol{f}^{s}_{n+1} \tag{3.9}$$

$$\boldsymbol{\Theta}^{p}_{n+1} = \boldsymbol{Q}_{n+1}\,\dot{\boldsymbol{u}}_{n+1} + \boldsymbol{H}_{n+1}\,\boldsymbol{p}_{n+1} - \boldsymbol{S}_{n+1}\,\dot{p}_{n+1} - \boldsymbol{f}^{p}_{n+1} \tag{3.10}$$

The above system 3.8 constitutes a set of coupled non-linear equations, which has to be solved iteratively $\{\Delta\,\ddot{\boldsymbol{u}}_n, \Delta\,\dot{\boldsymbol{p}}_n\}$. To this end, the Newton-Raphson procedure was used.

3.3 P-Z model for sand

In the present work, the generalised plasticity model with elements of bounding surface theory proposed by Pastor *et al.* (1990) and referred to as P-Z sand model, has been adopted to describe the saturated soil behaviour under static and cyclic loading. It should be noted that some minor modifications have been made to the flow rule to reflect the dependency of the stress state on the third deviatoric stress invariant (see Figure 3.1). The governing constitutive relations for the P-Z sand model are summarised below.

The P-Z model is expressed in terms of the following invariants:

$$p = \frac{1}{3}\sigma_{kk} \tag{3.11}$$

$$q = \sqrt{3J_2} \tag{3.12}$$

$$\theta = \frac{1}{3}\boldsymbol{sin}^{-1}\left(-\frac{3\sqrt{3}}{2}\times\frac{J_3}{J_2{}^{3/2}}\right) \quad \text{with} \quad \left(-\frac{\pi}{6}\le\theta\le\frac{\pi}{6}\right) \tag{3.13}$$

$$J_2 = \frac{1}{2}s_{ij}s_{ji} \tag{3.14}$$

$$J_3 = \frac{1}{3}s_{ij}s_{jk}s_{ki} \tag{3.15}$$

$$s_{ij} = \sigma_{ij} - \frac{1}{3}\sigma_{kk}\delta_{ij} \tag{3.16}$$

where p' is the mean effective stress obtained from the principal stresses, σ_{kk} (k=1,3), q is the deviatoric stress, θ is the Lode's angle, J_2 is the second invariant of the deviatoric stress tensor, J_3 is the third invariant of the deviatoric stress tensor, s_{ij} is the deviatoric stress tensor, σ_{ij} is the stress tensor and δ_{ij} is the Kronecker delta.

The following incremental quantities are also needed in the formulation of the P-Z model:

$$d\varepsilon_v = d\varepsilon_{kk} \tag{3.17}$$

$$d\varepsilon_s = \left(\frac{2}{3} de_{ij} de_{ji}\right)^{1/2} \tag{3.18}$$

$$de_{ij} = d\varepsilon_{ij} - \frac{1}{3} d\varepsilon_{kk} \delta_{ij} \tag{3.19}$$

where $d\varepsilon_v$, $d\varepsilon_{kk}$, de_{ij}, $d\varepsilon_s$, $d\varepsilon_{ij}$ are the increments of volumetric strain, principal strain, shear strain, deviatoric strain and strain tensor, respectively.

In the P-Z model, the dilatancy that reflects the plastic volumetric strains and the plastic shear strains can be approximated by a linear function of stress ratio $\eta=q/p'$ as first suggested by Nova & Wood (1979 & 1982) as follows:

$$d_g = (1+\alpha_g)(M_g - \eta) \tag{3.20}$$

where M_g is the slope of the critical state line and α_g is a material parameter. The direction of the unit normal $\boldsymbol{n}_g$ to the plastic potential defines the plastic strain directions as follows:

$$\boldsymbol{n}_g = \frac{1}{\sqrt{1+d_g^2+s_g^2}}\{d_g, 1, s_g\} \text{ with } s_g = -\frac{3qM_g}{2M_{gc}}\left(\frac{M_{gc}}{M_{ge}} - 1\right)\cos 3\theta \tag{3.21}$$

where M_{ge}, M_{gc} are additional model parameters obtained from triaxial extensions and compression tests, respectively.

The direction of the unit normal $\boldsymbol{n}_f$ to the yield function, which has a similar shape as the plastic potential, defines the loading direction as follows:

$$\boldsymbol{n}_f = \frac{1}{\sqrt{1+d_f^2+s_f^2}}\{d_f, 1, s_f\} \text{ with } s_f = -\frac{3qM_f}{2M_{fc}}\left(\frac{M_{fc}}{M_{fe}}-1\right)\cos 3\theta \tag{3.22}$$

where M_f, M_{fe} and M_{fc} are additional model parameters and α_f is defined as:

$$d_f = (1+\alpha_f)(M_f - \eta) \tag{3.23}$$

It should be mentioned that in the P-Z model, a non-associative flow rule is adopted by distinguishing the plastic potential (M_g, α_g) from the yield function (M_f, α_f).

The compression and the extension values for M_g and M_f can be related to the friction angles ϕ_c' and ϕ_e' and the Lode's angle θ as follows:

$$M = \frac{2M_e}{(1+C)-(1-C)\sin 3\theta} \text{ with } C = M_e / M_c \tag{3.24}$$

where the compression and the extension values can be related to the friction angles ϕ_c' and ϕ_e' as follows:

$$M_c = \frac{6\sin\phi_c'}{3-\sin\phi_c'} \text{ and } M_e = \frac{6\sin\phi_e'}{3+\sin\phi_e'} \tag{3.25}$$

Using the bounding surface concepts, the plastic modulus during loading in the P-Z model is obtained as follows:

$$H_L = H_0 p' H_f (H_v + H_s) H_D \tag{3.26}$$

where H_f, H_v, H_s and H_D are given by:

$$H_f = (1 - \frac{\eta}{\eta_f})^4 \quad \text{with} \quad \eta_f = (1 + \frac{1}{\alpha_f}) M_f \tag{3.27}$$

$$H_v = 1 - \frac{\eta}{M_g} \tag{3.28}$$

$$H_s = \beta_0 \beta_1 e^{-\beta_0 \xi} \tag{3.29}$$

$$\xi = \int d\xi \quad d\xi = (de_{ij}^p de_{ji}^p)^{1/2} \tag{3.30}$$

$$H_D = \left(\frac{\varsigma_{MAX}}{\varsigma} \right) \tag{3.31}$$

$$\varsigma = p' \left\{ 1 - \frac{\alpha_f}{1 + \alpha_f} \frac{\eta}{M_f} \right\}^{-1/\alpha} \tag{3.32}$$

where H_0, β_0, β_1 and γ are model parameters. In the case when the stress ratio η is equal η_f, Equation 3.26 implies that the plastic modulus H_L is zero. H_s represents the material degradation under accumulated distortional strain. Equations 3.27 and 3.28 suggest that for an isotropic path (η=0), the plastic modulus reduces to $H_L = H_0 p'^{\left(1 - \frac{1}{\alpha}\right)}$.

In order to predict plastic strains that allow rapid pore pressure to build up on unloading, the plastic modulus for unloading in the P-Z model is expressed as follows:

$$H_U = \begin{cases} H_{U0} \left(\frac{M_g}{\eta_U} \right)^{\gamma U} \; for \left| \frac{M_g}{\eta_u} \right| > 1 \\ H_{U0} for \left| \frac{Mg}{\eta_u} \right| \le 1 \end{cases} \tag{3.33}$$

where η_U is the stress ratio at the starting point of unloading, H_{U0} and γ_U are two additional model parameters.

The bulk and shear moduli are assumed to vary linearly with mean confining pressure, p', as follows:

$$K_{ev} = K_{ev0} p_a \left(\frac{p'}{p_a} \right)^{m_v} \tag{3.34}$$

$$G_{es} = G_{es0} p_a \left(\frac{p'}{p_a} \right)^{m_s} \tag{3.35}$$

where p_a is the atmospheric pressure, K_{ev0} and G_{es0} are the initial constant of the bulk and shear moduli and m_v and m_s are two model parameters.

3.3.1 Model Parameters

The P-Z sand model has 15 parameters used in the analysis and another two parameters describe the test condition, which are p'_0 and OCR, as shown in Table 3.1. These parameters can be identified by matching the experimental data of the routine triaxial tests, such as the consolidated-drained monotonic triaxial test (CD), the consolidated-undrained monotonic triaxial test (CU) and the consolidated-undrained cyclic triaxial test.

Table 3.1. List of P-Z sand model parameters

Material parameter	Description
M_f	Slope of the critical state line (CSL) for loading vector (dimensionless)
M_g	Slope of the critical state line (CSL) for plastic strain vector (dimensionless)
C	Ratio of the critical state line (CSL) (dimensionless)
α_f	Dilatancy parameter for plastic strain vector (dimensionless)
α_g	Dilatancy parameter (dimensionless)
G_{es0}	Initial constant of shear modulus (dimensionless)
K_{ev0}	Initial constant of bulk modulus (dimensionless)
m_v	Shear modulus exponent (dimensionless)
m_s	Bulk modulus exponent (dimensionless)
β_0	Shear hardening parameter 1 (dimensionless)
β_1	Shear hardening parameter 2 (dimensionless)
H_0	Plastic modulus on loading (kPa)
H_{U0}	Plastic modulus on unloading (kPa)
γ	Plastic deformation during reloading (dimensionless)
γ_U	Plastic deformation during unloading (dimensionless)
p'_0	The initial mean effective stress of the undrained triaxial test (kPa)
OCR	Over consolidation ratio

3.3.2 Calibration Procedure

These parameters are divided into two main groups: firstly, the parameters that can be identified by matching the results from a consolidated drained monotonic triaxial test (CD) and a consolidated undrained monotonic triaxial test (CU); these parameters are (M_g, M_f, C, α_g, α_f, K_{ev0}, G_{es0}, m_v, m_s, β_0, β_1, H_0). Secondly, the remaining three parameters, which are (H_{Uo}, γ, γ_U), can be identified by matching the result from a consolidated-undrained cyclic triaxial test. Furthermore, there are two

parameters required to start the analysis, namely the overconsolidation ratio (OCR) and the initial mean effective stress of the triaxial test (p'_0).

In order to estimate the first 12 parameters, it is sufficient to match the experimental results with simulation data. These curves can be obtained from either consolidated drained or undrained monotonic triaxial tests. The required curves are:

a) Consolidated-undrained monotonic triaxial test (CU), which is used in this study.

1) Axial strain (ε_a) and deviatoric stress (q) curve.

2) Axial strain (ε_a) and pore pressure (Δu) curve.

3) Effective mean principal stress (p') and deviatoric stress (q) curve (effective stress path).

4) Axial strain (ε_a) and stress ratio (η) curve.

b) Consolidated-drained monotonic triaxial test (CD).

1) Axial strain (ε_a) and deviatoric stress (q) curve.

2) Axial strain (ε_a) and volumetric strain (ε_v) curve.

3) Axial strain (ε_a) and stress ratio (η) curve.

4) Stress ratio (η) and dilatancy (d_g) curve.

The remaining three parameters can be estimated by matching the experimental results with simulation data of Consolidated-undrained cyclic triaxial test, which is used in this study. The required curves are:

1) Time history of cyclic deviatoric stress.

2) Time history of axial strain (ε_a).

3) Time history of pore pressure (Δu) or excess pore water pressure ratio (r_u).

4) Effective mean principal stress (p') and deviatoric stress (q) curve (effective stress path).

5) Axial strain (ε_a) and deviatoric stress (q) curve

6) Number of cycles and cyclic stress ratio curve (liquefaction strength curve)

The procedure used in this study to identify each parameter by the consolidated-undrained monotonic triaxial test (CU) and the consolidated-undrained cyclic triaxial test was as follows.

(M_g) is the slope of the critical state line (CSL) for the plastic strain vector that can be estimated by one of the following two methods:

1) Matching the q versus p' plot (effective stress path); M_g is equal to the tangent drawn from the origin to the residual stress path in a consolidated-undrained monotonic triaxial test (CU).

2) Estimated from the graph, stress ratio ($\eta = \frac{q}{p'}$) versus the shear strain or axial strain; M_g is approximately equal to the maximum value of stress ratio reached in the test.

M_f is the slope of the critical state line (CSL) for the plastic strain vector, and it can be estimated by one of the following three ways:

1) Matching the shape of the stress path in the q versus p' in a consolidated-undrained monotonic triaxial test (CU).

2) Matching the critical stress ratio ($\eta = \frac{q}{p'}$) where the soil behaviour changes from contractive to dilative behaviour in the dense sand case in a consolidated-undrained monotonic triaxial test (CU).

3) $M_f = D_r \text{ x } M_g$, where D_r is the relative density; this method gives the best starting value (Pastor *et al.*, 1985).

(C) is the ratio of the critical state line (CSL) on the side of extension and compression, but is usually taken as 0.80. It is often expressed in the following equation: the friction angles of extension and compression, ϕ'_c and ϕ'_e are the same as in Equation 3.24:

$$C = \frac{3}{3 + M_c} \tag{3.36}$$

The yield surface expressed in Equation 3.25 on II plane is shown in Figure 3.1 and the condition is required in order to maintain the outer convex shape.

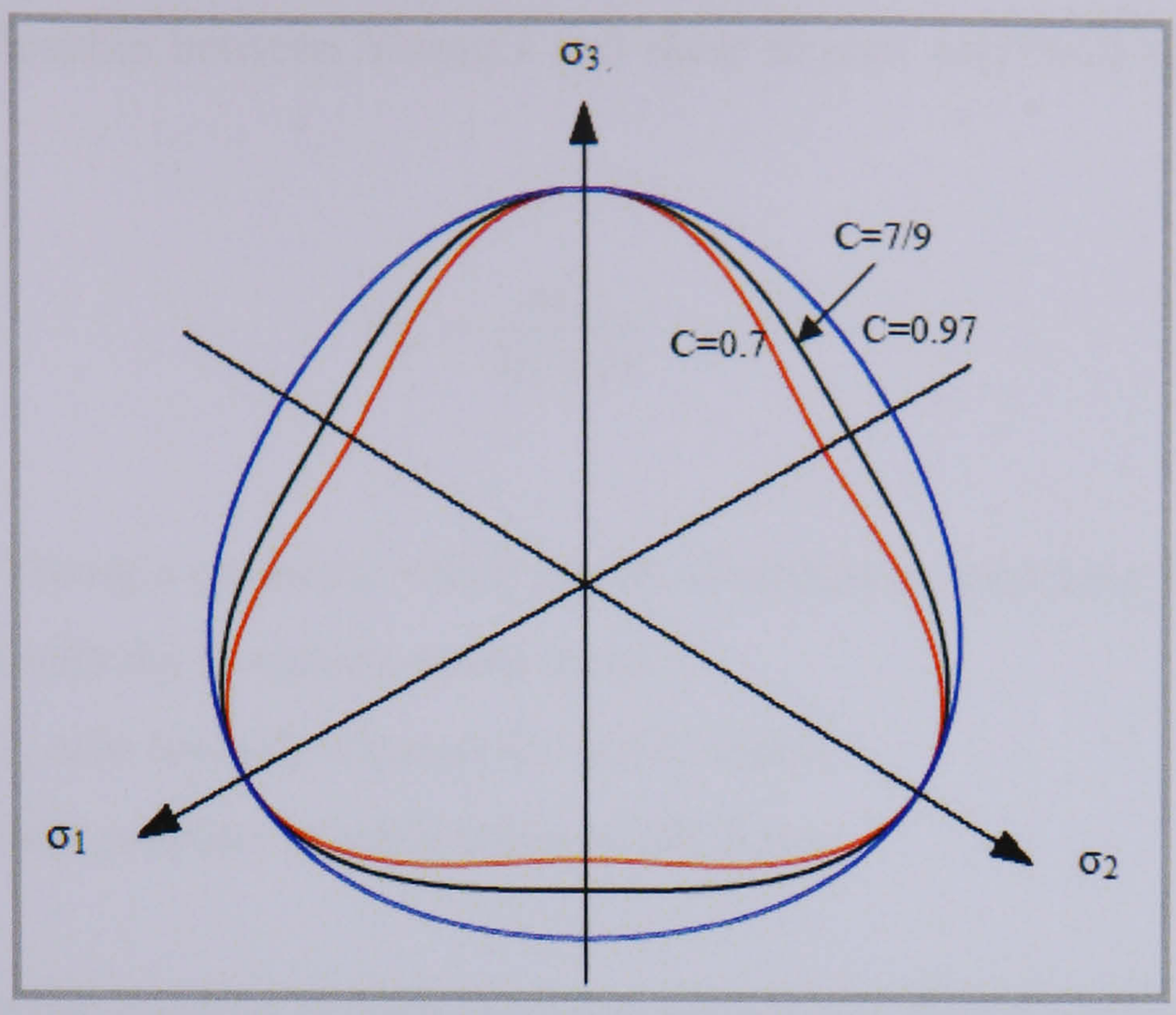

Figure 3.1. Yield surface shapes on II plane depending on the parameter C

(α_g) is the dilatancy parameter in the range of 0.4–0.5, usually taken as 0.45 as suggested by Pastor & Zienkiewicz (1986).

(α_f) is the dilatancy parameter for a plastic strain vector, and is usually taken to be the same as α_g as suggested by Pastor & Zienkiewicz (1986).

(m_s) is in the range 0.4–0.8, and is usually taken as 0.5.

(m_v) is usually taken to be same as m_s.

(G_{es0}) is the value of three times the coefficient of shear modulus at the initial effective mean principal stress (p'_0). Thus, it can be obtained by one of the following two methods:

1) Matching the axial strain versus deviatoric stress curve from a consolidated-undrained monotonic triaxial test (CU), or
2) From the following equation:

$$G_{es0} = \frac{3E_i}{2(1+v)p_a(p'_0/p_a)^{m_s}} \tag{3.37}$$

with the relationship between Young's and shear moduli expressed in the following equation:

$$G_{es} = \frac{3E_i}{2(1+v)} \tag{3.38}$$

where, E_i is Young's modulus, which can be identified by matching the initial slope of axial strain with the deviatoric stress curve.

v is Poisson's ratio (usually taken as 0.5 in CU tests).

p_a is atmospheric pressure (usually taken as 100 Kpa).

(K_{ev0}) is the initial constant of bulk modulus at the mean effective stress (p'_0). Thus, it can be obtained by one of the following two methods:

1) Matching the axial strain with a change in pore pressure curve from a consolidated-undrained monotonic triaxial test (CU), or
2) From the following equation:

$$K_{ev0} = \frac{2G_{es0}(1+v')}{9(1-2v')} \tag{3.39}$$

with the relationship between the bulk and shear moduli expressed in the following equation:

$$K_{ev} = \frac{2(1+v')G_{es}}{3(1-2v')3} \tag{3.40}$$

where v' is Poisson's ratio (usually taken as 0.2–0.3 in the CU test).

(β_0) is the shear hardening parameter 1; it is in the range 1–10 and it is usual to take 4.2 as an initial estimate.

(β_1) is the shear hardening parameter 2; it is in the range 0.1–0.9 and it is usually taken as 0.2 as an initial estimate.

(H_0) is the plastic modulus on loading; it can be obtained by one of the following three ways:

1) Matching the curve of axial strain against deviatoric stress from a consolidated-undrained monotonic triaxial test (CU); or
2) Matching the stress path shape of effective stress with deviatoric stress (effective stress path) from a consolidated-undrained monotonic triaxial test (CU).
3) It is recommended to take the value in Table 3.2 as the starting value because it correlates to some extent with relative density.

Table 3.2. H_0 and the relative density of sand

Sand type	**Relative density D_r**	**H_0**
Very loose	<0.2	50 ~ 200
Loose	0.2–0.4	200 ~ 400
Medium dense	0.4–0.6	400 ~ 600
Dense	0.6–0.8	600 ~ 800
Very dense	>0.8	800 ~ 1000

(H_{U0}) is the plastic modulus on unloading; it can be obtained by matching the initial slope of the first unloading curve of effective stress with the deviatoric stress curve (effective stress path) from the consolidated-undrained cyclic triaxial test. It is recommended to be equal to 6000 as an initial estimate.

(γ) is the plastic deformation during reloading. It can be obtained by:

1) Matching the slope of the first reloading curve of effective stress with deviatoric stress (effective stress path) from the consolidated-undrained cyclic triaxial test; or
2) Matching the number of cycles in a series of loading and unloading from the consolidated-undrained cyclic triaxial test.

(γ_U) is the plastic deformation during unloading. It can be obtained by:

1) Matching the slope of the first reloading curve of effective stress with the deviatoric stress (effective stress path) from the consolidated-undrained cyclic triaxial test; or

2) Matching the number of cycles in a series of loading and unloading from the consolidated-undrained cyclic triaxial test.

It is in the range 0–10, and it is best to start with the value of (γ -2).

Also, there are another two parameters that identify the experimental condition required in the analysis:

(p'_0) is the initial mean effective stress of the undrained triaxial test, and is expressed by the following equation:

$$p'_0 = \frac{\sigma_1 + \sigma_2 + \sigma_3}{3} \tag{3.41}$$

where σ_1 is the axial stress and σ_2 and σ_3: are the confining stresses; $\sigma_1 = \sigma_3$ in the triaxial test.

OCR is the overconsolidation ratio, usually taken as 1.0 for sand.

However, an example describing the P-Z sand model parameters iditification in more detail is given in Appendix B.

3.3.3 Model evaluation

To test the validity of the proposed model, simulations are compared with the published monotonic and cyclic tests of different types of sand under different confining pressures and initial relative densities. The experimental tests are those of Castro (1969), Toyota *et al.* (2004) and Taylor (1984) . The model requires a total of 15 parameters; these have been obtained by the procedure outlined in Section 3.3.2, and are listed in Table 3.3.

Figure 3.2 shows a comparison between the experimental undrained monotonic triaxial tests from Castro (1969) and the simulations for three relative densities of Dr=27%,44%, and 47%. It can be noticed that the response switches from softening behaviour (for the low density soil) to hardening behaviour (for the high density soil) are as would be expected under undrained loading conditions.

Figure 3.3 shows the comparison between the experimental and the simulations of stress:strain relationship for two relative densities of Dr=100% and 20% during drained monotonic triaxial tests conducted by Taylor (1984). It can be seen that the general shape of the stress:strain response for loose and dense states are well captured.

For the undrained triaxial cyclic tests, the soil samples were first isotropically consolidated to a mean effective stress p_0'=100 kPa and then cycles of constant deviator stress amplitude q = ±25 kPa were applied (Toyota *et al.*, 2004). The results are presented in Figure 3.4 and Figure 3.5 in terms of effective stress paths and stress:strain response for Toyoura sand and Masado sand, respectively. It can be seen that the model is remarkably successful in matching the general shape of stress:strain response and the decrease in mean effective stress resulting from the excess pore pressure generation. The number of cycles to reach liquefaction in each test agrees well with those measured.

These results indicate that the model is able to produce pore pressure build-up due to the change of mean effective stress and captures most of the important features of soil behaviour during liquefaction. This model has been implemented in the geotechnical finite element program UWLC, and can be applied to real geotechnical earthquake engineering problems.

a)

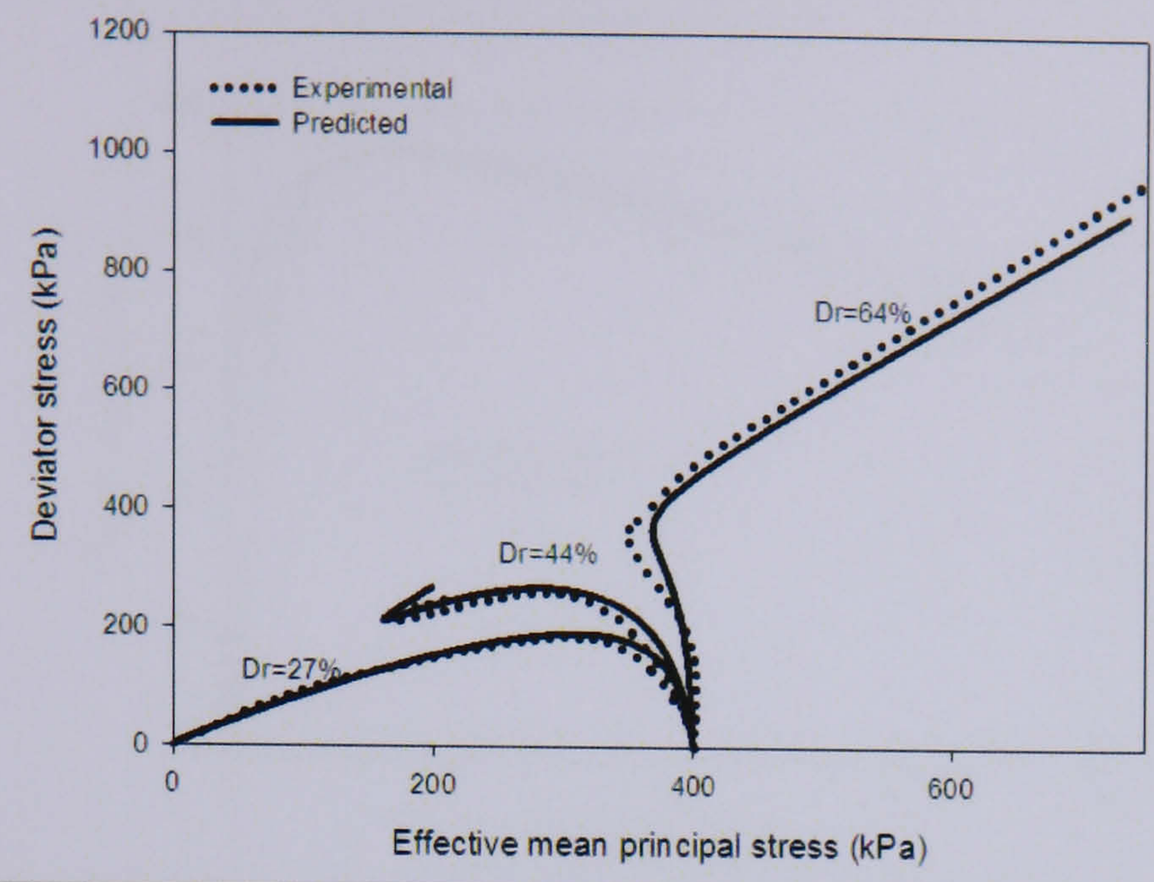

b)

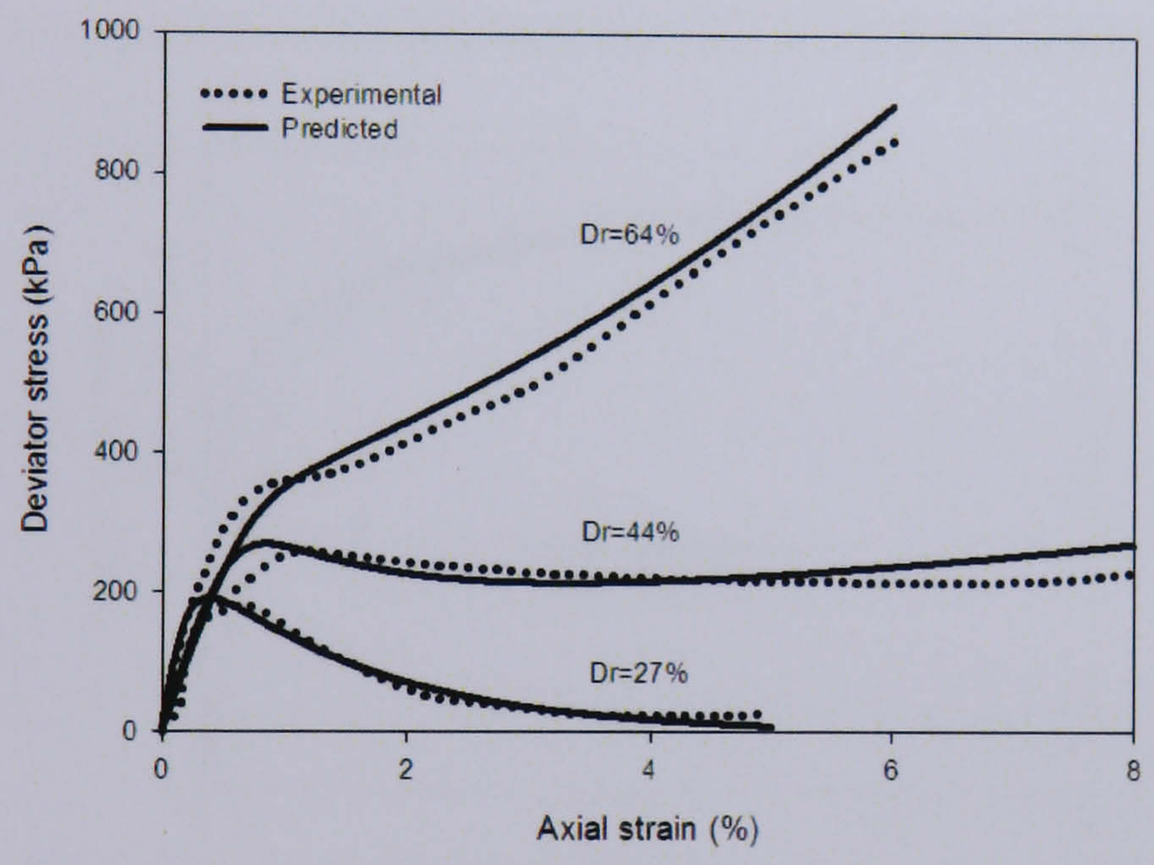

c)

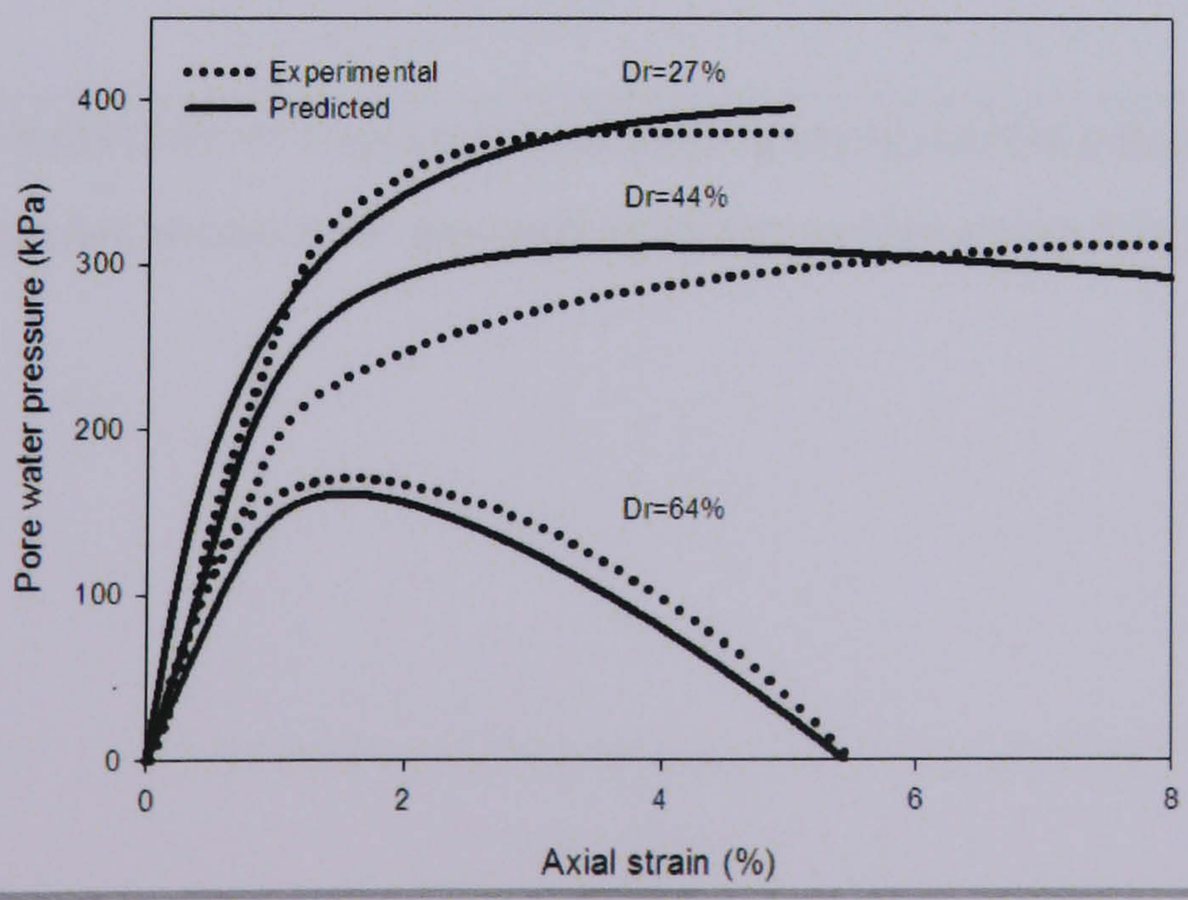

Figure 3.2. Simulation of experimental data from Castro (1969) under monotonic undrained loading: a) stress path and b) stress strain relationship and excess pore pressures

a)

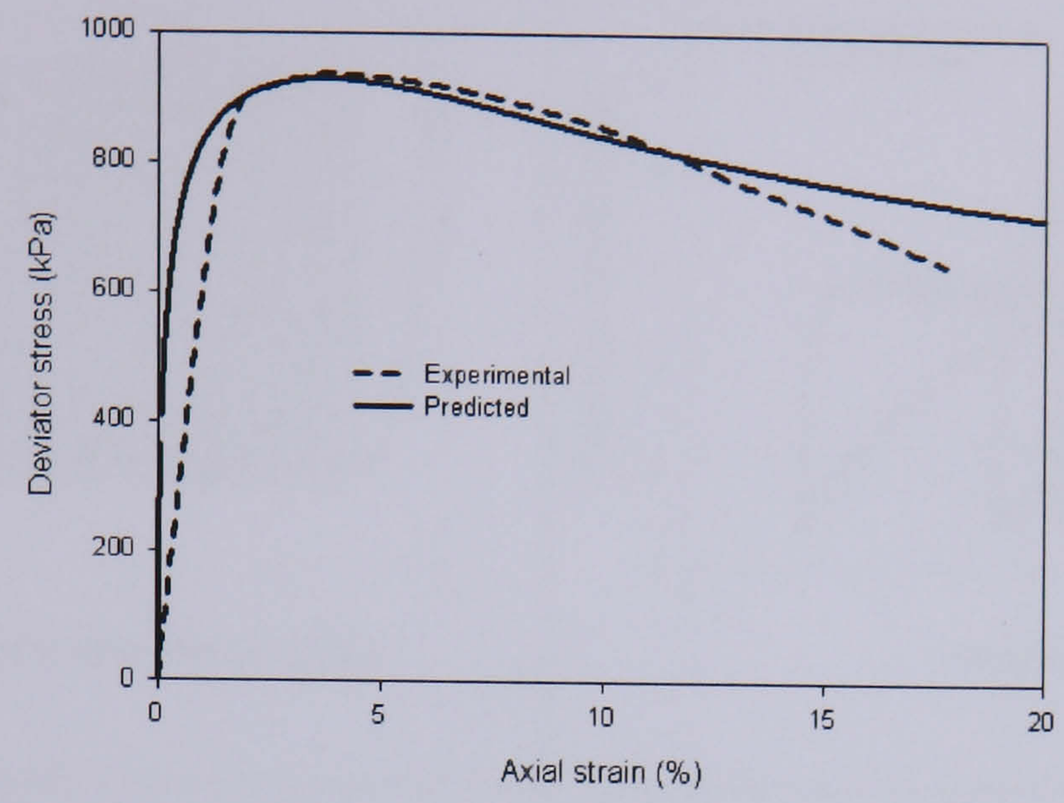

b)

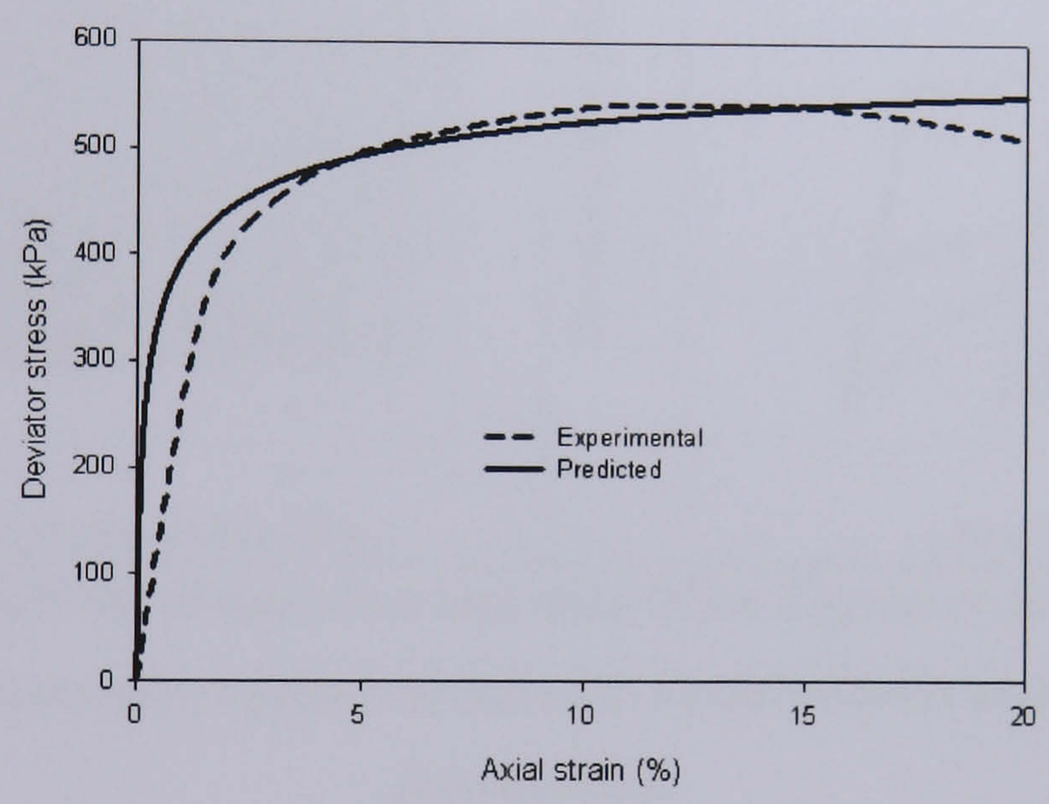

Figure 3.3. Simulations of experimental data of stress strain relationships from Taylor (1984) under monotonic drained loading: a) Dense sand and b) loose sand

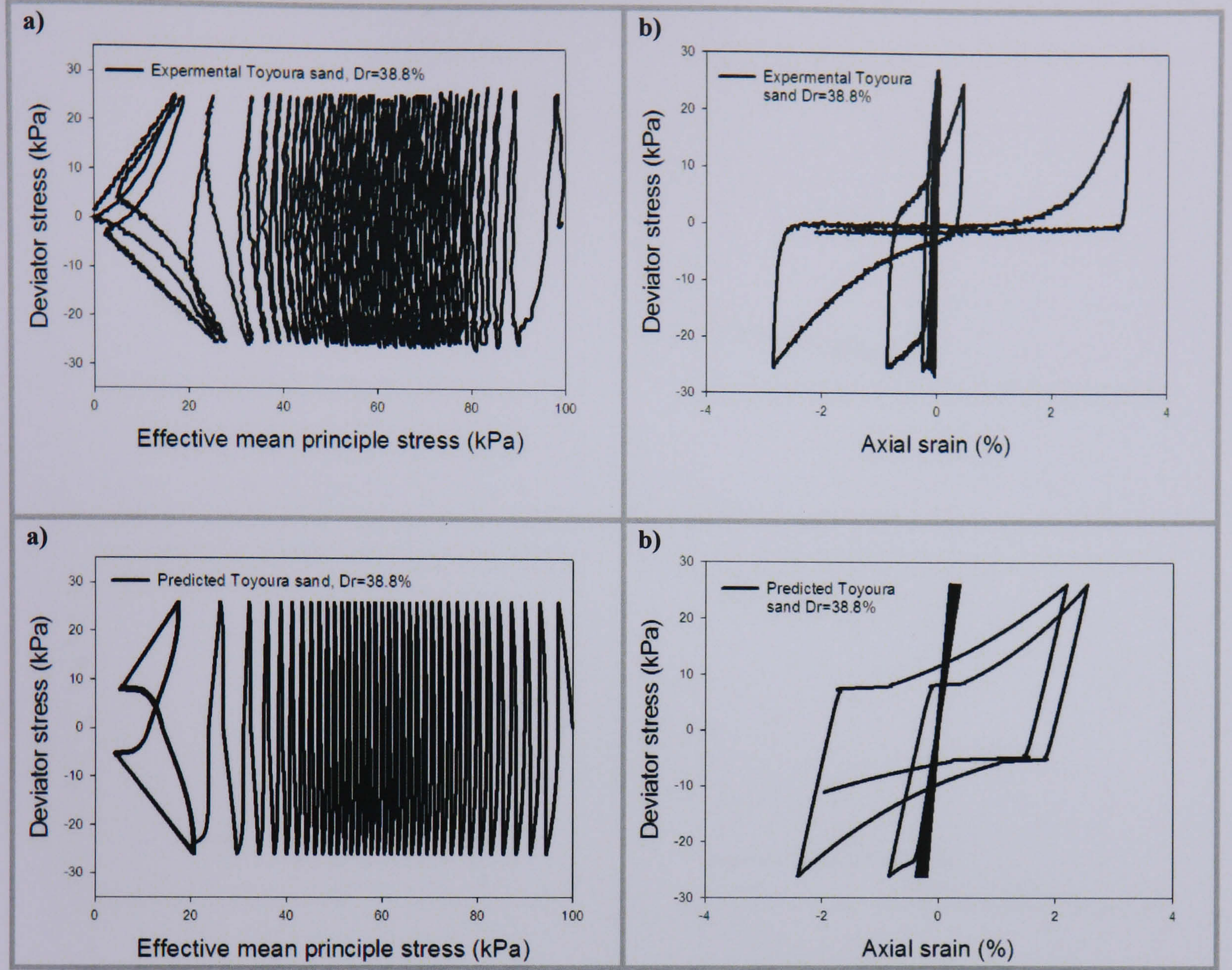

Figure 3.4. Simulations of experimental data from Toyota *et al.* (2004) of Toyora sand (Moist placement), cyclic triaxial test: a) stress path and b) stress strain relationship

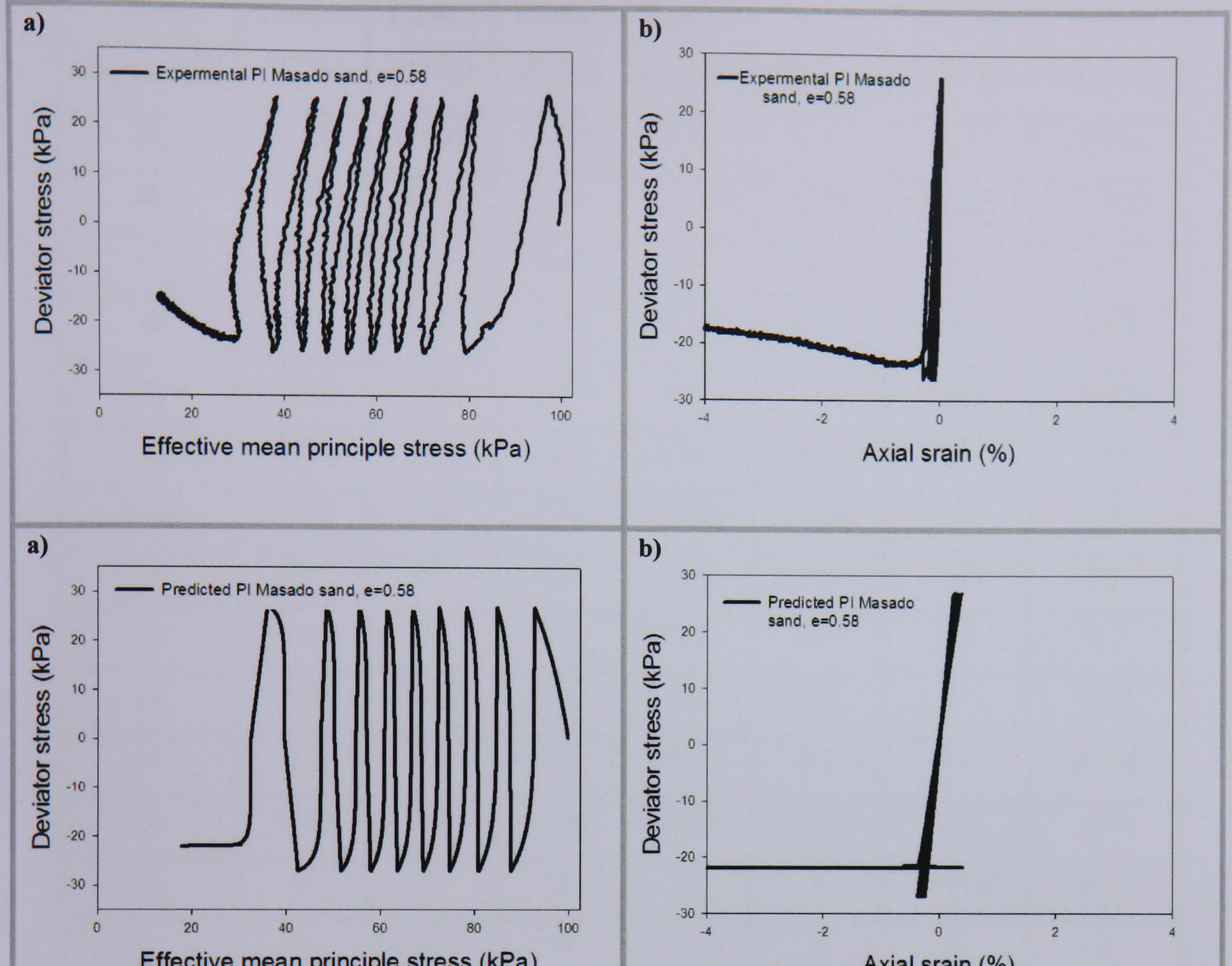

Figure 3.5. Simulation of experimental data from Toyota *et al.* (2004) of PI Masado sand (Moist placement), cyclic triaxial test: a) stress path and b) stress strain relationship

Table 3.3. Material parameters used in simulation of Figure 3.2 to Figure 3.5

Test / Parameter	Castro (27%)	Castro (44%)	Castro (64%)	Taylor (Loose)	Taylor (Dense)	Toyota (Toyora)	Toyota (Masado)
M_f	0.32	0.545	0.495	0.49	0.7	0.77	0.574
M_g	1.03	1.32	1	1.33	1.28	1.42	1.372
C	0.8	0.9	0.9	0.9	0.8	0.85	0.9
α_f	0.45	0.45	0.45	0.45	0.45	0.45	0.45
α_g	0.45	0.45	0.45	0.45	0.45	0.45	0.45
K_{ev0}	280	195	160	30000	30000	220	246
G_{es0}	600	300	250	50000	35000	140	120
m_v	0.5	0.5	0.5	0.5	0.5	0.5	0.5
m_s	0.5	0.5	0.5	0.5	0.5	0.5	0.5
β_0	4.2	4.2	4.2	4.2	4.2	6	4.45
β_1	0.2	0.2	0.2	0.2	0.2	0.3	0.189
H_0	1000	560	1900	16000	4000	520	470
H_{U0}	0	0	0	0	0	19200	6950
γ	0	0	0	0	0	6	6
γ_U	0	0	0	0	0	4.3	4.3
p'_0	400	400	400	207	207	100	100
OCR	1	1	1	1	1	1	1

3.4 Case history

Kobe Port is located in an area 6 km long and 12 km wide and there are two man-made islands, Port Island and Rokko Island. The soils used for landfill were excavated from the Rokko Mountains to the north west of Kobe city; this soil is called PI Masado (Ikuo *et al.* (1996); Inagaki *et al.* (1996); Sugano *et al.* (1996)) . Figure 3.6 shows Port Island, which is divided into two phases; the first, referred to as phase 1, was constructed on the northern half of Port Island between 1966 and 1981, the rest is referred to as phase 2; land filling in the southern half of Port Island was almost complete when the Hyogoken-Nanbu earthquake hit Kobe City in January 1995 (Toyota *et al.*, 1996) .

Kobe Port had significant ground subsidence as a result of liquefaction during the earthquake; the extent of liquefaction was intense on Port Island and over 250 caissons type quay walls were damaged there with a repair cost exceeding US$11 billion (Ishihara, 1997) . These walls were constructed on loose saturated decomposed granite, which had been used to replace the alluvial clay layer in order to attain the required bearing capacity for the foundations. The typical types of damage observed after the earthquake were: seaward displacement, approximately 5 m maximum and approximately 3 m average; the walls also settled approximately 1 to 2 m and tilted approximately 4 degrees (Ichii, 2004) .

Caisson type quay walls in Kobe Port including Port Island and Rokko Island were designed using the pseudo-static method, with limit equilibrium mechanics based on the Mononobe-Okabe method developed by Okabe (1924) and Mononobe & Matsuo (1929) using horizontal seismic coefficients ranging from 0.1 to 0.15 (Inagaki *et al.*, 1996) .

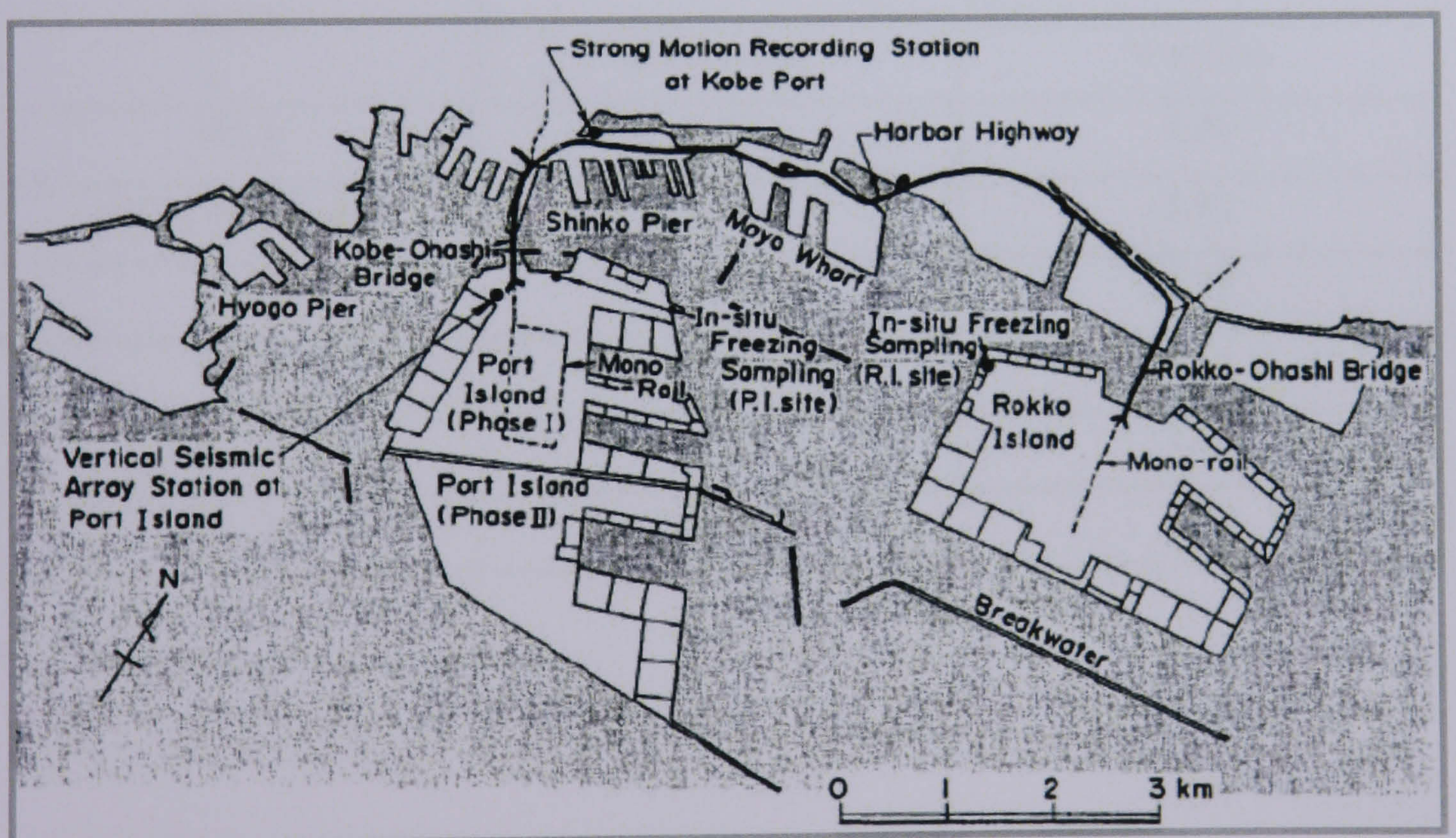

Figure 3.6. Plan of Kobe Port, showing the location of the recording station, quay walls and sites for geotechnical investigation, after Inagaki *et al.* (1996)

This study focuses on the analysis of a typical Port Island caisson quay wall failure during the 1995 Hyogoken-Nanbu earthquake. The quay wall considered here

as a case study is called PC1, and it was constructed in phase one and is depicted in Figure 3.7. The design specifications have been described by Towhata *et al.* (1996); the friction angle used in the design was 30 degrees, except beneath the wall where a friction angle of 40 degrees was employed; the safety factor was 1.2. The horizontal seismic coefficient was 0.1 and the vertical seismic coefficient was zero.

The measured horizontal and vertical displacements for Port Island quay walls PC1–PC5 are presented in Table 3.4. All these walls have the same specifications (i.e. they are identical to PC1 used in the analysis). As shown in Table 3.4, these walls displaced seaward by approximately 2.3 m to 3.13 m, settled approximately 0.79 m to 1.4 m and tilted approximately 3 degrees on average (Ministry of Transport, Japan, 1997).

Table 3.4. Summary of measured displacements of PC berths at Port Island after the 1995 Kobe earthquake (Ministry of Transport, Japan, 1997)

Berth	Displacements (m)	
	Horizontal	Vertical
PC 1	2.75	1.36
PC 1 extension	3.13	1.01
PC 2	2.33	0.79
PC 3	2.46	1.14
PC 4	2.37	1.40
PC 5	2.30	1.38

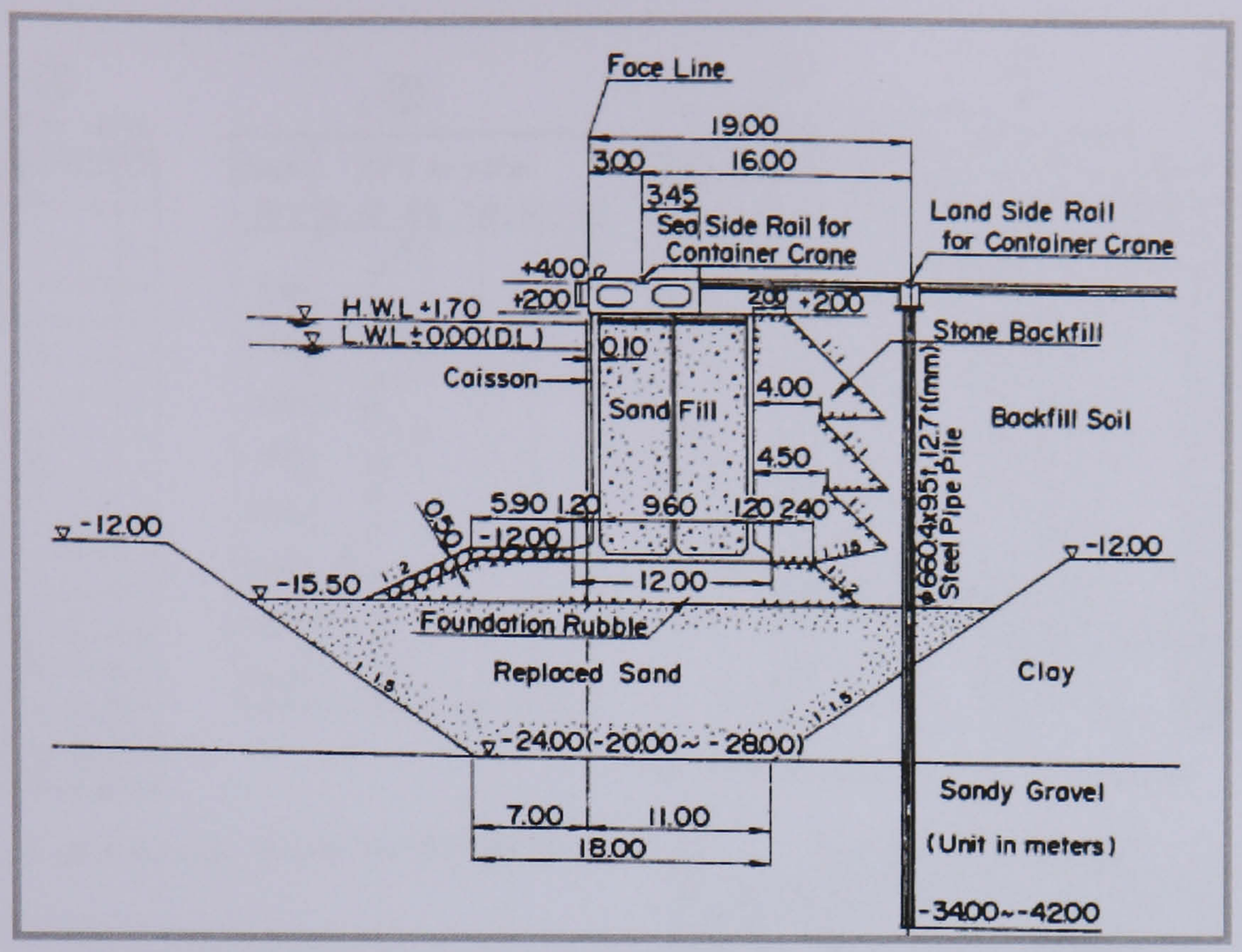

Figure 3.7. Cross section of a quay wall PC1 at Port Island, after Inagaki *et al.* (1996)

The relative density of the backfill soil was obtained from the Standard Penetration Test (SPT) data conducted by Inagaki *et al.* (1996) and shown in Figure 3.8. These data are calculated using the following empirical correlation between SPT, N value and relative density, developed by Cubrinovski & Ishihara (2001).

$$D_r = \left\{ N_1 \left(e_{\max} - e_{\min} \right)^{1.7} \right\}^{0.5} / 3 \text{ with } N_1 = \left(98 / \sigma'_v \right)^{0.5} N \tag{3.42}$$

where σ'_v is the effective vertical stress (kPa) and $e_{\max}$ and $e_{\min}$ represent the maximum and minimum void ratios, respectively. A simple empirical relationship between $e_{\max} - e_{\min}$ and D_{50} exists for all types of sand including gravely sand, clean sands and sands with fines, given by:

$$e_{\max} - e_{\min} = 0.23 + 0.06 / D_{50} \tag{3.43}$$

where D_{50} is the median formation sand diameter. The relative density for each metre depth of backfill soil for PC1 is illustrated in Figure 3.8 and calculated in Table 3.5; the average relative density was found to be $D_r = 41.7\%$.

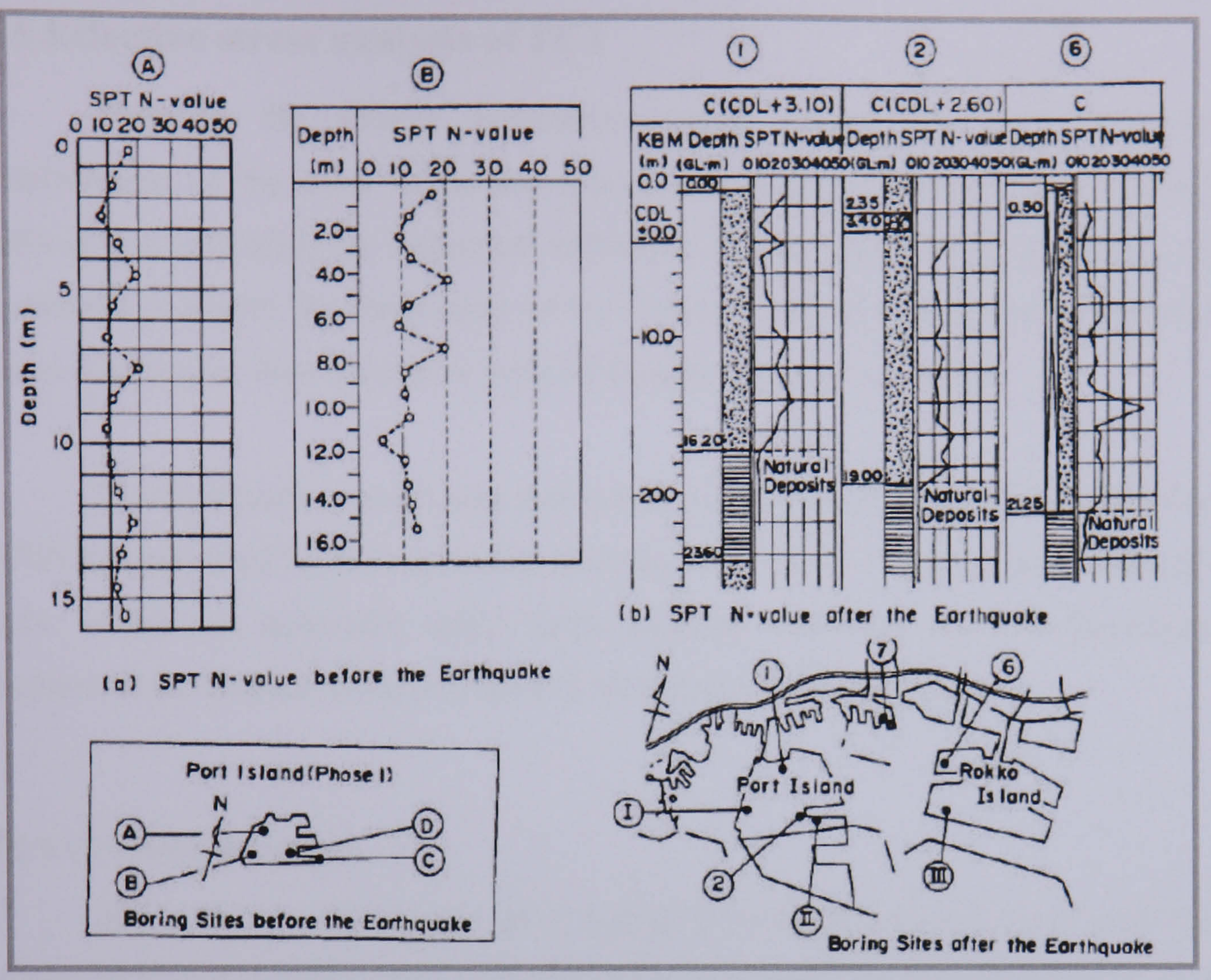

Figure 3.8. SPT N-value before and after the earthquake, after Inagaki *et al.* (1996)

Table 3.5. Calculated relative density from N value

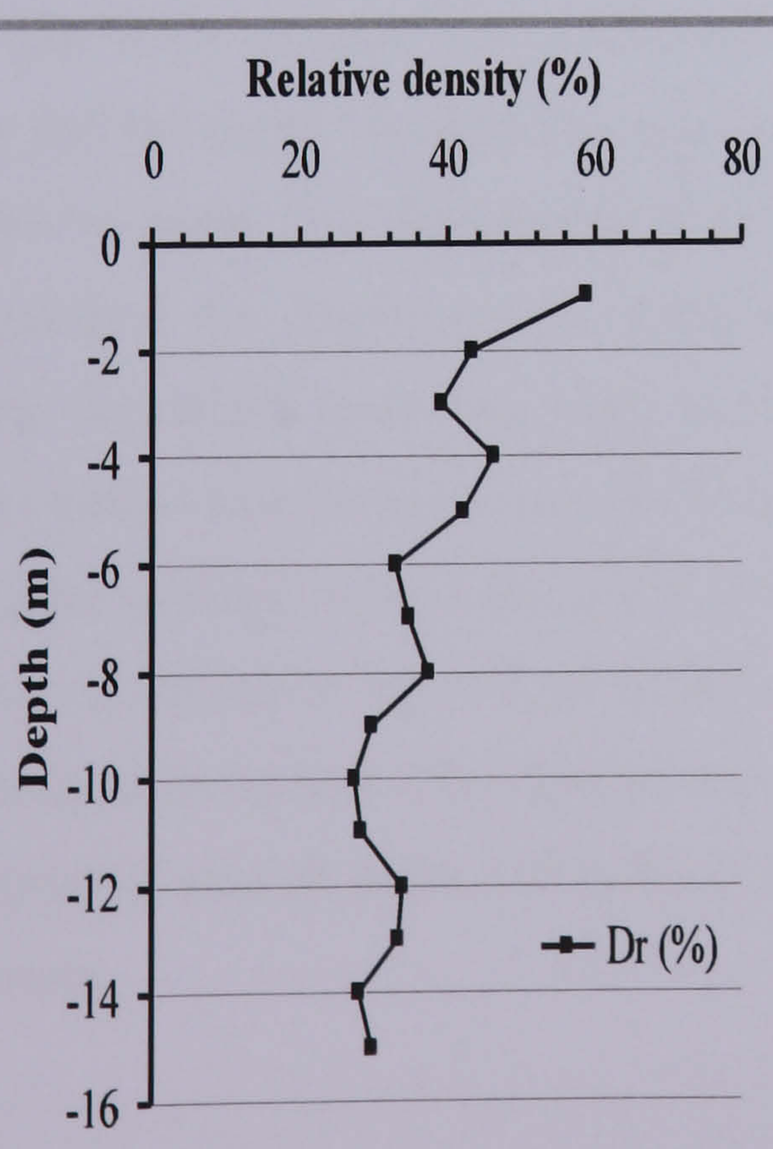

Depth	N value	D_r (%)
-1	13	58.70
-2	10	43.29
-3	10	39.12
-4	16	46.05
-5	15	42.17
-6	10	32.90
-7	12	34.67
-8	15	37.49
-9	10	29.73
-10	9	27.47
-11	10	28.27
-12	15	33.88
-13	15	33.21
-14	11	27.92
-15	13	29.83
Average relative density		41.7 %

3.5 Effective stress analysis of PC1

Although the sliding mechanism could explain the large horizontal displacement of the quay walls, this mechanism does not explain the other large deformations including the settlement and tilting. Hence, effective stress analysis was conducted to clarify the mechanism of the damage, and the applicability of effective stress analysis for these extensive areas of damage was also confirmed.

The constitutive model was incorporated into a finite element computer code (UWLC) then used for the numerical analysis; this code is a fully coupled numerical code, which can undertake initial stress analysis, and one- and two-dimensional dynamic finite element analyses based on total and effective stress.

3.5.1 Creating the mesh

The seismic performance of a typical Port Island caisson quay wall PC1 shown in Figure 3.7 has been modelled using a dynamic non-linear effective stress analysis method in order to evaluate the applicability of effective stress analysis for these areas of extensive damage.

The finite element was performed considering two-dimensional plane strain analysis and the mesh idealisation consisted of 644 elements as shown in Figure 3.9. It should be noted that four-noded elements for pore pressure variation and eight-noded element for displacement variation elements were used in the simulations. However, the model resolution and convergence have been verified in Appendix A. As both vertical and horizontal accelerations were modelled, the boundary conditions of the finite element mesh were fixed in both the x and y directions on the bottom. The sides of the mesh were fixed in both x and y directions because it is far away from the caisson system. The domain used for the finite element analysis covered a cross sectional area of about 115 m by 27 m in the horizontal and vertical directions, respectively.

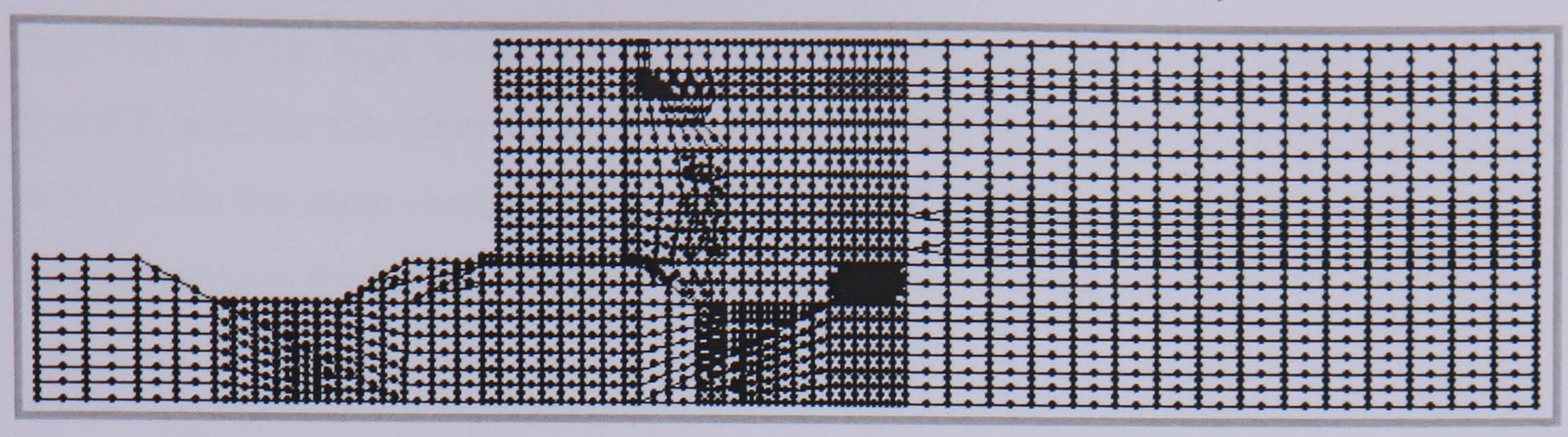

Figure 3.9. Geometry mesh of the Port Island PC1 quay wall

3.5.2 Plain strain element properties

Five materials divided into nine zones were used in the analysis. Each material zone was constructed using a number of elements and then those elements in each material zone were given the same material properties. These different material zones could be assigned different types of constitutive relations. The materials and their properties are listed in Table 3.6. Figure 3.10 shows the Geometry (in natural scale) and material zones of the Port Island PC1 quay wall; zone 1 is saturated backfill soil, zones 2 and 3 are submerged backfill and foundation soil, zones 4 and 5 are backfill and foundation rubble, zones 6 and 7 are alluvial clay, zone 8 is the caisson wall and zone 9 is the interface.

Table 3.6. Material properties for model, after Iai *et al.* (1998) and Dakoulas & Gazetas (2005)

Materials	Density (Mg/m^3)	Friction angle(^{o})	Permeability (m/s)
Saturated backfill	1.8	37	$4*10^{-5}$
Submerged backfill and foundation	0.8	37	$4*10^{-5}$
Caisson wall	2.1		
Alluvial clay	1.7	30	$1*10^{-8}$
Rubble in backfill and foundation	2.0	40	$4*10^{-4}$
Friction angle at bottom of concrete caisson =30 deg. Friction angle at back of concrete caisson =15 deg.			

As the active earth pressure on the wall is considered to be the failure force, whether the low water level or the high water level is considered as the worst design case is, in practice, not significant. In the low water level case, the active pressure is

less than in the high water level, the reason being the reduction in the density of backfill soil; on the other hand, the stability weight of the caisson wall will also be reduced for the same reason, and equally, the density of soil and the density of caisson will increase in the high water level case.

For practical engineering, it is known that it is vital to design the caisson wall for both cases and then the worst case is taken. In this model, the low water level is considered in the calculation as recommended by Elsharnoby *et al.* (2004), because it produces the worst case concerning stress at rock base level. This problem will be investigated in Chapter 4.

As a result, the backfill layer is divided into layers; the top layer is saturated soil with unit weight γ = 1.8 Mg/m^3 and 4 m thickness, the submerged soil is measured under the water level with a submerged unit weight of γ = 0.8 Mg/m^3. Rayleigh damping coefficients (α = 0.1714 and β = 0.00174) were used to ensure the stability of the numerical analysis process. Also, the horizontal and vertical permeability coefficients are used for each material as illustrated in Table 3.6.

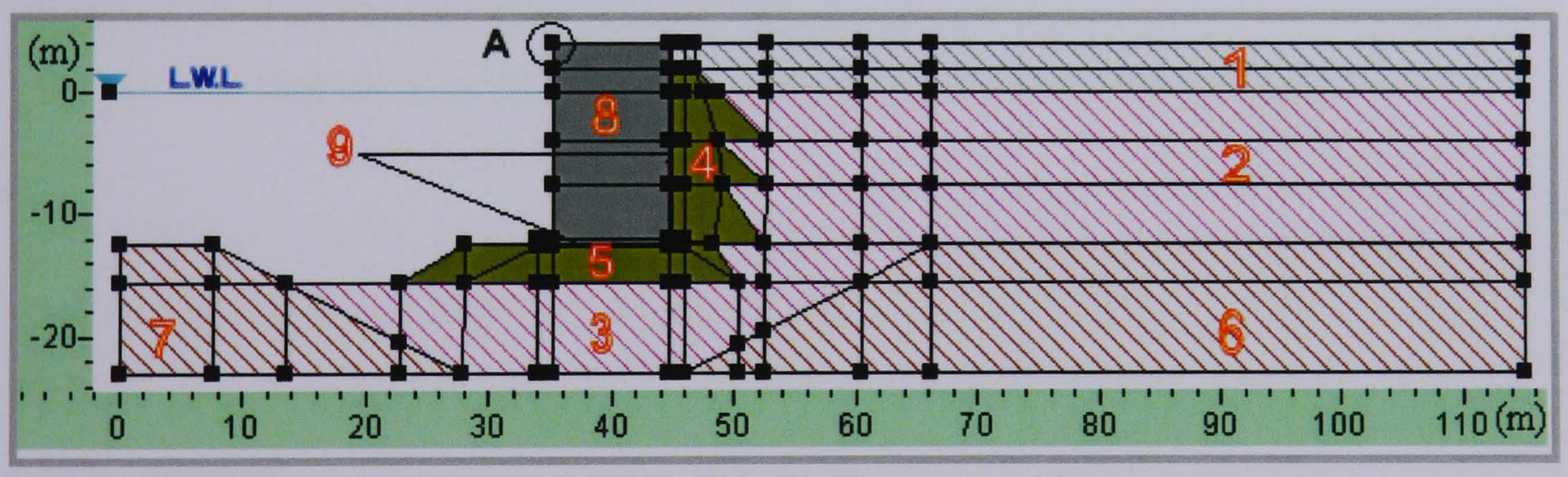

Figure 3.10. Geometry (in natural scale) and material zones of the Port Island PC1 quay wall

3.5.3 Constitutive model parameters

The backfill and foundation layers are modelled using the P-Z sand modified constitutive model described in Section 3.2 for which the parameters used in the calculation were obtained from the series of cyclic triaxial tests conducted prior to the earthquake by Nigase *et al.* (1995) and presented by Ishihara *et al.* (1996). In their

work, undisturbed frozen samples of Massado soils excavated from the northern section of Port Island were tested for different overconsolidation ratios (OCR=1, 2 and 4) and different relative densities (D_r = 37%, 54% and 57%), as shown in Figure 3.11.

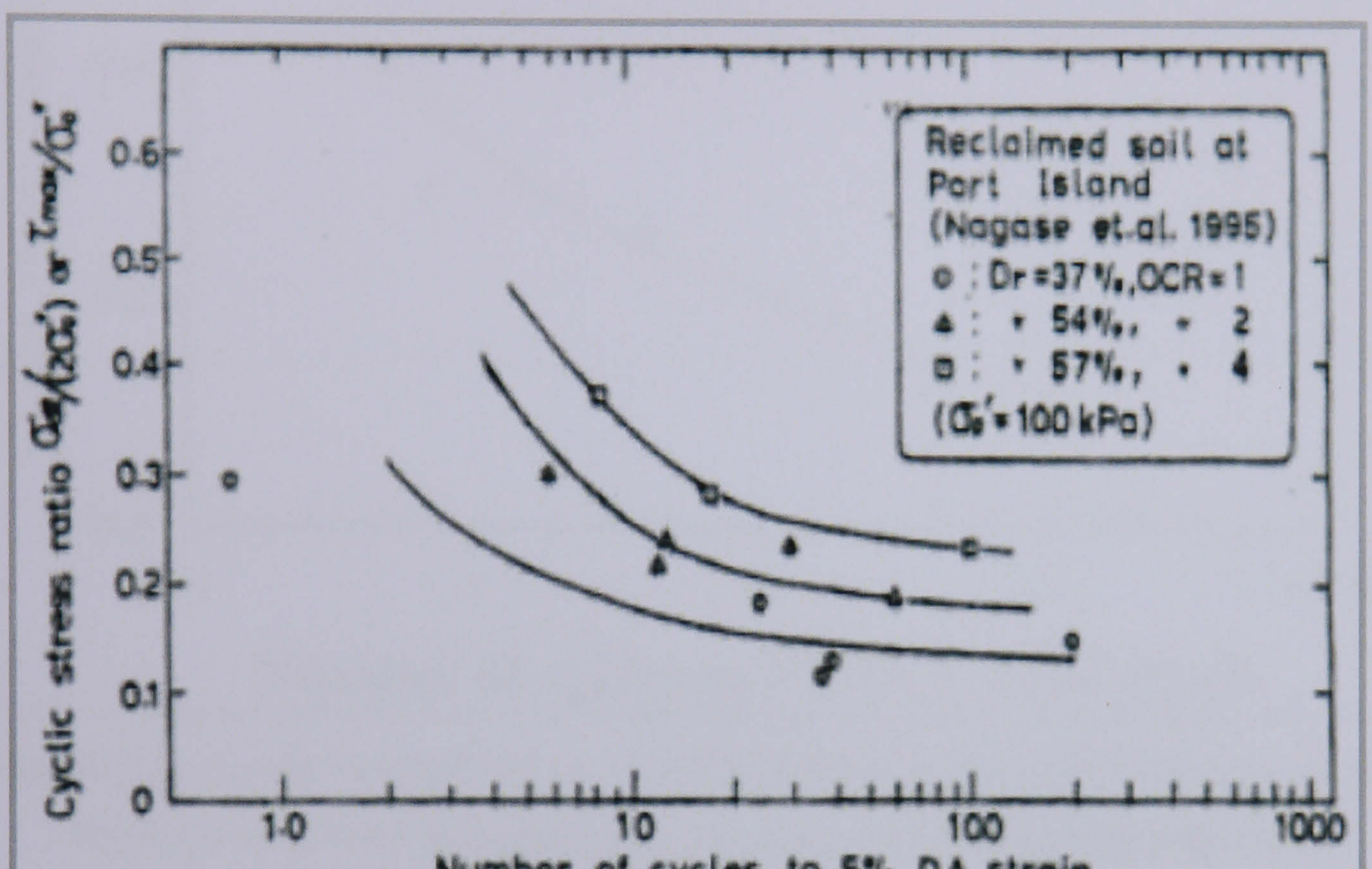

Figure 3.11. Cyclic strength curves of reclaimed soil at Port Island performed by Nigase *et al.* (1995), as reported by Ishihara *et al.* (1996)

Since the SPT-N value tests of Kobe Port Island presented by Inagaki *et al.* (1996) showed the average density for reclaimed Port Island sand to be 41.7% (see Section 3.4), the results of the sample with D_r = 37% performed by Nigase *et al.* (1995) are used in the present study. The results of the calibration procedure in terms of the cycles required to generate cyclic development of 5% double-amplitude axial strain as describe in Section 3.3.2, were estimated by back-fitting the liquefaction strength curve obtained by cyclic triaxial tests on samples from Port Island conducted by Nigase *et al.* (1995). These are shown in Figure 3.12 together with the corresponding parameters shown in Table 3.7.

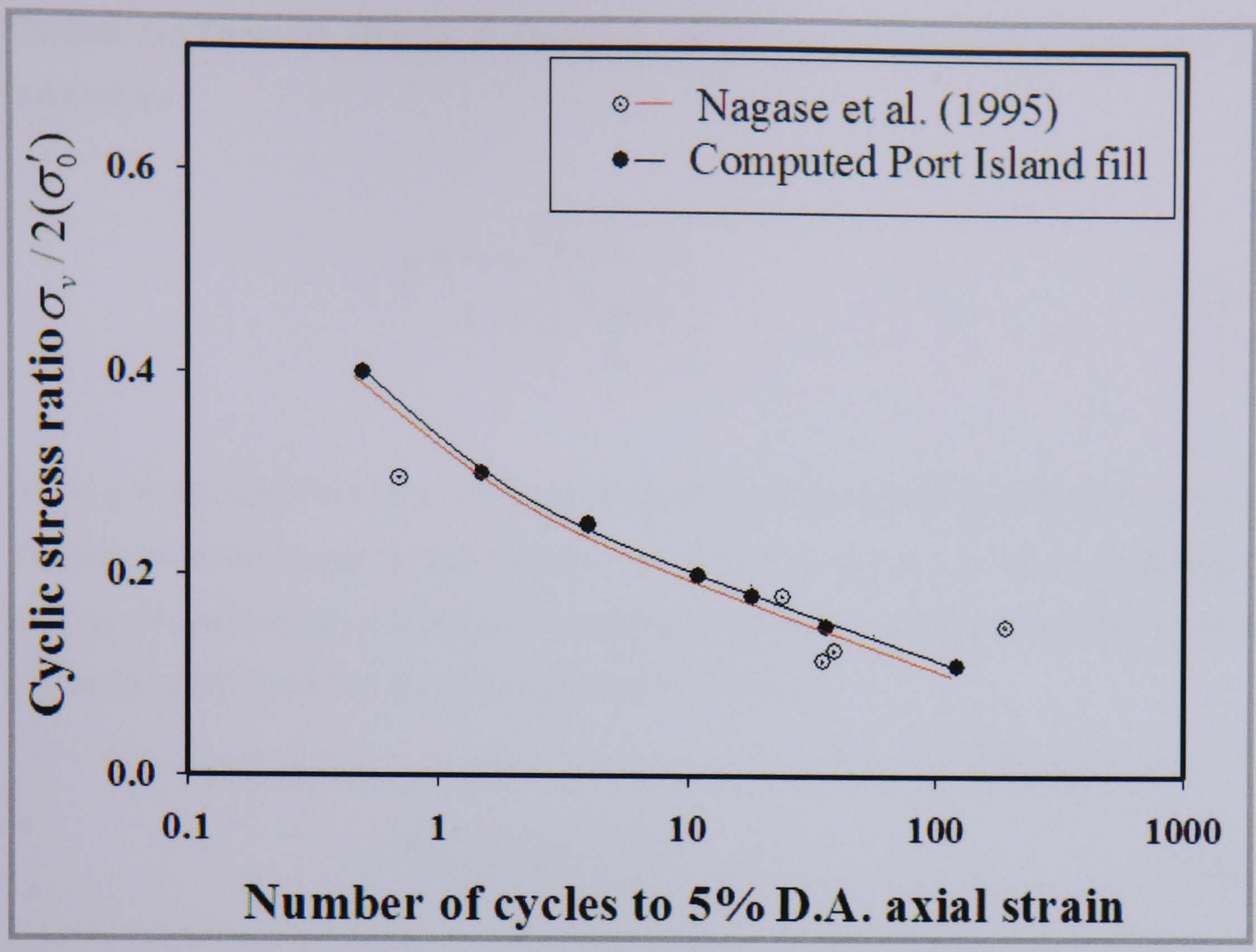

Figure 3.12. Cyclic strength curves of reclaimed soil at Port Island performed by Nigase *et al.* (1995); as reported by Ishihara *et al.* (1996) compared with predictions using the modified P-Z sand model

Table 3.7. Model parameters for relative density, D_r= 41.7%

M_f	M_g	C	α_f	α_g	K_{ev0}	G_{es0}	m_v	m_s	β_0	β_1	H_0	H_{U0}	γ	γ_U	p'_0
0.58	1.3	0.9	0.45	0.45	340	175	0.5	0.5	6	0.76	680	3000	8	7.1	100

The caisson wall is modelled as a homogeneous elastic material with the following properties assigned to the wall: Young's modulus E = 20 GPa and Poisson's ratio v =0.25. It should be noted that interface elements were used to take into account the sliding and separation between the quay wall and the soil. The selected interface properties along the base of caisson were: Young's modulus E = 208 MPa, Poisson's ratio v = 0.3, cohesion C = 1 KN/m^2 and friction angle ϕ = 30°. The interface properties behind the caisson were the same as those of the base, except for friction angle, which was taken as ϕ = 15° as used by Iai *et al.* (1998) and Dakoulas & Gazetas (2005). The stress:strain response of the clay layers was described by the modified

Hardian and Drnevich (Hardin & Drnevich, 1972) relationship given in term of *p-q* notation as:

$$q = \frac{G_{max}\varepsilon_a}{1 + R_f\left(\frac{G_{max}\varepsilon_a}{q_f}\right)} \tag{3.44}$$

where q is the shear stress; ε_a is the shear strain; q_f is the maximum shear stress is a function of friction angle ϕ_c and cohesion C_c of the clay and R_f is a material constant. In order to capture the influence of confining pressure on stiffness degradation, the maximum shear modulus, G_{max}, is calculated as follows:

$$G_{\max} = G_0 p_a \left(\frac{p'_0}{p_a}\right)^m \tag{3.45}$$

where G_0 is the value at the reference confining pressure p'_0, m is a material constant that controls the rate of decay of stiffness with stress and p_a is the atmospheric pressure. The material parameters used in the simulations for the typical clay are listed in Table 3.8.

Table 3.8. Modified Hardin-Drnevish model (HD) parameters for clay layer

G_0	p'_0	m	v_c	C_c	ϕ_c	R_f
75 MPa	143 kPa	0.5	0.4	5 kPa	30°	1

3.5.4 Input motion for dynamic analysis

The seismic excitation input file in both horizontal (E-W) and vertical (U-D) directions were recorded by a seismometer installed at a depth of 32 m in the northern area of the Port Island site, very close to PC1, adopted by the development Division, Kobe city, in October 1991 and reported by Iwasaki & Tai (1996). There are three readings in three directions: south-north (S-N), east-west (E-W) and up-down (U-P).

The PC1 caisson wall is located at the western area of Kobe Port and runs in a north-south direction; therefore (E-W) and (U-D) motions are taken in this study. The peak acceleration values recorded reached 4.80 (m/sec^2) and 2 (m/sec^2) as shown in Figure 3.13. The digital data were collected from Ichii (2006).

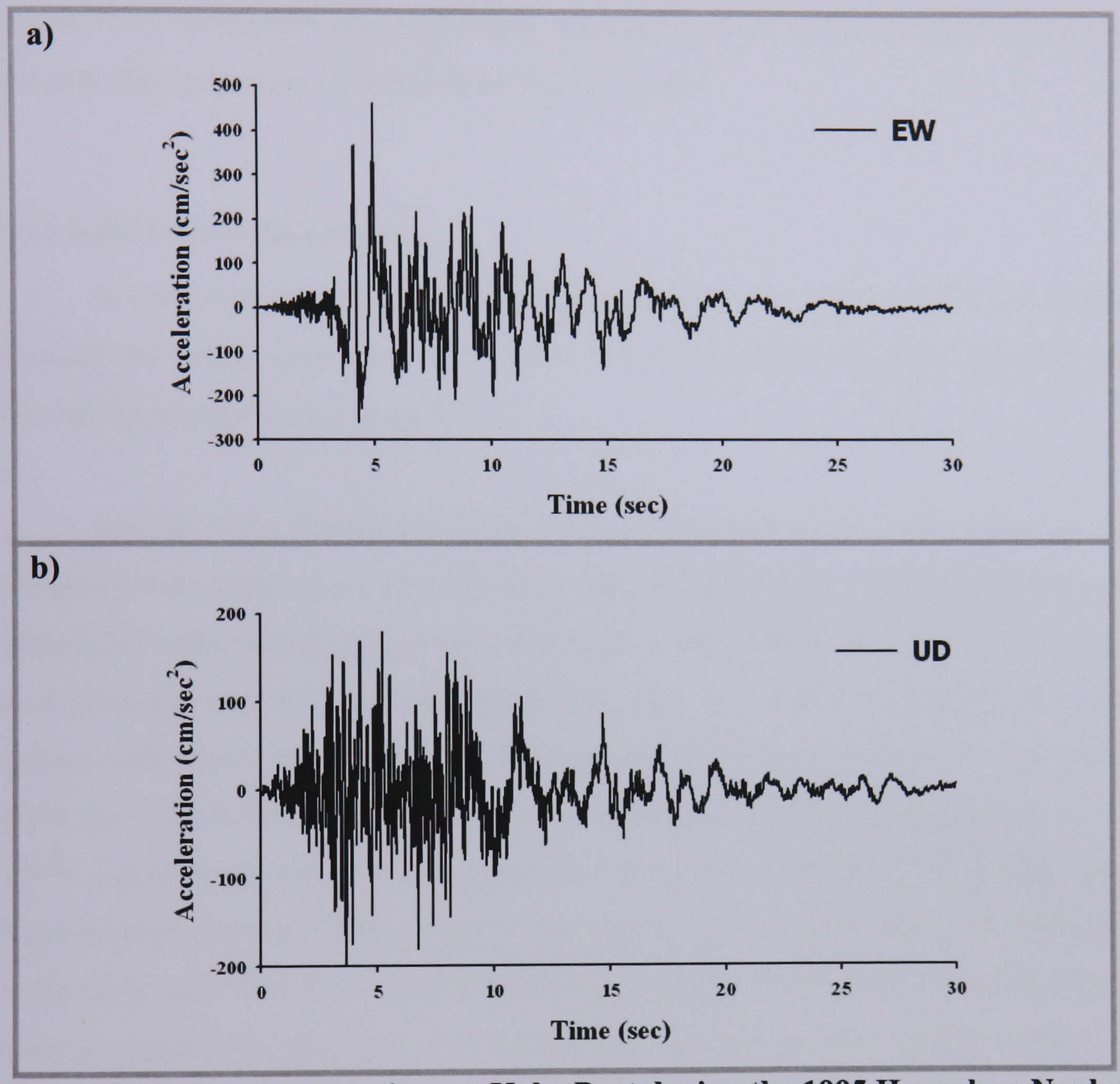

Figure 3.13. Recorded motions at Kobe Port during the 1995 Hyogoken-Nanbu earthquake; a) Horizontal (E-W) component and b) Vertical (U-D) component, reported by Iwasaki & Tai (1996). The digital data were collected from Ichii (2006)

3.6 Results of effective stress analysis

The dynamic analysis was performed in two steps. The first step consisted of an elastic static analysis, which is necessary to take into account the effect of the soil self-weight before the earthquake. In the second step, a dynamic analysis for the period of the earthquake was performed, starting from the initial effective stress state and pore fluid pressures obtained from the first step.

3.6.1 Initial stress distribution

A static analysis was performed before the dynamic response analysis, both to simulate the initial stress distributions and to take the effect of gravity into account. The results are shown in Figure 3.14.

Results using Rankin theory as discussed in Section 2.2.1 are computed and compared with initial stress distribution results in Figure 3.14. First, section a-a (just behind the wall) had computed earth pressures at rest, which are consistent with the earth pressures used in current design practice, (i.e. $k_0 = 0.35$). Section b-b below the caisson wall shows that the vertical stress below the wall corresponds to the design stress (i.e. 300 kPa). This result is also consistent with practice design (Iai *et al.*, 1997). At the front area of sand replacement, section c-c in Figure 3.14 (a) shows that the horizontal stress is almost equal to the vertical stress. This is due to the influence of the quay wall. However, it seems that these complex initial stress conditions might have a significant effect on the mechanism of gravity quay walls during the earthquake. The final displacement at point A on the seaward corner of the quay wall was 0.01 m in the horizontal direction and 0.09 m in the vertical direction.

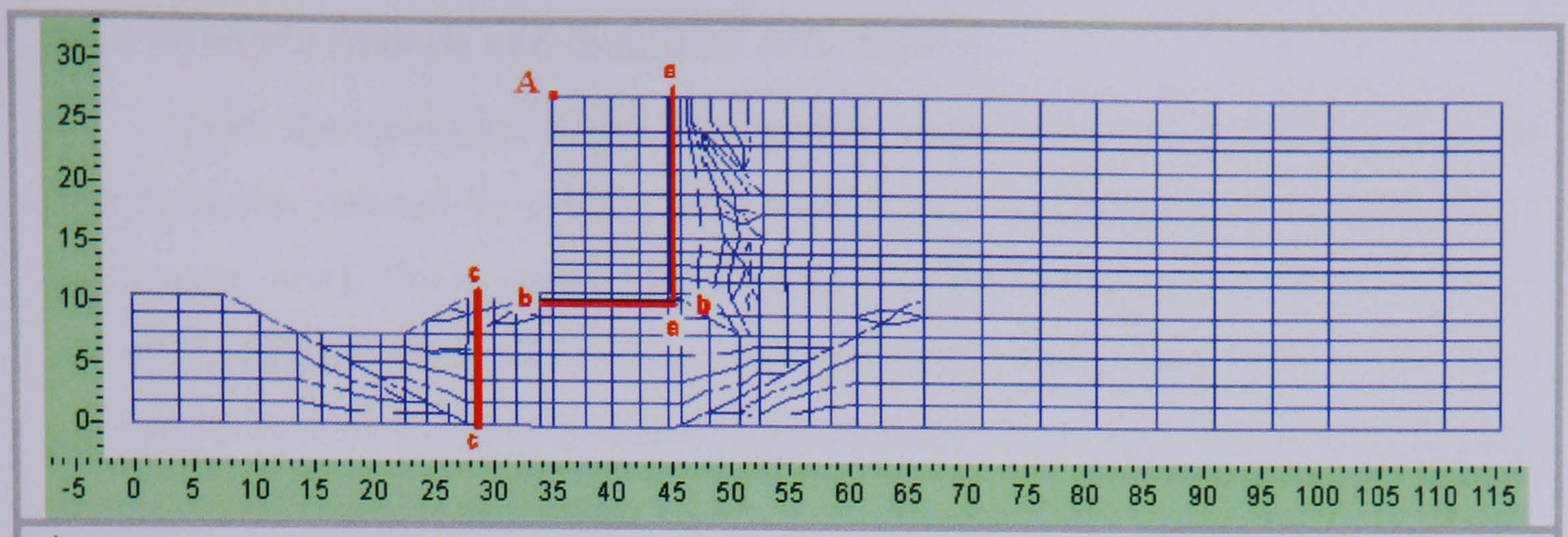

a)

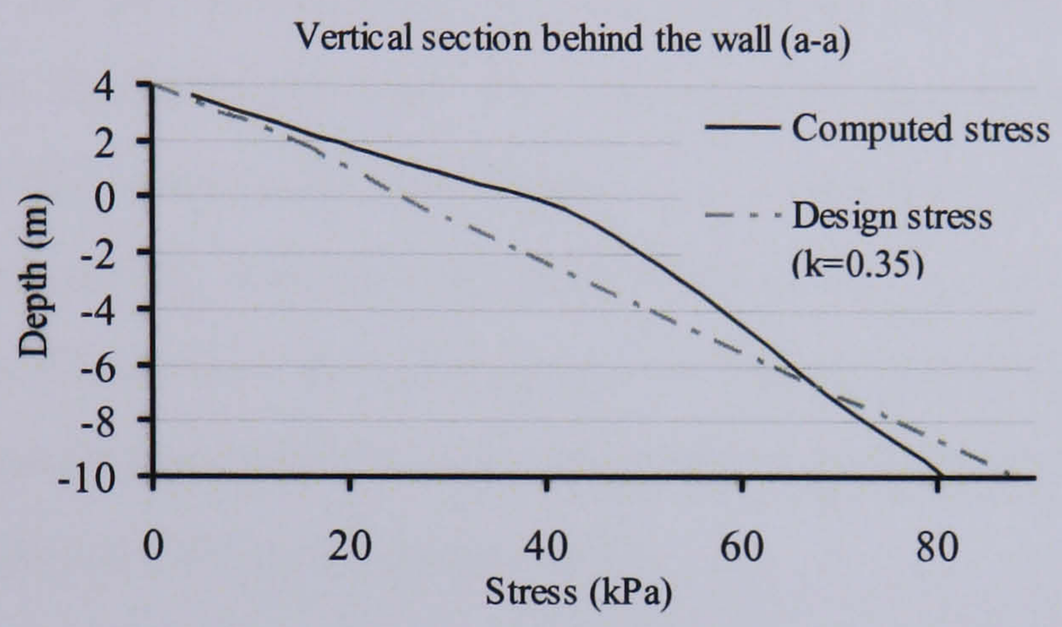

b)

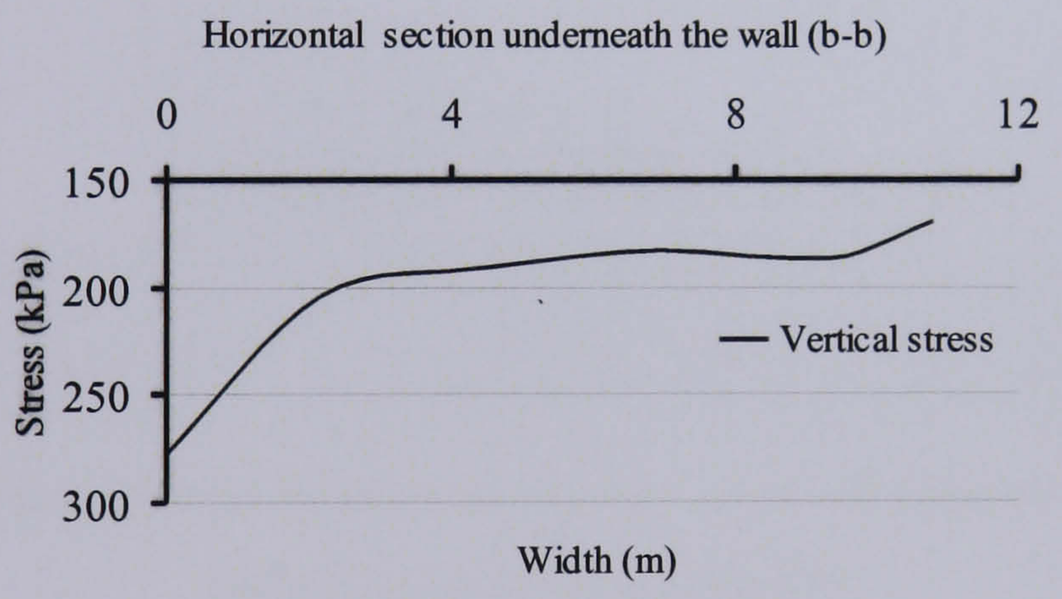

c)

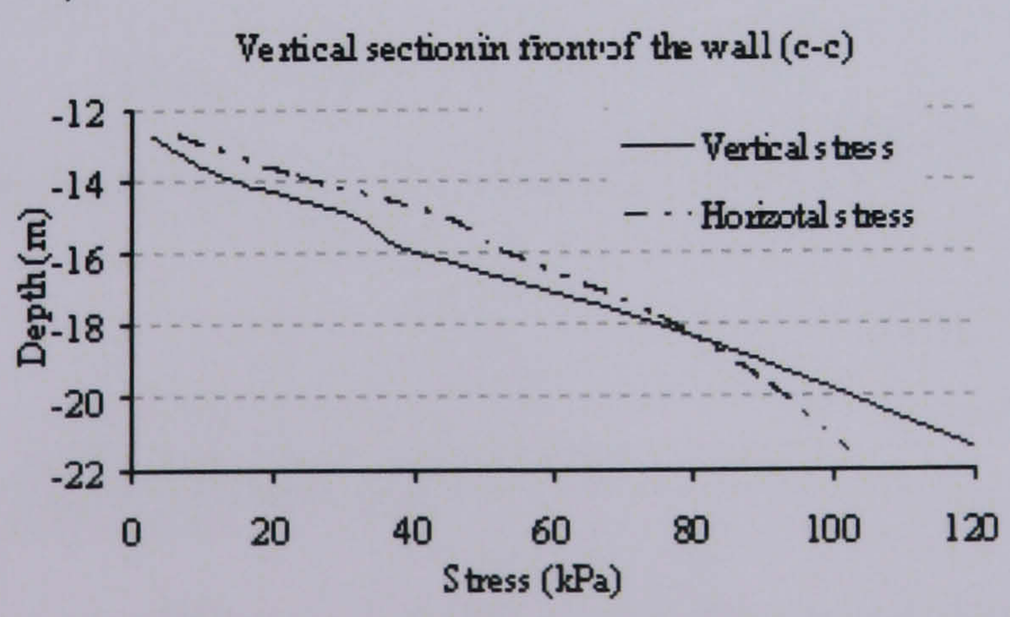

Figure 3.14. Initial stress distributions for different sections. a) Vertical section behind the wall (a-a), b) Horizontal section underneath the wall (b-b), and c) Vertical section in front of the wall (c-c)

3.6.2 Dynamic analysis and computed deformation

After the equilibrium state was reached by performing the static analysis, the displacements induced by gravity were reset to zero and the stresses at each Gauss point were saved. These values were then used as the initial state for the subsequent dynamic analysis. Figure 3.15 shows the deformed mesh of the typical quay wall section of PC1 at the end of shaking (30 seconds). It can be seen that significant seaward displacement and tilting of the wall has occurred. As the wall is rigid, its movement is due to the deformation of the foundation rubble, which creates a significant heave at the toe of the wall. The computed displacement at point A on the seaward corner of the quay wall (see Figure 3.15) was 3.28 m (2.3 m to 3.13 m measured), the wall settled vertically by about 0.73 m (0.79 m to 1.40 m measured) and tilted into the foundation by 4.2 degrees (3 degrees measured). The computed residual deformation results for PC1 were consistent with field observations shown in Figure 3.16 (Ministry of Transport, Japan, 1997).

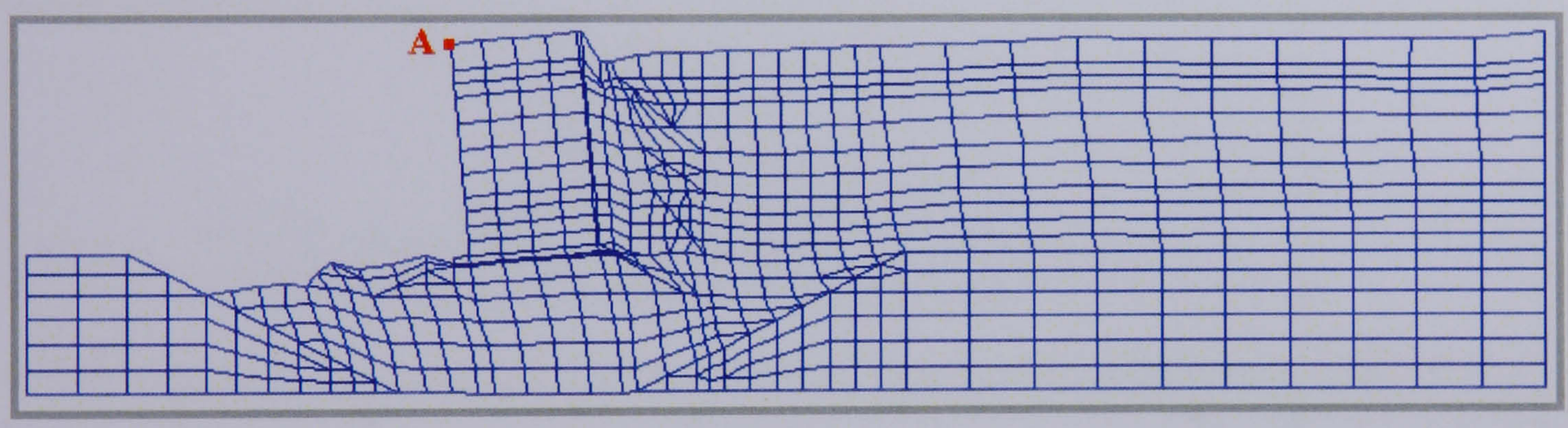

Figure 3.15. Computed deformation at the end of earthquake ($t = 30$sec) of Port Island caisson quay wall PC1

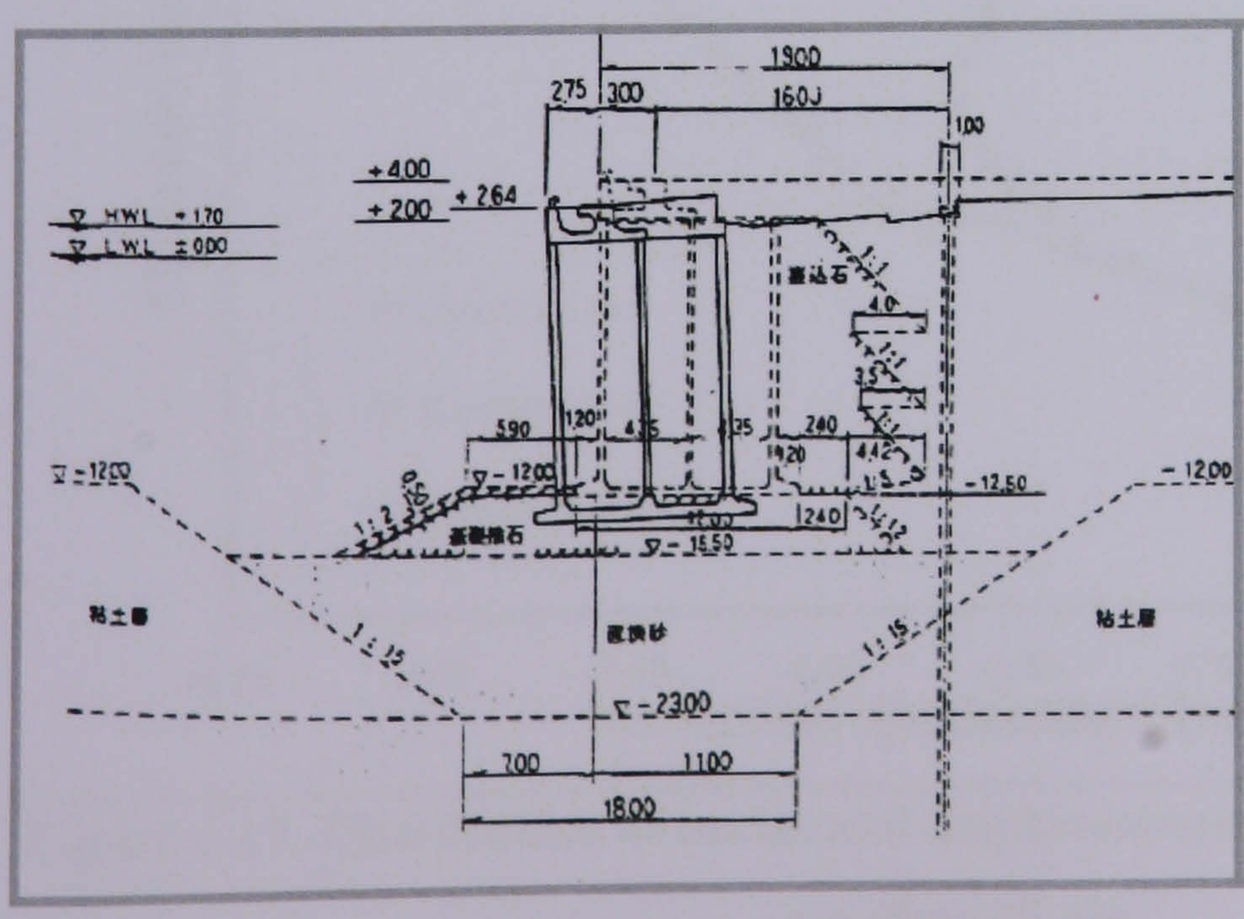

Figure 3.16. Cross section of the caisson quay wall PC1 in Port Island with observed residual deformation after Kobe 1995 earthquake, after Ministry of Transport, Japan (1997)

Figure 3.17 shows the computed horizontal displacement profiles at different sections of the backfill behind the quay wall PC1. It can be seen that section c-c, which is situated about 80 m from the wall, had approximately zero horizontal displacement until about mid-height; thereafter it displaced outward by 0.4 m. This part of the response is quite similar to the lateral spreading observed over a distance of 50-200 m from Rokko Island quay walls (Ishihara *et al.,* 1996). Since the displacements are relatively small, this also suggests that the model boundary has been located sufficiently far from the quay wall to have negligible influence on the results. At section b-b, which is situated approximately 20 m from the wall, no displacement can be noted in the clay layer. However, the total surface displacement is approximately 2.8 m at section a-a while the displacement level with the base of the wall is approximately 1.8 m. At this location it is possible to observe the small influence of the interface elements placed beneath the wall, which has allowed the wall to slip horizontally by approximately 0.3 m.

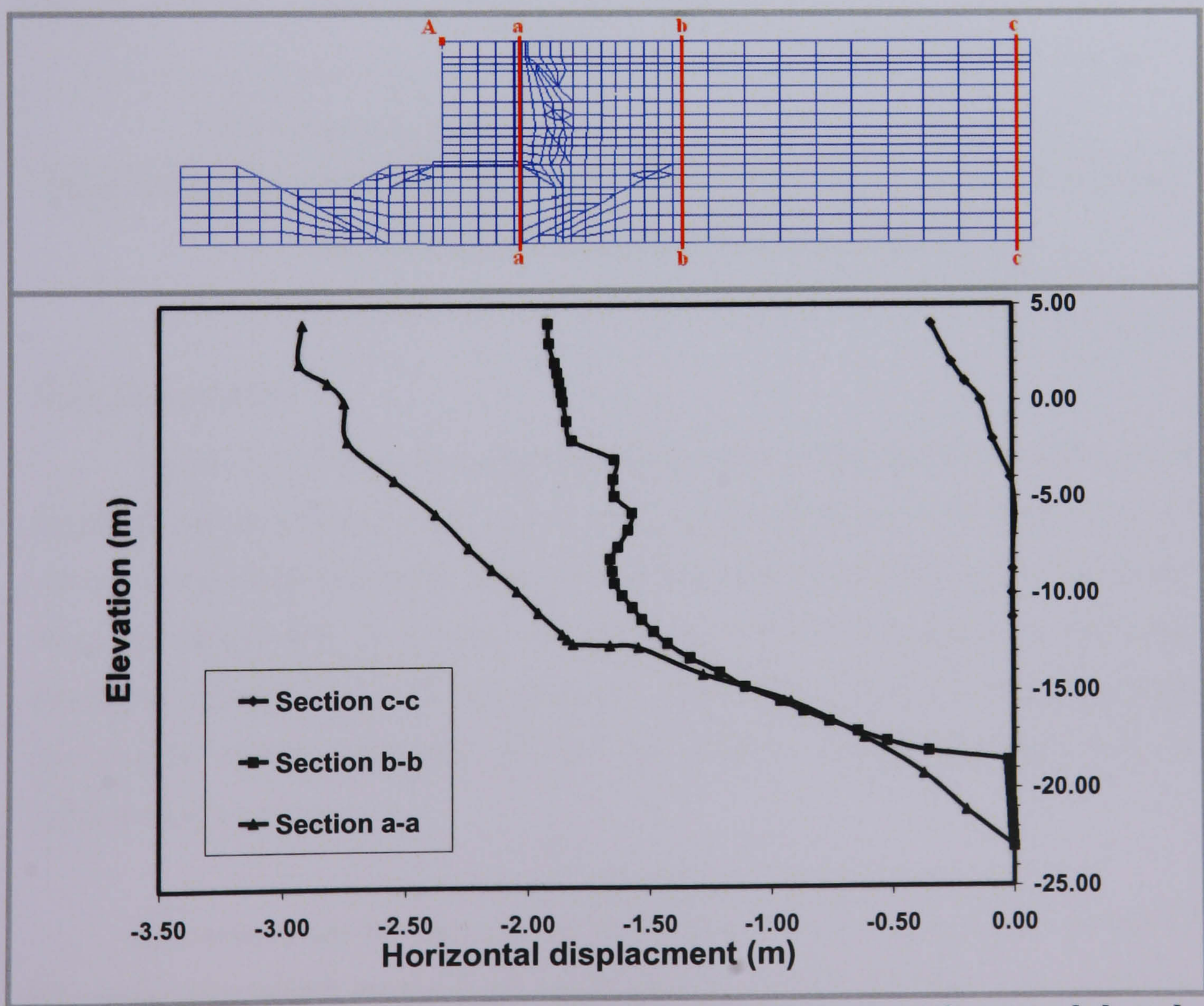

Figure 3.17. Distribution of horizontal displacements along sections a-a, b-b and c-c after 30 sec

The computed lateral displacements and settlements at the service level behind the wall and the observed results from Ishihara *et al.* (1996) are shown in Figure 3.18. It can be seen that the computed results are in good agreement with the observed results. However, Figure 3.18 shows that the maximum lateral displacement occurred directly behind the wall, thereafter reducing until reaching about 30 m distance behind the wall, afterward remaining steady while the maximum settlement occurred at 29m from the wall. While significant differences between the computed and the observed deformations exist, the general shape and maximum magnitudes are similar.

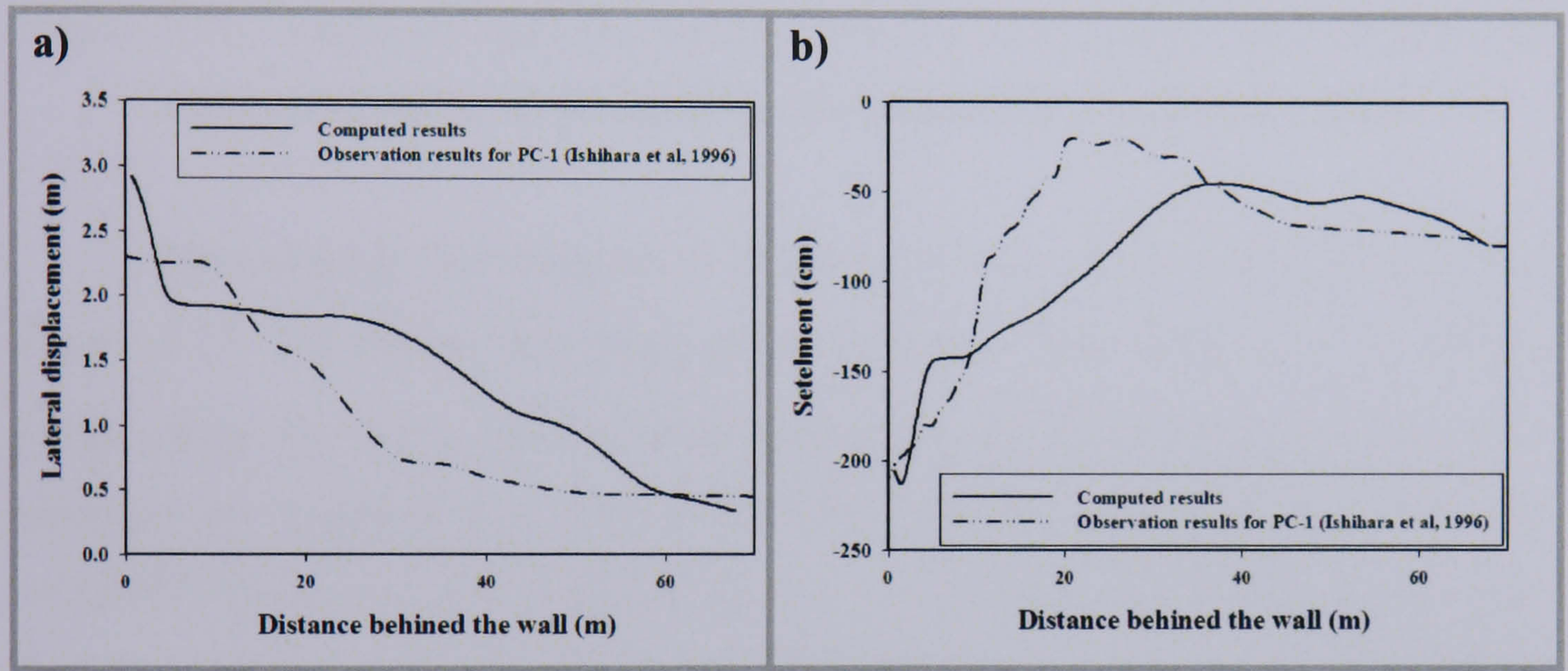

Figure 3.18. Computed and observation results, a) Lateral displacement behind the wall and, b) Settlement behind the wall

3.6.3 Time history

Figure 3.19 depicts the response time history of the horizontal and vertical displacements at the top seaside corner of the quay wall (point A on Figure 3.10). It can be noticed that the seaside corner settled vertically by approximately 0.73 m and displaced horizontally by as much as 3.28 m as a result of liquefaction. The large horizontal displacement is due to significant rotation of the wall (4.2 degrees), which has caused further settlement of the soil retained behind the quay wall of approximately 1.83 m.

However, it can be seen that the displacement is still increasing at the end of the earthquake, which means if the earthquake had been more than 30 seconds, the displacements would be greater.

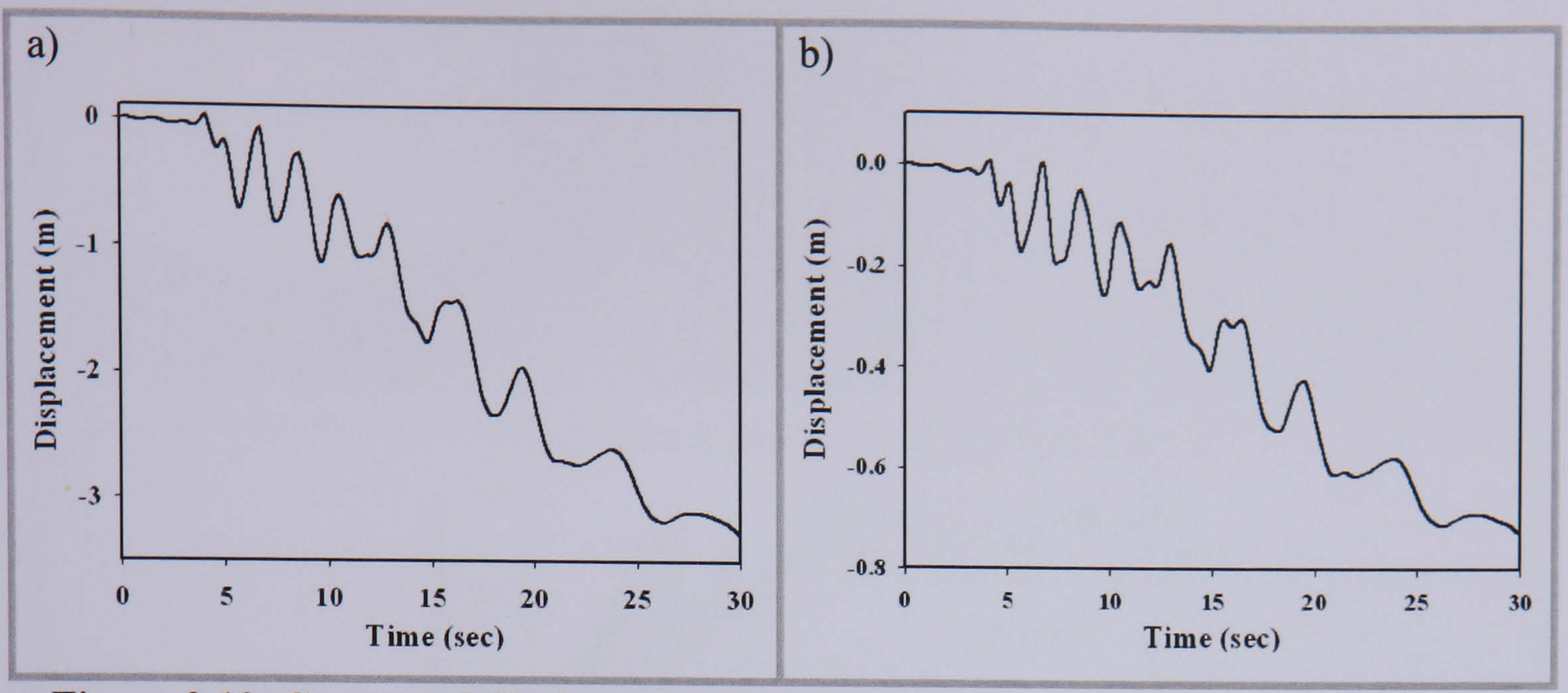

Figure 3.19. Computed displacement time history at the upper seaward corner of caisson (point A). a) Horizontal direction and b) Vertical direction

The computed time histories of excess pore water pressure ratios are shown in Figure 3.20. The excess pore water pressure ratio is represented by $r_u = \Delta u/\sigma v'_0$, where Δu is the excess pore pressure and $\sigma v'$ is the initial vertical stress. Three elements are selected: two behind the wall and one underneath the wall. The computed excess pore water pressure ratio in the foundation soil as shown for element C only reached a maximum of 0.8 and then reduced to be negative at the end of the shaking. That is because the settlement of the wall, which resulted in compaction of the soil beneath the wall, increases the confining pressure. Also, the computed excess pore water pressure ratio for element B far inland shows that the excess pore water pressure ratio (r_u) quickly reached the maximum value of 1, whereas at element A, just behind the wall, there is a slight reduction in (r_u) after reaching its maximum.

These results are consistent with observed evidence of the liquefaction of the backfill in the surrounding area of the caisson wall, i.e. the lateral displacement due to the liquefaction of the backfill was less than the lateral displacement accrued in land fill about 30 m or further behind the wall, as reported by Ishihara (1997).

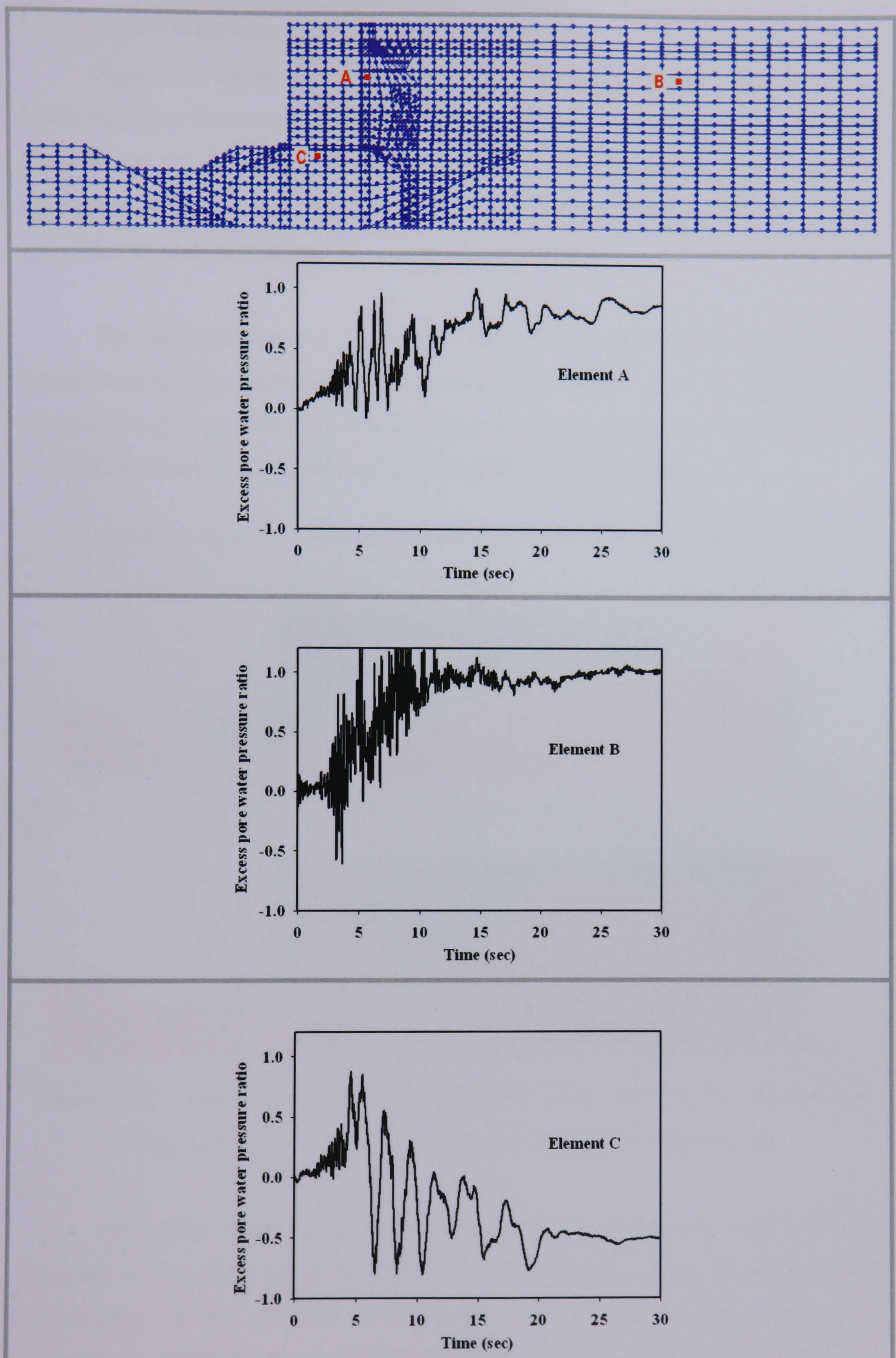

Figure 3.20. Computed time history of excess pore water pressure ratios

3.6.4 Contour diagrams

Figure 3.21 (a) and (b) portray the contour diagrams of horizontal and vertical displacements at the end of shaking at $t = 30$ seconds. In Figure 3.21 (a) the computed contours of the horizontal displacements show the formation of slip surface mechanisms that have developed within the quay wall, indicating a problem of global stability at the end of shaking.

The contour diagram in Figure 3.21 (b) shows that the retained soil behind the caisson wall settled significantly (with maximum settlement about 1 m), following the seaward movement of the caisson wall. These results are in excellent agreement with the field observation as reported by Ishihara (1997) shown in Figure 3.22.

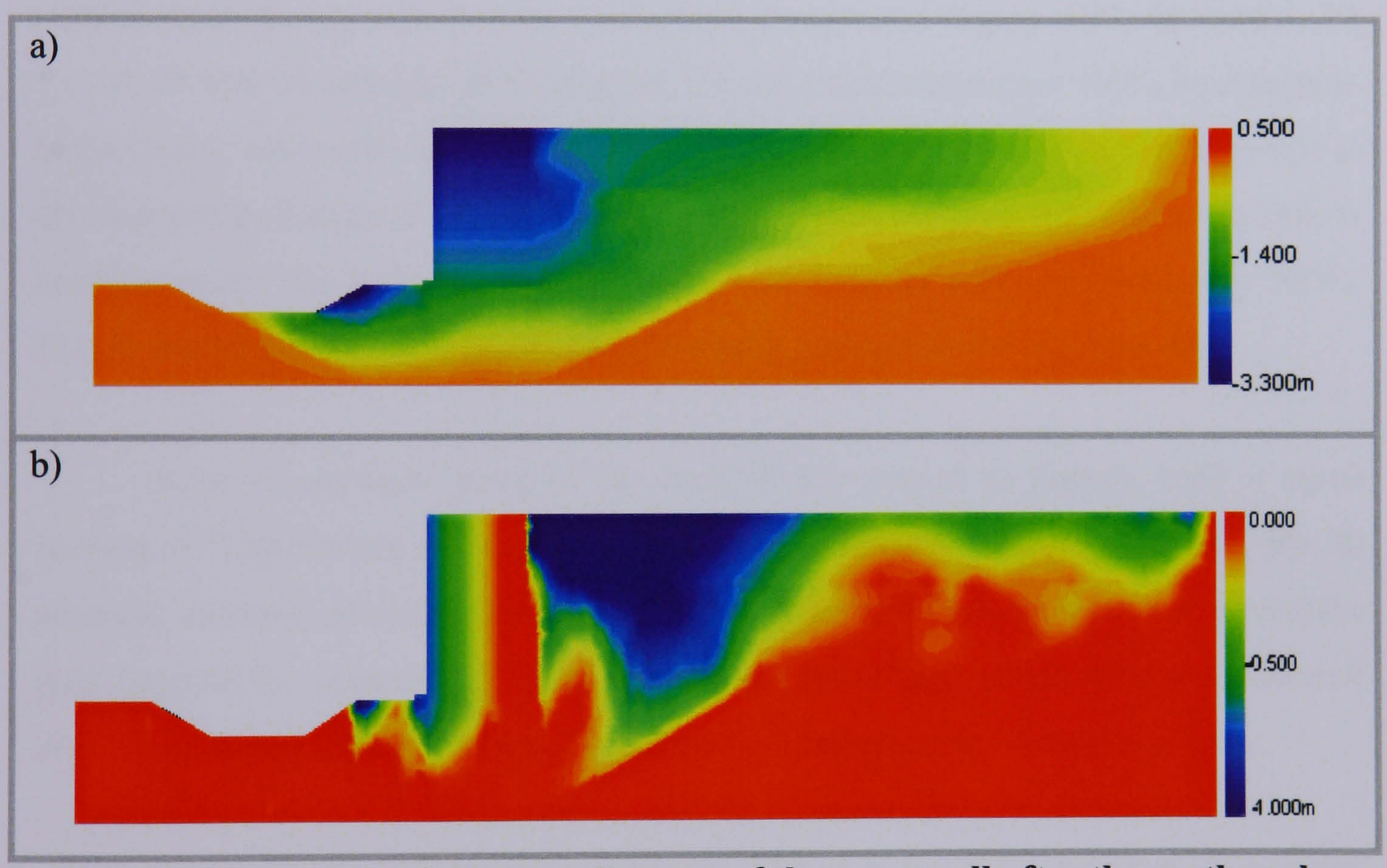

Figure 3.21. Computed contour diagram of the quay wall after the earthquake (t=30); a) horizontal displacements and b) vertical displacements

The results from the computer simulation are within the range of those observed in the field (refer to PC1 in Table 3.4) and clearly demonstrate the performance of the effective stress analysis carried out in this case study. Investigation of the interface elements placed between the wall and the foundation rubble shows negligible slip between those surfaces.

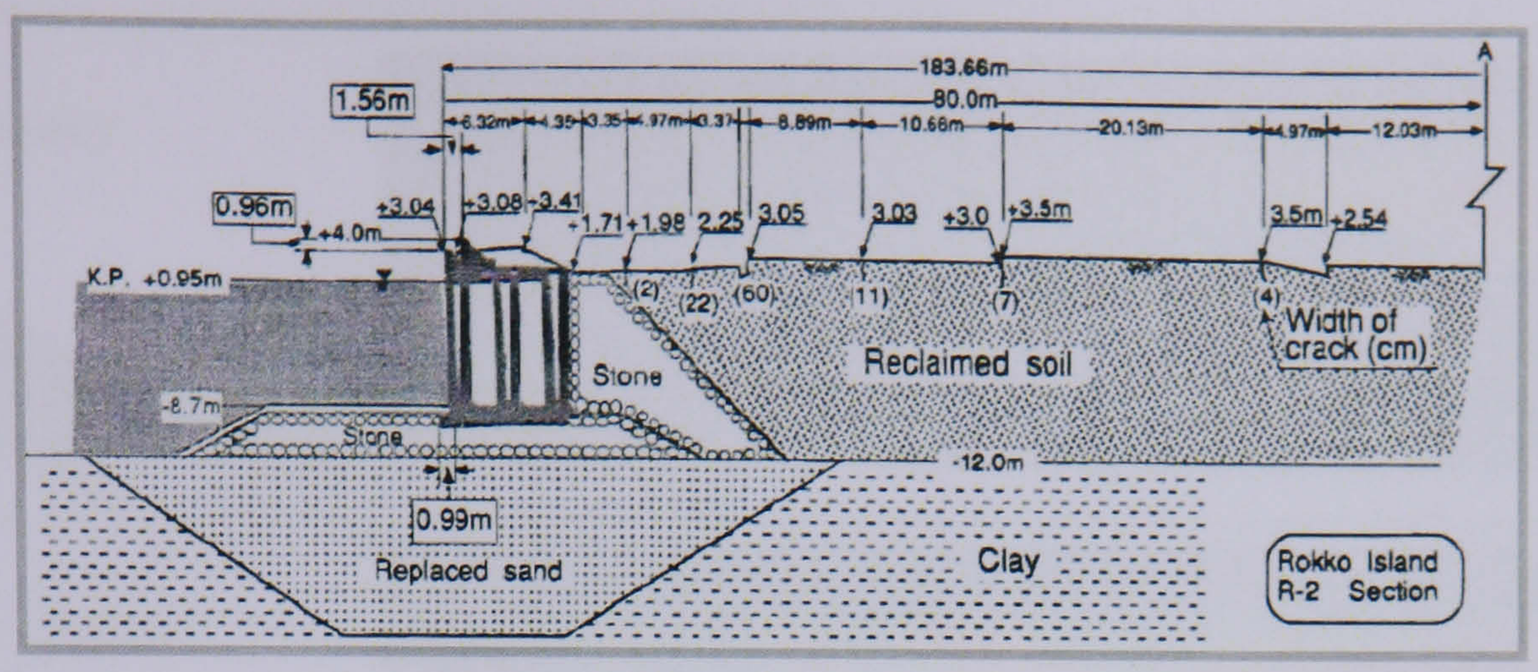

Figure 3.22. Detailed profile of the ground deformation at R-2 section in Roko Island, after Ishihara (1997)

3.6.5 Computed distributions of excess pore water pressure ratio

Computed distributions of excess pore water pressure ratio for the quay wall at various times during and after the earthquake are given in Figure 3.23, for state 5, 10, 15, 20, 25 and 30 seconds. In this figure, the red colour represents 100% liquefaction. Liquefaction starts after only 5 seconds furthest from the wall. This is probably due to the impervious nature of the caisson wall. At this time, the pore water pressure ratio is smallest under the wall and directly behind the caisson wall (approximately 50%). This is due to the wall providing extra confining pressure to the soil beneath.

After 10 seconds, most of the backfill has started to liquefy, with a small amount of liquefaction occurring at the model boundary beneath the wall. By 20 seconds, virtually all the backfill has liquefied. After this time, the pore water pressure ratio beneath the caisson wall starts to reduce. This is because the weight of the wall above has caused the sand to settle and therefore compacts the foundation layer.

This is verified by looking at Figure 3.24 showing the vertical displacements of point A at the upper seaward corner of the caisson. In Figure 3.24 (a) the top left hand corner vertical displacement is plotted, in Figure 3.24 (b) the vertical displacement in the middle of the wall surface is plotted, and in Figure 3.24 (c) the right hand corner vertical displacement is plotted. In Figure 3.24 (b), it can be seen that the centre of the wall stops settling after approximately 20 seconds, whereas in Figure 3.24 (a) the settlement increases and in Figure 3.24 (c) it reduces after 20 seconds. It can be concluded that the wall finishes settling after 20 seconds and only rotates after this time.

Figure 3.23. Computed distribution of excess pore water pressure ratio r_u for the quay wall at various times during and after the earthquake

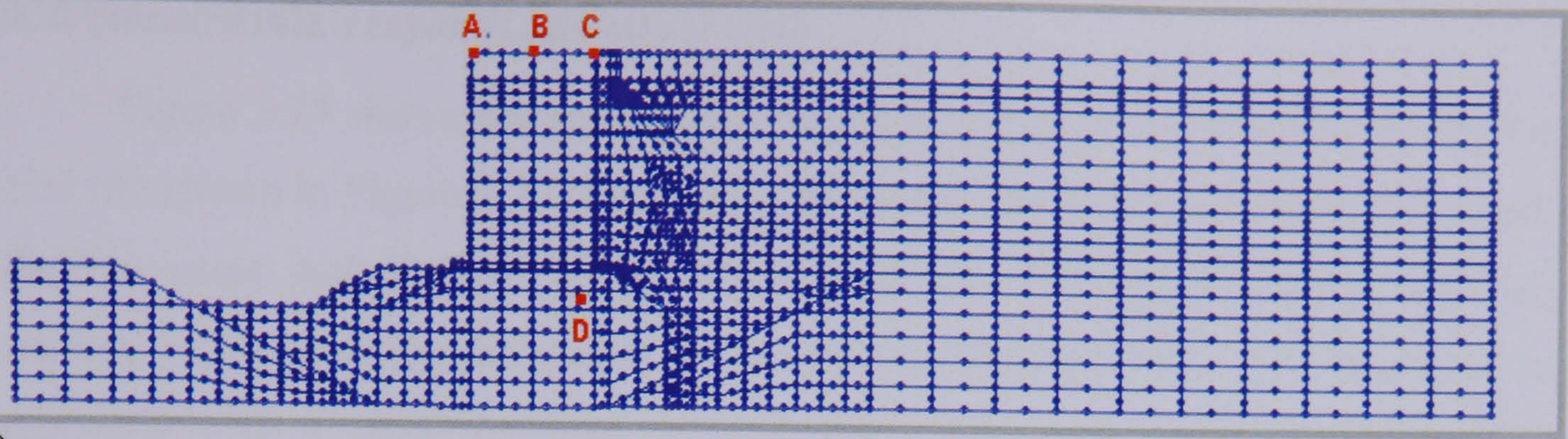

a)

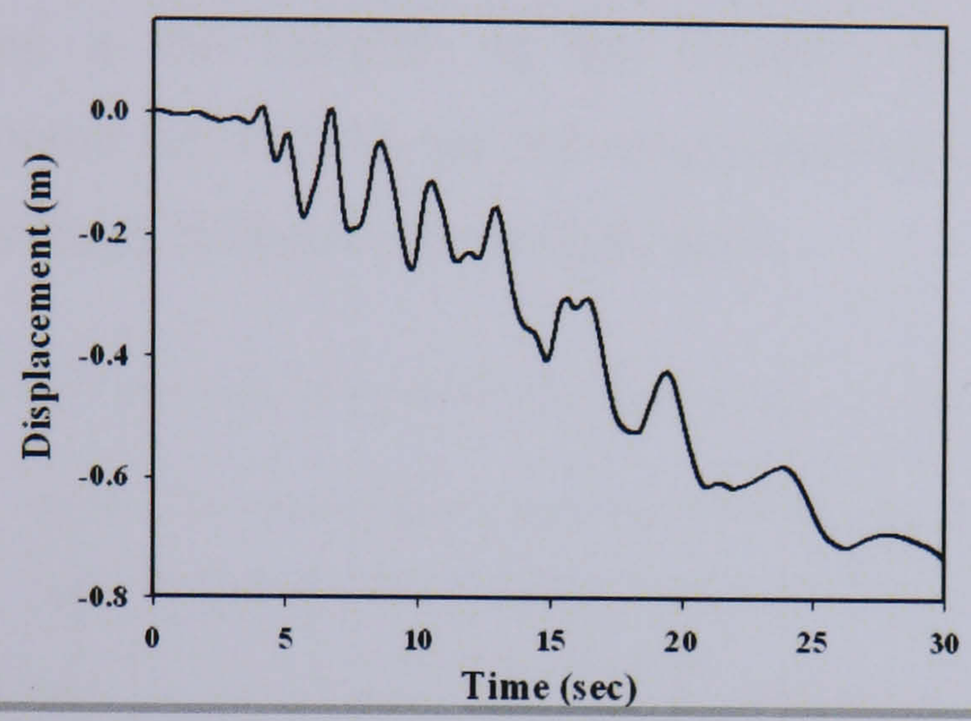

b)

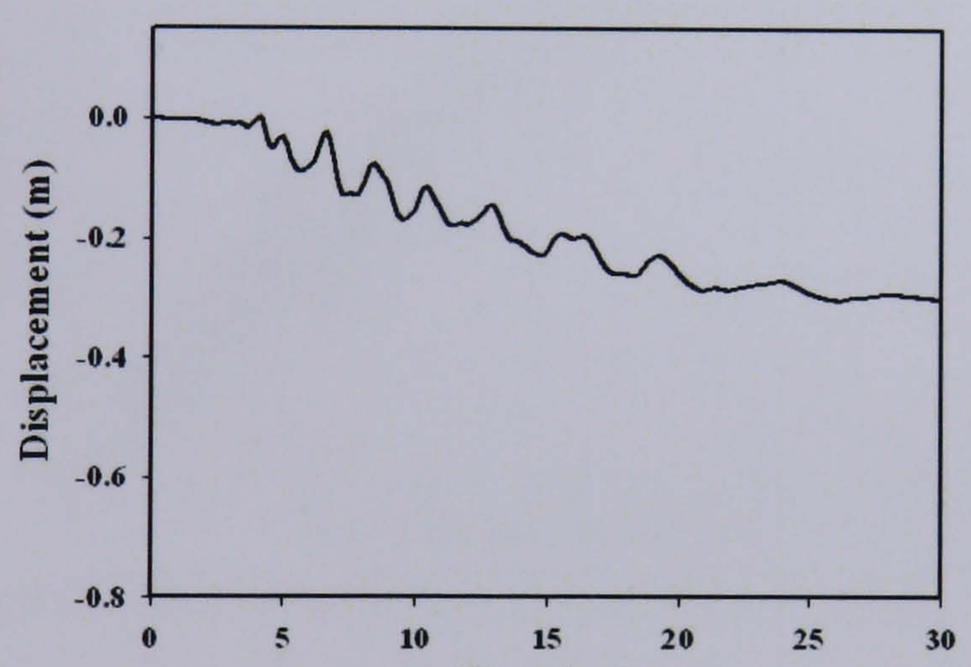

c)

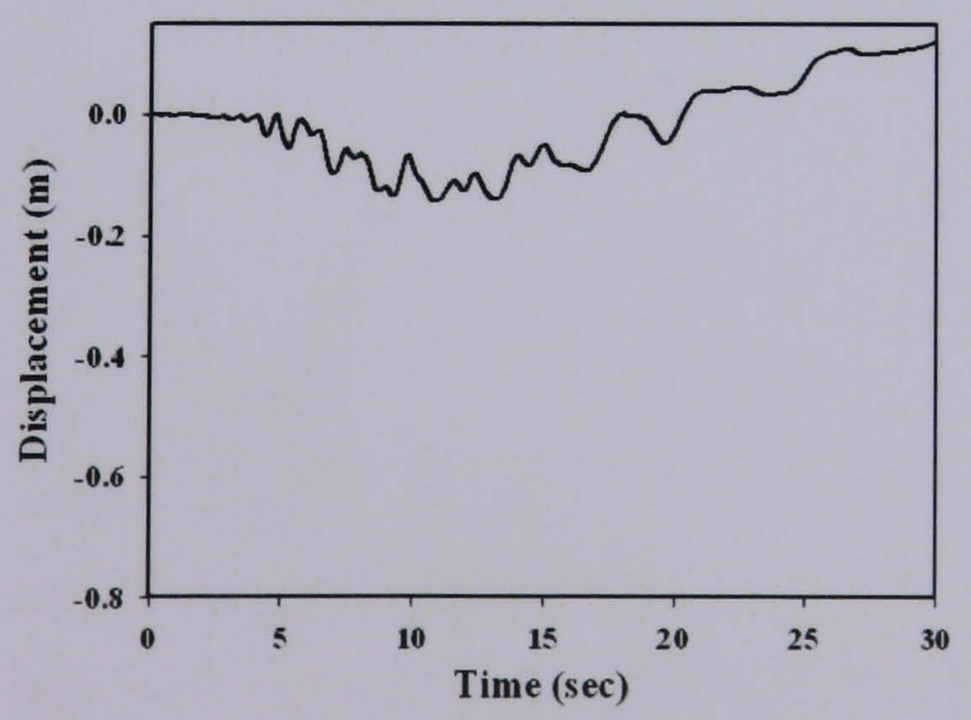

Figure 3.24. Computed vertical displacements; a) vertical displacement for point A, b) vertical displacement for point B and c) vertical displacement for point C

3.6.6 Stress:strain response and stress path

Figure 3.25 shows the stress:strain response and effective stress paths for the point (A) shown in Figure 3.20 (just behind the wall). The figure shows that the mean effective stress and deviator stress at the point (A) fell rapidly during shaking, resulting in the stress path migrating to the origin of the stress axis. This behaviour is associated with a rapid increase in pore water pressures, which indicates that liquefaction occurred in the backfill. At this location, the backfill underwent considerable shear strains (up to 20%) and the stress:strain response clearly exhibited a significant degradation of stiffness with increase strain.

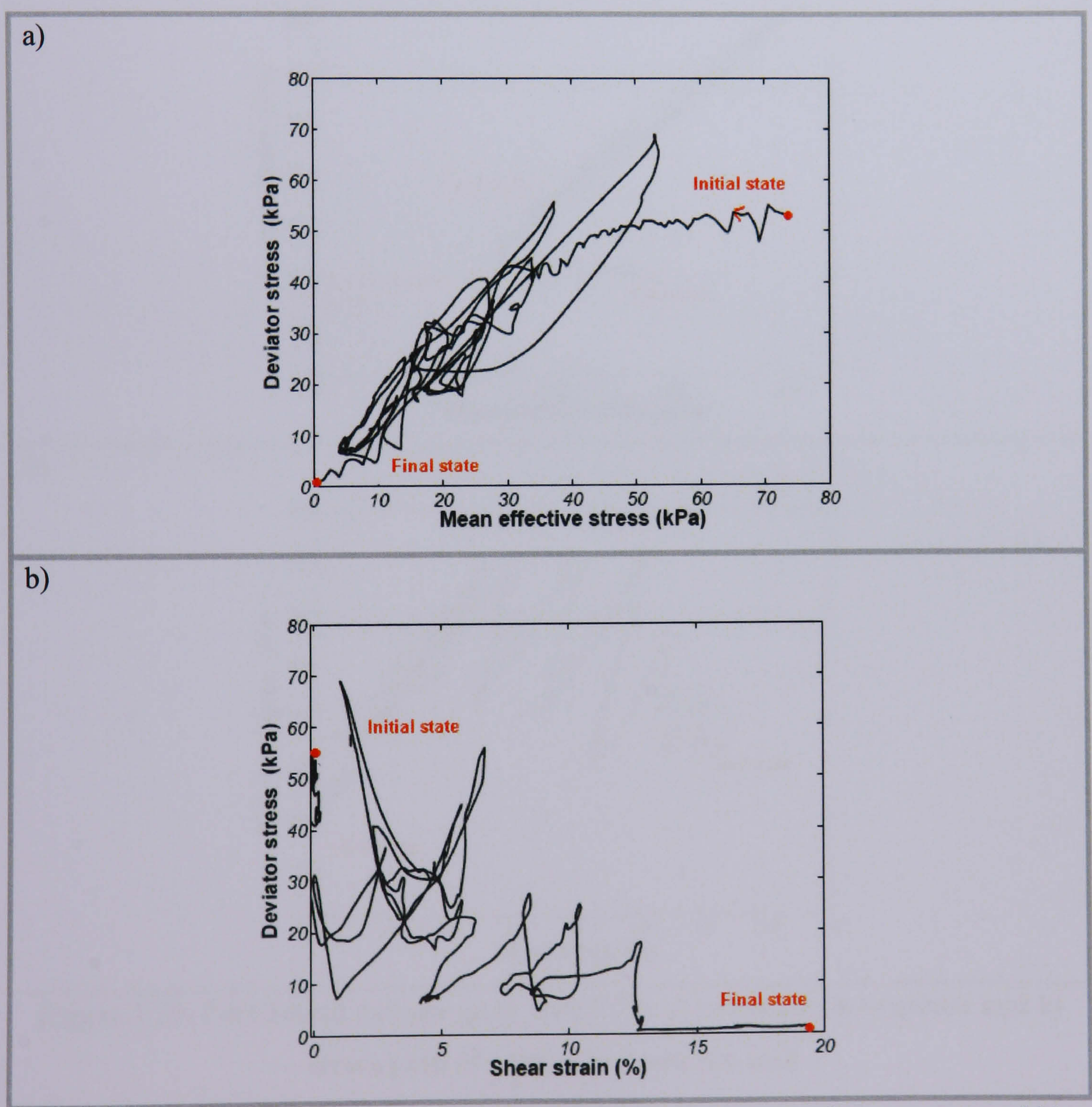

Figure 3.25. Port Island caisson quay wall PC2: a) stress:strain response and b) stress path of a point behind the wall

Figure 3.26 shows the stress:strain response and effective stress path at a point situated in the foundation rubble beneath the wall (point C on Figure 3.20). By contrast, the effective stress path moved to the left of the *in situ* stress and converged toward the ultimate strength on the critical state inertia transmitted by reaching the *phase transformation point* (Ishihara *et al.,* 1975). The maximum shear strain reached approximately 13% with a gradual loss of stiffness (to zero) as the soil reaches a critical state.

a)

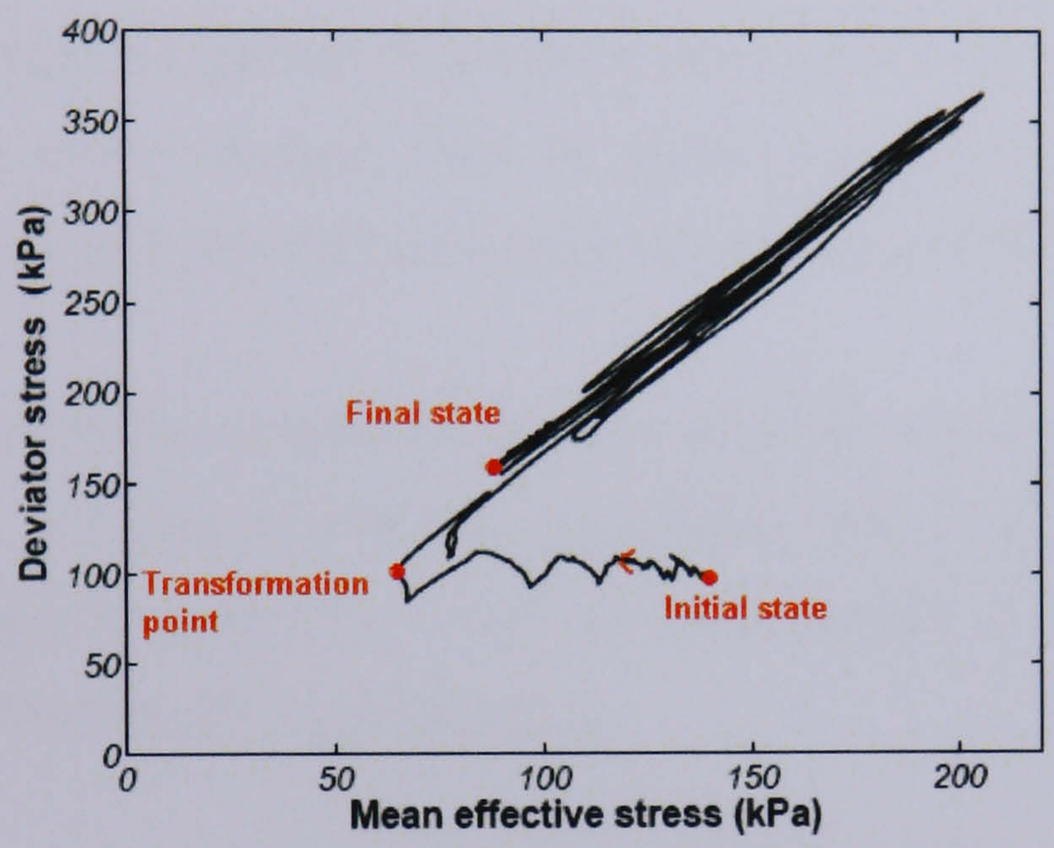

b)

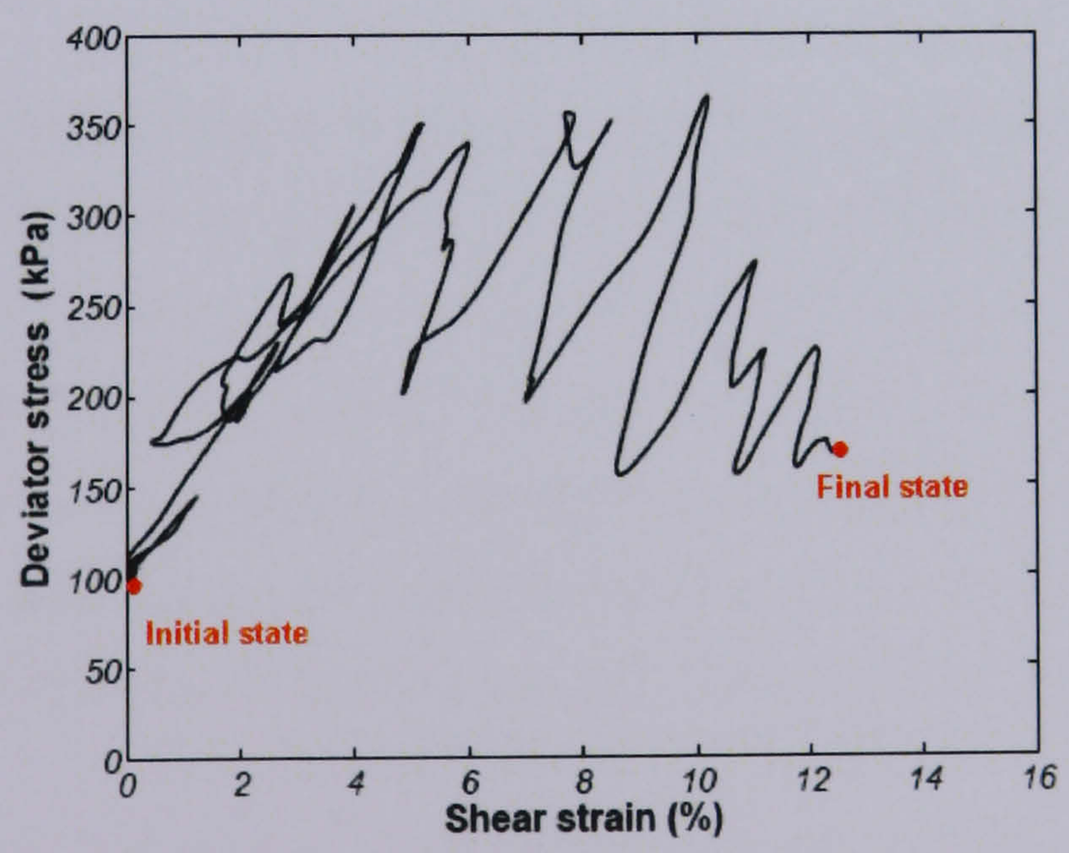

Figure 3.26. Port Island caisson quay wall PC2: a) stress:strain response and b) stress path of a point beneath the wall

3.7 Summary

A two-dimensional, effective-stress finite element procedure in conjunction with a generalised elasto-plastic constitutive model of Pastor *et al.* (1990), with slight modifications, has been conducted. The model was first validated by simulating published monotonic and cyclic test results.

The results of the monotonic tests showed excellent agreement between the experiments results and numerical simulations with successful prediction of the dilative and contractive behaviour of sand. For the cyclic tests, the model was successful in matching the general shape of the stress:strain response and the decrease in mean effective stress resulting from the excess pore pressure generation. The number of cycles to reach liquefaction in each test agreed well with those measured.

To demonstrate the validity of the finite element procedure, a model of Port Island quay walls was then developed using a finite element package UWLC. Both vertical and horizontal accelerations were applied to the model and the results were compared to the observed field measurements.

Comparison of computed and observed results show:

1. Computed overall displacements and rotations of the caisson wall were similar to those observed in the field. The computed displacement at point A (see Figure 3.10) on the seaward corner of the quay wall was 3.28 m (2.3 m to 3.13 m measured), the wall settled vertically by about 0.73 m (0.79 m to 1.40 m measured) and tilted into the foundation by 4.2 degrees (3 degrees measured).
2. The computed excess pore water pressure ratios were consistent with observed evidence of the liquefaction phenomenon reported by Ishihara *et al.* (1996).

The final aim of this thesis is to assess the seismic safety of quay walls in Jeddah Port. As part of this assessment, recommendations will be made on how to improve existing quay wall specifications as well as recommending rehabilitation strategies for existing walls that have insufficient seismic capacity.

To do this the PZ sand model will now be used to study how various soil parameters and quay wall geometry affect liquefaction behaviour. The results of this parametric study will be used to inform mitigation strategies developed later in this thesis.

CHAPTER FOUR

4. PARAMETRIC STUDY

4.1 Introduction

This chapter presents the results of computer simulations that investigate the effects of various soil parameters, wall geometry and seismic excitation on the seismic performance of gravity quay walls. The results of this parametric study were used to design the computer simulations (investigated in Chapter 6) conducted for Jeddah Port quay walls. The effects of the major parameters, such as wall dimensions, tidal range, intensity of the seismic excitation (represented by the seismic design coefficient) and the friction angle of the backfill, on the seismic behaviour of gravity quay walls were investigated by Elsharnoby *et al.* (2004). This study was based on a simplified method (a pseudo-static approach), which did not consider the effect of liquefaction. This study uses a soil model that can account for the liquefaction behaviour of the soil and therefore will better inform practicing engineers on the effects of these parameters on the seismic resistance of quay walls.

In order to identify the effect of major parameters on the residual deformation of gravity quay walls constructed on liquefiable soil, the effective stress analysis technique, verified in Chapter 3, is used for various structural and geotechnical parameters. Twenty-six cases of effective stress analysis with variations of tidal range, soil permeability, soil relative densities, wall width size and direction of seismic excitation were performed. The cross section used for the parametric study is the typical Port Island PC-1 caisson type quay wall, which was damaged by the 1995 Hyogoken-Nanbu earthquake and shown in Figure 3.10 in Chapter 3.

4.2 Influence of tidal range

Stability of gravity walls is achieved by the stabilising forces (vertical weight) being able to accommodate the destabilising forces. The major destabilising force on a gravity wall is due to the active earth pressure. The water level affects both stabilising and destabilising forces to different extents. Whether the worst case scenario is caused by either low water level (L.W.L.) or high water level (H.W.L.) has

been under investigation by Elsharnoby *et al.* (2004). In the case of low water level, the active pressure is more than at high water. On the other hand, the effective weight of the gravity wall is enlarged and *vice versa* in high water conditions.

For practicing engineers, it may be better for the design of gravity walls to analyse both scenarios (L.W.L.) and (H.W.L.), from which the worst case is considered. However, Elsharnoby *et al.* (2004) used the pseudo-static approach to investigate whether the design of gravity quay walls in the low water level or the high water level is the worst case. Their results have indicated that low water level may produce the worst case considering stress at rock base level.

4.2.1 Results of numerical analysis

In this study, two cases are examined by using the effective stress analysis method; Case 1, shown in Figure 4.1, represents the conditions at low water level. As a result, the backfill is divided into layers: the top layer is saturated soil with a unit weight of γ=1.8 Mg/m^3 and 4 m thickness, the submerged soil is measured below the water level with a submerged unit weight of γ=0.8 Mg/m^3. Also, the top layer of the concrete wall has a unit weight of γ=2.1 Mg/m^3 and 4 m thickness; the submerged concrete wall is measured below the water level with a submerged unit weight of γ=1.1 Mg/m^3. Case 2, shown in Figure 4.2, represents the conditions at high water level; in this case, the top layer was thinner with a thickness of 2 m. All soil parameters for the P-Z sand model are identical to those used in Chapter 3.

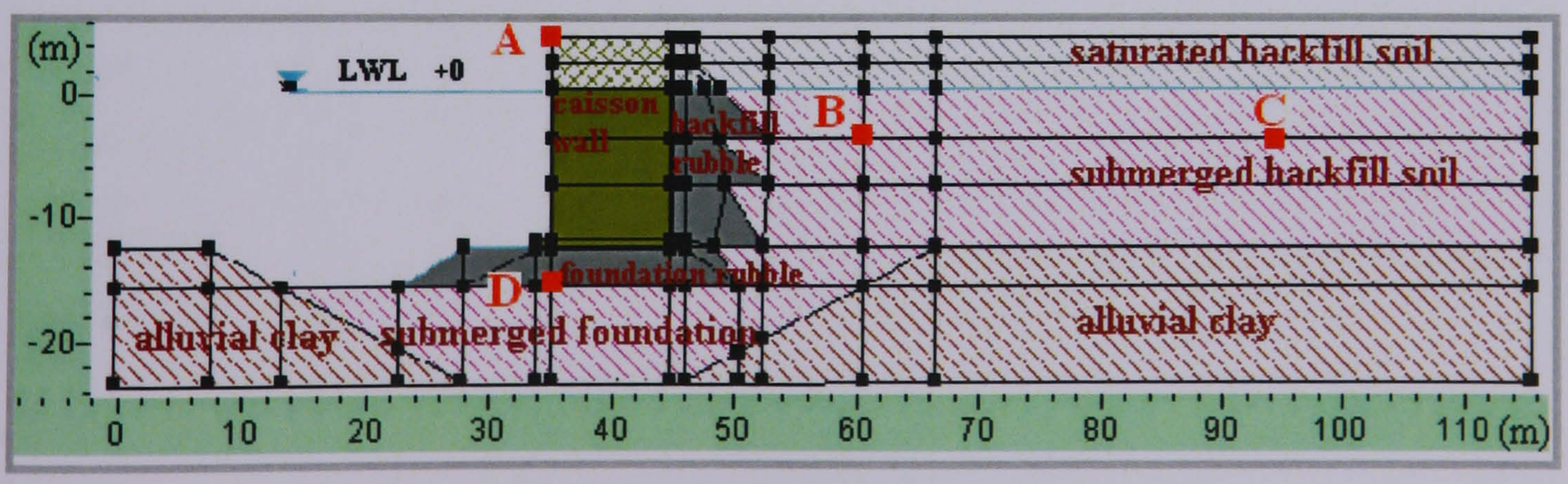

Figure 4.1. Geometry (in natural scale) of the Port Island PC1 quay wall in the L.W.L. case

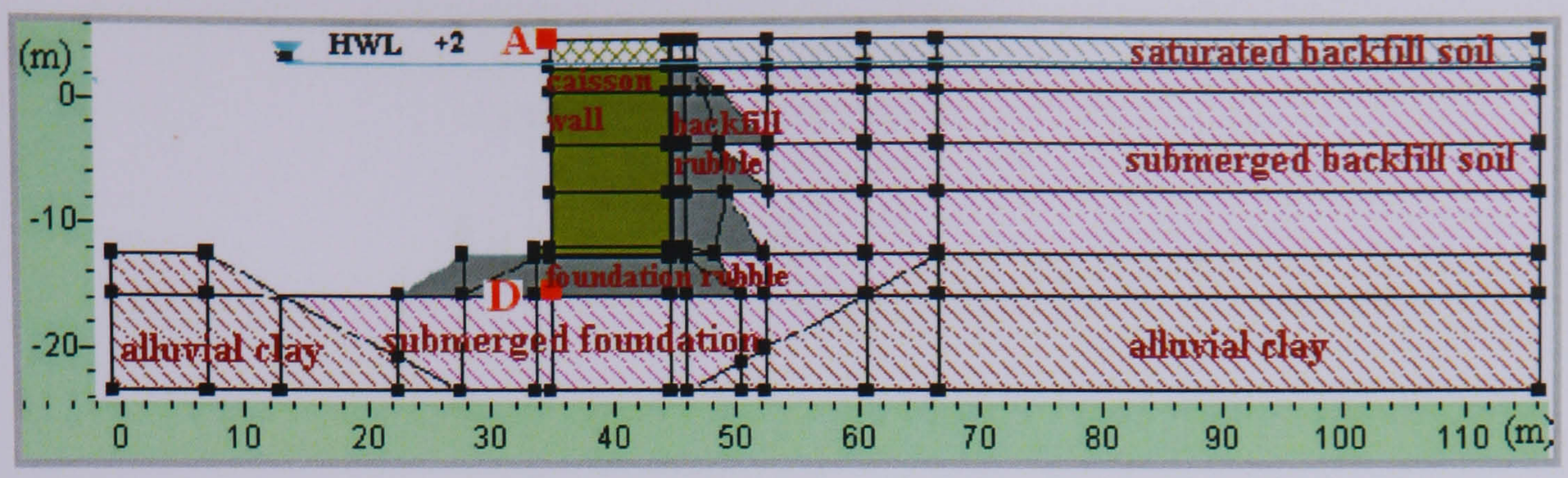

Figure 4.2. Geometry (in natural scale) of the Port Island PC1 quay wall in the H.W.L. case

The final residual deformations for both cases (L.W.L.) and (H.W.L.) are listed in Table 4.1 and shown in Figure 4.3. From the table and figure, it can be seen that L.W.L. produces the worst case condition, including both horizontal and vertical displacements.

As a conclusion, it is clear that in the case of low water level more residual deformation is produced. That is because the increase in the saturated backfill layer in case 1 (L.W.L.) causes an increase in active earth pressure. Also case 1 (L.W.L.) produces the worst case considering stress at rock base level. This may be seen, for example, in Figure 4.4 and Figure 4.5.

Table 4.1. Summary of computed results of parameter study for quay wall PC1

Case	Backfill		Caisson wall		Displacements (m)	
	γ (Mg/m^3)	Thickness (m)	γ (Mg/m^3)	Thickness (m)	Horizontal	Vertical
Case 1 (L.W.L)	2.1	4	2.1	4	3.28	0.73
	1.8	12	2	12		
Case 2 (H.W.L)	2.1	2	2.1	2	2.91	0.58
	1.8	14	2	14		

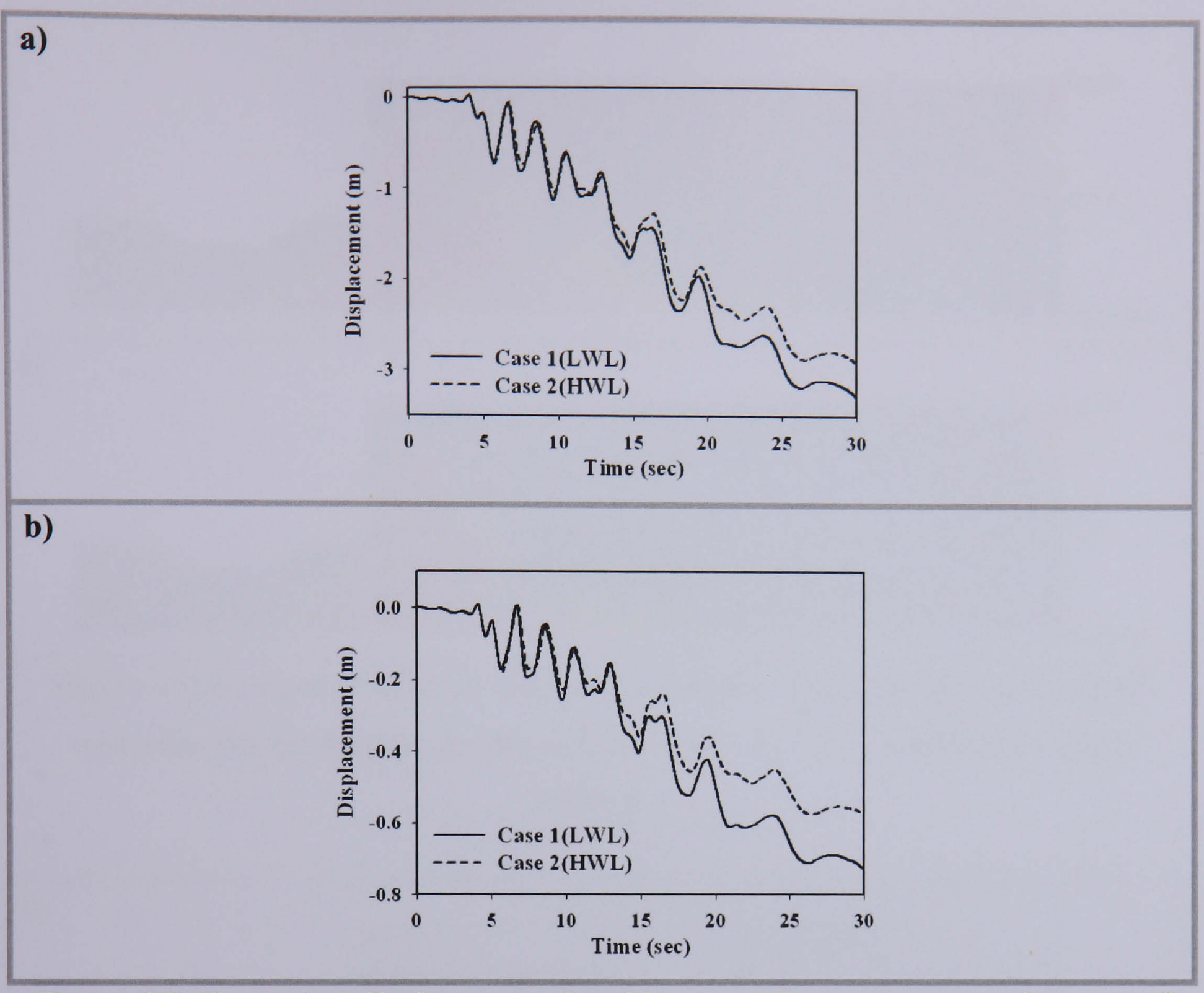

Figure 4.3. Computed displacement time history at the upper seaward corner of caisson at point (A). a) Horizontal direction for both cases, and b) Vertical direction for both cases

Figure 4.4 (a) and (b) show the computed contour diagram of effective shear stresses of the quay wall after the earthquake (t = 30) for Case 1 (L.W.L.) and Case 2 (H.W.L.), respectively. From the figures it is clear that the effective shear stresses at rock base level in Case 1 is greater than those produced in Case 2.

Figure 4.5 (a) and (b) show the computed stress time history beneath the caisson wall at point D (see Figure 4.1 or Figure 4.2) for both cases in the horizontal and vertical directions. The results demonstrate the effect of tidal range on the horizontal and vertical stresses at the end of shaking (t = 30 sec).

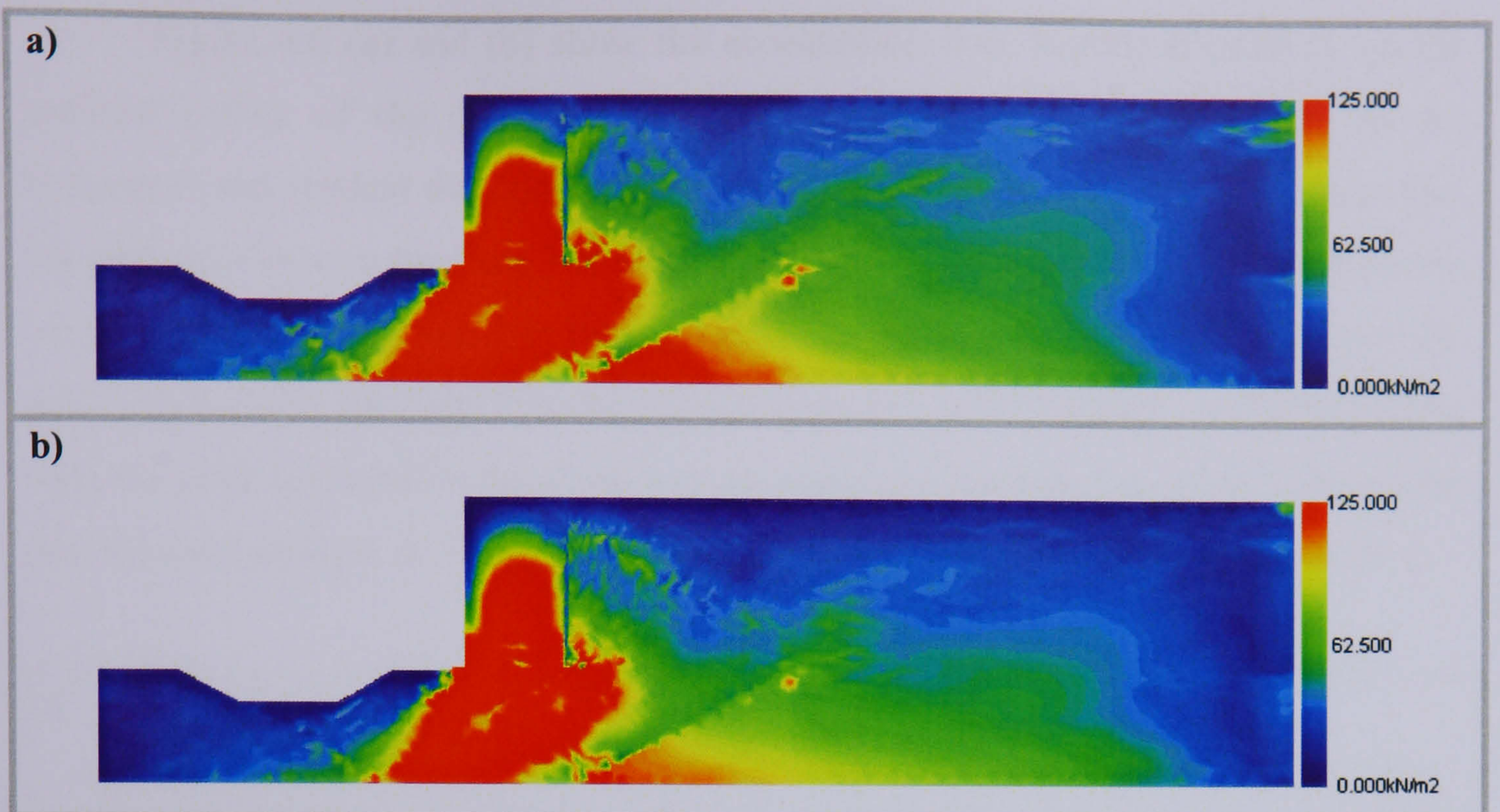

Figure 4.4. Computed contour diagram of effective shear stresses of the quay wall after the earthquake (t=30); a) For Case 1 (L.W.L.) and b) For Case 2 (H.W.L.)

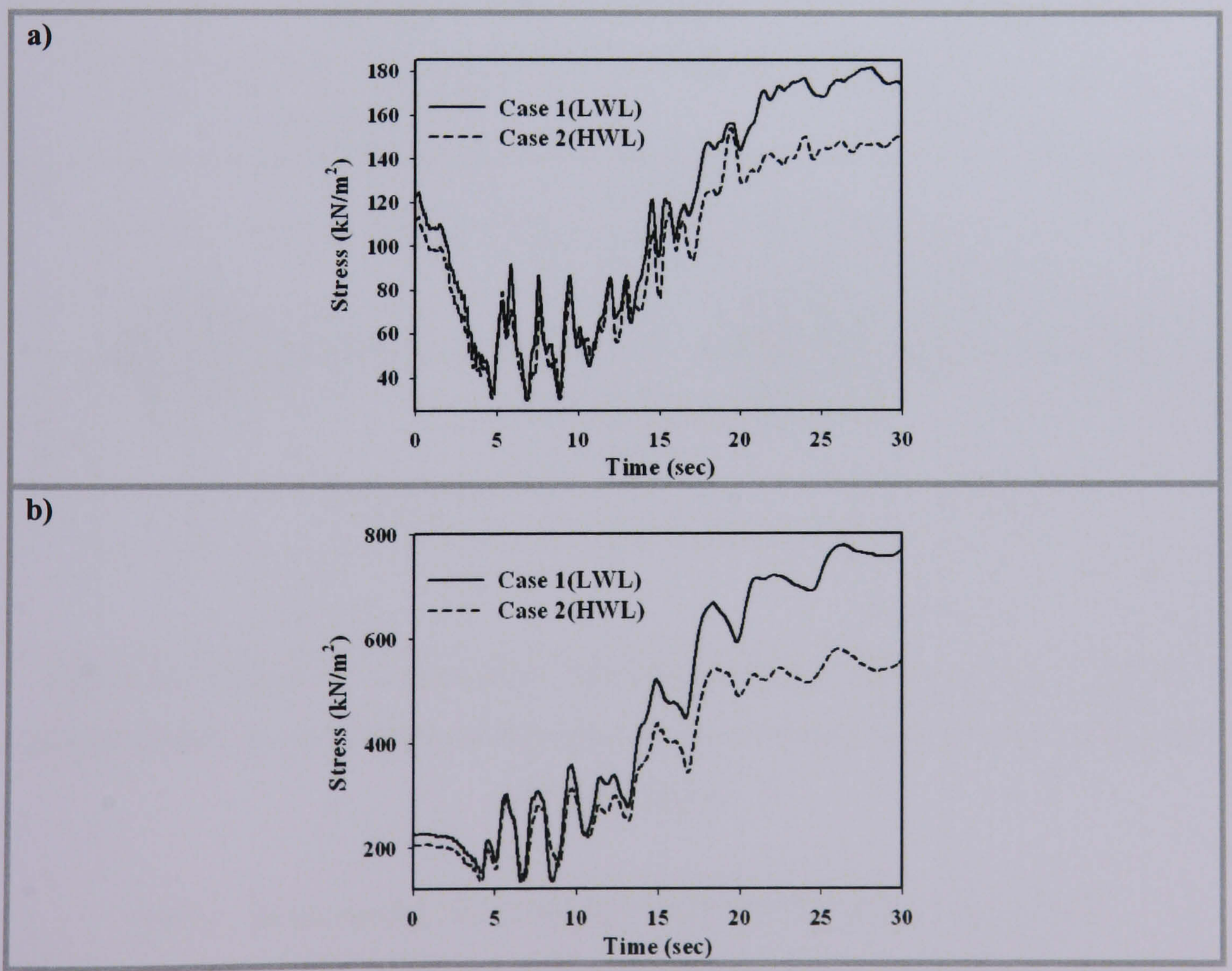

Figure 4.5. Computed stress time history at the upper seaward corner of caisson at point (A), a) Horizontal direction for both cases, and b) Vertical direction for both cases

Figure 4.6 (a) and (b) show the acceleration time history at point A on the seaward corner of the quay wall for both cases (L.W.L.) and (H.W.L.) in the horizontal and vertical directions, respectively. From the figures, it can be seen that the peak acceleration for Case 1 in the horizontal direction is 6.42 m/sec^2, whereas the peak acceleration for Case 2 in the horizontal direction is 4.4 m/sec^2. In addition, the peak acceleration for Case 1 in the vertical direction is 4.18 m/sec^2, which is greater than the peak acceleration for Case 2 in the vertical direction (3.4 m/sec^2). It is clear that the accelerations of the wall are about 1.5 times higher at L.W.L. than at H.W.L.

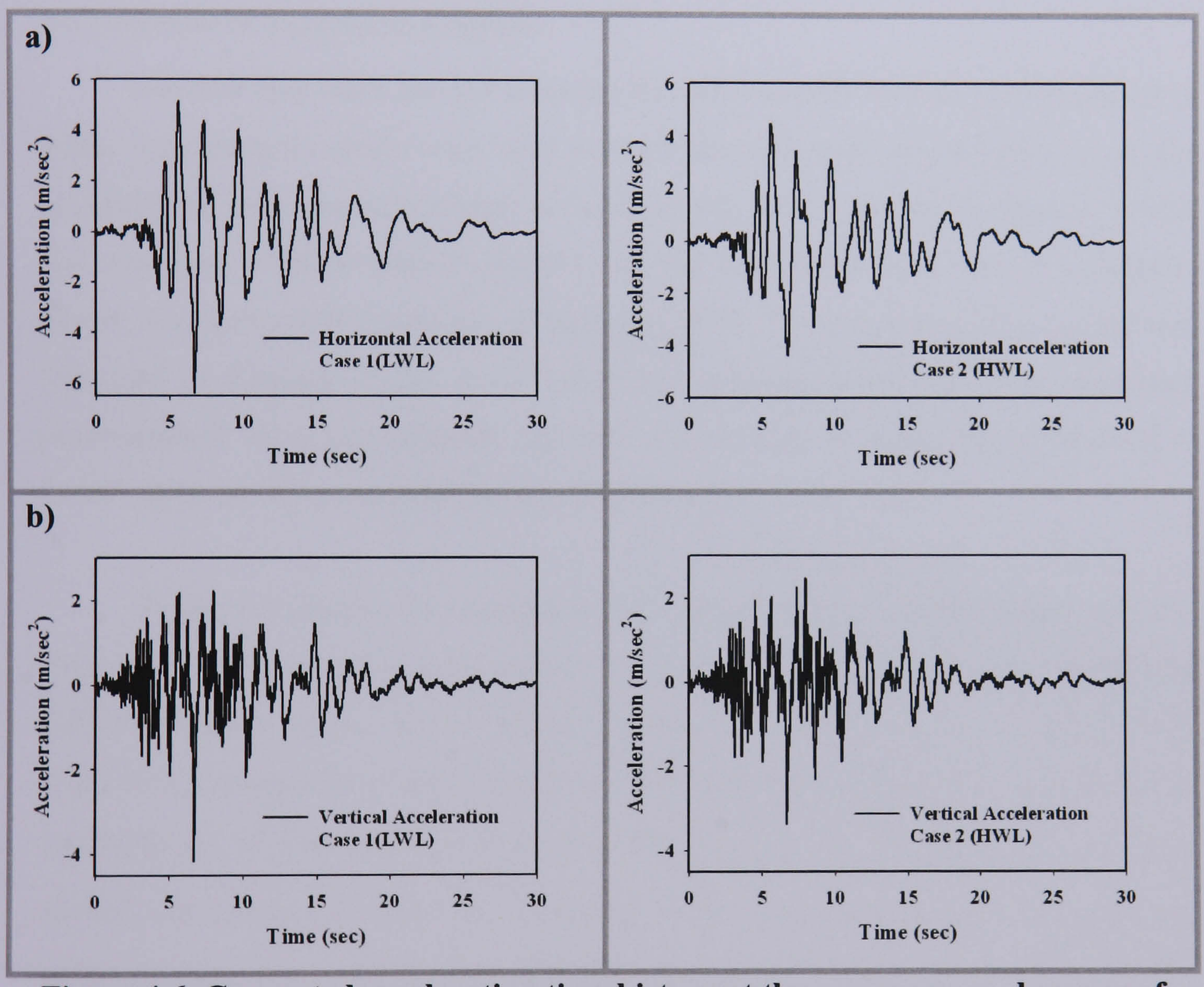

Figure 4.6. Computed acceleration time history at the upper seaward corner of caisson (point A). a) Horizontal direction for both cases, and b) Vertical direction for both cases

Finally, these results are consistent with the findings of Elsharnoby *et al.* (2004); the low water level case is the worst case to be considered by practical engineers in the design stage of gravity quay walls.

4.3 Influence of permeability

For seismic performance of gravity quay walls, the permeability is considered to be among the most important factors in dictating the liquefaction behaviour of backfill material. It has been found that low permeability restricts the pore water movement leading to accumulation of pore water pressure. For highly permeable soil deposits, the dissipation of pore water pressure can occur at a faster rate than pore water pressure generation, thus preventing the sand from liquefying (PIANC, 2001).

4.3.1 Results of numerical analysis

As silts and clays are not used for backfill material in well engineered quay walls, only medium sands were used to study the influence of permeability on the generation of pore pressure behind the wall. In this study, the relative density of the soil was kept constant with D_r=41.7% and three permeabilities were investigated. Firstly, the permeability used the *in situ* case of PC1 constructed in Port Island and discussed in Chapter 3; (k= 4×10^{-5} m/s) was simulated and then two additional permeabilities were investigated. The first corresponds to sandy gravel with (k = 5×10^{-4} m/s), the latter corresponds to gravel with ($k = 5\times10^{-3}$ m/s).

Figure 4.7 depicts the computed time history of excess pore water pressure ratio, $r_u = \Delta u/\sigma'_{v0}$ where u is the current pore water pressure and σ'_{v0} is the current vertical effective stress, at two points (B and C) (see Figure 4.1 or Figure 4.2) immediately behind the caisson. The plots show that when permeability increases the accumulation of pore pressure decreases. However, in the case of sand, r_u quickly reached the maximum value of 1 whereas in the case of sandy gravel there is a reduction in r_u after reaching the maximum. For gravel, r_u only reached a maximum of 0.5 and then reduces to nearly 0.

If the acceleration record of Figure 3.13 in Chapter 3 is considered, it can be seen that strong shaking occurs for approximately 11 seconds, moderate shaking occurs from this point to approximately 20 seconds, with the shaking tapering off after this. This is reflected in Figure 4.7, where in the case of the gravel and the sandy gravel, the pore water pressures develop during strong shaking, is maintained during

moderate shaking and reduces thereafter. In the case of the sand, the permeability is such that the pore water pressure cannot dissipate. It can also be noted that the relative increases in pore water pressure reduce with distance from the wall.

As a conclusion, the results show that when permeability increases the accumulation of pore pressure is reduced. Furthermore, if the permeability is low enough the pore water pressure will not readily dissipate. The change of permeability has also significant effect on the residual deformation of the quay wall as shown in Table 4.2. Similar trend has been observed by Dakoulas & Gazetas (2005) in term of effect of permeability on the rotation of cassion walls.

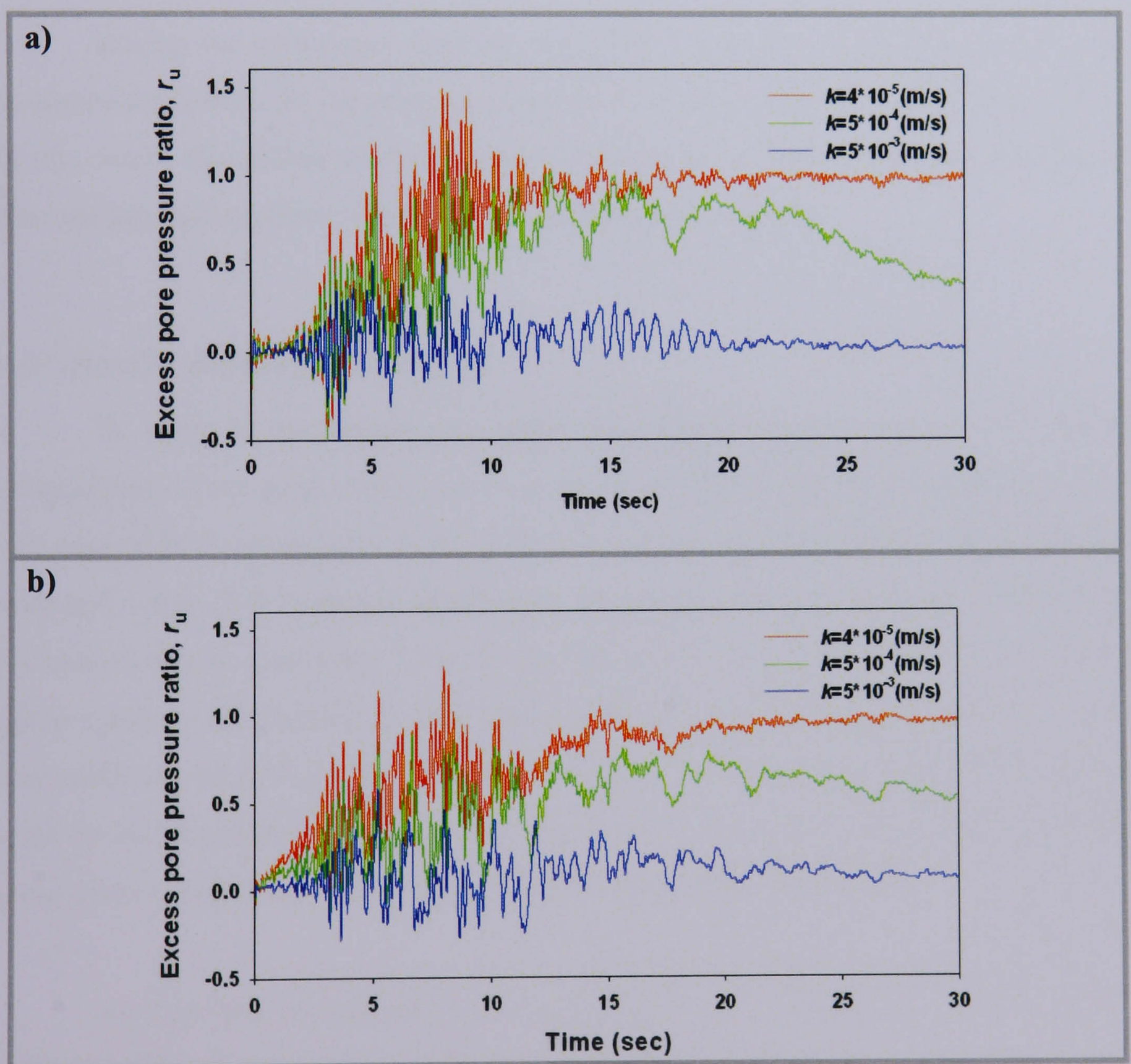

Figure 4.7. Computed pore water pressure ratio for three different permeabilities; a) At point B (15 m to the right of quay wall), and b) At point C (40 m to the right of quay wall)

Table 4.2. Summary of computed results of different permeabilities for quay wall PC1

Case	Permeability (m/sec)	Displacements (m)		Rotation (degree)
		Horizontal	Vertical	
Case 1	$K = 4 \times 10^{-5}$	3.28	0.73	4.2
Case 2	$K = 5 \times 10^{-4}$	3.50	0.77	4.3
Case 3	$K = 5 \times 10^{-3}$	4.52	1.16	4.8

4.4 Influence of density

During the earthquake shaking, the relative density or void ratio of soil plays an important role in the liquefaction potential of a soil deposit (Seed & Idriss, 1971) . In this study, the influence of the relative density of backfill and foundation soils on the residual deformation of gravity quay walls is investigated.

4.4.1 Results of numerical analysis

In order to investigate the effect of ground improvement on the residual deformation of the quay walls, four cases are considered. The first is similar to the *in situ* case of PC1 constructed in Port Island and discussed in Chapter 3. This case was analysed using P-Z material parameters of loose sand, for both the backfill and foundation layers. Secondly, Case 2 was analysed using P-Z material parameters of dense sand for the foundation and loose sand for the backfill layer. Thirdly, Case 3 was analysed using P-Z material parameters of dense sand for the backfill and loose sand for the foundation layer. The last case, Case 4, was analysed using P-Z material parameters of dense sand for both the backfill and foundation layers.

As there are no experimental results for dense soil for OCR=1 with which to calibrate the soil parameters, it was not possible to simulate a soil with a specific density. Therefore the soil parameters obtained from the triaxial tests on samples from Port Island conducted by Nigase *et al.* (1995) that are associated with density were modified to increase the number of cycles required to develop 5% double-

amplitude axial strain. The liquefaction strength curves using these parameters are shown in Figure 4.8, while the actual values of the parameters are shown in Table 4.3.

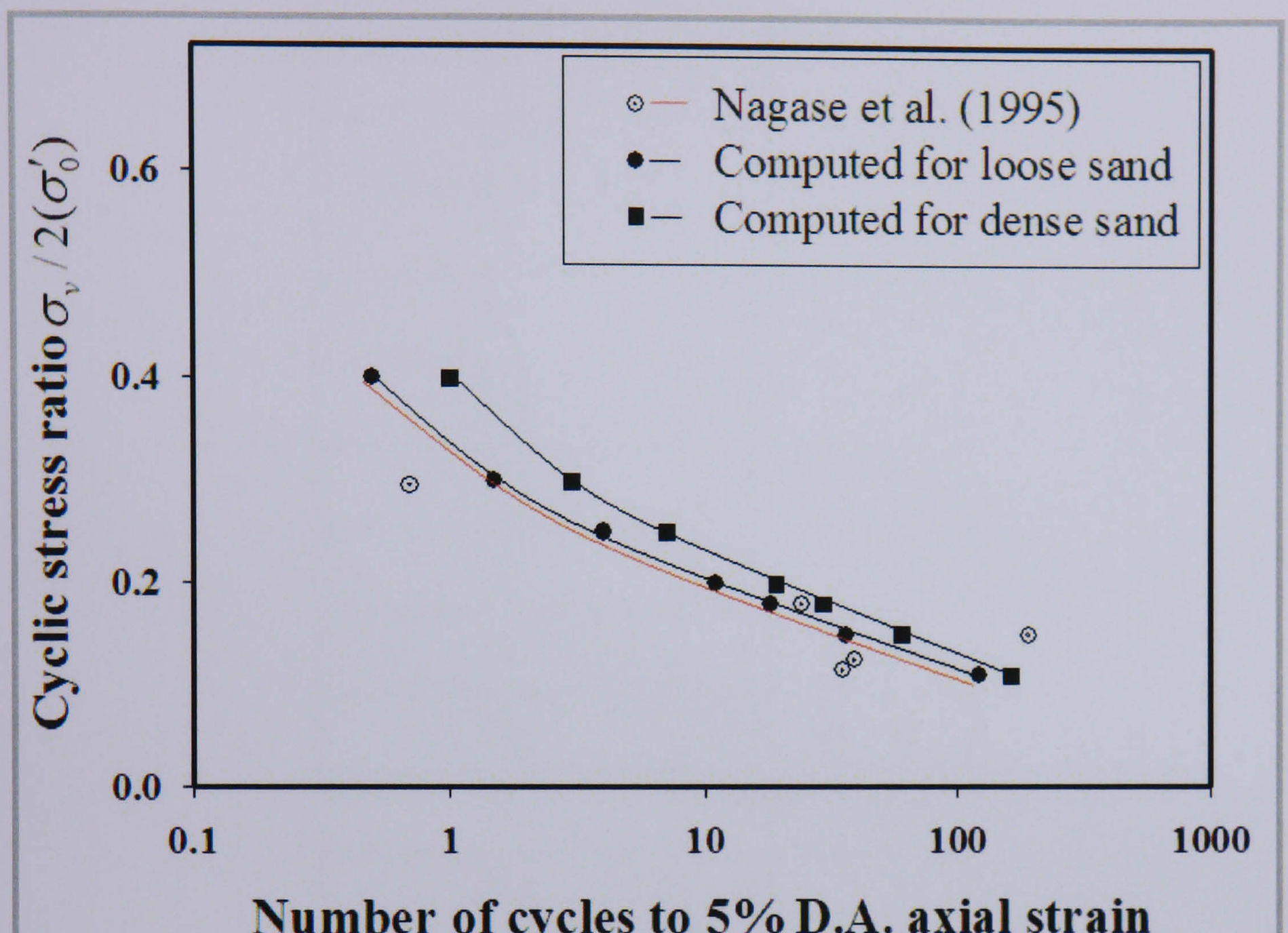

Figure 4.8. Cyclic strength curves of reclaimed soil at Port Island performed by Nigase *et al.* (1995), as reported by Ishihara *et al.* (1996). Comparison with predictions using modified P-Z sand model, for loose and dense sands

Table 4.3. Model parameters for loose and dense sands

Material parameter	Loose	Dense
M_f	0.58	0.78
M_g	1.3	1.55
C	0.9	0.9
α_f	0.45	0.45
α_g	0.45	0.45
K_{ev0}	340	360
G_{es0}	175	200
m_v	0.5	0.5
m_s	0.5	0.5
β_0	6	6
β_1	0.76	0.76
H_0	680	700
H_{U0}	3000	3300
γ	8	8
γ_U	7.1	7.1
p'_0	100	100

The computed results are shown in Table 4.4 and Figure 4.9. The figure demonstrates that the soil improvement of the foundation in Case 2 leads to a reduction in the maximum displacement at point A on the seaward corner of the quay wall to 0.61 m, from 3.28 m in Case 1. The settlement at point A is reduced from 0.73 to 0.09 m. In Case 3, although the backfill is improved, the settlement is increased from 0.73 to 1.10 m. This can be explained by the fact that when the foundation consisting essentially of loose material liquefied, the denser backfill material then applied increased forces upon the wall, which the weakened foundation could not support. Case 4 represents the case when both the foundation and the backfill are

improved; in this case, the seaward displacement and the settlement are reduced from 3.28 to 0.74 m and from 0.73 to 0.20 m, respectively.

Table 4.4. Summary of computed results of different relative densities for quay wall PC1

Case	Foundation Densification	Backfill and Land fill densification	Displacements (m)		Rotation (degree)
			Horizontal	Vertical	
Case 1	Loose	Loose	3.28	0.73	4.2
Case 2	Dense	Loose	0.61	0.09	1.3
Case 3	Loose	Dense	2.50	1.10	3.6
Case 4	Dense	Dense	0.74	0.20	1.5

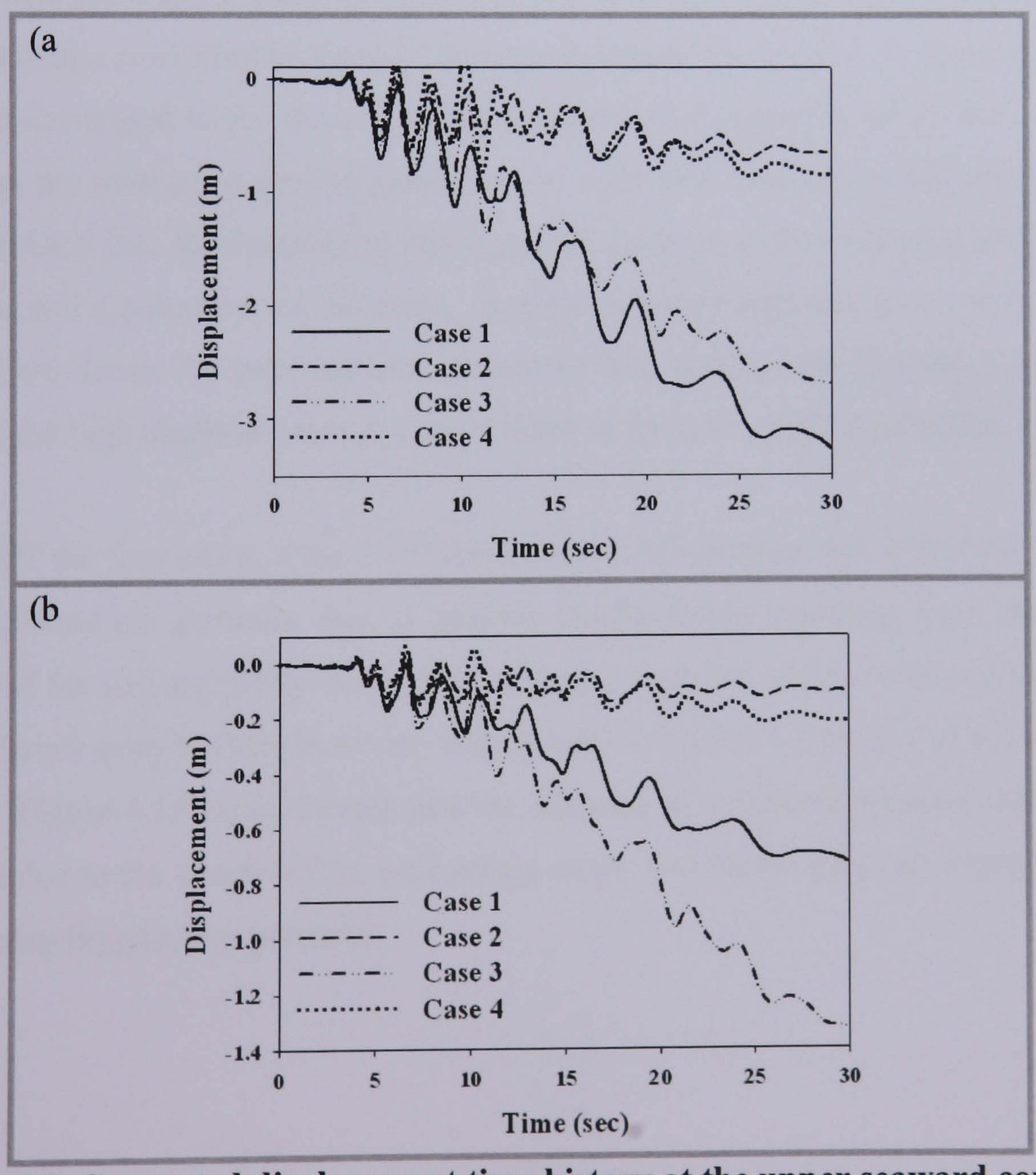

Figure 4.9. Computed displacement time history at the upper seaward corner of caisson (point A) for all cases; a) Horizontal direction, and b) Vertical direction

It can be deduced from Table 4.4 that when the foundation is improved and the backfill remains loose, less residual deformation is obtained compared to the case when both the foundation and backfill are improved (see Case 2 and Case 4). One of the reasons is that the backfill is less dense, which leads to a reduction in the active earth pressure acting on the wall during the shaking and results in a reduction in the tilting of the foundation.

Computed distributions of excess pore water pressure ratio for the quay wall at various times during and after the earthquake are given in Figure 4.10. From the figure, it can be seen that in Case 1 the maximum pore pressures were generated in the backfill rather than underneath the wall. This is because of a high confining pressure, resulting from the weight of the wall, which reduces the liquefaction potential of the soil. In Case 2, the pore pressure generated in the backfill layer was greater than for Case 1 while the dense foundation layer had a slightly smaller pore pressure when compared to Case 1. In Case 3, where the backfill is dense, the pore pressure developed in the loose foundation layer was the greatest of all the tests. In this case, the pore pressure was greater on the right side than on the left side because the wall tilted into the foundation, leading to an increase in the confining pressure on the front and a reduction on the back. In Case 4, where both the foundation and the backfill are dense, the pore pressure generated was greater than in Case 3; this was because the high displacements in Case 3 allowed the pore water to dissipate

Of the four cases, Case 2 in which only the foundation has improved, has the best performance, partially due to smaller inertia forces resulting from the lower density of the soil and partly due to the soil being liquefied and therefore reducing the lateral forces even further; however, it does lead to greater settlement of the backfill. Finally, Figure 4.10 demonstrates that the increase in confining pressure underneath the wall due to the weight of the wall acting on the foundation plays an important role in reducing liquefaction potential.

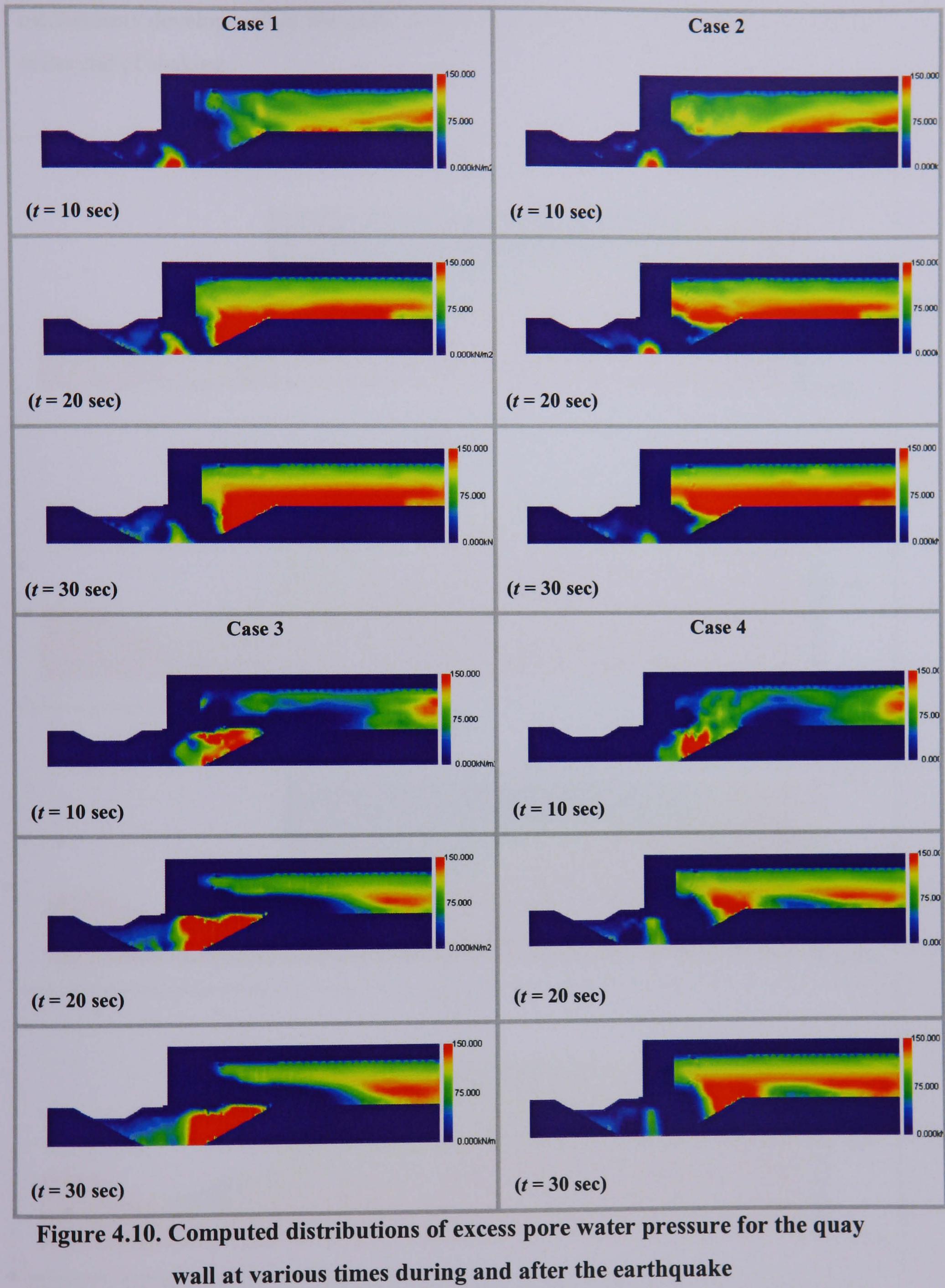

Figure 4.10. Computed distributions of excess pore water pressure for the quay wall at various times during and after the earthquake

Figure 4.11 shows the deformed geometry and the contours of horizontal displacements of the quay wall. In all cases it can be observed that slip surface

mechanisms develop within the quay wall, which indicates global stability problems at the end of shaking.

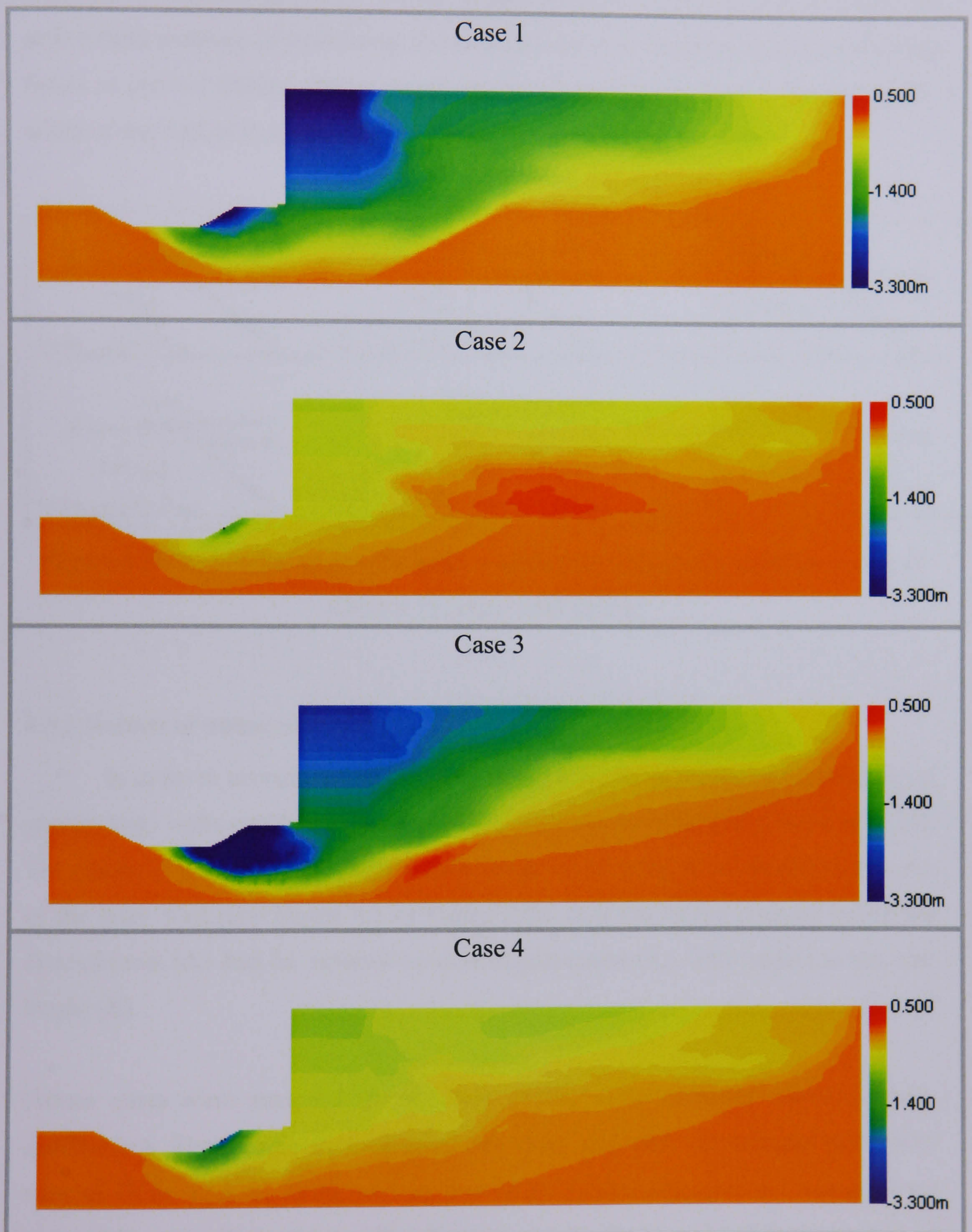

Figure 4.11. Deformed geometry and contours of horizontal displacements of the quay wall at the end of shaking (t = 30 sec)

4.5 Influence of wall width

Increasing the width of the wall is known to increase its stability, because it increases the stabilising forces. As the design seismic coefficient (k_h) increases, the active earth pressure (destabilising forces) also increase, requiring greater stabilising forces to prevent failure. These stabilising forces can be provided by increasing the width of the wall as shown in Figure 4.12.

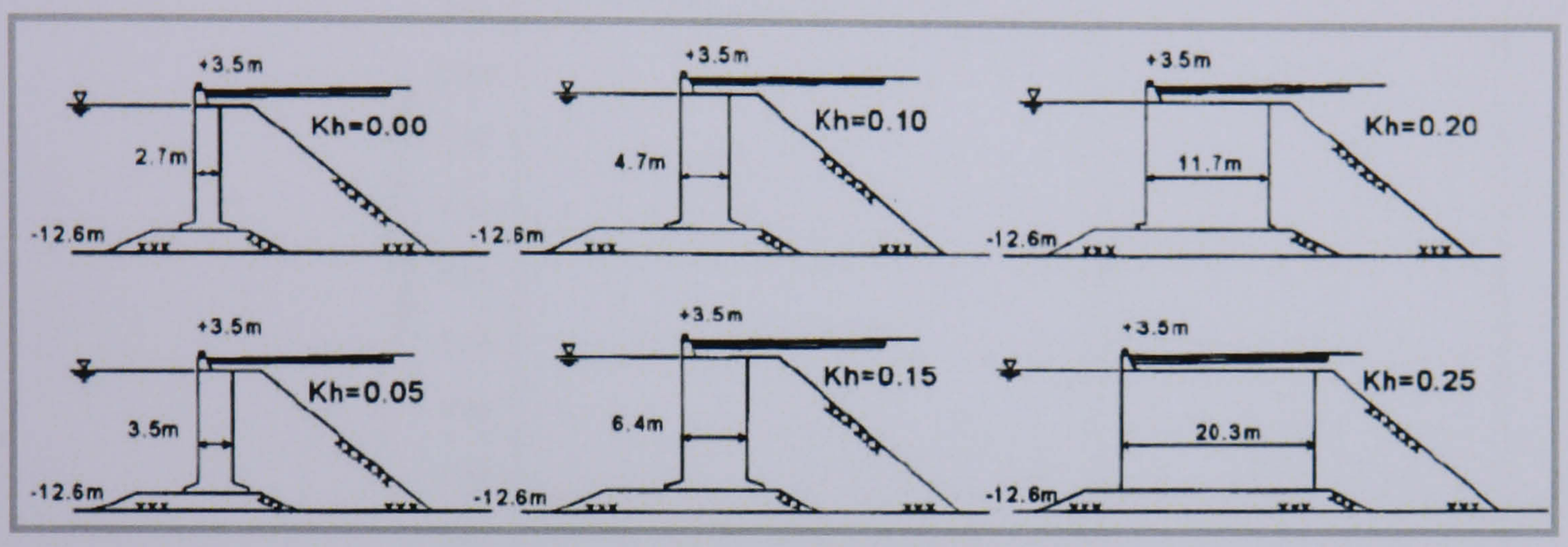

Figure 4.12. Examples of gravity quay wall design for seismic coefficient (k_h) of 0.0 to 0.25, after Ichii (2003)

4.5.1 Results of numerical analysis

In order to investigate the effect of the wall width on the seismic behaviour of gravity quay walls constructed on liquefiable soil, a parametric study was conducted. The results of the parametric study were normalised for point A on the seaward corner of the quay wall (see Figure 4.1 or Figure 4.2), in terms of the residual horizontal displacement (d_x) and the residual vertical displacement (d_y) with respect to the wall height (H).

Fifteen cases were analysed for different widths under different relative density distributions. These cases were grouped into three sets; each set includes wall width sizes of 10 m, 11.5 m, 13 m, 14.5 m, and 16 m. Afterwards, each set was analysed under different soil conditions. The first set was analysed using P-Z parameters of loose sand for the foundation and loose sand for the backfill layer. The second set was analysed using P-Z parameters of dense sand for the backfill and loose sand for the foundation layer. The last set was analysed using P-Z parameters of dense sand for

both the backfill and foundation layers. The effect of width to height ratio (W/H) on the displacement in both directions for different relative soil densities is shown in Figure 4.13.

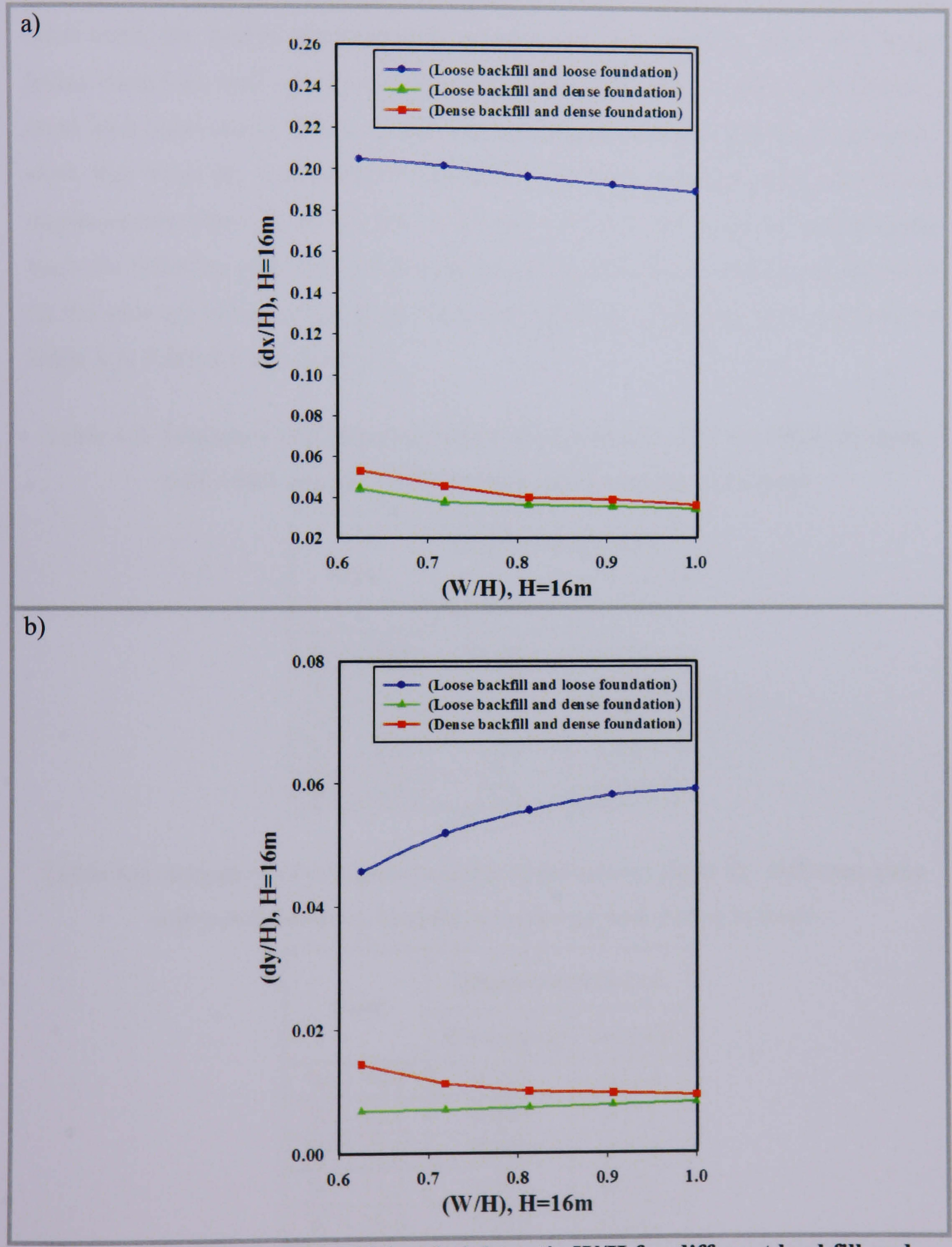

Figure 4.13. Effect of the width to height ratio W/H for different backfill and foundation density. a) Horizontal displacement to height ratio, and b) Vertical displacement to height ratio

From these results it can seen that cases with a loose sand layer behind the wall and dense sand beneath the wall have less deformation than other cases, for reasons that are explained in Section 4.4. Also, in the case when both layers are loose, when the wall width is increasing the horizontal displacements are decreased; on the other hand, the vertical displacements are increased. In addition, cases with loose layers behind the wall and dense layers beneath the wall give the same indications as those with loose layers. However, the results of the cases when both layers are dense show that when the wall width is increased by 1.5 m, both horizontal and vertical displacements reduce by about 10%. A summary of computed results of the parameter study for different quay wall width sections under different soil conditions at point A on the seaward corner of the quay wall (see Figure 4.1 or Figure 4.2) are listed in Table 4.5, Table 4.6 and Table 4.7.

Table 4.5. Summary of computed results of parameter study for different quay wall width sections, both backfill and foundation are loose

Case	Displacements (m)	
	Horizontal	Vertical
W = 10.0	3.28	0.730
W = 11.5	3.23	0.830
W = 13.0	3.15	0.890
W = 14.5	3.09	0.930
W = 16.0	3.04	0.945

Table 4.6. Summary of computed results of parameter study for different quay wall width sections, backfill is loose and foundation is dense

Case	Displacements (m)	
	Horizontal	Vertical
W = 10.0	0.710	0.110
W = 11.5	0.605	0.111
W = 13.0	0.580	0.117
W = 14.5	0.570	0.125
W = 16.0	0.554	0.131

Table 4.7. Summary of computed results of parameter study for different quay wall width sections, both backfill and foundation are dense

Case	Displacements (m)	
	Horizontal	Vertical
W = 10.0	0.850	0.230
W = 11.5	0.730	0.180
W = 13.0	0.640	0.160
W = 14.5	0.625	0.155
W = 16.0	0.581	0.149

This procedure can be used in a new design code to evaluate the expected deformation of a wall constructed on soil deposits that could liquefy due to earthquake shaking if the applicable seismic excitation level were provided. In contrast, the available procedures based on the simplified method (pseudo-static approach) do not take into account the effect of liquefaction that can occur behind and beneath the wall. It should be noted that this parametric study can be applied not only for the caisson type quay wall studied here but also for other types of quay walls, such as block types that will be studied in Chapter 6.

4.6 Influence of seismic excitation input

The effect of using either one or two directions of seismic input on the residual deformation of the wall was also tested. Two cases were considered; Case 1 analysed two directions of Kobe Port 1995 Hyogoken-Nanbu acceleration while the second case analysed one direction acceleration. The directions of excitation were the horizontal (E-W) component and the vertical (U-D) component for Case 1 and the horizontal (E-W) component for Case 2. The accelerographs are shown in Figure 3.13 in Chapter 3.

The computed residual deformation results at point A on the seaward corner of the quay wall (see Figure 4.1 or Figure 4.2) are listed in Table 4.8. From the results it can seen that the residual deformations of the quay wall are similar for both cases. These results indicate that for this earthquake record, it is sufficient to analyse the finite element meshes using the one direction acceleration record only. The reason for

this is that firstly the vertical component will have little influence on the horizontal deformations and secondly the vertical accelerations are much smaller than the horizontal accelerations and therefore do not contribute significantly to the liquefaction.

Table 4.8. Summary of computed results of parameter study for quay wall PC1

Case	Displacements (m)		Rotation
	Horizontal	Vertical	(degree)
Case 1	3.28	0.73	4.2
Case 2	3.15	0.78	4.3

4.7 Summary

The influence of various soil parameters, wall geometry and seismic excitation on the seismic performance of gravity quay walls was investigated using effective stress analysis. The performance of the quay wall obtained from this parametric study is summarised as follows:

1. Two cases of tidal range, one at low water level and the other at high water level, were considered. The results indicate that the low water level case is the worst and that this should be considered by practicing engineers.

2. Three different values of permeability were analysed to investigate the influence of permeability on the development of pore pressure behind the wall. The results showed that when permeability increases the accumulation of excess pore pressure is reduced. Furthermore, if the permeability is low enough, the pore water pressure will not easily dissipate.

3. Improving the backfill and the foundation soils of caissons reduces the vertical settlement at the toe of the wall by over 73%, while the horizontal displacement is reduced by over 77%.

4. Improving the foundation while keeping the backfill loose, as represented by Case 2 of this study, caused a lower residual deformation of the caisson compared to when both the foundation and backfill were improved. The reason for this is partially due to smaller inertia forces resulting from the lower density of the soil and partly due to the soil being liquefied and therefore reducing the lateral forces even further.

5. The weight of the wall acting on the foundation leads to increased confining pressure beneath the wall, which reduces the susceptibility to liquefaction.

6. Increasing the width of the wall also reduced the horizontal displacement of the wall; however the relative reduction in displacements is less than the relative increase in the wall width. Increasing the width of the wall also increases the vertical settlement slightly.

7. It is sufficient to analyse the finite element meshes using an acceleration record in one direction only (i.e. the horizontal component, instead of horizontal and vertical).

CHAPTER FIVE

5. SITE INVESTIGATION OF JEDDAH PORT

5.1 Introduction

The documented failures of gravity quay walls world-wide due to earthquake loading have encouraged researchers to predict the safety levels of existing quay walls located in regions of seismic activity. This is often done by developing numerical models of the quay walls and subjecting them to earthquake accelerations. Before any numerical model can be developed, the constitutive properties of the soil must be assessed.

This chapter describes an experimental programme developed to measure the properties of both the backfill soil and the foundation soil of quay walls that have been constructed in Jeddah Port, Saudi Arabia. The soil properties to be used in the soil liquefaction models are measured by conducting triaxial tests. As the soil that is tested in the triaxial tests must have the same properties as the *in situ* soil, it is necessary to obtain the relative density of the landfill soil. This was achieved by conducting Standard Penetration Tests (SPT). The test procedure for this, as well as the method for obtaining the relative density, is described in this chapter.

To obtain the best data possible, the test results obtained as part of this research programme, were supplemented with the results of other tests conducted by the Saudi Port Authority (Saudi Ports Authority, 2006). A statistical analysis has been conducted to ensure that the most reliable value of relative density has been obtained from the SPT results.

A series of monotonic and cyclic triaxial tests were conducted under undrained conditions for Jeddah Port sand, with different relative densities. The purpose of these tests was to characterise basic soil properties and hence assess the liquefaction characteristics of Jeddah Port sand, which was a previously untested material. The results will provide a framework for calibration and validating numerical models that can be used for simulating soil response in different geotechnical engineering applications.

5.2 SPT and other geotechnical investigations

In investigating the soil properties of Jeddah Port, *in-situ* tests were conducted. These tests consisted of the SPT carried out at the site to a depth of 20 m. The site is a vacant area within the Jeddah Port. It is located in the Northern Container Berths bounded by an asphalt road to the east and south and the Red Sea to the other sides. The test location is about 850 m from the face of berths number 4, 5 and 6. The ground surface at the site is almost flat and has the same level as the surrounding asphalt road at the western part of the site as shown in Figure 5.1.

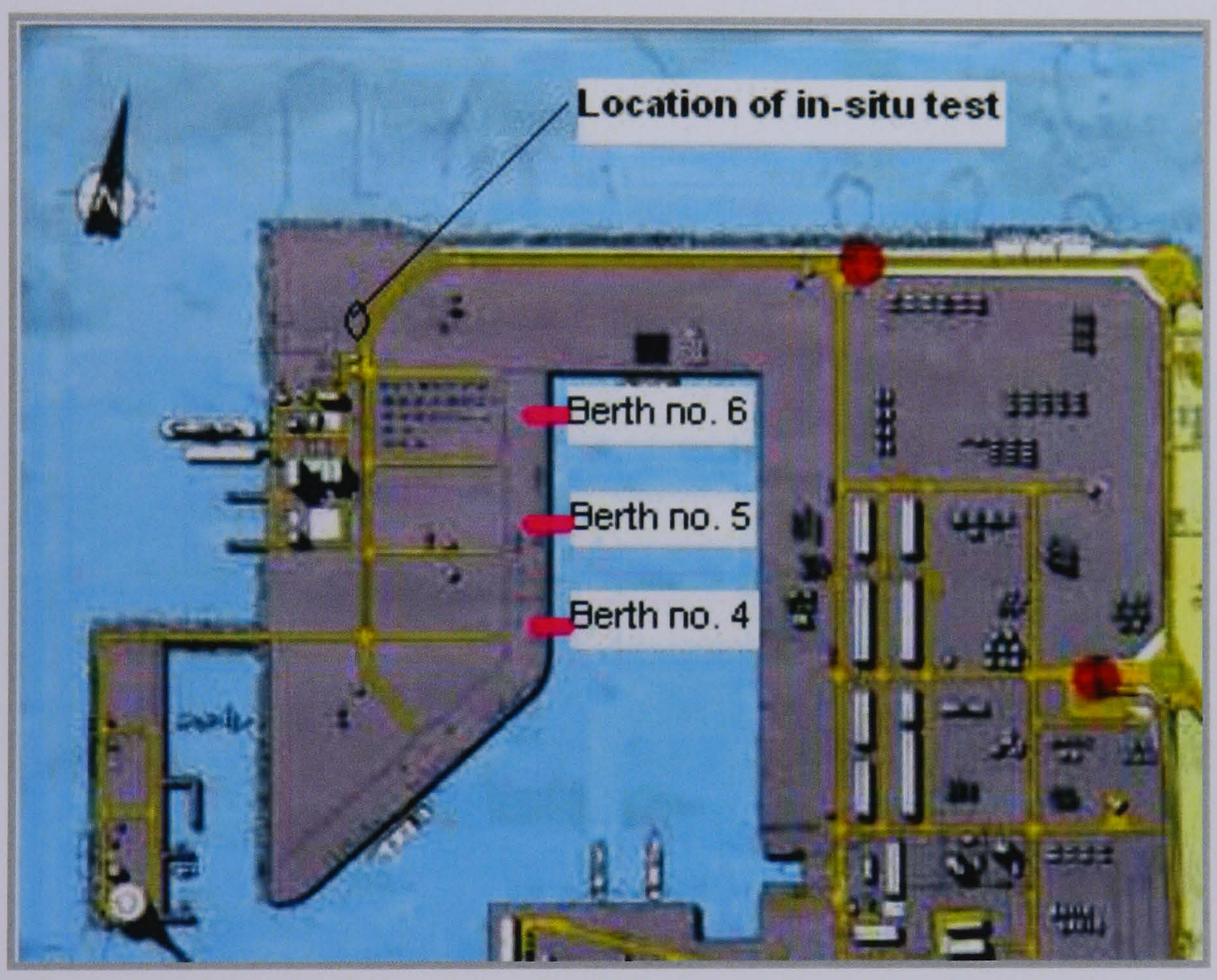

Figure 5.1. Location of *in situ* test

The drilling of one borehole was done using a truck-mounted hollow stem auger drilling machine Mobile (B-57). The Standard Penetration Test (SPT) was carried out according to BS 5930:1999 at 1.5 m intervals, using a 63.5 kg hammer, falling freely from a height of 760 mm. The number of blows required to drive 150 mm of split spoon sampler (Raymond Sampler) into the ground was recorded. The total number of blows for the last 300 mm of penetration gave the SPT N-value. Images of the testing procedure are shown in Figure 5.2. The SPT N-values are shown in the last column of

the borehole logs in Figure 5.3. The field work was completed in one day on the 8th of November 2006.

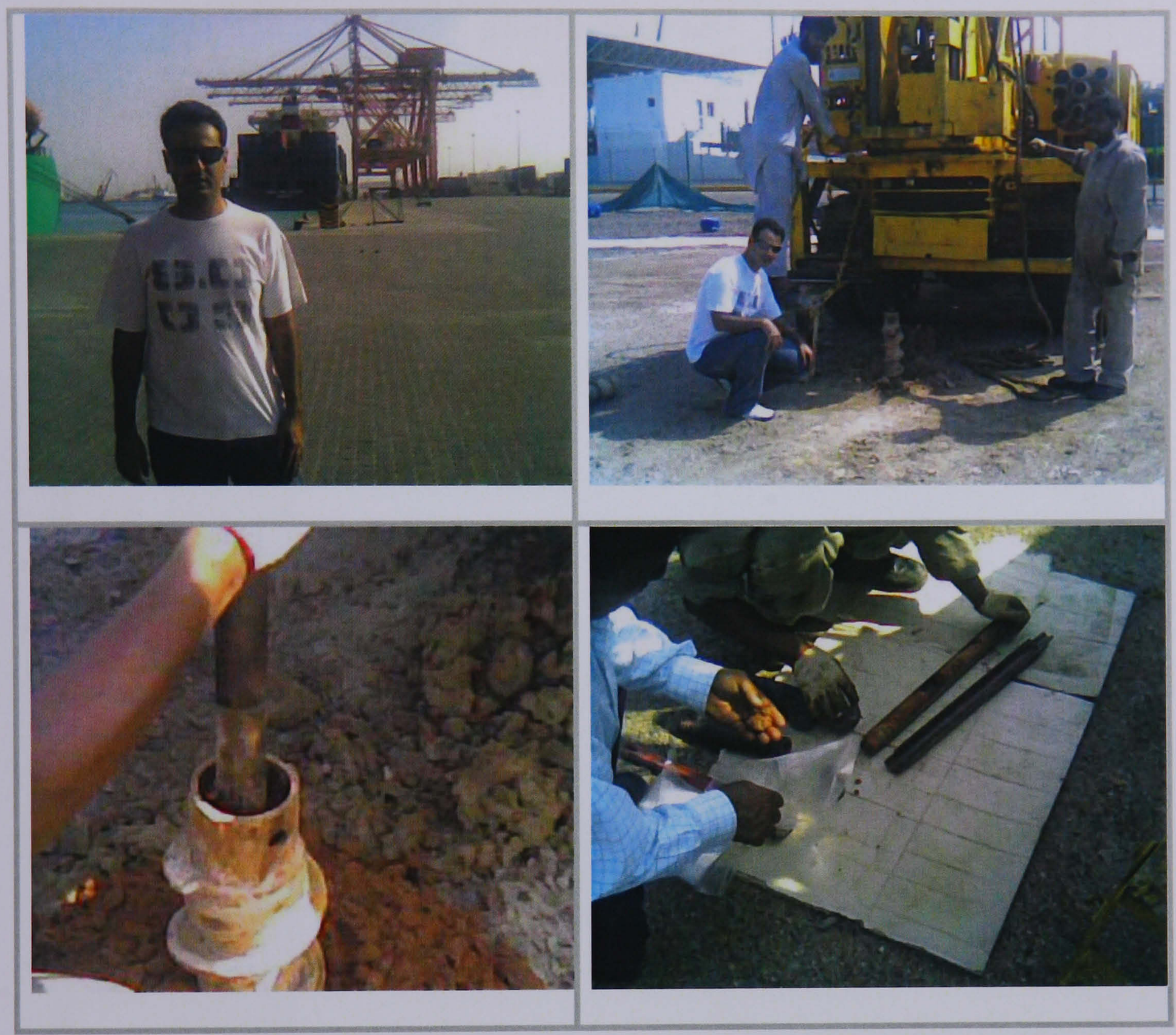

Figure 5.2. Images of the testing procedure

Depth (M)	Legend	Description	S.P.T. N VALUE 20 40 60 80 100 % M. C.	N Value
		Pale Brown		13
1.0		Carbonate poorly graded		
		sand with conglomerate		
2.0		fragments		5
		Loose to medium dense		
3.0				
		Light gray		15
4.0		Coralline conglomerate		
		with cavities and channels		
5.0		infilled with silty sand		26
		Medium dense		
6.0				
				17
7.0				
8.0				19
9.0				
				18
10.0				
11.0				10
12.0				
				9
13.0				
14.0				28
15.0				
				11
16.0				
17.0				11
18.0				
				17
19.0				
20.0				17

Figure 5.3. Borehole log completed by the author

5.2.1 Ground conditions of the site

Overlying the site from the surface to about 2.50 m depth is a loose to medium dense fill material, brown, dry to wet, very clayey, gravely sand. SPT N- values showed a range of 5 – 13 blows/300 mm. Based on the laboratory test results and according to the Unified Soil Classification System (BSCS) BS 5930:1999, the soil is classified as SCL. Below this layer to 20.0 m depth, loose to medium dense, light grey, wet, coralline, very gravely and very silty sand was encountered. SPT N-values showed a range of 9 – 28 blows/300 mm. Based on the laboratory test results and according to BSCS, the soil is classified as SML. It is also believed to be a fill material. Groundwater was encountered at 2.00 m from the ground surface during drilling.

Six SPTs were carried out by the Saudi Port authority in 1993 in the same area as the tests reported here; their locations are shown in Figure 5.4. These tests are closer to Berths 4, 5 and 6 for which the performance against earthquake loading will be studied in Chapter 6. The distances from the location of each test to the face of the wall are summarised in Table 5.1. The results are similar to the results of the test conducted by the author. The SPT results are presented in Figure 5.5.

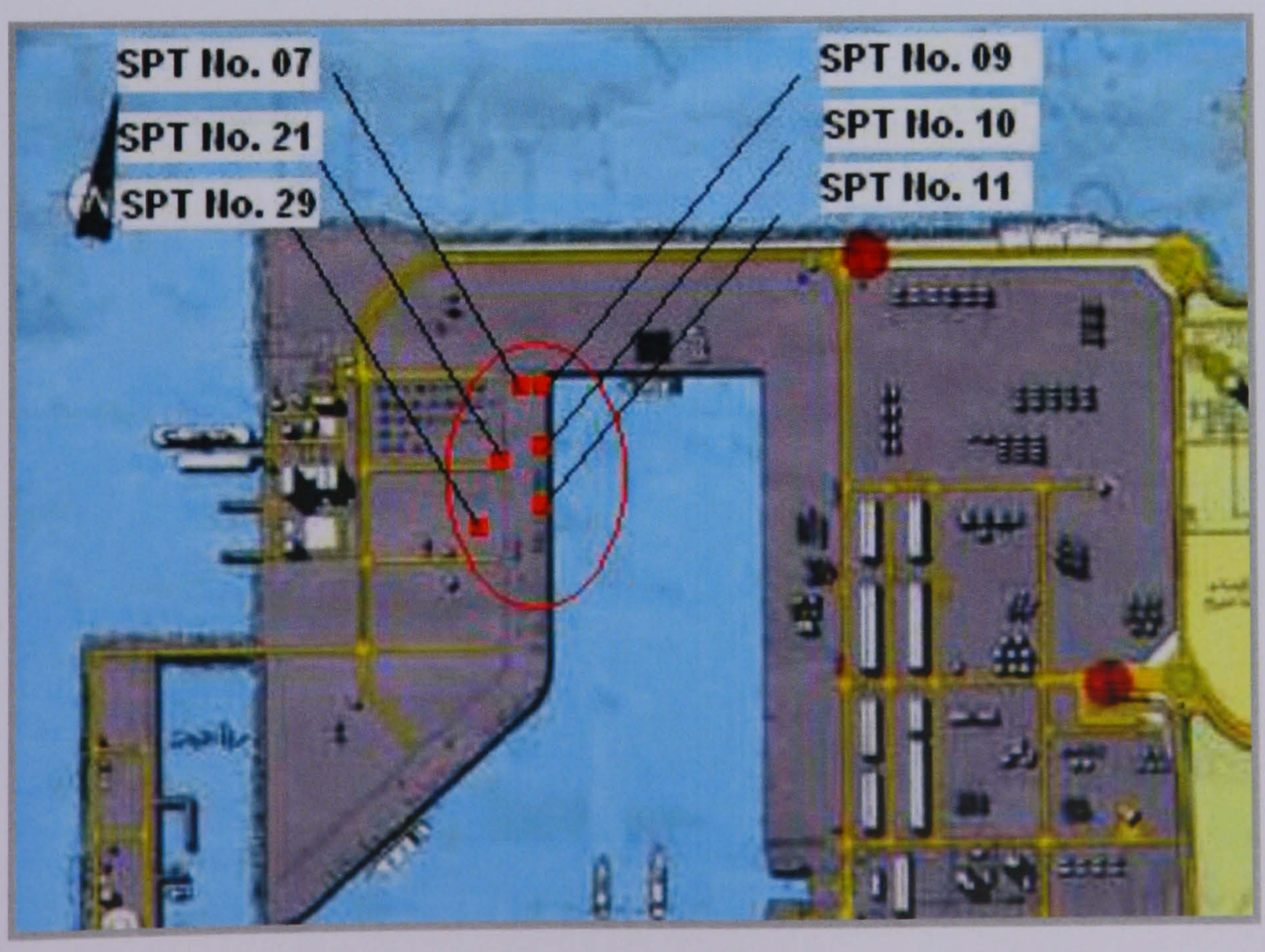

Figure 5.4. Location of SPTs conducted by Saudi Port authority in 1993

Table 5.1. Distance from the location of SPT to the face of wall

SPT No.	Distance from the location to the face of wall (m)
09	20
10	20
11	20
07	130
21	260
29	350

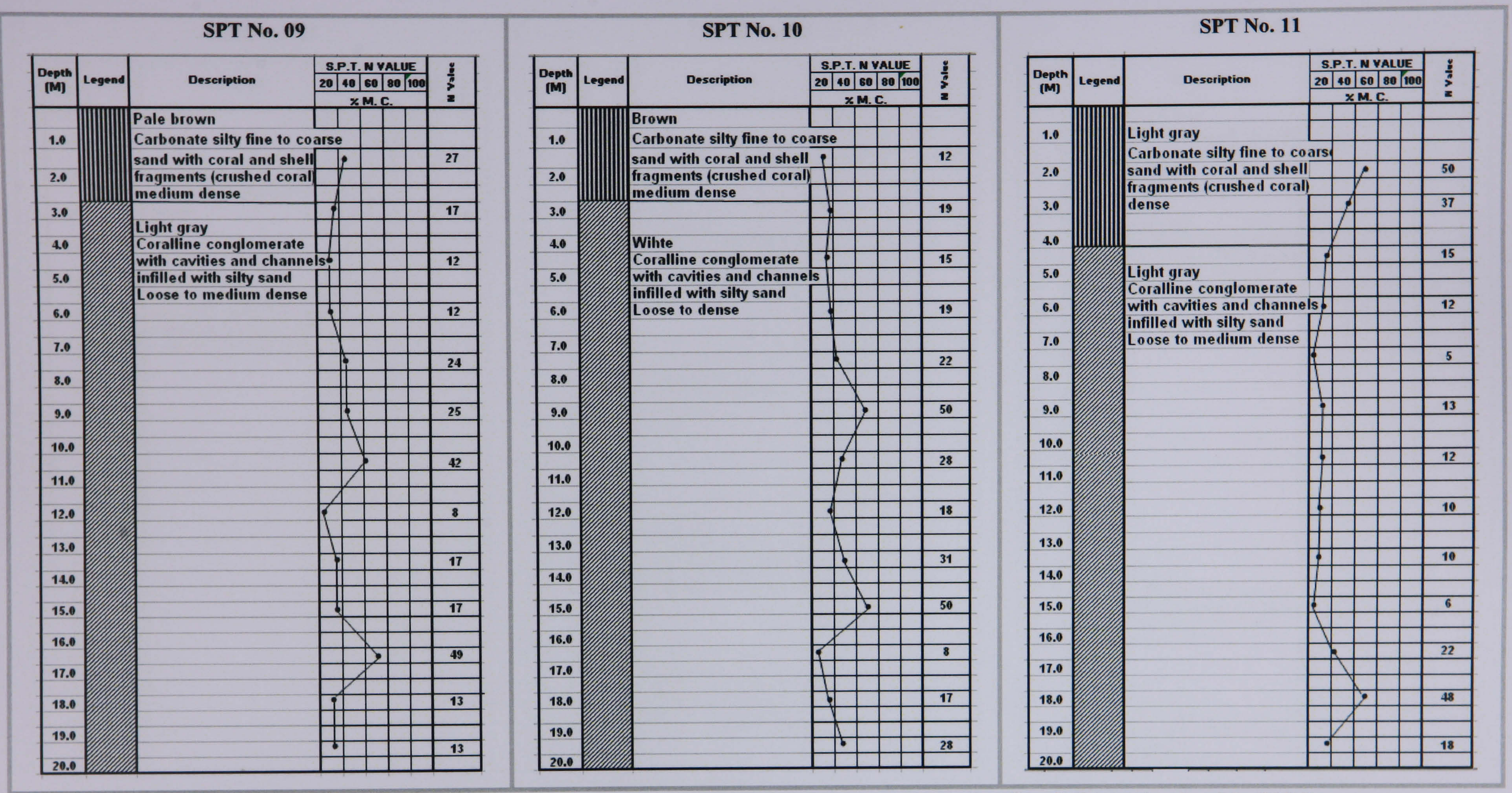

Figure 5.5. Results of SPTs conducted by Saudi Port authority in 1993, after Saudi Ports Authority (2006)

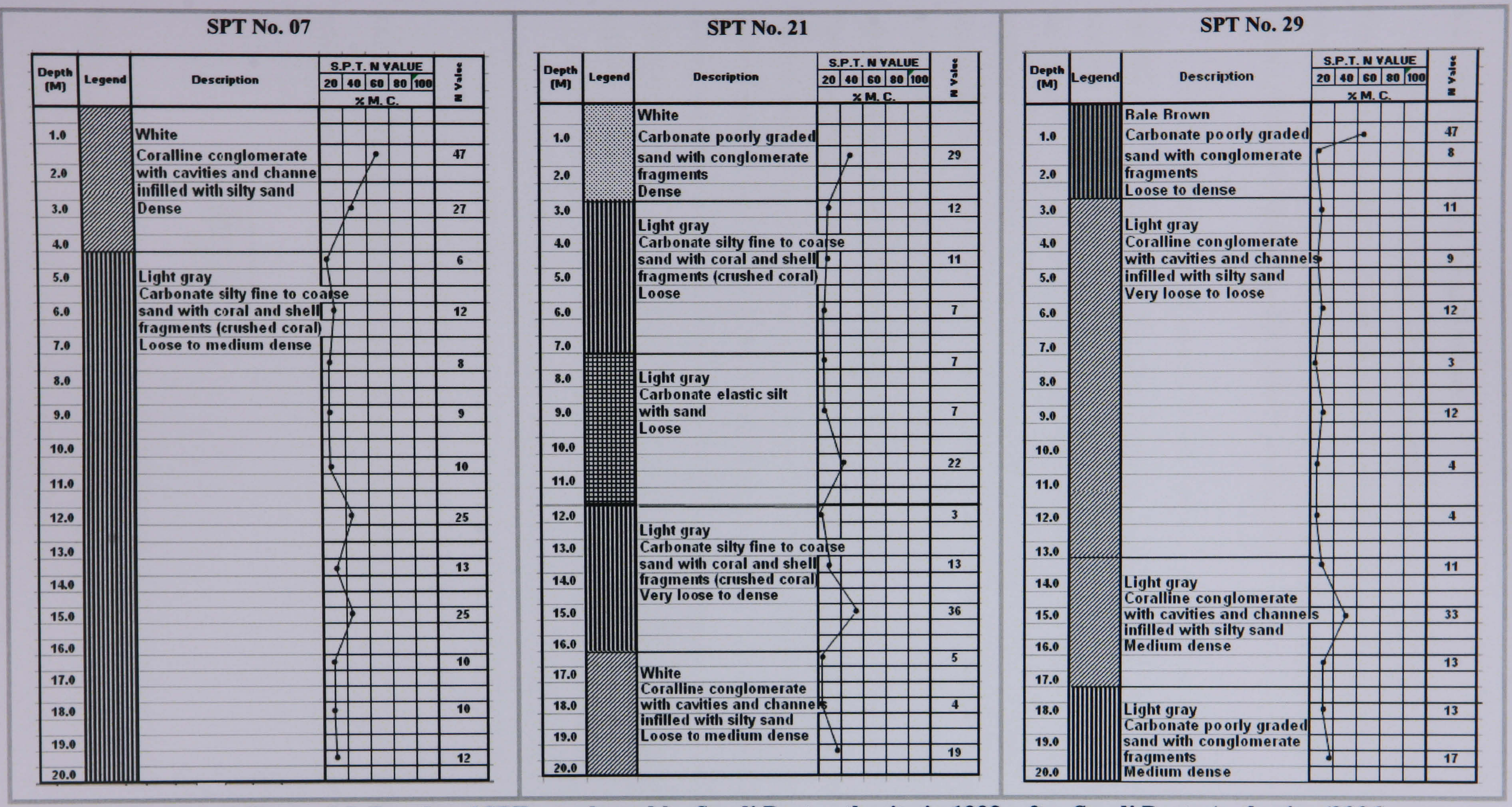

Continued Figure 5.5. Results of SPTs conducted by Saudi Port authority in 1993, after Saudi Ports Authority (2006)

5.2.2 Relative density from N values

The relative density of the backfill soil was obtained by the Standard Penetration Test (SPT). These data were calculated using the empirical correlation between SPT, N value and relative density, developed by Cubrinovski & Ishihara (2001). This correlation was discussed in Section 3.4.

In the finite element model which will be presented in Section 6.4.2, the landfill and the foundation are represented as a single layer. Therefore, the most relevant value of density needs to be chosen and the laboratory specimens prepared to this density. Since the results of the SPTs at the sites tested by the Saudi Port authority are similar to the one conducted as a part of this research, it can be concluded that the SPT results obtained by the Saudi Port Authority are valid. This allows all SPT results to be pooled in order to increase the reliability of the final SPT adopted. Rather than take the average of all tests, a sensible lower bound was adopted. This was chosen as site 7 because its mean was smaller than the average mean of all the test results (i.e. it is a lower bound) and it had the lowest standard error (i.e. the values changed the least with depth and therefore it is not only consistently a lower bound, but also a implies that the material and the compaction procedure was the most consistent). It was also less than the mean as shown in Table 5.2. The standard error (of the means $s_{\bar{y}}$) of these tests is calculated as follows:

$$s_{\bar{y}} = \frac{s}{\sqrt{n}} \tag{5.1}$$

where $s_{\bar{y}}$ is the standard error, n is the size of sample and s is the standard deviation, which can be calculated as follows:

$$s = \sqrt{\frac{\Sigma(y-\bar{y})^2}{n-1}} \tag{5.2}$$

where $(y-\bar{y})$ is the distance between each reading and the mean.

After Equation 5.1 had been applied to all the SPT results, Table 5.2 shows the results which indicate that SPT No. 7 has the lowest standard error of 2.33%. Therefore, this test can be considered as representative of all the other tests in giving an acceptable value of D_r. A relative density of 81.7% was allocated to the upper layer situated at a depth of 3 m below the ground service. In addition, a relative density of 35.7% is given to the soil of Jeddah Port quay walls situated at a depth of approximately 19.5 m below the ground surface level.

Table 5.2. SPT's relative Density and Standard errors

Depth (m)	σ'_v : The effective vertical stress (kPa)	SPT No. 07		SPT No. 09		SPT No. 10		SPT No. 11		SPT No. 21		SPT No. 29		SPT conducted as a part of this study	
		N-value	Relative density (D_r)(%)	N-value	Relative density (D_r)(%)	N-value	Relative density (D_r)(%)	N-value	Relative density (D_r)(%)	N-value	Relative density (D_r)(%)	N-value	Relative density (D_r)(%)	N-value	Relative density (D_r)(%)
1.5	27.6	47	100	27	75.6	12	50.4	50	103	29	78.4	8	41.2	13	69.1
3	55.2	27	64	17	50.5	19	53.4	37	74.5	12	42.4	11	40.6	5	30.3
Average D_r (%)			**81.7**		**63.1**		**51.9**		**88.7**		**60.4**		**40.9**		**49.7**
4.5	45.5	6	31.5	12	44.5	15	49.8	15	49.8	11	42.6	9	38.6	15	53
6	60.6	12	41.4	12	41.4	19	52.1	12	41.4	7	31.6	12	41.4	26	63.8
7.5	75.7	8	32	24	55.4	22	53.1	5	25.3	7	29.9	3	19.6	17	48.3
9	90.9	9	32.4	25	54	50	76.4	13	39	7	28.6	12	37.4	19	48.5
10.5	106.1	10	32.9	42	67.4	28	55	12	36	22	48.8	4	20.8	18	45.2
12	121.3	25	50.3	8	28.5	18	42.7	10	31.8	3	17.4	4	20.1	10	32.5
13.5	136.4	13	35.2	17	40.2	31	54.4	10	30.9	13	35.2	11	32.4	9	29.9
15	151.6	25	47.6	17	39.2	50	67.3	6	23.3	36	57.1	33	54.6	28	51.2
16.5	166.7	10	29.4	49	65	8	26.3	22	43.6	5	20.8	13	33.5	11	31.3
18	181.9	10	28.7	13	32.7	17	37.5	48	63	4	18.2	13	32.8	11	30.6
19.5	197	12	30.9	13	32.1	28	47.1	18	37.8	19	38.8	17	36.7	17	37.2
Average D_r (%)			**35.7**		**45.5**		**51.1**		**38.4**		**33.6**		**33.5**		**42.3**
Standard error			**0.022**		**0.04**		**0.041**		**0.034**		**0.038**		**0.032**		**0.034**

5.3 Physical and engineering proprieties of JPS

To further categorise Jeddah Port Sand, samples were taken from the same location as the SPT test at a depth of approximately 13 m. Figure 5.6 shows a specimen of Jeddah Port sand where particles larger than 2 mm have been removed. These samples were first subjected to index and classification tests and then both monotonic and cyclic triaxial tests. The results of the index and classifications include particle size distribution, Atterberg limits, particle density, maximum and minimum density as well as consolidation derived coefficients.

Figure 5.6. Jeddah Port sand

Particle Size Distribution was determined using the wet sieving methods in accordance with BS 1377-2: 1990 part 9.2. The wet sieving method was the definitive method of BS 1377. The particle size distribution curves are shown in Figure 5.7.

Curve 1 represents the results for dry sieve analysis on *in situ* Jeddah Port sand. The soil is uniformly graded and contains particles up to medium sized gravel. Curve 2 represents the definitive particle size distribution for Jeddah Port sand used in this investigation where particles larger than 2 mm have been removed by sieve. The wet sieving method reveals that Jeddah Port sand consists of 82% sand and 18% silt.

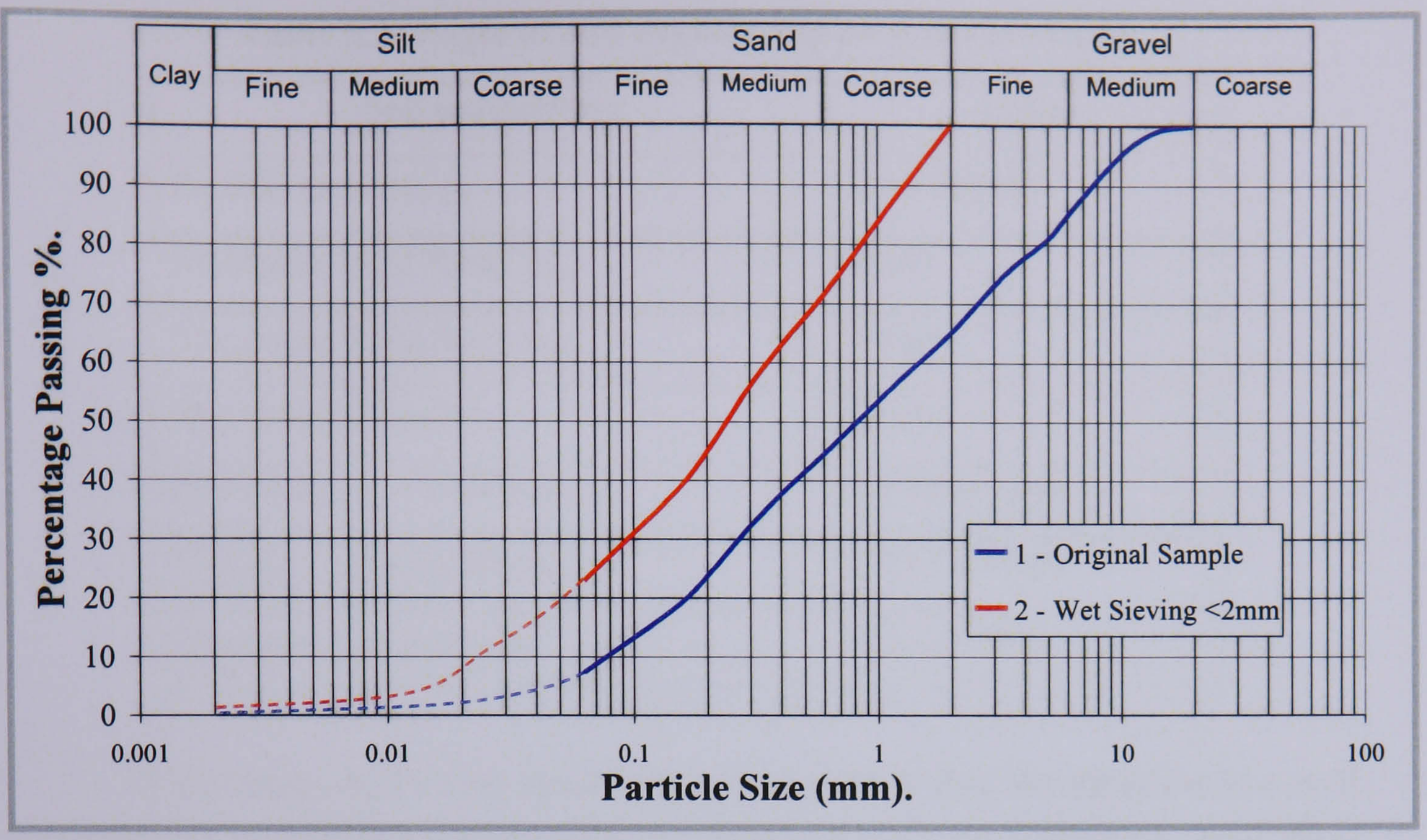

Figure 5.7. Particle Size Distribution Curves of JPS

Liquid Limit was determined using the Cone Penetrometer method in accordance with BS 1377-2: 1990 part 4.3. The results are valid for particles passing the 425 μm sieve, which makes up 64% of the soil by weight. The results are listed in Table 5.3.

Particle density, and maximum and minimum void ratios were measured by British standard BS 1377-2: 1990 part 8.2, BS 1377-4: 1990 part 4.2 and BS 1377-4: 1990 part 4.4, respectively. The results are listed in Table 5.3.

Coefficient of Consolidation, Volume Compressibility and Permeability were determined following the consolidation stage of sample preparation, in accordance with BS 1377-8: 1990 part 6.3. The results are listed in Table 5.3.

Table 5.3. Physical and engineering proprieties of JPS

Soil parameters	Value
Particle Density, ρ_s	2.64 Mg/m^3
Minimum Void Ratio, e_{min}	0.487
Maximum Void ratio, e_{max}	0.943
The liquid limit, W_L	25.5%
Consolidation Coefficient, c_v	26.33 m^2/year
Volume Compressibility, m_v	0.282 m^2/MN
Permeability (loose), k	$2.3x10^{-3}$ m/s

It has been shown that Jeddah Port sand used in this investigation is a well graded soil consisting of 82% sand and 18% silt and finer fractions. The fines contained within the soil have a Liquid Limit w_L= 25% and are non plastic in nature. Soil particles are angular to sub-angular in nature. These findings demonstrate that Jeddah Port sand meets the requirements of a potentially liquefiable soil as determined by Wang (1979) as discussed in Section 2.5.2.1.

5.4 Monotonic and Cyclic Triaxial tests

In this study, a series of monotonic and cyclic triaxial tests were conducted under undrained conditions for Jeddah Port sand. The sand was taken from the reclaimed ground of Jeddah quay walls and was formed into a remoulded sample. The results of these tests provide a framework for calibration and validating numerical models that can be used for simulating soil response in different geotechnical engineering applications.

5.4.1 Triaxial testing equipment and test procedures

The stress:strain behaviour of soils can be investigated under a relatively simple set of boundary conditions in triaxial tests. Although the triaxial apparatus is widely used to determine the stress:strain characteristics of soils, it has major limitations such as:

- Two of the principal stresses have to be identical, because the samples are cylindrical.

- The principal stress and strain directions coincide and are fixed with reference to the soil sample.

The apparatus is further limited by its inability to accommodate the strains that can result if the axes of anisotropy of the soil specimen (for instant in a sample taken in the field) do not coincide with the imposed principal axes of the apparatus. The top and the bottom end rigid platen faces are assumed to be smooth and to remain horizontal during a test so that the top and bottom faces of the sample are principal planes. This is not of great concern for this type of soil.

5.4.1.1 Triaxial Apparatus

The apparatus used to carry out the monotonic and cyclic tests on Jeddah Port sand was the GDS Cyclic Triaxial Automated System (GDSCTAS) (GDS, 2005). The apparatus uses a traditional load frame and triaxial cell to allow high load static work with an additional +/-5kN dynamic actuator for dynamic cyclic work as shown in Figure 5.8 (a). The top of the triaxial cell is modified to use low friction bearings for the load ram. Force is measured in the vertical axis by a submersible internal load cell. Axial displacement is measured externally by a linear potentiometer.

The cell base houses the hydraulic connections for back pressure (top of specimen), pore pressure (bottom of specimen) and cell pressure conditions. The cell top is held in place on the cell base by six tie rods. The axial piston is controlled vertically by a pneumatic bellofram actuator capable of generating loads of up to 5 kN with a stroke of 50 mm. The bellofram actuator is controlled by a separate unit consisting of a pneumatic valve, air buffer and dump valve, and runs on compressed air from an external compressor.

The pressure/volume controller is used to apply the back pressure and subsequently measure changes in volume of the test specimen. The controller consists of a standard Pressure/Volume Controller (STDDPC) with pressure ranges from 1 to 4MPa, serial PC connectivity and 200cc volumetric capacity (see Figure 5.8 (b)). In addition, data acquisition is performed by the GDSLAB control and acquisition software manufactured by GDS Instruments, Hook Hampshire.

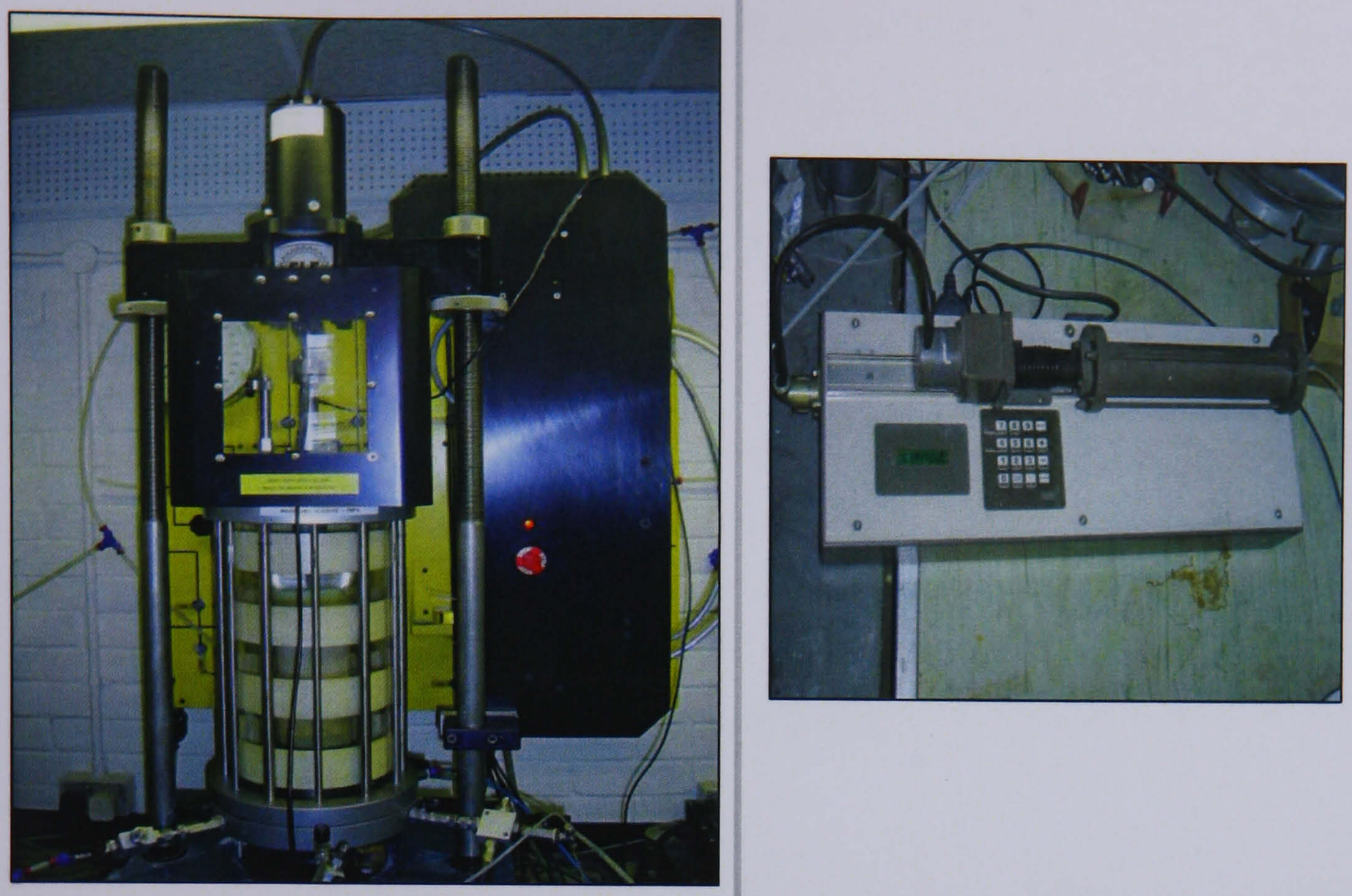

Triaxial test apparatus used in this study | Pressure/Volume controller

Figure 5.8. Monotonic and cyclic triaxial test apparatus

5.4.1.2 Sample preparation, saturation and consolidation stages

Specimens for the monotonic and cyclic triaxial tests were prepared using the moist tamping method as described by Ishihara (1993). This method complies with the requirements of British Standard BS 1377-8: 1990 part 4.1.3.2.4. In this method, it is relatively easy to prepare specimens to a specific density. For the experiments three different densities were chosen: loose (which represents the *in situ* density), medium and dense. The three different sets correspond to relative densities of 35%, 55% and 75%, respectively. As it is not possible to prepare samples to an exact density, the above densities were actually target densities. During experimentation all samples were prepared to be within 2% of target density. This demonstrated that the tamping method chosen is a good method to achieve control densities.

A latex membrane is sealed around a porous disc and the pedestal of the triaxial testing machine, using two rubber O-rings. The membrane is stretched over a split mould 70 mm in diameter and 180 mm high. A pre-determined amount of soil with moisture content w = 5% is then compacted into seven 25 mm layers using a

square compaction foot measuring 250 mm^2. The split mould and compaction foot used in sample preparation are shown in Figure 5.9 (a). This method ensures a constant void ratio and density throughout the sample. Another porous stone is placed on the top of the specimen before the top cap and rubber membrane are sealed around it, again using two rubber O-rings. The back pressure hose is connected from the top cap to the hydraulic connection. Figure 5.9 (b) shows a prepared sample.

The average specimen height is then measured as the distance between the two porous discs. Similarly an average of three diameters, taken from the top, middle and bottom of the sample, is calculated. The initial sample volume may then be determined. Because the specimen volume is almost known, the required weight to achieve the specific relative density can be calculated as:

$$Dr = \frac{e_{max.} - e_{in-situ}}{e_{max.} - e_{min.}} \tag{5.3}$$

where e_{max} and e_{min} are the maximum and minimum void ratio, respectively. e is the void ratio giving by:

$$e = \frac{\rho_s}{\rho_b}(1 + w) - 1 \tag{5.4}$$

where ρ_s is particle density, w is water content, and ρ_b is bulk density given by:

$$\rho_b = \frac{MassOfSample}{VolumeOfSample} \tag{5.5}$$

Afterwards, the specimens were saturated based on British Standard BS 1377-8: 1990 part 5.3. The objective of this stage is to ensure that all the voids are filled with water. This can be achieved by increasing the pore pressure in the specimen to that level which is enough for the water to absorb in solution all the air originally in the voids and is measured by its B-value. The pore pressure can be increased by applying back pressure to the specimen, and at the same time increasing the cell

pressure in order to maintain a small positive effective stress. A B-value of approximately 0.95 was attempted for the entire test prior to consolidation and consequent testing of specimens. However, in some cases, it was difficult to achieve a saturation level where the B-value is greater or equal to 0.95, because the increasing confining pressure is transmitted to the soil fabric and not entirely to an increase in pore pressure (Bishop & Henkel, 1962). As a consequence, the degree of saturation was calculated and is used alongside the measured B value.

When the specimen is saturated, a certain confining pressure was applied to consolidate the specimen isotropically. The objective of this stage is to bring the specimen to the state of effective stress required for carrying out the compression test. Finally, due to the consolidation process, the specimen dimension will differ from the original dimensions after sample preparation. The new volume should be considered to determine the final relative density.

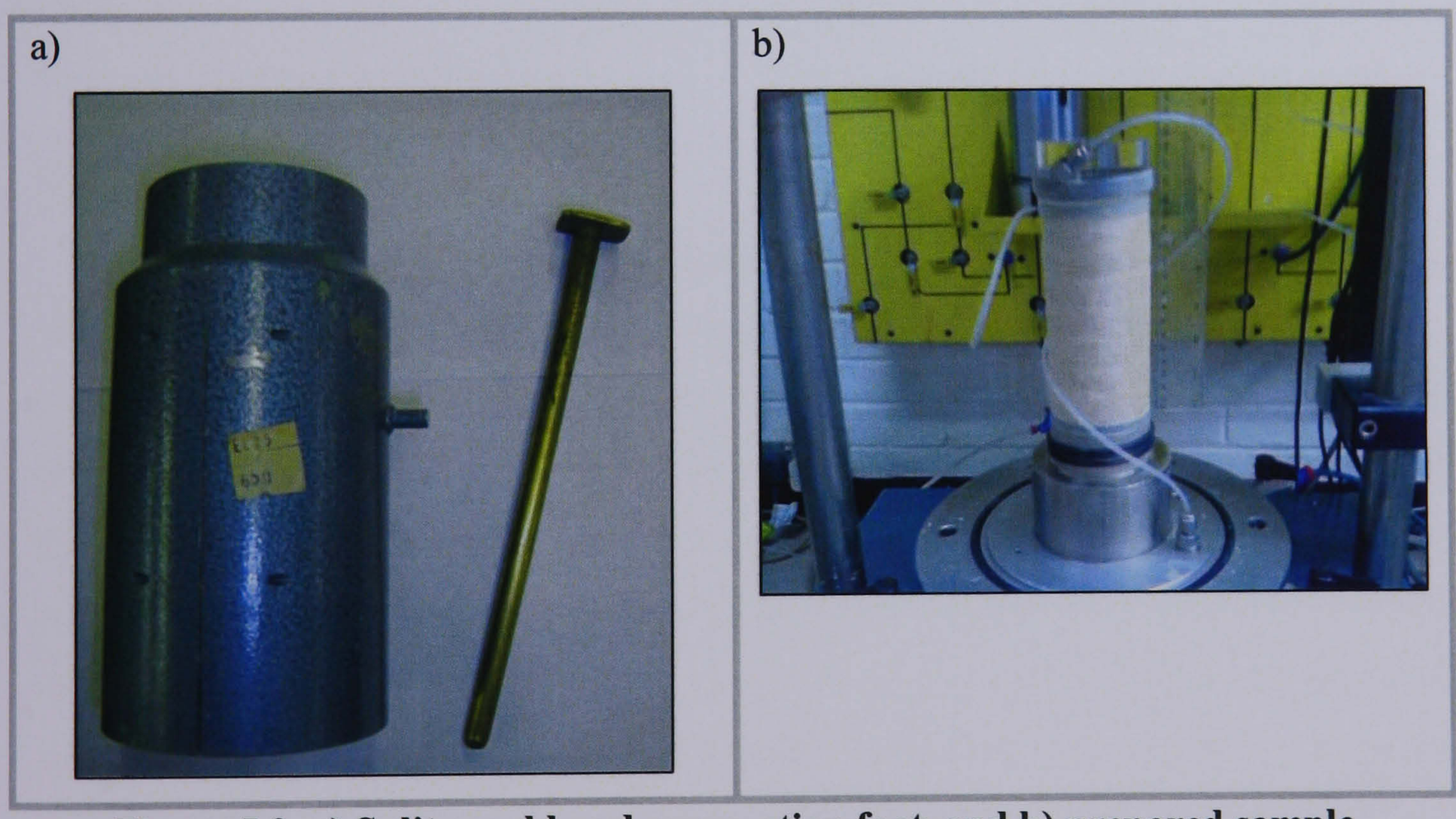

Figure 5.9. a) Split mould and compaction foot, and b) prepared sample

5.4.1.3 Monotonic Test method

The monotonic triaxial tests conducted in this study were isotropically consolidated undrained tests and were performed under constant cell pressures with axial strain rates of 0.1 mm/min. The test was terminated once the axial strain reached 15%. Axial strain and excess pore pressures were measured at both the top and the bottom of the sample. These tests were conducted based on BS 1377-8: 1990 part 7. These tests are summarised in Table 5.4.

Table 5.4. Monotonic triaxial tests list

Test	Relative density D_r (%)	Confining pressure p' (kpa)	Axial strain ε_a (%)
M01	35	100	15
M02	55	100	15
M03	75	100	15

5.4.1.4 Cyclic test method

The cyclic triaxial tests conducted during this study were isotropically consolidated undrained and were performed under constant cell pressure conditions at three different amplitudes of deviator stresses; q=±40, q=±50 and q=±60 kPa. Testing was terminated once the axial strain reached 5% double amplitude as recommended by Ishihara (1993). Samples were prepared using the moist tamping method as discussed in Section 5.4.1.1. A cyclic loading rate of 1 Hz as recommended by Ghosh & Madabhushi (2003) was adopted. It should be noted that the cyclic test method is not included in the British Standard. Therefore, these tests were conducted based on ASTM: D 5311-92 (1996), *The Standard Test Method for Load Controlled Cyclic Triaxial Strength of Soil.* This method allows the determination of the cyclic strength for a reconstituted soil in undrained conditions. The cyclic tests are summarised in Table 5.5.

Table 5.5. Cyclic triaxial tests list

Test	Relative density D_r (%)	Confining pressure p' (kPa)	Axial strain ε_a (%)	Amplitude $\pm q$ (kPa)	Frequency f (Hz)
C01	35	100	5	40	1
C02	35	100	5	50	1
C03	35	100	5	60	1
C04	55	100	5	40	1
C05	55	100	5	50	1
C06	55	100	5	60	1
C07	75	100	5	40	1
C08	75	100	5	50	1
C09	75	100	5	60	1

Finally, specimen parameters of suggested Monotonic and Cyclic triaxial tests are illustrated in Table 5.6.

Table 5.6. Specimen parameters

Test	Sample	$D_{int.}$ (mm)	$H_{int.}$ (mm)	$V_{int.}$ (mm^3)	Soil mass (g)	ρ_{int} (Mg/m^3)	$Dr_{int.}$ (%)	$e_{int.}$	$\Delta V_{int.}$ (mm^3)	$\rho_{con.}$ (Mg/m^3)	$Dr_{con.}$ (%)	$e_{con.}$	*B-value*	S_r
Monotonic CU	M01	67.60	134.0	480937	700	1.455	26.0	0.817	12000	1.493	35.3	0.771	0.92	93.8
Monotonic CU	M02	67.47	136.7	488742	760	1.555	49.8	0.700	6600	1.576	54.5	0.677	0.90	106.1
Monotonic CU	M03	67.60	137.0	491704	810	1.647	69.4	0.605	9500	1.680	75.8	0.574	0.92	90.8
Cyclic CU	C01	67.67	133.3	479415	700	1.460	27.1	0.811	12000	1.498	36.4	0.765	0.86	94.4
Cyclic CU	C02	67.00	135.3	477020	700	1.467	29.0	0.802	8500	1.494	35.6	0.770	0.86	105.4
Cyclic CU	C03	68.27	134.0	490517	700	1.427	18.5	0.853	20700	1.490	34.6	0.775	0.85	94.3
Cyclic CU	C04	67.63	136.7	491063	760	1.548	48.2	0.708	6600	1.569	52.9	0.685	0.90	98.6
Cyclic CU	C05	68.80	135.3	502996	760	1.511	39.7	0.750	20400	1.575	54.2	0.679	0.88	116.1
Cyclic CU	C06	68.07	135.7	493834	760	1.539	46.2	0.718	11200	1.575	54.2	0.679	0.96	97.9
Cyclic CU	C07	68.00	137.0	497540	810	1.628	65.5	0.624	9500	1.660	71.9	0.593	0.92	88.1
Cyclic CU	C08	67.40	136.3	486301	810	1.666	73.0	0.587	6200	1.687	77.2	0.567	0.90	108.7
Cyclic CU	C09	68.03	135.3	491800	810	1.647	69.3	0.605	6400	1.669	73.6	0.584	0.85	113.7

D Diameter
H Height
V Volume
ρ Bulk density
D_r Relative density
e Void ratio
S_r Degree of saturated

int. Before consolidation reading
con. After consolidation reading
CU Consolidation undrained

5.4.2 Testing results

Monotonic and cyclic tests were conducted under undrained conditions. Soil samples tested in undrained conditions are not capable of changing volume, as the water cannot escape. The soil, therefore, transfers stresses from the grain structure to the pore water, thus changing the effective stresses.

5.4.2.1 Monotonic tests results

A series of strain-controlled, isotropically consolidated undrained monotonic triaxial tests were performed on samples of Jeddah Port sand at different densities, with similar initial mean effective stresses. Figure 5.10 shows the combined, stress:strain relationships, excess pore pressure:axial strain and stress paths plots for tests; M01, M02 and M03. These samples are subjected to undrained monotonic compression to 15 % axial strain, and were carried out at the same effective confining stress of 100 kPa.

For the loose specimen (M01), it can be observed that the maximum shear stress reached 50 kPa at 0.75% axial strain. This is followed by strain softening behaviour to a residual strength of 12 kPa at large strain (see Figure 5.10 (a)). From Figure 5.10 (b), it can be seen that following the initial and rapid increase in pore pressure due to the sample undergoing contraction, the rate at which excess pore pressure generated gradually decreases, leading to the reduction in shear strength and ultimately to the *liquefaction* of the sample (see Figure 5.10 (c)).

The medium dense soils (M02) initially exhibited a contractive behaviour up to the point of phase transformation (Ishihara *et al.*, 1975) after which the dilative behaviour started (see Figure 5.10 (c)). This leads to a reduction in excess pore pressure and strain hardening occurs. This behaviour is known as *limited liquefaction*.

By contrast, the dense specimen (M03) initially contracted until reaching 1% axial strain then dilated with increasing shear stress and effective mean principal stress, leading to the reduction in excess pore pressure. This behaviour is known as *dilation*.

The three stress paths plotted in p'-q space allow the Failure line of the soils to be determined. The effective internal friction angle of the soil ϕ' is obtained as follows:

$$\phi' = \sin^{-1}\left(\frac{3M}{6+M}\right) \tag{5.6}$$

where M is the slope line of Failure line, which is obtained from Figure 5.10 (c) and it is equal to 1.5. From the above equation, the internal friction angle of the soil ϕ' is equal to 36.8°.

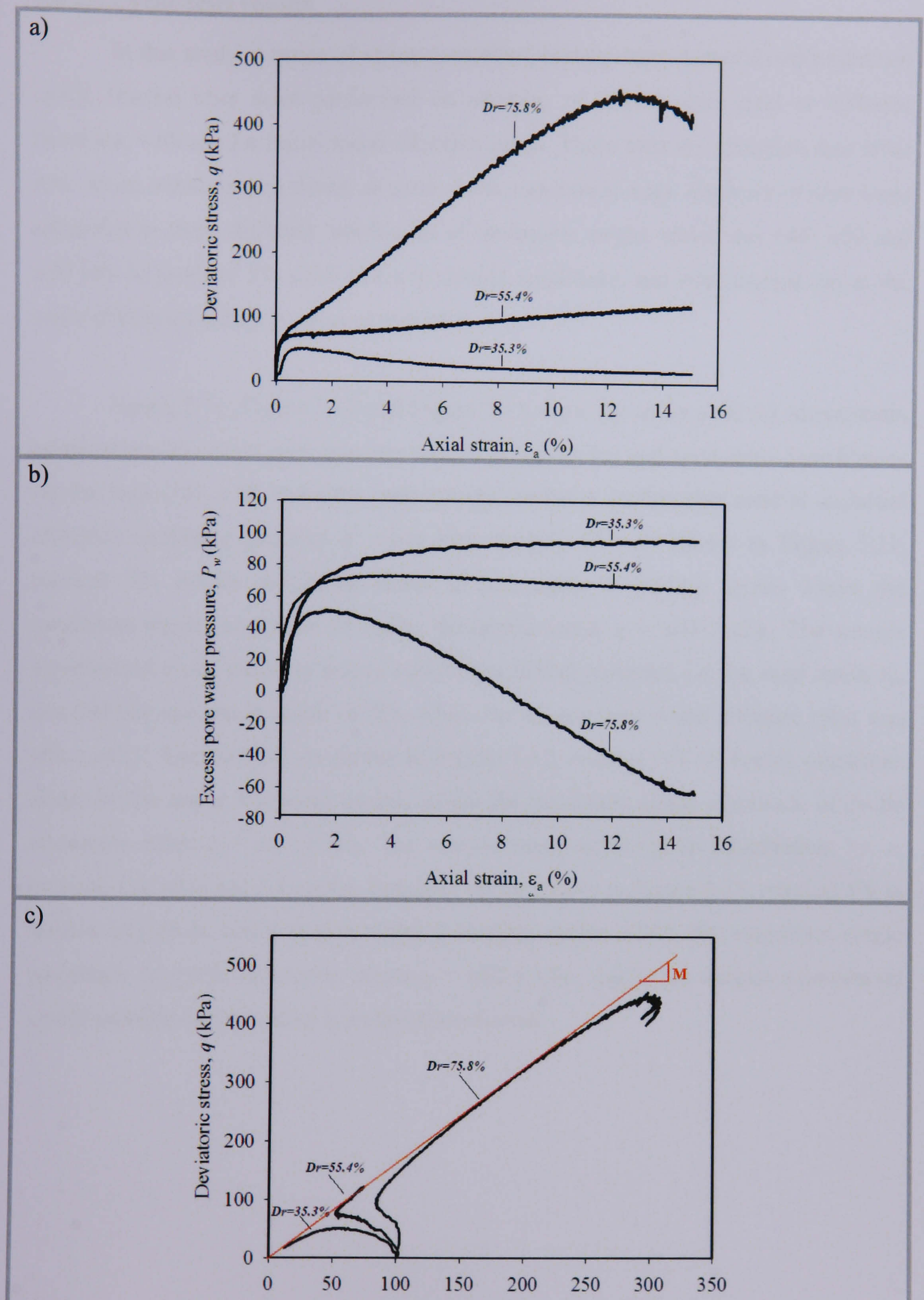

Figure 5.10. Effect of density for Jeddah Port sand in undrained trixial compression tests: a) stress:strain relationships, b) excess pore pressure : axial strain and c) stress paths

5.4.2.2 Cyclic tests results

In this study, a series of stress-controlled, isotropically consolidated undrained cyclic triaxial tests were performed on samples of Jeddah Port sand at different densities, with similar initial mean effective stress. These tests are classified into three sets: loose, medium and dense, as used in the monotonic tests. Each set of tests were subjected to three different amplitudes of deviatoric stress, which are ±40, ±50 and ±60 kPa to produce 5% axial strain in double amplitude, and were carried out at the same effective confining stress of 100 kPa.

Figure 5.11, Figure 5.12 and Figure 5.13 show the stress path (a), stress:strain relationship (b) excess pore pressure ratio time history (c) and axial strain time history (d) for tests C01, C02 and C03, respectively, on loose Jeddah Port sand at an initial effective confining pressure p' =100 kPa. Sample C01 as shown in Figure 5.11, reached 5% double amplitude strain in just under 8 loading cycles where the maximum single amplitude of cyclic deviatoric stress q = ±41.7 kPa. The sample experienced cyclic mobility before initial liquefaction occurred, i.e. the axial strain, ε_a, reached the maximum value of 5%, while the excess pore water pressure ratio was still r_u=0.7. Sample C02, as shown in Figure 5.12, reached 5% in double amplitude strain in just under 4 loading cycles, where the maximum single amplitude of cyclic deviatoric stress q = ±47.6 kPa. The sample experienced cyclic liquefaction, i.e. r_u reached 1.0, after just 3.2 cycles. Sample C03, as shown in Figure 5.13, reached 5% in double amplitude strain in just under 2 loading cycles where the maximum single amplitude of cyclic deviatoric stress q = ±62.5 kPa. Again the sample experienced cyclic mobility before initial liquefaction occurred.

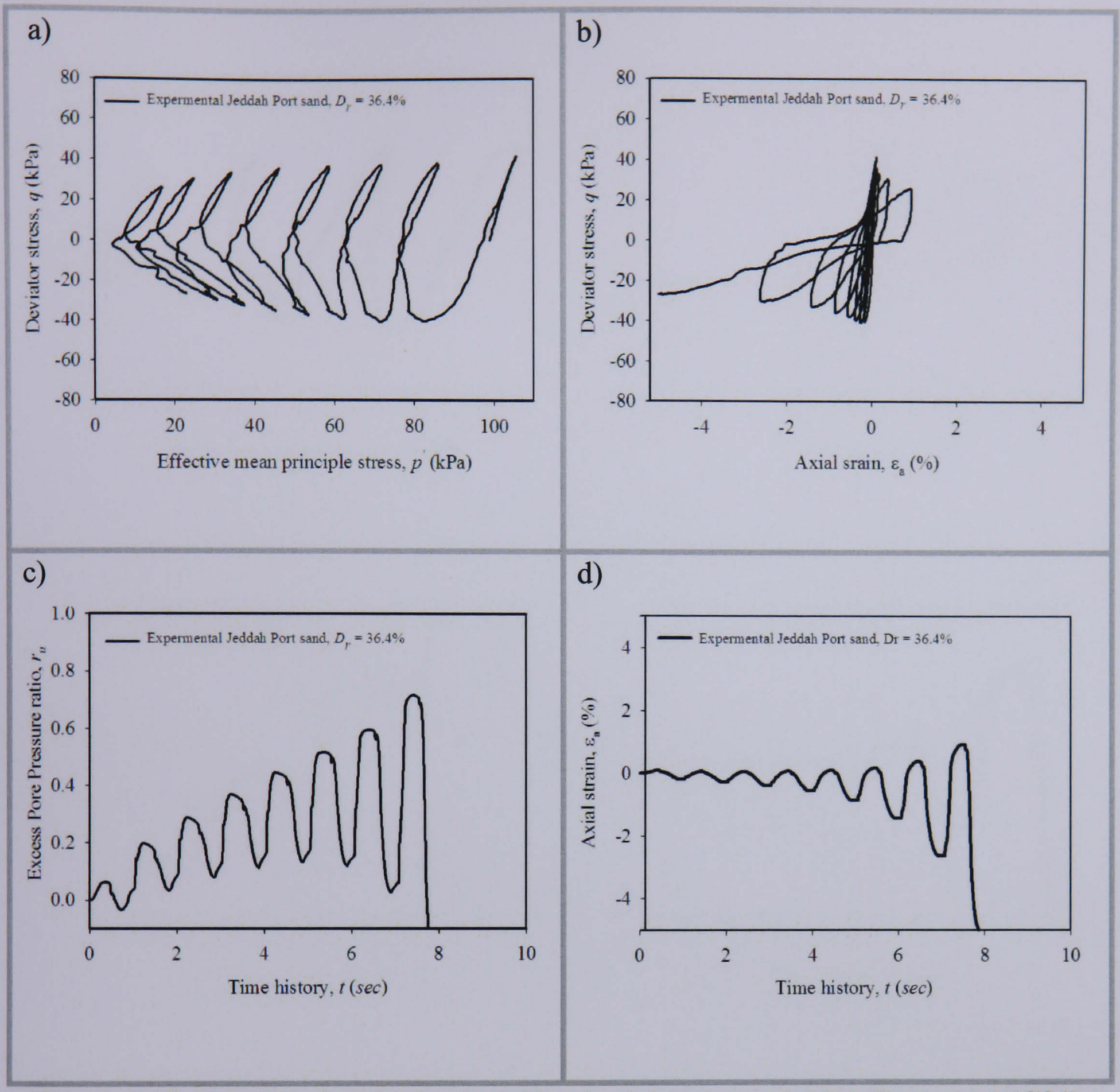

Figure 5.11. Results of undrained cyclic triaxial tests on Jeddah Port sand (C01) (Relative density, D_r=36.4% & Peak Amplitude, q=41.7 kPa): a) stress path ; b) stress:strain relationship; c) excess pore pressure ratio time history and d) axial strain time history

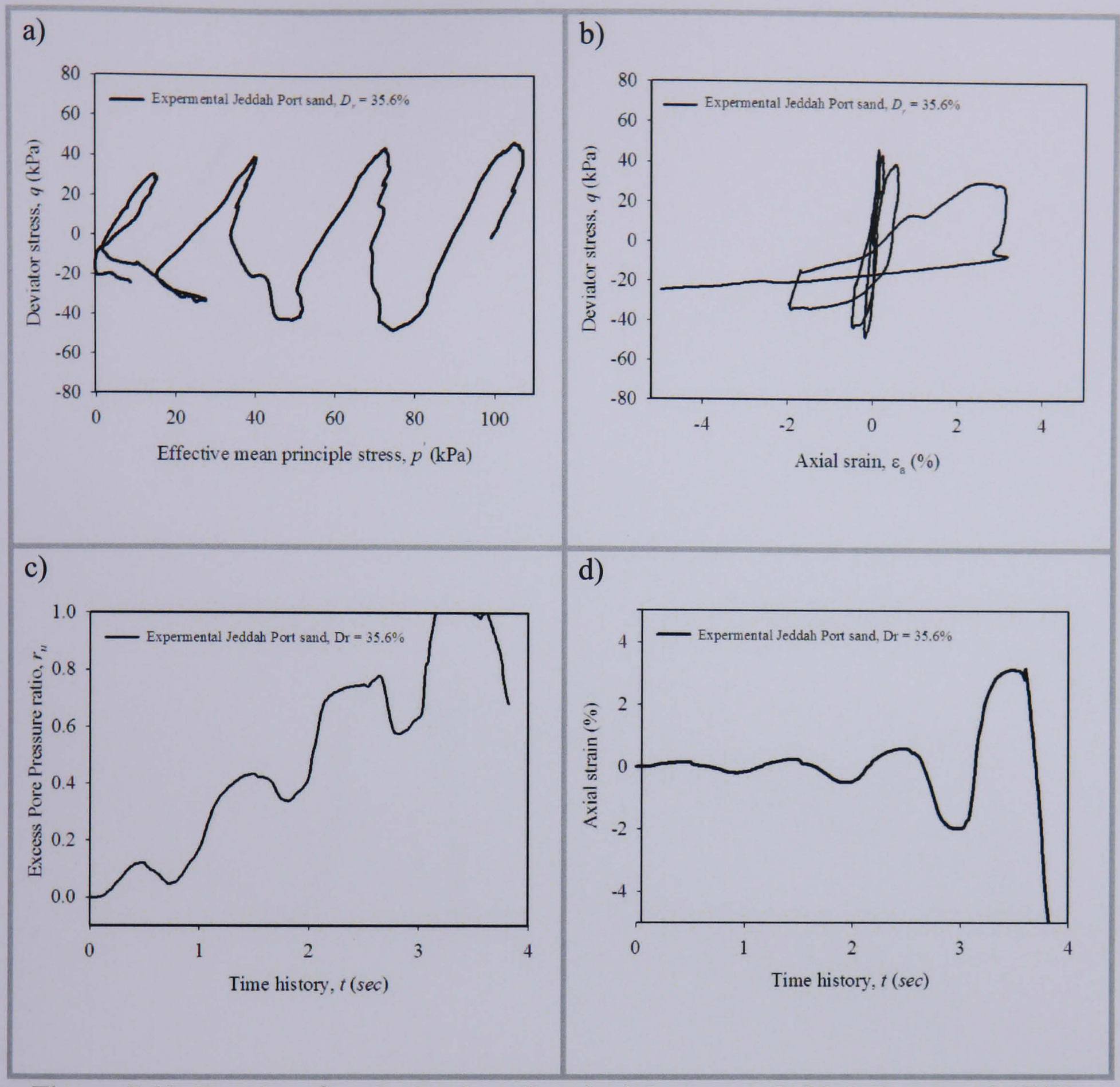

Figure 5.12. Results of undrained cyclic triaxial tests on Jeddah Port sand (C02) (Relative density, D_r=35.6% & Peak Amplitude, q=47.6 kPa): a) stress path ; b) stress:strain relationship; c) excess pore pressure ratio time history and d) axial strain time history

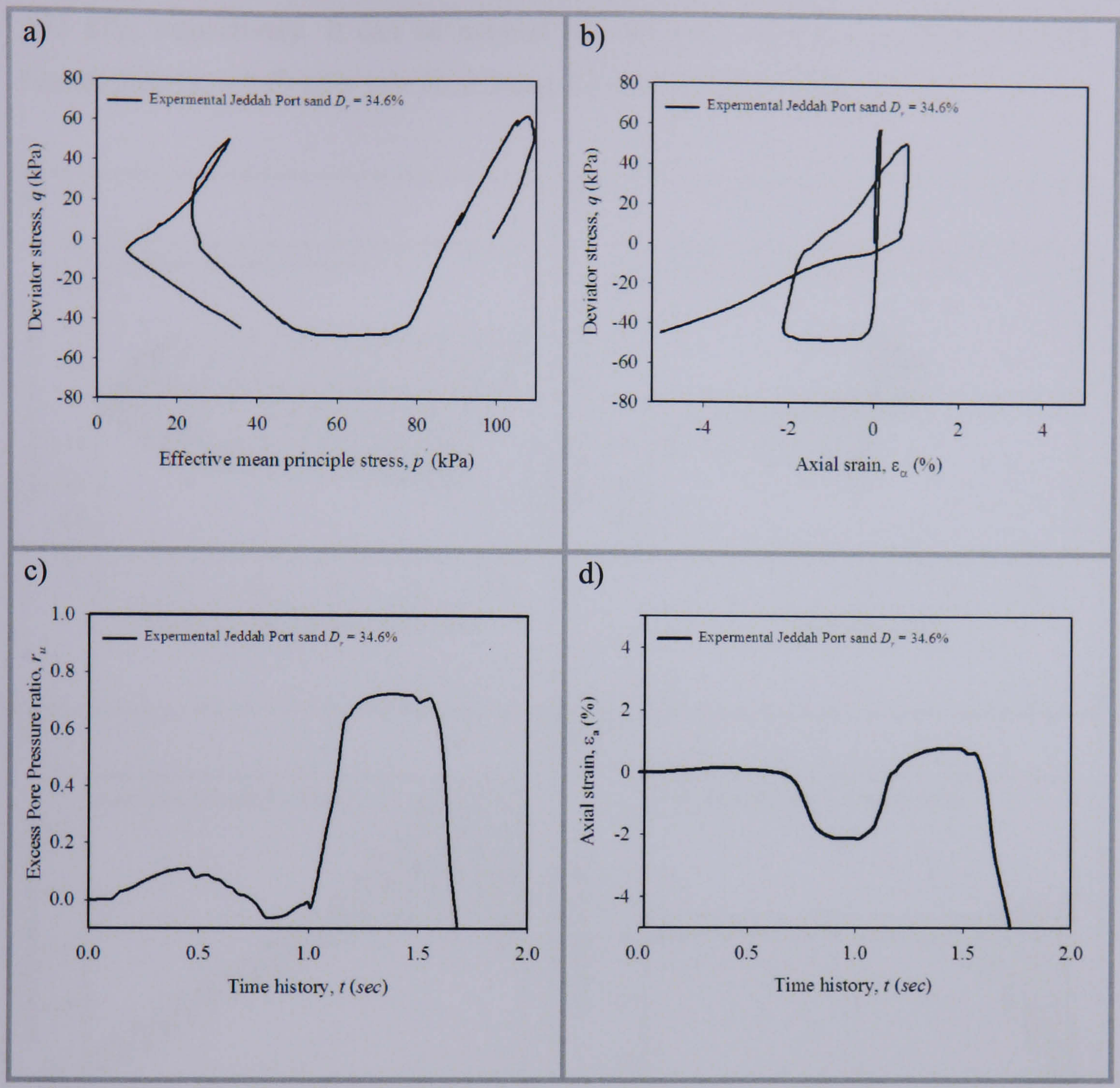

Figure 5.13. Results of undrained cyclic triaxial tests on Jeddah Port sand (C03) (Relative density, D_r=34.6% & Peak Amplitude, q=6.2.5 kPa): a) stress path ;b) stress:strain relationship; c) excess pore pressure ratio time history and d) axial strain time history

The undrained cyclic tests for medium dense specimen results are presented in Figure 5.14, Figure 5.15 and Figure 5.16 for tests C04, C05 and C06, respectively. Again, each test was carried out at different amplitudes of deviatoric stress q = ±40 kPa, q = ±50 kPa and q = ±60 kPa, respectively.

From Figure 5.14, Figure 5.15 and Figure 5.16, it can be seen that the samples C04, C05 and C06 reached 5% in double amplitude strain in just under 20, 10 and 5 loading cycles, respectively. The maximum single amplitude of cyclic deviatoric

stress to which the samples were subjected were q = ±38.7 kPa, q = ±48.8 kPa and q = ±62 kPa, respectively. It can be noticed that all three samples experienced cyclic liquefaction (r_u = 1.0) after just 16, 8.3 and 4.2 cycles, respectively.

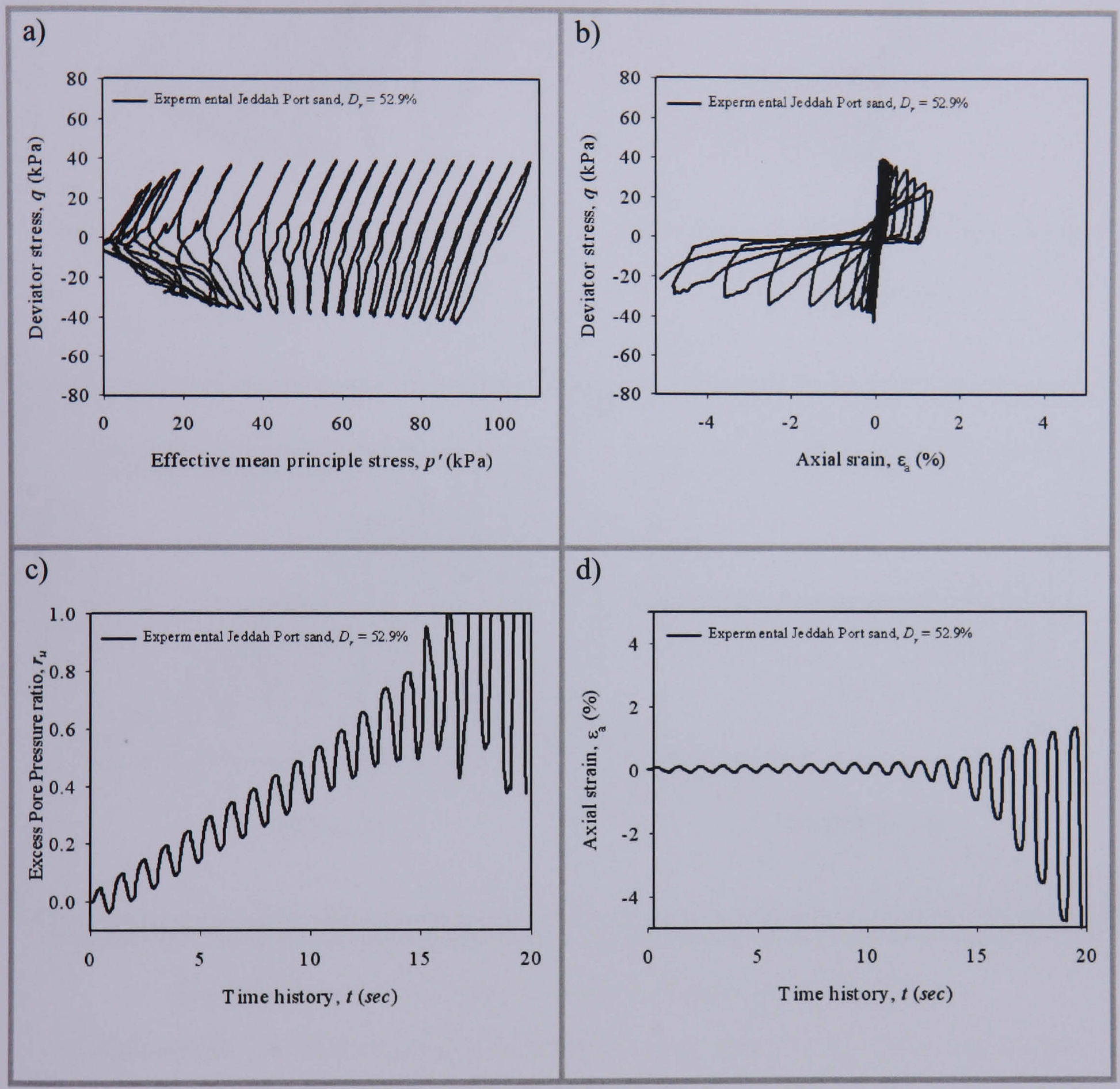

Figure 5.14. Results of undrained cyclic triaxial tests on Jeddah Port sand (C04) (Relative density, D_r=52.9% & Peak Amplitude, q=38.7 kPa): a) stress path ;b) stress:strain relationship; c) excess pore pressure ratio time history and d) axial strain time history

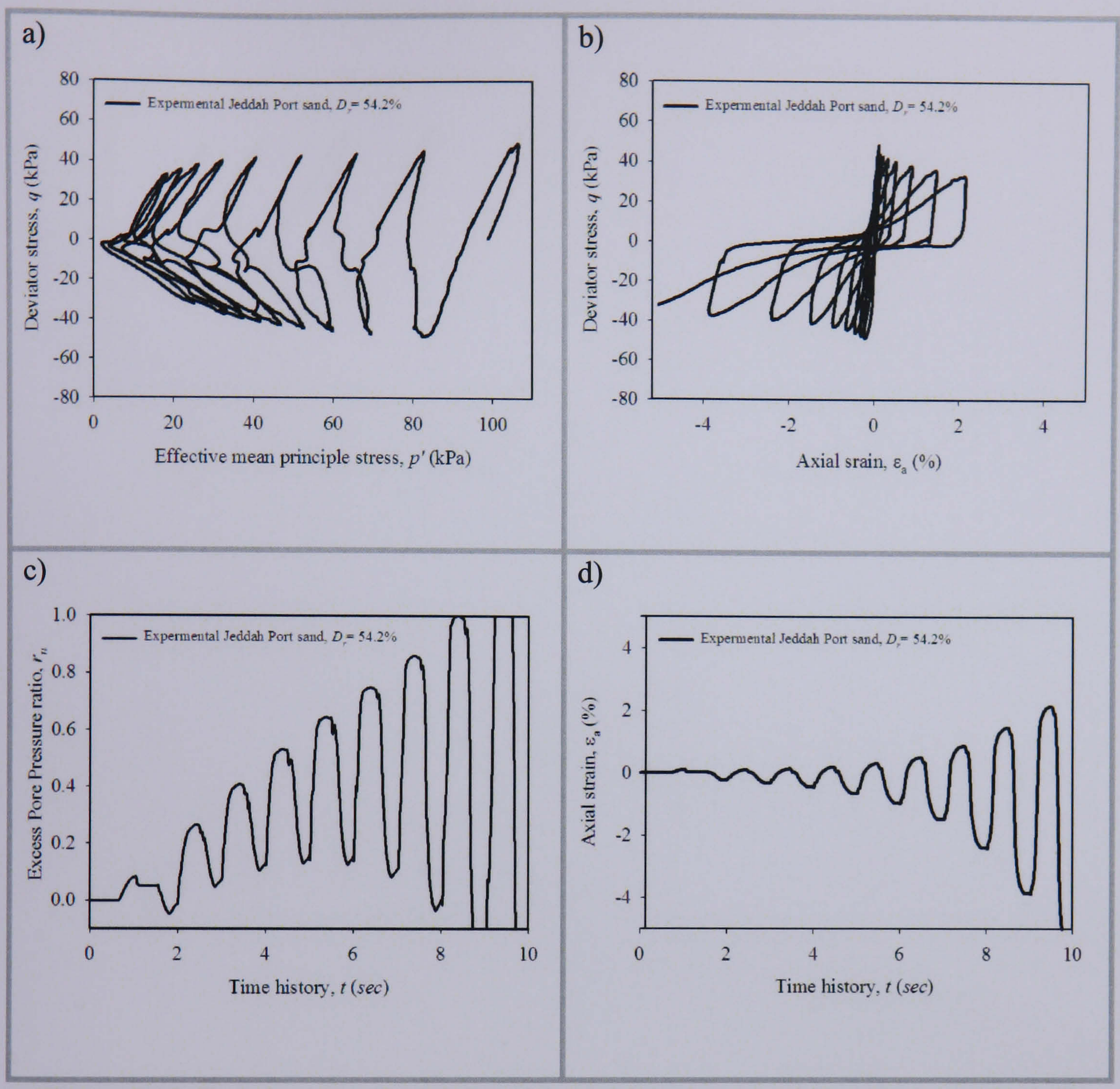

Figure 5.15. Results of undrained cyclic triaxial tests on Jeddah Port sand (C05) (Relative density, D_r=54.2% & Peak Amplitude, q=48.8 kPa): a) stress path ; b) stress:strain relationship; c) excess pore pressure ratio time history and d) axial strain time history

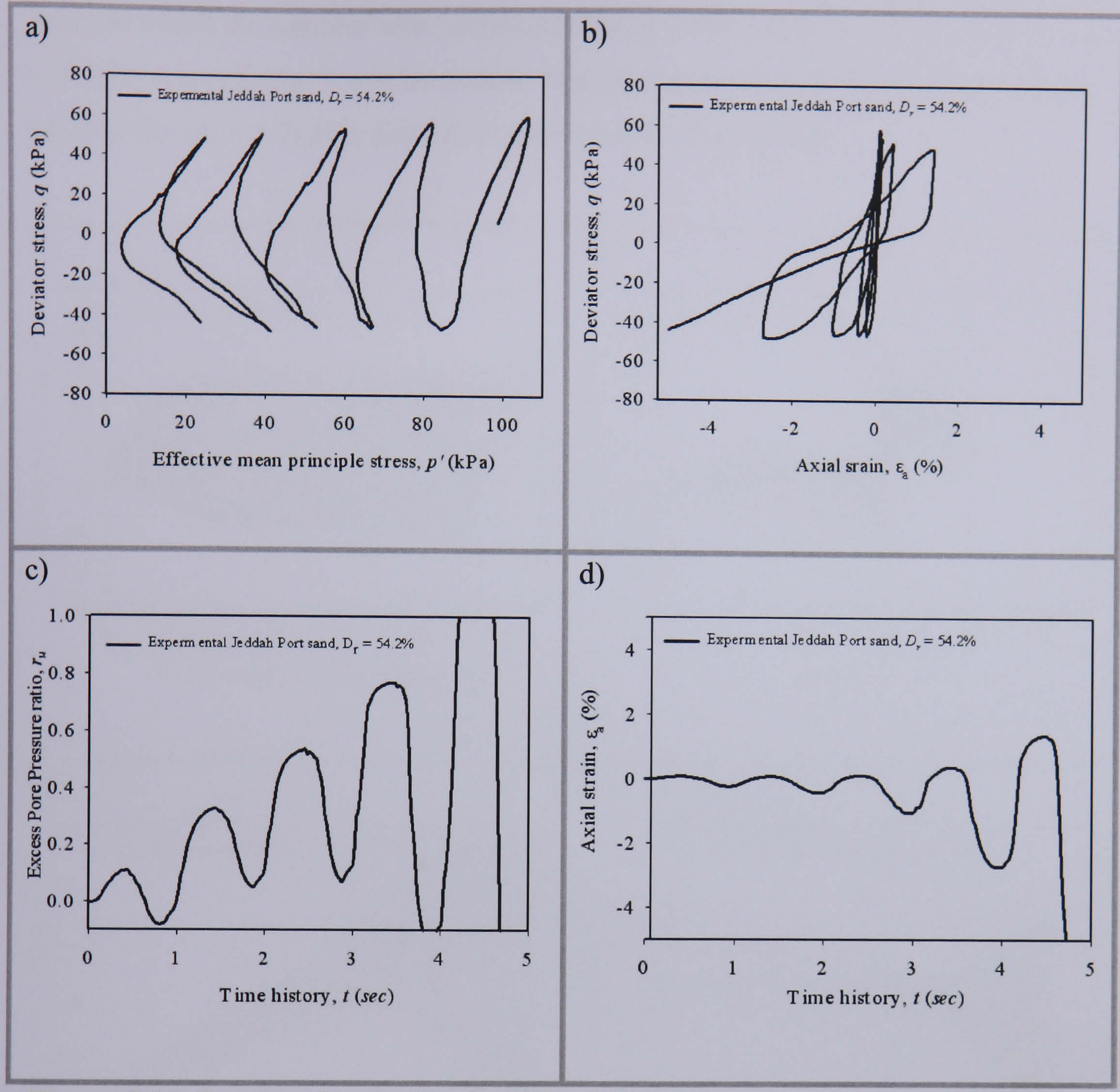

Figure 5.16. Results of undrained cyclic triaxial tests on Jeddah Port sand (C06) (Relative density, D_r=54.2% & Peak Amplitude, q=62.0 kPa): a) stress path ;b) stress:strain relationship; c) excess pore pressure ratio time history and d) axial strain time history

The undrained cyclic test results for medium dense specimens are presented in Figure 5.17, Figure 5.18 and Figure 5.19 for test C07, C08 and C09, respectively. Again, each test was carried out at different amplitudes of deviatoric stress: q = ±40 kPa, q = ±50 kPa and q = ±60 kPa, respectively.

From Figure 5.17, Figure 5.18 and Figure 5.19, it can be seen that the samples C07, C08 and C09 reached 5% in double amplitude strain in just under 23, 18 and 7

loading cycles, respectively. The maximum single amplitude of cyclic deviatoric stress to which the samples were subjected were q = ±44.1 kPa, q = ±48.4 kPa and q = ±60 kPa, respectively. It can be noticed that all the three samples experienced cyclic liquefaction (r_u = 1.0) after just 18, 11 and 4 cycles, respectively.

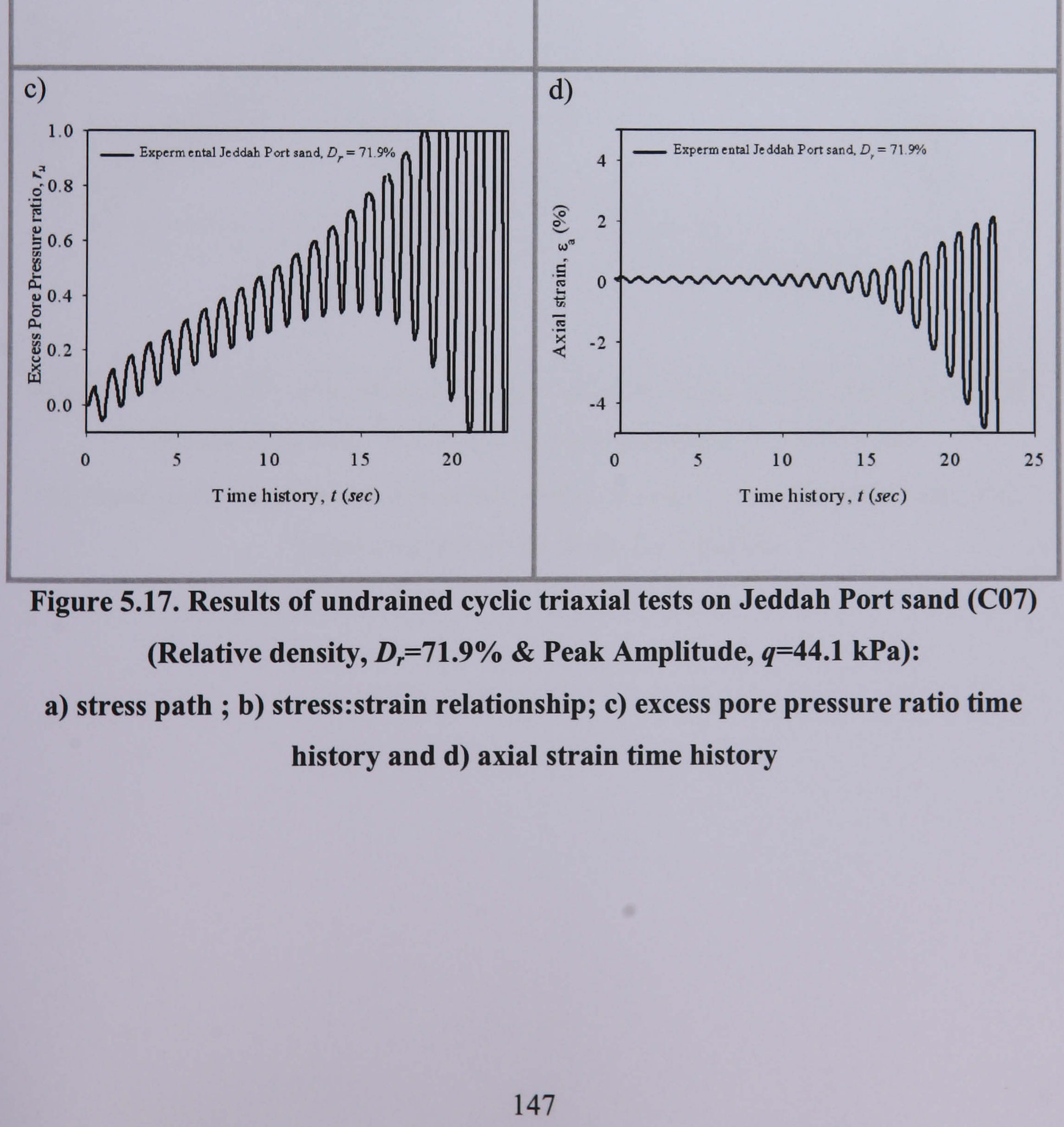

Figure 5.17. Results of undrained cyclic triaxial tests on Jeddah Port sand (C07) (Relative density, D_r=71.9% & Peak Amplitude, q=44.1 kPa): a) stress path ; b) stress:strain relationship; c) excess pore pressure ratio time history and d) axial strain time history

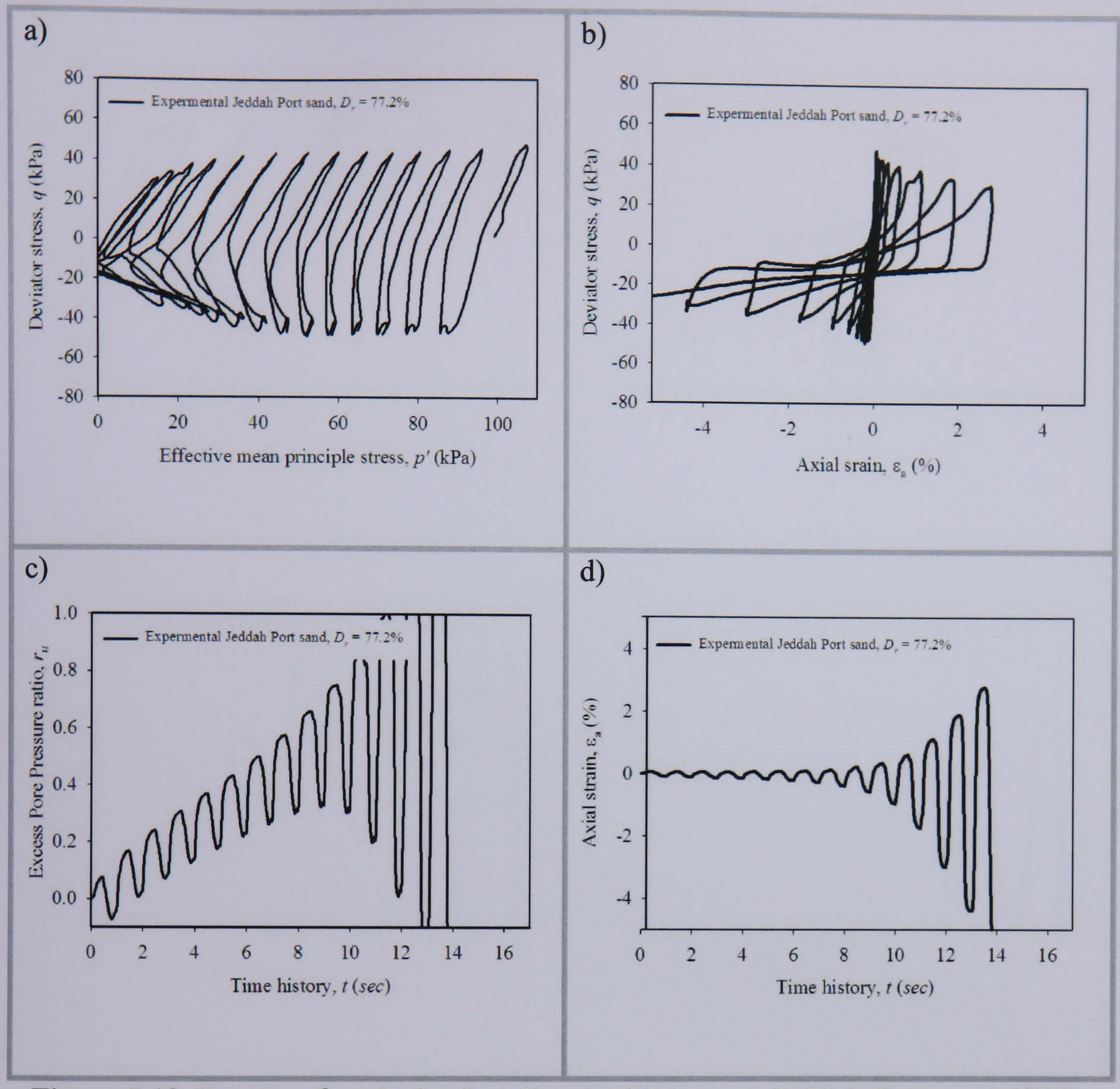

Figure 5.18. Results of undrained cyclic triaxial tests on Jeddah Port sand (C08) (Relative density, D_r=77.2% & Peak Amplitude, q=48.4 kPa): a) stress path ; b) stress:strain relationship; c) excess pore pressure ratio time history and d) axial strain time history

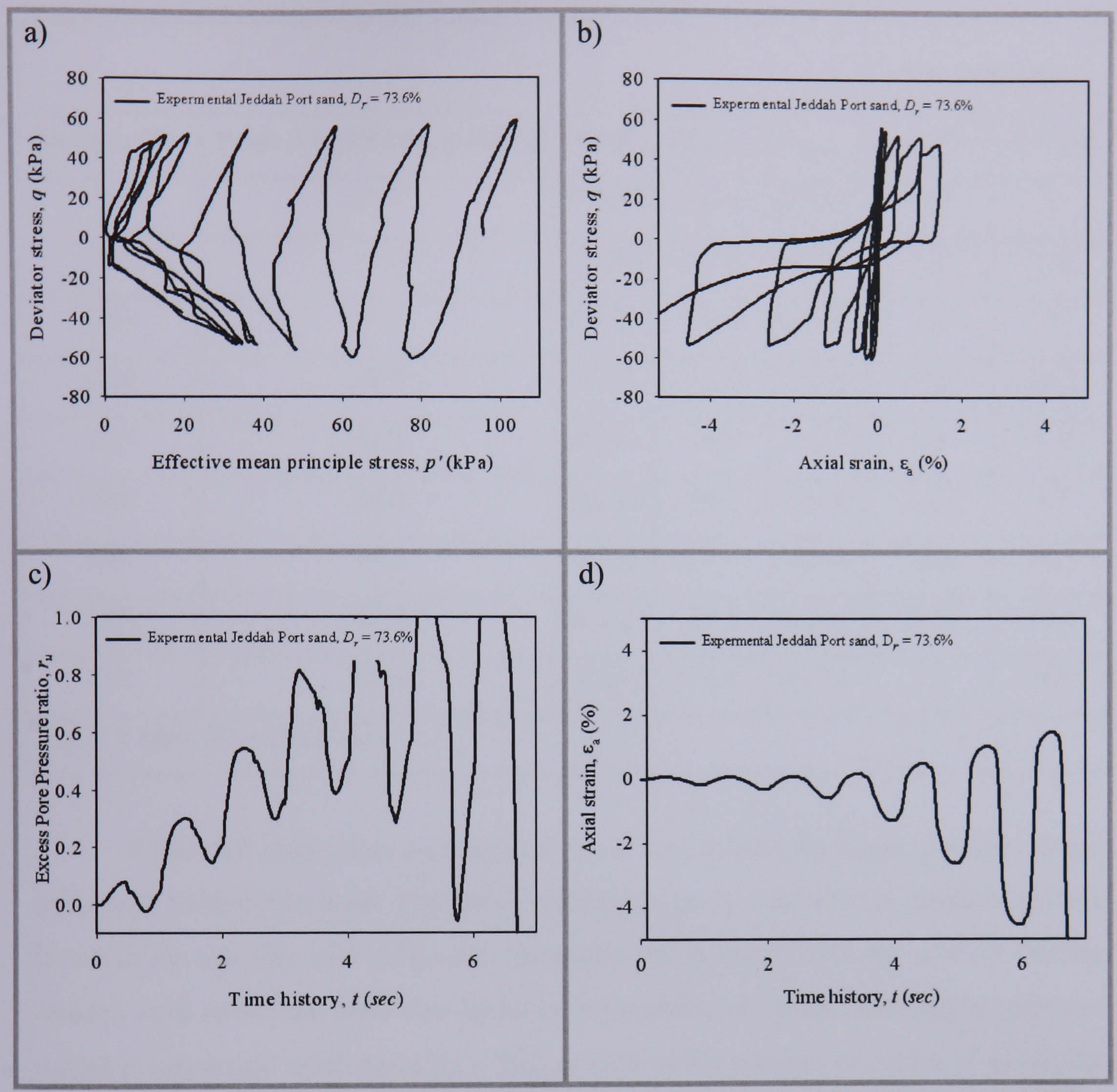

Figure 5.19. Results of undrained cyclic triaxial tests on Jeddah Port sand (C09) (Relative density, D_r=73.6% & Peak Amplitude, q=60.0kPa): stress path ; b) stress:strain relationship; c) excess pore pressure ratio time history and d) axial strain time history

Table 5.7. Undrained cyclic triaxial test results of Jeddah Port sand

					No. of Cycles	
Sample No.	**Peak Amplitude, q (kPa)**	**CSR**	**D_r (con.)**	**e (con.)**	**$\varepsilon_a = 5\%$**	**$r_u = 1.0$**
C01	41.7	0.209	36.4	0.765	7.9	*
C02	47.6	0.238	35.6	0.770	3.8	3.2
C03	62.5	0.313	34.6	0.775	1.7	*
C04	38.7	0.194	52.9	0.685	19.8	16.2
C05	48.8	0.244	54.2	0.679	9.8	8.4
C06	62.0	0.310	54.2	0.679	4.7	4.2
C07	44.1	0.221	71.9	0.593	22.8	18.3
C08	48.4	0.242	77.2	0.567	13.9	11.4
C09	60.0	0.300	73.6	0.584	6.7	4.1
* $r_u < 1$ after 5% axial strain						

Table 5.7 shows the summary of cyclic test results for loose, medium dense and dense Jeddah Port sand. The table contains the peak amplitude in deviatoric stress to which the samples were subjected, the cyclic stress ratio (CSR), the relative density and the void ratio. The table also includes the number of cycles necessary to produce a double amplitude axial strain ($\varepsilon_a = 5\%$) as well as the number of cycles at which the cyclic liquefaction occurs ($r_u = 1.0$).

It can be seen that for loose samples that the cyclic strain reaches 5% before the onset of cyclic liquefaction. This behaviour occurs only in loose sand and is related to the failure line of the soil obtained by monotonic tests shown in Figure 5.10 (c). It is supposed that for samples C01 and C03, the stress state of the soil during cyclic loading reached the Cyclic Liquefaction Surface, resulting in a flow failure before cyclic liquefaction $r_u = 1.0$ could occur. However, for sample C02, cyclic liquefaction was observed before the axial strain reached 5%. From Figure 5.12 (b), it appears that the steady state strength was reached towards the end of the third cycle when the sample was in maximum extension, which would have led to a flow type failure. However, the cyclic loading then switched phase and the sample was

subjected to compression. This had the effect of generating further pore water pressure before the stress state could reach the cyclic liquefaction surface in the compressive region of the steady state line, causing initial liquefaction before the 5% axial strain was reached.

On the other hand, in samples C04 – C09, (medium and dense specimens) cyclic liquefaction was observed before large strains could accumulate. This behaviour is again related to the steady state strength of the soil. For medium dense and dense samples, the steady state strength of Jeddah Port sand is greater than the imposed cyclic shear stress, which explains the occurrence of cyclic mobility, rather than flow type failures.

Ishihara (1993) found that for loose samples, large strains accumulate at the onset of cyclic liquefaction. This study has found that for loose sands, large strains develop before cyclic liquefaction, typically when $r_u \approx 0.8$. Larger strains can be expected when loose samples reach cyclic liquefaction. Ishihara also found that for medium dense and dense sands, cyclic liquefaction produces strains of about 5% whereas in Jeddah Port sand initial liquefaction when r_u =1.0 produces smaller strains, typically 2–3%.

5.4.2.3 Liquefaction strength curve

Figure 5.20 shows the liquefaction strength curves for loose, medium dense and dense Jeddah Port sand at an initial effective confining pressure p' = 100 kPa. The figure represents the number of cycles necessary to induce 5% double amplitude strain against the Cyclic Stress Ratio (CSR). It can be noticed that as density increases, the number of cycles required to induce 5% double amplitude strain increases. It is also observed that as the cyclic stress ratio increases, the number of cycles leading to failure decreases. Ishihara (1993) notes that it is routine practice to determine the CSR value required to produce 5% double amplitude axial strain in 20 cycles as a factor for quantifying and relating the liquefaction resistance of sands for a given relative density. These curves shown in Figure 5.20 are necessary for understanding the susceptibility of soils to cyclic mobility and are commonly used to

determine the parameters required for numerical modelling of soils. This will be discussed in Chapter 6.

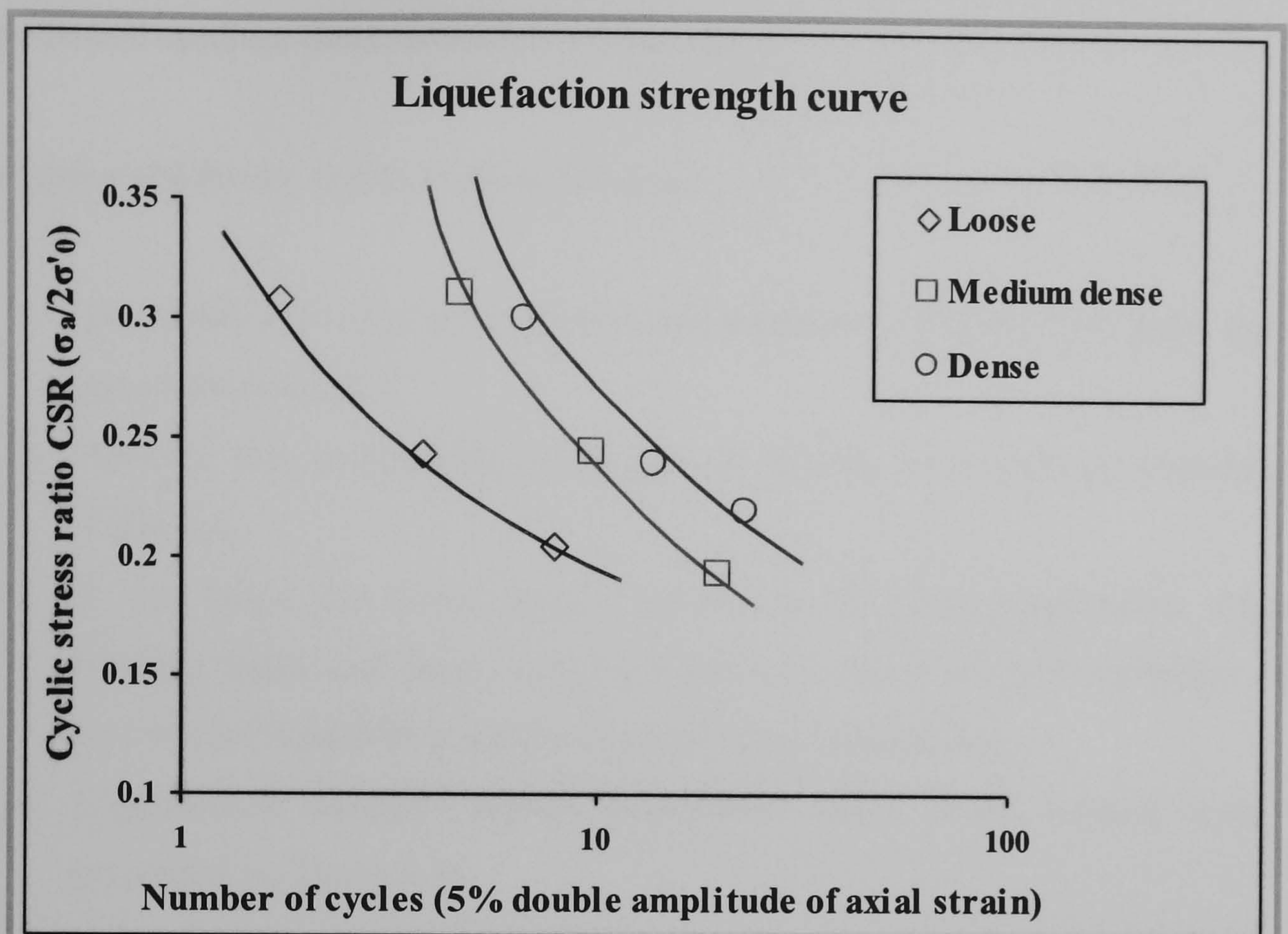

Figure 5.20. Liquefaction strength curve for JPS

5.5 Summary

This chapter described the mechanical properties of Jeddah port soil. These properties were measured using both monotonic and cyclic tests. To ensure that the tests were representative of the *in situ* conditions, SPT tests were conducted at Jeddah Port and the results compared to other tests conducted by the Saudi Port Authority (Saudi Ports Authority, 2006). The tests gave consistent results and showed the relative density of the *in situ* soil to be 35%.

Index and classification tests for samples that were obtained from the North Container Terminal at Jeddah Port have also been conducted. The results include particle size distribution, Atterberg limits, particle density, maximum and minimum density as well as consolidation derived coefficients. These results showed that Jeddah Port sand used in this investigation consists of 82% sand and 18% silts. Also the sand is angular in nature and fines are non plastic, making Jeddah Port sand

susceptible to liquefaction. In addition, Samples with this density were prepared in the lab and a series of undrained triaxial tests were conducted for three different relative densities; D_r = 35%, 55% and 75%. These represent loose (equal to *in situ* conditions), medium dense and dense, respectively.

The major results are summarised as follows:

1. The relative density of reclaimed soil retained by Jeddah Port quay walls is approximately 35%.
2. Physical and engineering proprieties of Jeddah Port sand are presented in Table 5.4.
3. It was found that loose samples failed due to cyclic liquefaction, whereas medium dense and dense samples failed as a result of cyclic mobility. This proves that Jeddah Port sand is susceptible to liquefaction.
4. Liquefaction strength curves determined using cyclic triaxial tests are presented in Figure 5.20.

These results of monotonic, cyclic and liquefaction strength curves will be used in Chapter 6 to identify the soil parameters of the P-Z sand model. This model will then be used to assess the seismic capacity of gravity quay walls at Jeddah Port.

CHAPTER SIX

6. PERFORMANCE-BASED DESIGN METHOD APPLIED TO JEDDAH PORT

6.1 Introduction

The data recorded from 1965 to 2004 show that at 2:41 AM on August 3 1967, an earthquake of magnitude M_s=6.7 (Richter scale) occurred of the coast of Jeddah. The faulting mechanism was a Strike/Slip type (Al-Amri, 2004). This earthquake occurred before the Jeddah Port was built. Therefore, no damage due to this earthquake is recorded. On the other hand, the results presented in Chapter 5 indicate that Jeddah Port sand (JPS) has a susceptibility to liquefy and therefore subsequent earthquakes may cause considerable damage.

This chapter assesses the safety levels of existing quay walls that have been constructed in Jeddah Port using the performance-based design method. This method allows geotechnical structures such as quay walls to be designed more economically and rationally using non-linear elasto-plastic dynamic analysis. The theory and the applicability of this method were explained in detail in Chapter 3. In addition, the vulnerability of Jeddah Port quay walls to liquefaction resulting from seismic events will be investigated.

In order to predict the seismic resistance resulting from failure due to liquefaction, the quay walls of Berths 4, 5 and 6 of Jeddah Port were investigated. This group of quay walls were the last berths to be constructed in Jeddah Port and were completed in 1983. A typical cross section of Berth 4, which represents the Northern Container Berths, was considered as a case study in this research. The modified P-Z sand model parameters used in this analysis were derived from the results of the monotonic and cyclic triaxial test conducted on Jeddah Port sand, as discussed in Chapter 5. To evaluate the expected deformation and to enhance the seismic performance of those quay walls, a number of earthquake records were used to provide two levels of earthquake intensity were applied under different compaction

conditions. As a conclusion, a flowchart illustrating a reasonable seismic design procedure for existing and new gravity quay walls is proposed.

6.2 Jeddah Port

Jeddah Port has a working area of about 11.5 km^2 with 58 berths as shown in Figure 6.1 with alongside water depths from 10 m to 16 m. The total length of berths is 11,700 m. The warehousing area covers more than 3.5 km^2. The port is located in the south western part of Jeddah City, Saudi Arabia, and has an excellent location in the middle of the international shipping routes between east and west and is considered to be the biggest port in the Middle East. The location is close to the main shipping routes, requiring minimal deviation, lies on the Red Sea coast at latitude 21° 28' north and longitude 39° 10' east. The port handles 65% of the containers coming into the Saudi Arabia, 60% of total imports and 65% of the total food imports. The port has two separate container terminals with a total of 12 berths, with a depth alongside ranging from 15 m to 16 m. The total terminal storage area is 3,414,746 m^2, capable of storing 91,000 containers and a total capacity of 3 million TEU annually (Saudi Ports Authority, 2006).

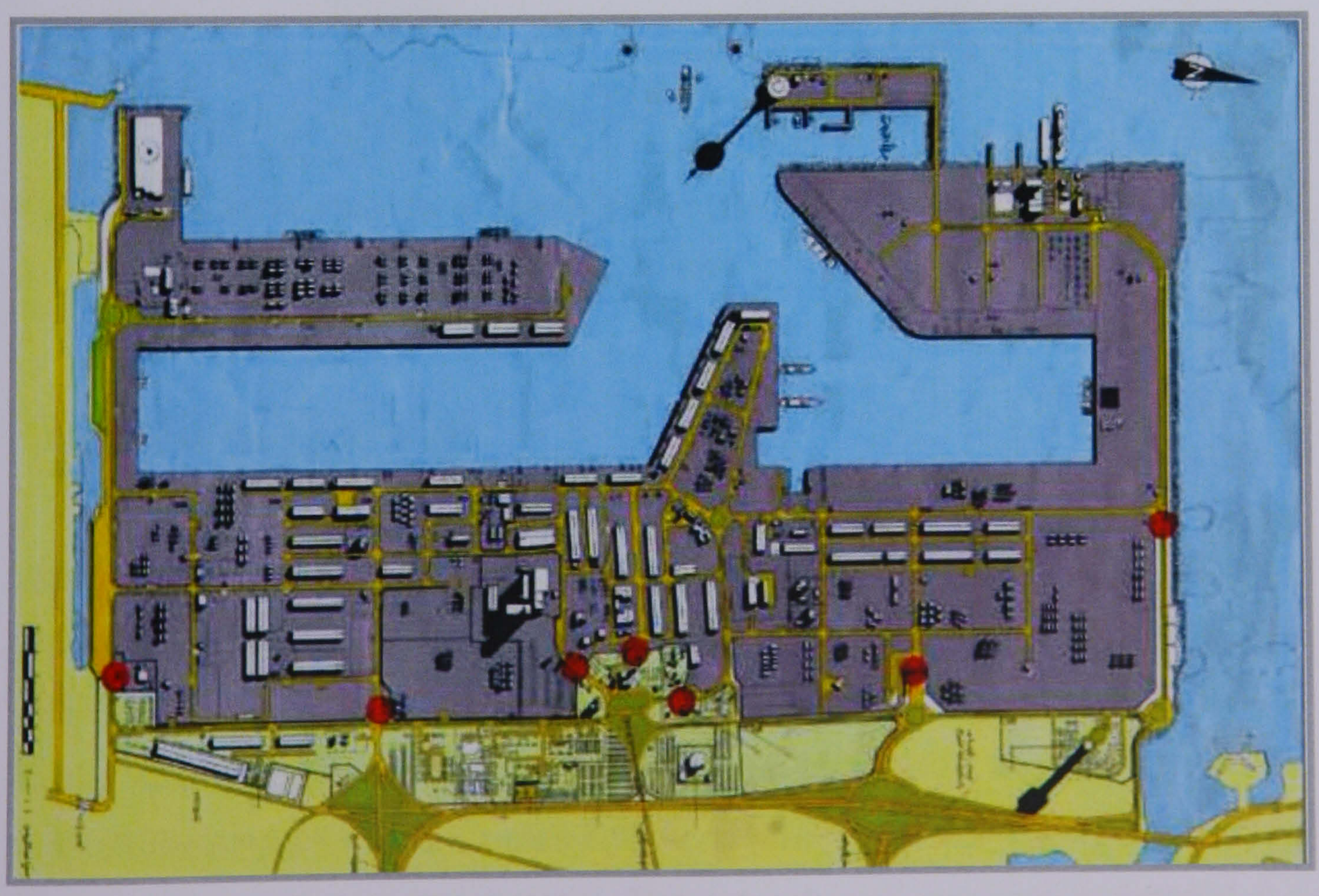

Figure 6.1. Plan of Jeddah Port, after Saudi Ports Authority (2006)

6.2.1 Seismic activity in Jeddah Port

The data recorded from 1965 to 2004 show that at 2:41 AM on August 3 1967, an earthquake of magnitude 6.7 (Richter scale) struck Jeddah, with the fault type being Strike/Slip (Al-Amri, 2004). This earthquake occurred before the present port was built. Therefore, no damage was recorded. However, Al-Haddad *et al.* (1994) reported that the maximum credible magnitude for the coordinate 21.4N, 39.1E where Jeddah Port is located is 7.0 (Richter scale). The 50-year iso-acceleration map that was developed by Al-Haddad *et al.* (1994) as shown in Figure 6.2 shows that the suggested peak ground acceleration (PGA) in the study area is 0.15 g = 1.5 m/s^2.

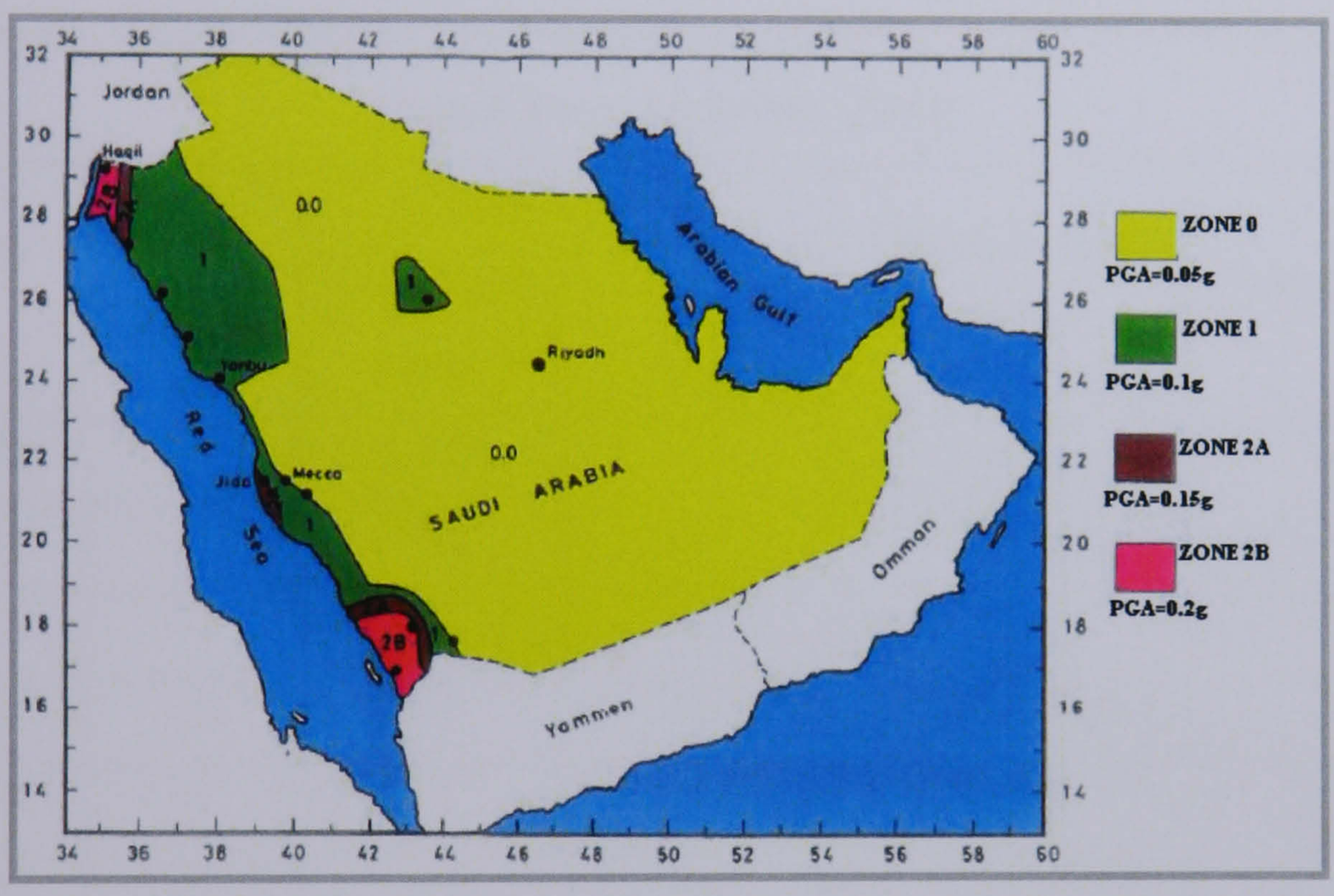

Figure 6.2. The 50-year iso-acceleration map of Saudi Arabia, after Al-Haddad *et al.* (1994)

6.2.2 Jeddah Port quay walls

The gravity quay walls constructed at Jeddah Port are mainly the block type. This type is quite easy to install but has higher costs in construction materials compared to other high performance types of quay walls, which can reach deep seabed levels (CUR, 2005). Jeddah quay walls were all built using pre-cast concrete blocks bedded on foundation materials placed in and above a dredged trench. The depth of the dredged trench depends both upon the depth of the original sea bed and on the quality of the sea bed material. The concrete wall was usually founded at a

level equivalent to that of the general dredging adjacent to it. Thus a 12 m berth provides a quay wall to a depth of -12 m relative to the contract datum, and the adjacent general dredging will also be at a depth of 12 m relative to contract datum. In each case, a margin of safety is provided because the lowest water record is 0.35 m above the contract datum. The quay walls were preloaded then completed with an *in situ* concrete capping block into which are cast the bollards, access ladders, small-boat steps, fender fixings, bunkering points, ship-to-shore telephone points and other services (Halcrow & Partners, 1982). The quay walls are listed by berth number in Table 6.1, which also shows the geometry of each section and the construction period.

Table 6.1. Characteristics and construction period of Jeddah Port berths, after Saudi Ports Authority (2006)

Berth	Depth (m)	Capping block		Construction period	Length (m)
		Cope level (m)	Width (m)		
Ro-Ro	-8	+2.78	12	1975	320
4-6	-14	+3	10.5	1981-1983	1,000
9	-12	+3	8.6	1976	170
10	-12	+3	8.6	1980-1981	135
11-14	-8	+3	7	1976	680
20-23	-11	+3	8.6	1967-1969	
24-28	-11	+3	8.6	1969-1971	1,810
29-36	-12	+3	8.6	1974-1978	1,260
37-38	-12	+3.6	8.6	1976-1977	
39-49	-12	+3.6	8.6	1977-1979	2,480
50-53	-16.1	+3.6	12	1978-1980	720
54-56	-16.1	+3.6	12.5	1977-1979	750

6.2.3 Quay wall design: loading and method

The type of quay wall chosen at Jeddah Port was dictated by the variability of the bed material encountered. To combat the large differential settlements envisaged, the design incorporated individual columns of pre-cast concrete hollow blocks, and carefully prepared foundations of rock and sand/gravel fill, which were introduced to reduce bearing pressure. A system of preloading of individual columns was decided upon in order to take up as much settlement as possible prior to the construction of the *in situ* capping block. The latter's *in situ* construction enables a consistent surface to be produced by eliminating differences in the levels of the pre-cast blocks, and facilitates the incorporation of services. The individual blocks are designed to maintain their centre of gravity to the rear of the wall, thus increasing the stability of the completed wall system.

Oval and semicircular voids in the blocks are subsequently concreted up to produce vertical shear keys. The latter voids were only partially concreted to enable free-draining, thus enabling the possibility of differences in water pressures to be ignored in the design.

Checks against slip circle failure, sliding failure and overturning have all been carried out with minimum factors of safety of 1.3, 1.8 and 2, respectively. The maximum bearing pressure established under the base block is 300 kN/m^2. The static design method based on Coulomb's wedge theory for earth retaining structures was used in the design.

Although Jeddah is located in a seismically active region (Zone 2A) with a horizontal seismic coefficient (k_h) of 0.15, as shown in Figure 6.2, there is no evidence that the Jeddah quay walls were designed to resist earthquakes by using the pseudo-static method (Halcrow & Partners, 1982). Hence, with respect to the stability of Jeddah quay walls, it is necessary to investigate the affect of earthquake loading, especially when liquefaction in the landfill may occur.

In order to predict the seismic resistance due to liquefaction, the quay walls of Berths 4, 5 and 6 of Jeddah Port shown in Figure 5.1 in Chapter 5 with identical cross

sections shown in Figure 6.3, were investigated. The material properties of the foundation and backfill of those quay walls are summarised in Table 6.2 (Saudi Ports Authority, 2006).

Table 6.2. The material properties of Berths 4, 5 and 6, after Saudi Ports Authority (2006)

Materials	**Friction angle ϕ (°)**	**Submerged density γ_{sub} (Mg/m^3)**	**Saturated density γ_{sat} (Mg/m^3)**
Sand fill	30	1.03	1.875
Rock in backfill and foundation	40	1.03	1.875
Caisson wall	-	1.30	2.3
Friction between Wall/Backfill and Wall/Foundation $\delta = 13.3^0$			

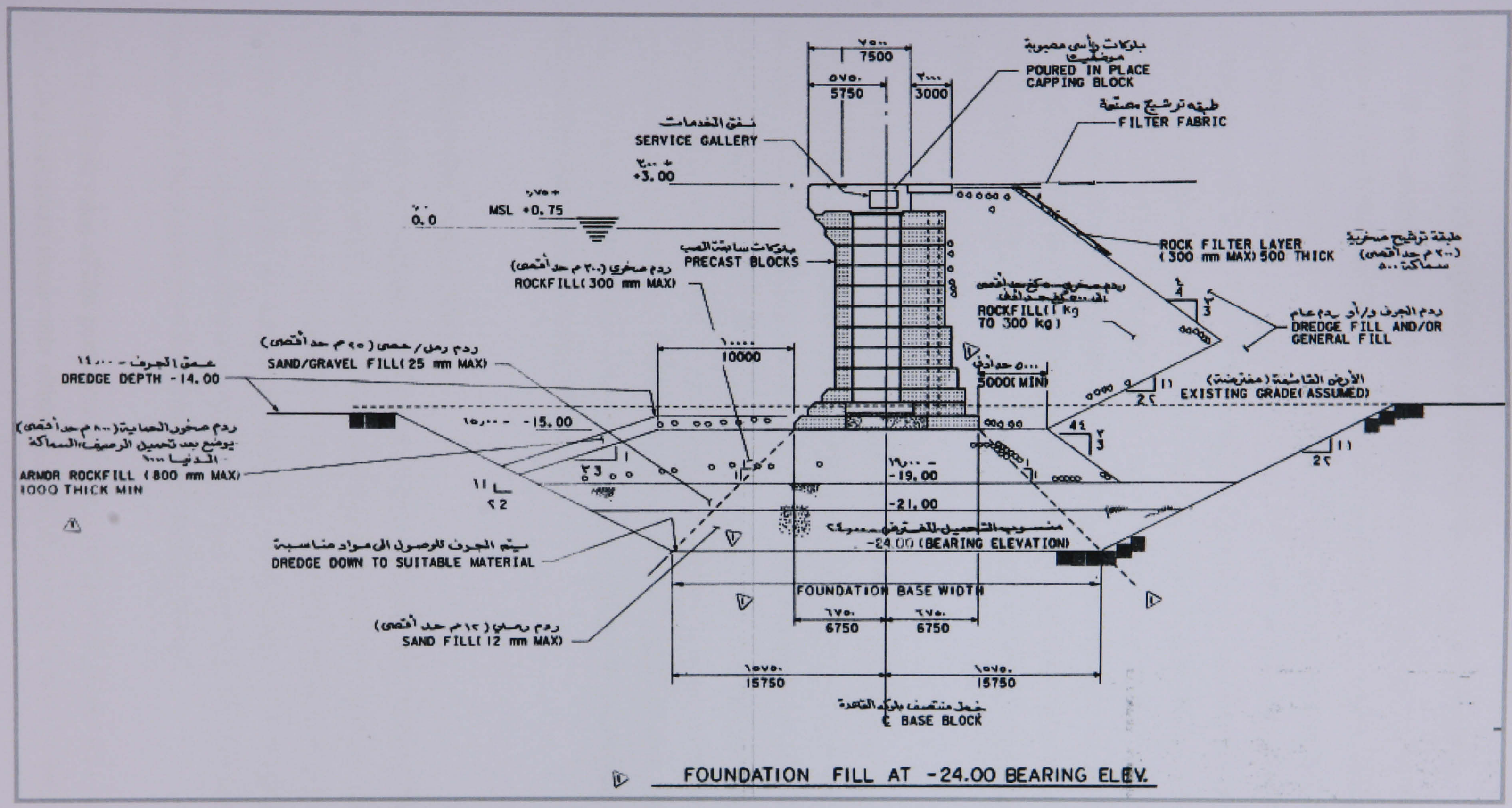

Figure 6.3. Cross section of a quay wall (Berths 4, 5 and 6) at Jeddah Port, after Saudi Ports Authority (2006)

6.3 Parameter identification of JPS for the P-Z sand model

In this section, the consolidated undrained monotonic and cyclic triaxial test results of Jeddah Port sand that were presented in Chapter 5 are used to identify the P-Z sand model parameters. The formulation of this model as well as the associated parameters is explained in Section 3.3. The P-Z sand model subroutine has been incorporated into the UWLC finite element package to facilitate the comparison between the predicted model responses and the experimental results. It should be noted that, undrained monotonic and cyclic triaxial tests, which can be easly performed, are choosen in the parametric determination procedure of the P-Z sand model. In addition, the liquefaction strength curve is obtained from at least three cyclic triaxial tests. The procedure used to identify each of the model parameters is as follows.

The twelve P-Z sand model parameters (M_g, M_f, C, α_g, α_f, K_{ev0}, G_{es0}, m_v, m_s, β_0, β_1, H_0), and two additional state parameters (p'_0 and OCR) are firstly assigned by matching monotonic triaxial compression tests with simulated results. However, before any simulations can be performed, initial values of these parameters must be estimated. Wherever possible, initial values were chosen from the recommendations in the literature and these are discussed in detail later. The remaining three parameters (H_{Uo}, γ, γ_U) are assigned values of 0.0, as they are not relevant for monotonic tests and are later identified from the cyclic triaxial tests.

6.3.1 Monotonic tests parameters

In order to calibrate Jeddah Port sand parameters, the results of the strain-controlled, isotropically consolidated undrained monotonic triaxial tests were performed on samples of Jeddah Port sand at different densities are used. These samples are subjected to undrained monotonic compression to 15 % axial strain, carried out at the same effective confining stress of 100 kPa. The P-Z sand model parameters of these tests were obtained in the following manner.

(M_g) The initial value of this parameter was estimated from the stress ratio:axial strain plot as the maximum stress ratio obtained in the monotonic triaxial compression test.

Figure 6.4 shows that the maximum values of the stress ratio up to 15% of axial stain level are 1.53, 1.65 and 1.61 for loose, medium and dense sands, respectively. These initial values for M_g are later modified to improve the prediction results of the model.

a)

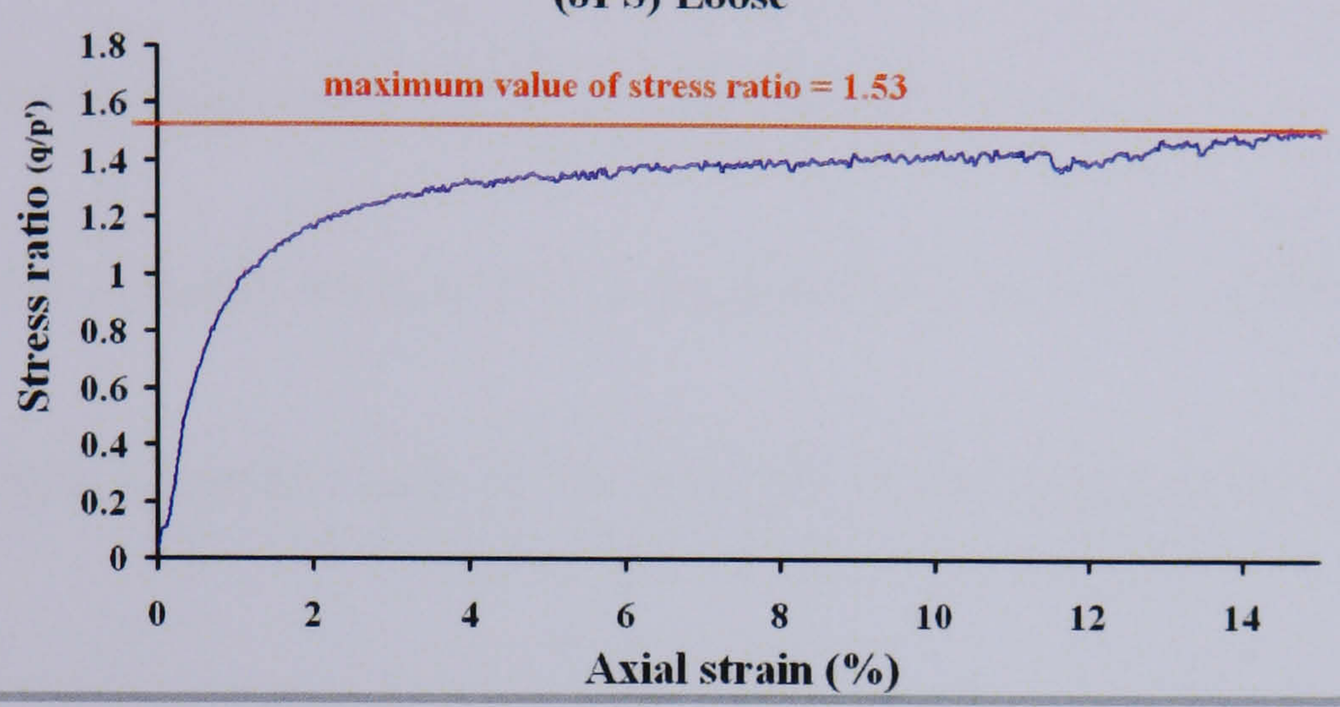

b)

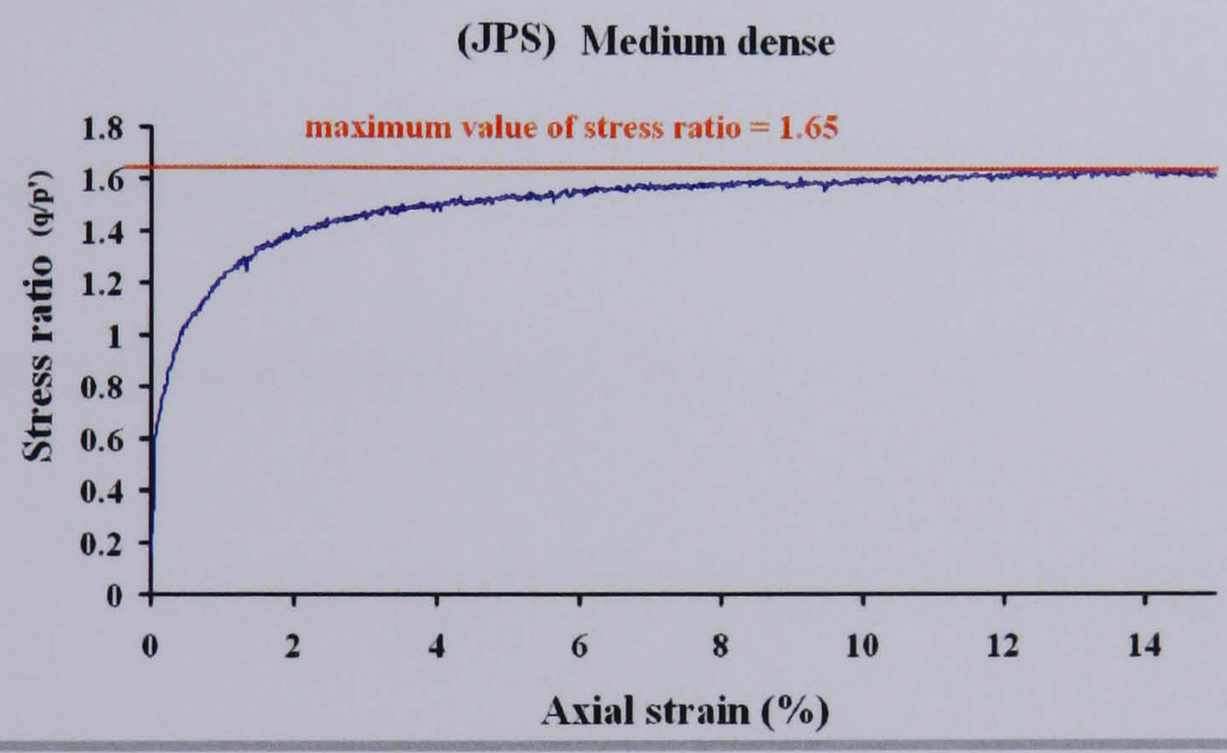

c)

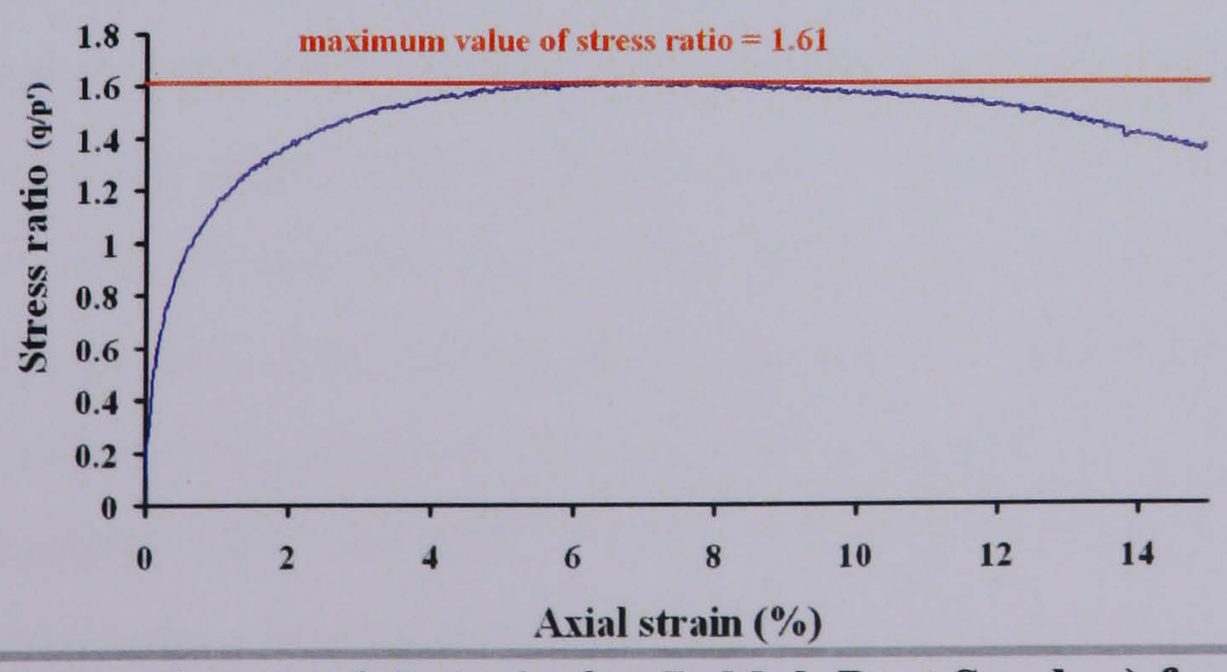

Figure 6.4. Stress ratio vs. axial strain for Jeddah Port Sand: a) for loose sand, b) medium dense sand, and c) dense sand

(M_f) The initial value of this parameter was calculated from the equation $M_f = D_r * M_g$ as suggested by Pastor *et al.* (1985). The calculated values from the above equation are 0.57, 0.91 and 1.21 for loose, medium and dense sands, respectively. Simulations were then conducted by adjusting the values of M_f to improve the match between the predicted and the experimental results. Table 6.3 shows the final values of M_g and M_f.

(C) This value is usually taken as 0.80 as explained in Section 3.3.2.

(α_g) This value is usually taken as 0.45 as suggested by Pastor *et al.* (1985).

(α_f) This value is usually taken to be equal to (α_g) as suggested by Pastor *et al.* (1985).

(m_s) This value is usually taken as 0.5 as explained in Section 3.3.2.

(m_s) This value is usually taken as 0.5 as explained in Section 3.3.2.

(G_{es0}) This value was obtained by using the following equation:

$$G_{es0} = \frac{3E_i}{2(1+v)p_a(p_0'/p_a)^{m_s}} \tag{6.1}$$

where the meaning of each parameter is given in Equation 3.37. By assuming an undrained Poisson's ratio $v = 0.5$, the Young's Modulus E_i was obtained by matching the initial slope of the stress:strain relationship curve (see Figure 5.10 (b)), which is equal to 11 111 kPa, 28 000 kPa and 29 700 kPa for loose sand, medium sand and dense sand, respectively. The atmospheric pressure p_a is usually taken as 100 kPa. The calculated value of G_{es0} from the above equation is equal to 111, 280 and 297 for loose sand, medium sand and dense sand, respectively. These values will be considered as final values for G_{es0} in both monotonic and cyclic tests.

(K_{ev0}) This value was obtained by using the following equation:

$$K_{ev0} = \frac{2G_{es0}(1+v')}{9(1-2v')} \tag{6.2}$$

where the meaning of each parameter is given in Equation 3.39. By assuming a value of 0.25 for the effective Poisson's ratio, v'= 0.25, the calculated value of K_{ev0} from the above equation is equal to 61.7, 155 and 165 for loose sand, medium sand and dense sand, respectively. These values will be considered as final values for K_{ev0} in both the monotonic and cyclic tests.

(β_0) Pastor *et al.* (1985) suggested a value of 4.2 as an initial estimate. This was used in the first set of simulations that were conducted to obtain the value of M_g. Once this parameter was fixed, other simulations were conducted to further improve the fit by adjusting β_0. In these simulations, β_0 was found to vary from 1.0 to 10.

(β_1) This was suggested by Pastor *et al.* (1985) to be 0.2 as an initial estimate. A similar procedure to that used for β_0 was used to obtain β_1. Using this procedure, the value of β_1 was found to be in the range of 0.1 to 0.9.

(H_0) This value was taken from Table 3.2; for loose sand it is recommended to start with 200, 400 for medium dense and 600 for dense sand. Slight adjustments are needed to improve the simulation results.

(p'_0) The value of preconsolidation stress was calculated as follows:

$$p'_0 = \frac{\sigma_1 + \sigma_2 + \sigma_3}{3} = \frac{100+100+100}{3} = 100 \text{ kPa}$$

(*OCR*) The samples tested are normally consolidated; thus this value was taken to be 1.0.

Table 6.3 shows the final values of the P-Z model parameters obtained from the calibration exercise of the monotonic triaxial tests.

6.3.2 Cyclic tests parameters

In order to calibrate Jeddah Port sand parameters for cyclic response, the results of stress-controlled, isotropically consolidated undrained cyclic triaxial tests performed on samples of Jeddah Port sand at different densities are used. These tests are classified into three sets, loose, medium and dense, as used in the monotonic tests. Each set of tests were subjected to three different amplitudes of deviatoric stress, which are ±40, ±50 and ±60 kPa to produce 5% axial strain in double amplitude, and were carried out at the same effective confining stress of 100 kPa. The P-Z sand model parameters of these tests were obtained as follows.

In the cyclic tests, the same parameters are used, except M_g in loose sand was adjusted to be 1.29 instead of 1.38. Also, β_0 and β_1 were adjusted to be 6.0 and 0.7, respectively, for all sand types. However, β_1 was further adjusted to be 0.5 for dense sand.

In addition, as mentioned earlier, there are three additional parameters (H_{Uo}, γ, γ_U) to be used in conjunction with cyclic response. The procedure to identify these model parameters is as follows.

(H_{Uo}) A value of 6 000 is recommended as an initial estimate as explained in Section 3.3.2. This value was adopted in both medium and dense sand but was adjusted to 3,100 in loose sand.

(γ) A value of 8 is recommended as an initial estimate as explained in Section 3.3.2. This value affects the number of cycles before the onset of liquefaction, especially in loose sand. Therefore, this value was adjusted to 3, 6 and 6.5 for loose sand, medium sand and dense sand, respectively, to improve the match between the experimental and simulation results.

(γ_U) A value of γ -2 is recommended as an initial estimate as explained in Section 3.3.2. This value affects the number of cycles before the onset of liquefaction, especially in loose sand. To improve the predictions, this value was adjusted to be 4.6,

5 and 4.8 for loose sand, medium sand and dense sand, respectively. It can be mentioned that in loose sand γ_U was greater than γ .

Table 6.3 summarises the final P-Z sand model parameter obtained from the calibration procedure. However, an example describing the P-Z sand model parameters iditification for medium dense in more detail is given in Appendix B.

Table 6.3. Summary of the P-Z sand model parameters of JPS

Test / parameter	Monotonic (35%) Loose	Monotonic (55%) Medium dense	Monotonic (75%) Dense	Cyclic (35%) Loose	Cyclic (55%) Medium dense	Cyclic (75%) Dense
M_f	0.57	0.91	1.21	0.57	0.91	1.21
M_g	1.38	1.4	1.46	1.29	1.4	1.46
C	0.8	0.8	0.8	0.8	0.8	0.8
α_f	0.45	0.45	0.45	0.45	0.45	0.45
α_g	0.45	0.45	0.45	0.45	0.45	0.45
K_{ev0}	61.7	155	165	61.7	155	165
G_{es0}	111	280	297	111	280	297
m_v	0.5	0.5	0.5	0.5	0.5	0.5
m_s	0.5	0.5	0.5	0.5	0.5	0.5
β_0	1.0	1.0	1.8	6.0	6.0	6.0
β_1	0.1	0.1	0.1	0.7	0.7	0.5
H_0	210	450	700	210	450	700
H_{U0}	0	0	0	3,100	6,000	6,000
γ	0	0	0	3.0	6.0	6.5
γ_U	0	0	0	4.6	5.0	4.8
p'_0	100	100	100	100	100	100
OCR	1	1	1	1	1	1

Figure 6.5 shows the comparison between the experimental undrained monotonic triaxial tests and the simulation for three different relative densities of 35.7%, 55.4 and 75.8. It can be observed that the general trend is very well captured in terms of stress path, stress:strain relationship and excess pore water pressure:axial strain.

In terms of stress:strain response, very good agreement between the behaviour of experimental and simulation results was obtained for loose and medium dense sand. For dense sand, the model matched the stress strain response quite well up to 2% axial strain. However, at large shear strain, the shape was under predicted as seen on Figure 6.5 (b).

In terms of the generated excess pore pressure, the simulations are in good agreement with the observed data. However, for dense sand the pore water pressure is slightly over predicted by approximately 15%, as can be seen in Figure 6.5 (c)

Figure 6.6 to Figure 6.14 present the results of the stress path, stress:strain relationship and the time history of the axial strain for the cyclic tests. Figure 6.6, Figure 6.7 and Figure 6.8 show the loose soil loaded by three different amplitudes, q of ±41 kPa, ±48.7 kPa and ±61.6 kPa, respectively. Figure 6.9, Figure 6.10 and Figure 6.11 show the same results but for medium dense samples and amplitudes of ±38.65 kPa, ±48.8 kPa and ±62 kPa, respectively. Figure 6.12, Figure 6.13 and Figure 6.14 present the results of the dense samples under amplitudes of ±44 kPa, ±48 kPa and ±60 kPa, respectively.

As recommended by Ishihara, (1993), the test was terminated at 5% axial strain. At this value of axial strain, Figure 6.6 (a) and (c) show that the effective mean principal stress had reduced to almost zero, while in 6.7 (b) the effective mean principal stress had reduced to zero. This means that only the second sample had actually liquefied; however, if the test had continued, the other two samples would have liquefied also.

For medium and dense sands, as shown in Figure 6.9 to Figure 6.14, it can be seen that after several cycles, the soil element starts to experience stress dilatancy

after large deformations. The effective confining stress decreases during the cyclic loading due to pore water pressure build up. Under these conditions strain amplitudes increase remarkably but complete collapse does not occur, which explains the occurrence of cyclic mobility. Some differences may be recognised between the computed and experimental results. A reason for these differences is explained by Iai *et al.* (1993); the computed results are for the average soil properties whereas the experimental results contain deviations from the average.

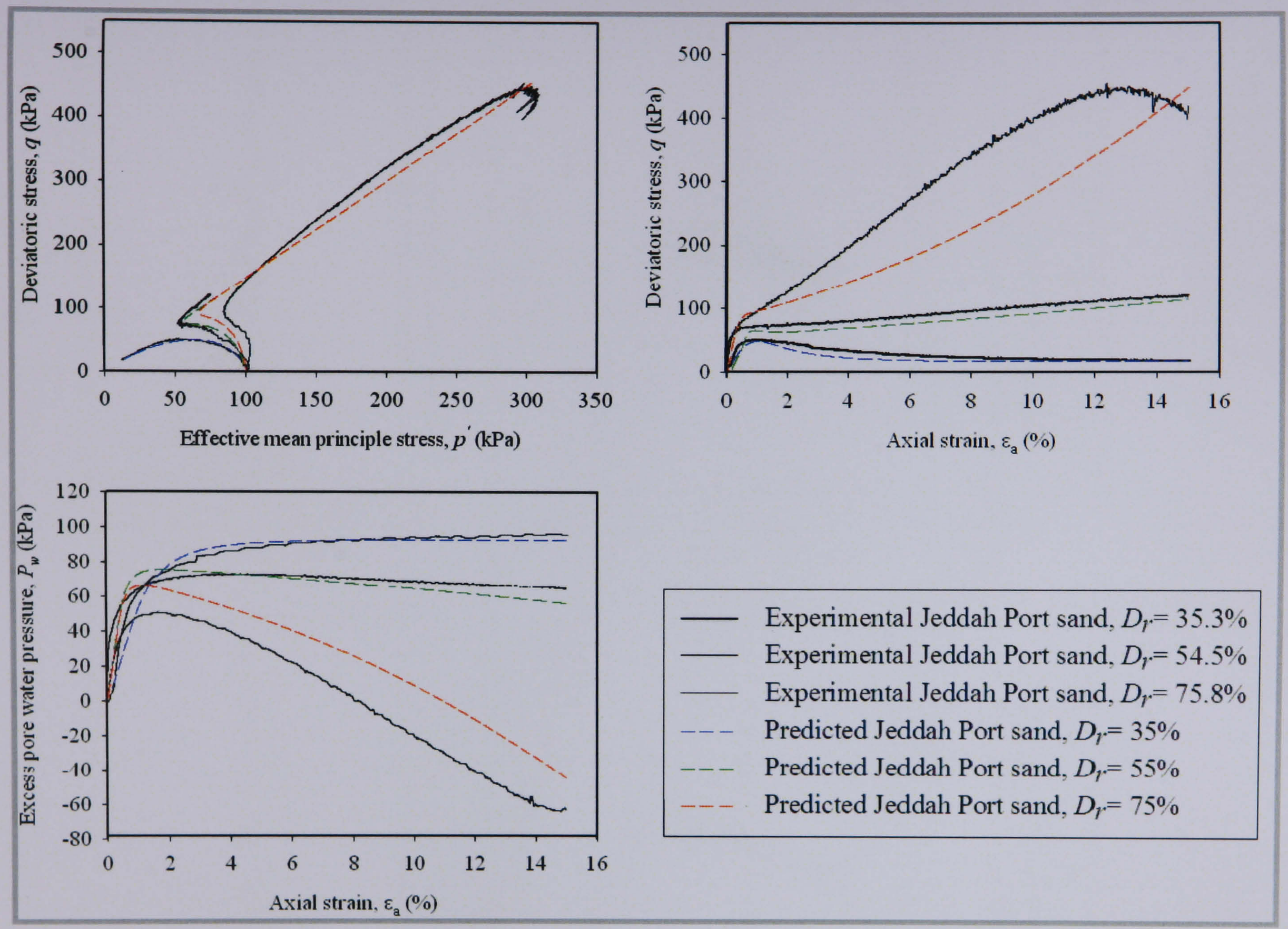

Figure 6.5. Simulation of experimental data of tests M01, M02 and M03, under monotonic undrained loading: a) stress path, b) stress: strain relationship and c) excess pore pressures: axial strain.

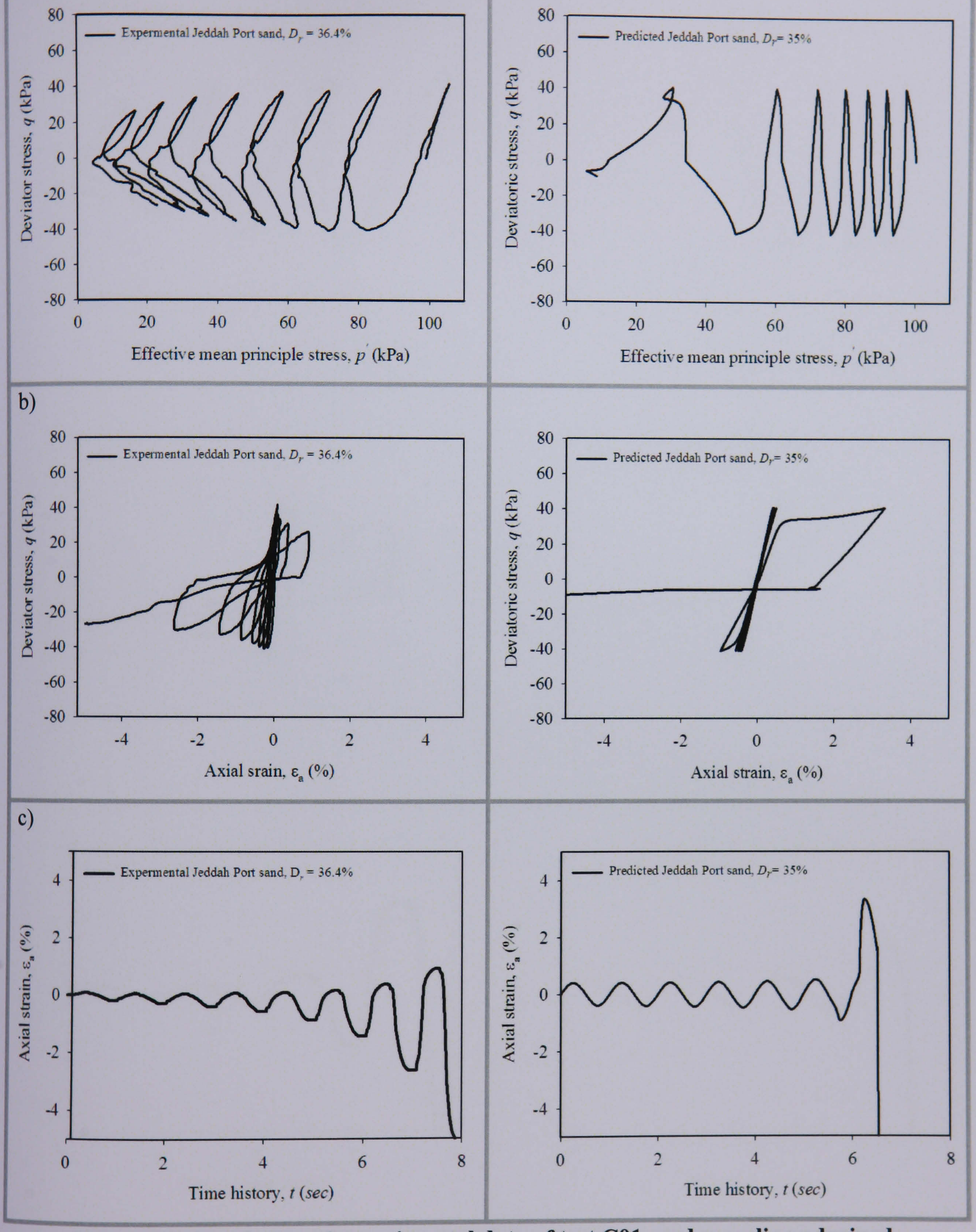

Figure 6.6. Simulation of experimental data of test C01, under cyclic undrained loading where the axial stress equals ±41.7 kPa: a) Stress path, b) Stress:strain relationship and c) Axial strain time history

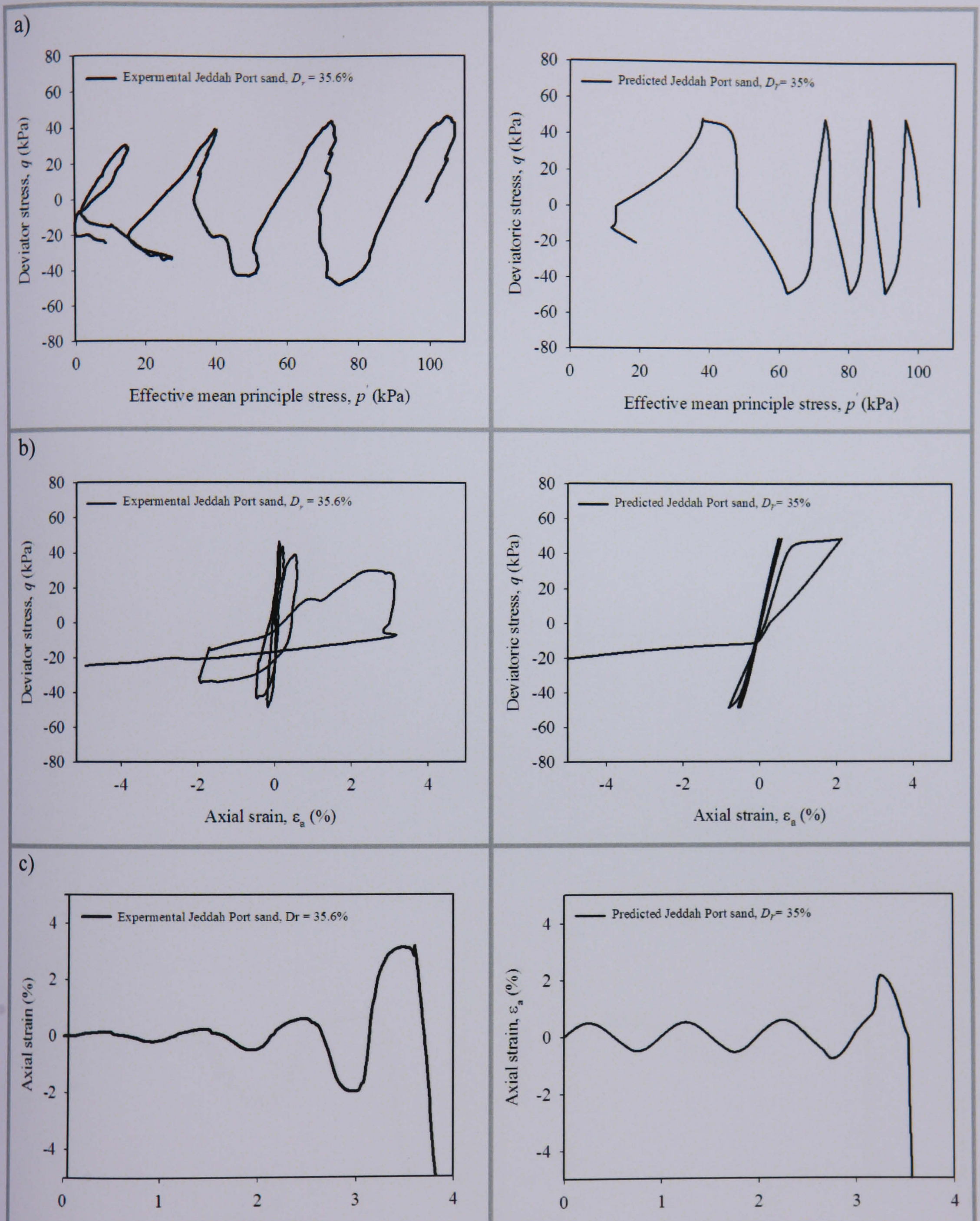

Figure 6.7. Simulation of experimental data of test C02, under cyclic undrained loading where the axial stress equals ±47.6 kPa: a) Stress path, b) Stress:strain relationship and c) Axial strain time history

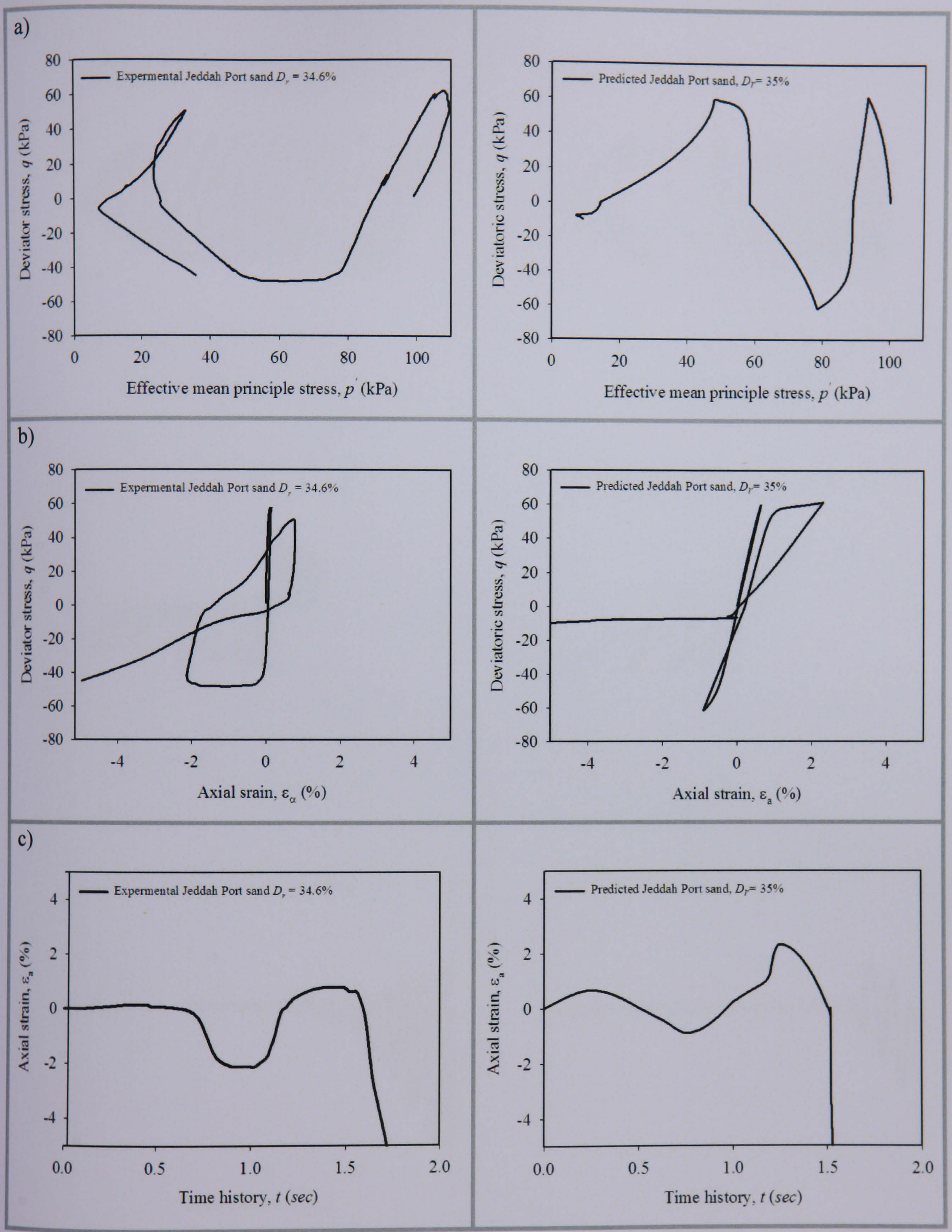

Figure 6.8. Simulation of experimental data of test C03, under cyclic undrained loading where the axial stress equals ±62.5 kPa: a) Stress path, b) Stress:strain relationship and c) Axial strain time history

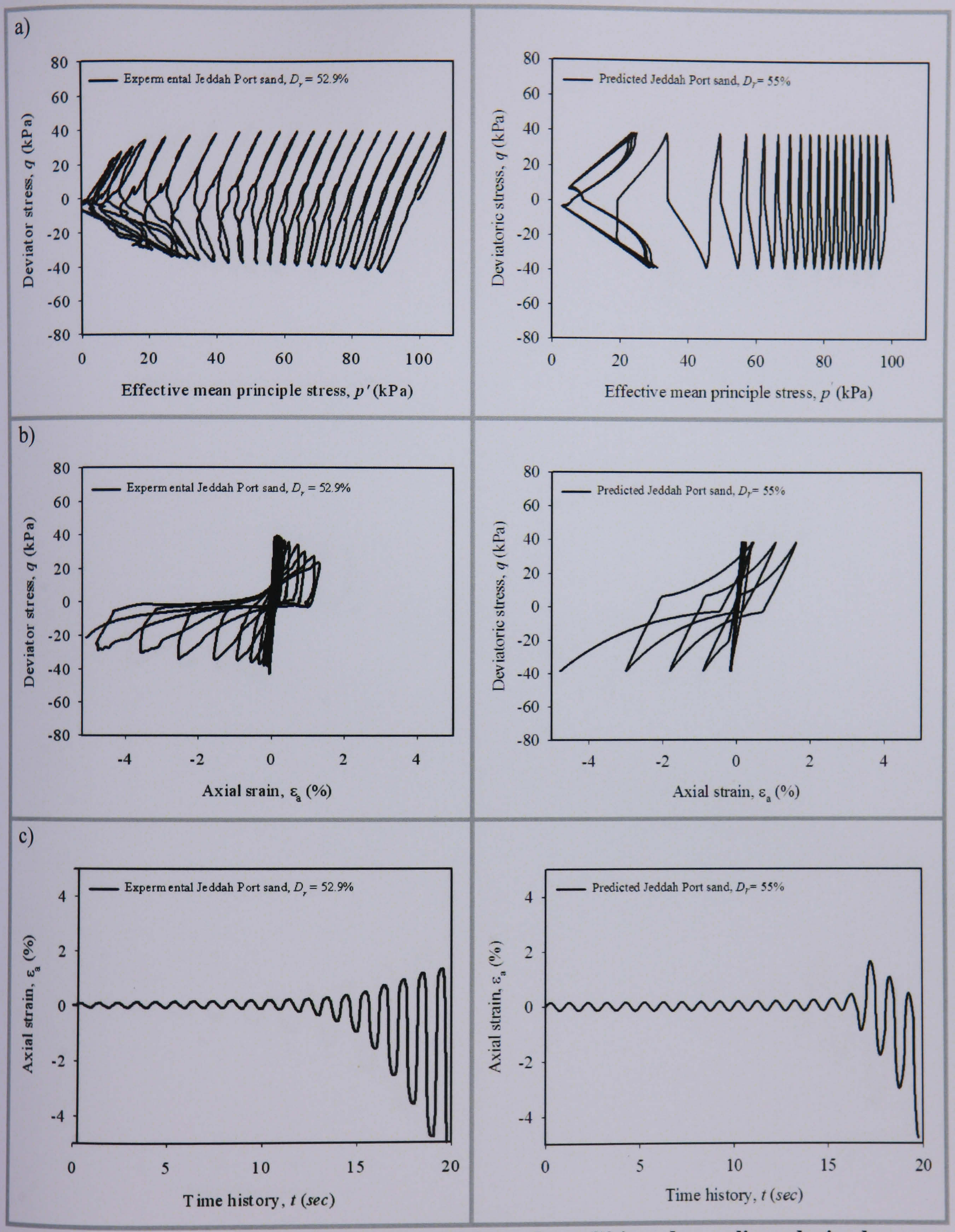

Figure 6.9. Simulation of experimental data of test C04, under cyclic undrained loading where the axial stress equals ±38.7 kPa: a) Stress path, b) Stress:strain relationship and c) Axial strain time history

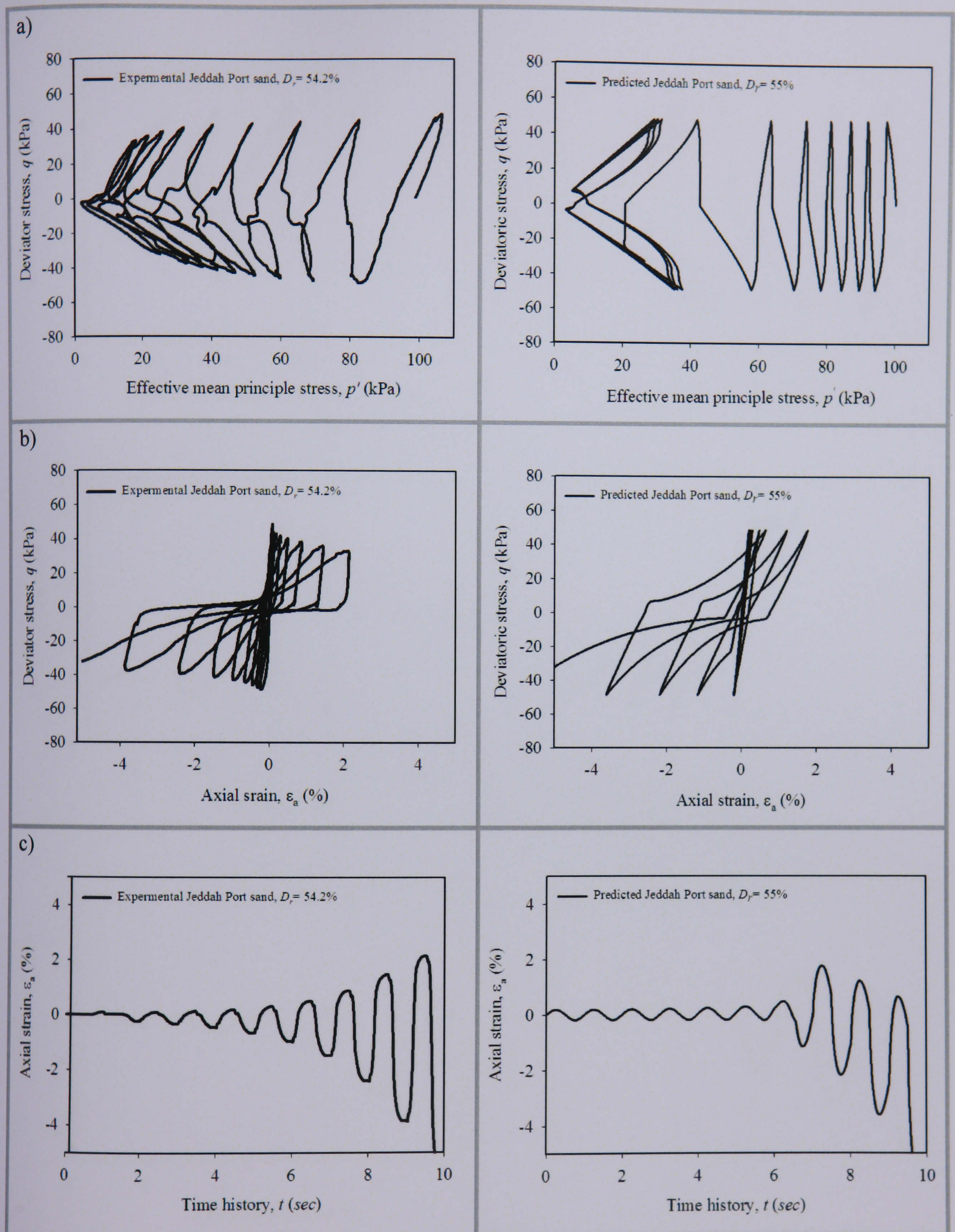

Figure 6.10. Simulation of experimental data of test C 05, under cyclic undrained loading where the axial stress equals ±48.8 kPa: a) Stress path, b) Stress:strain relationship and c) Axial strain time history

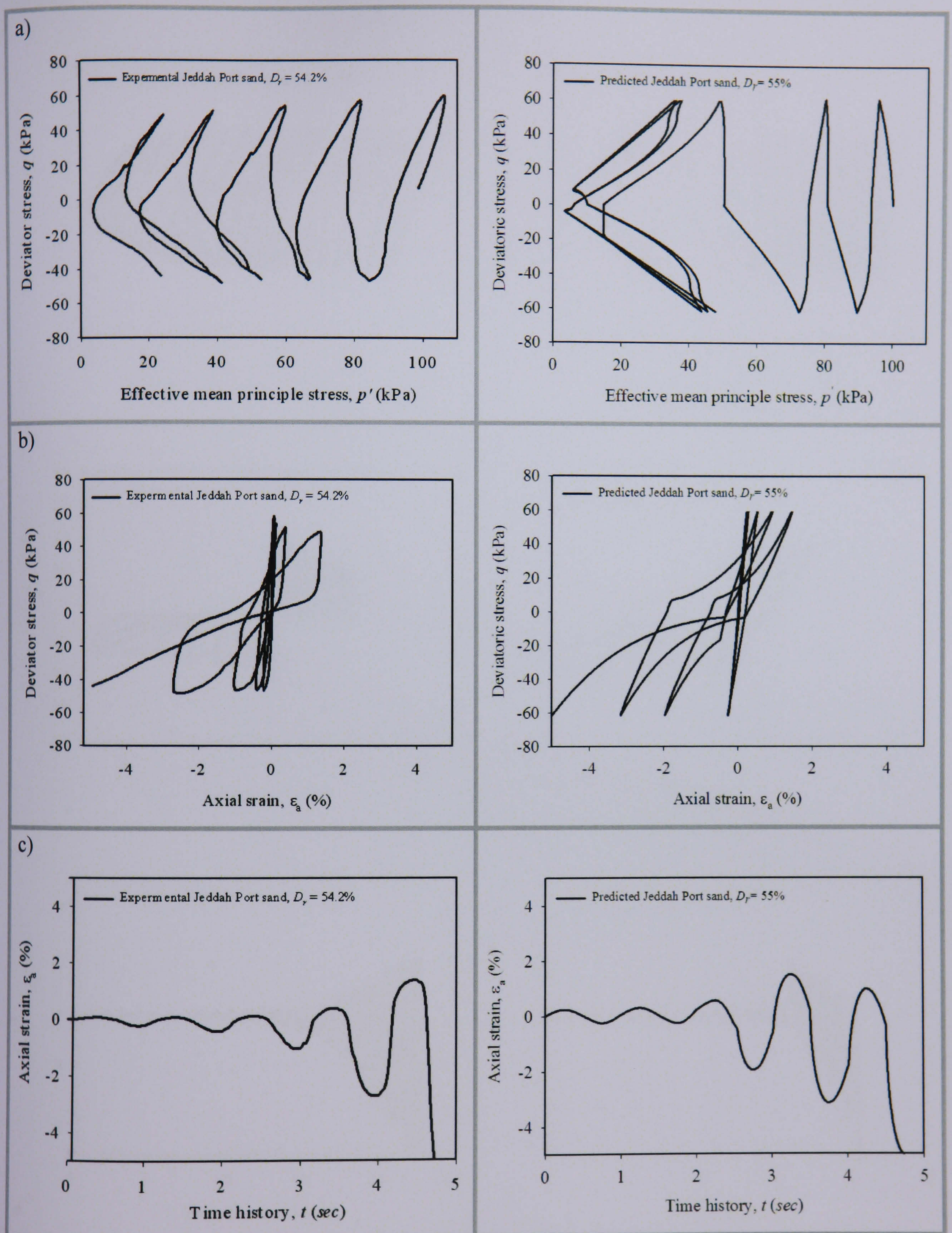

Figure 6.11. Simulation of experimental data of test C06, under cyclic undrained loading where the axial stress equals ±62 kPa: a) Stress path, b) Stress:strain relationship and c) Axial strain time history

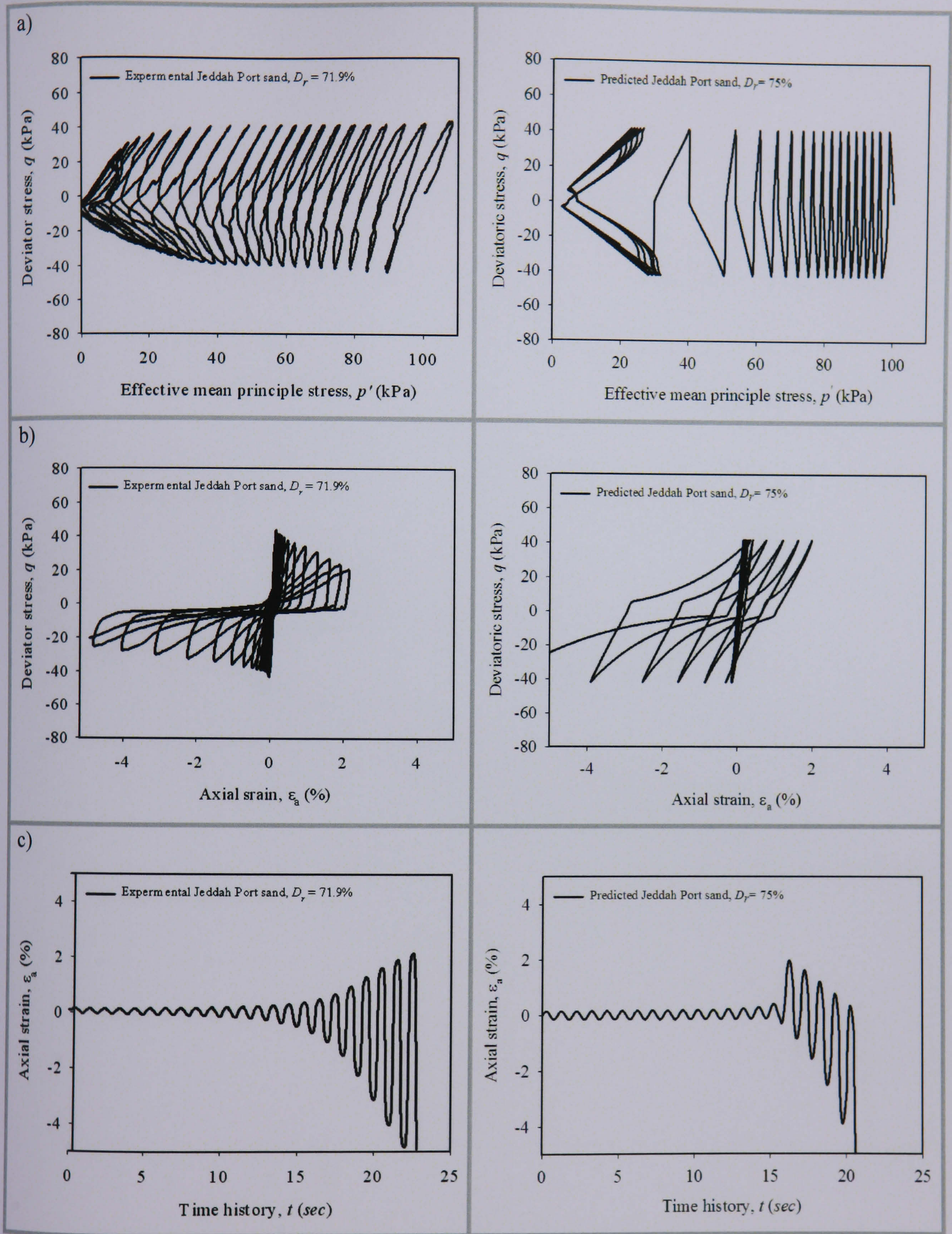

Figure 6.12. Simulation of experimental data of test C 07, under cyclic undrained loading where the axial stress equals ±44.1 kPa: a) Stress path, b) Stress:strain relationship and c) Axial strain time history

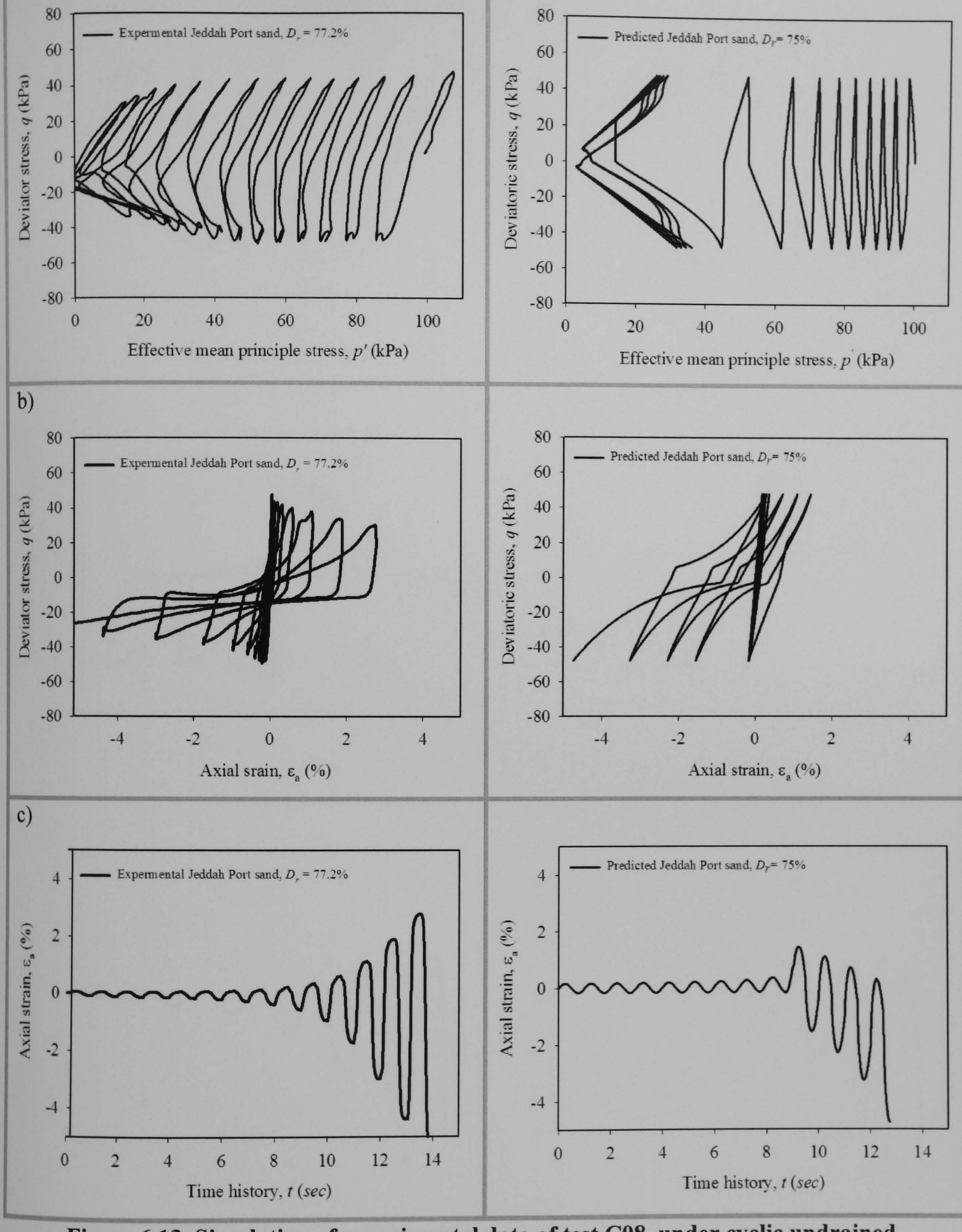

Figure 6.13. Simulation of experimental data of test C08, under cyclic undrained loading where the axial stress equals ±48.4 kPa: a) Stress path, b) Stress:strain relationship and c) Axial strain time history

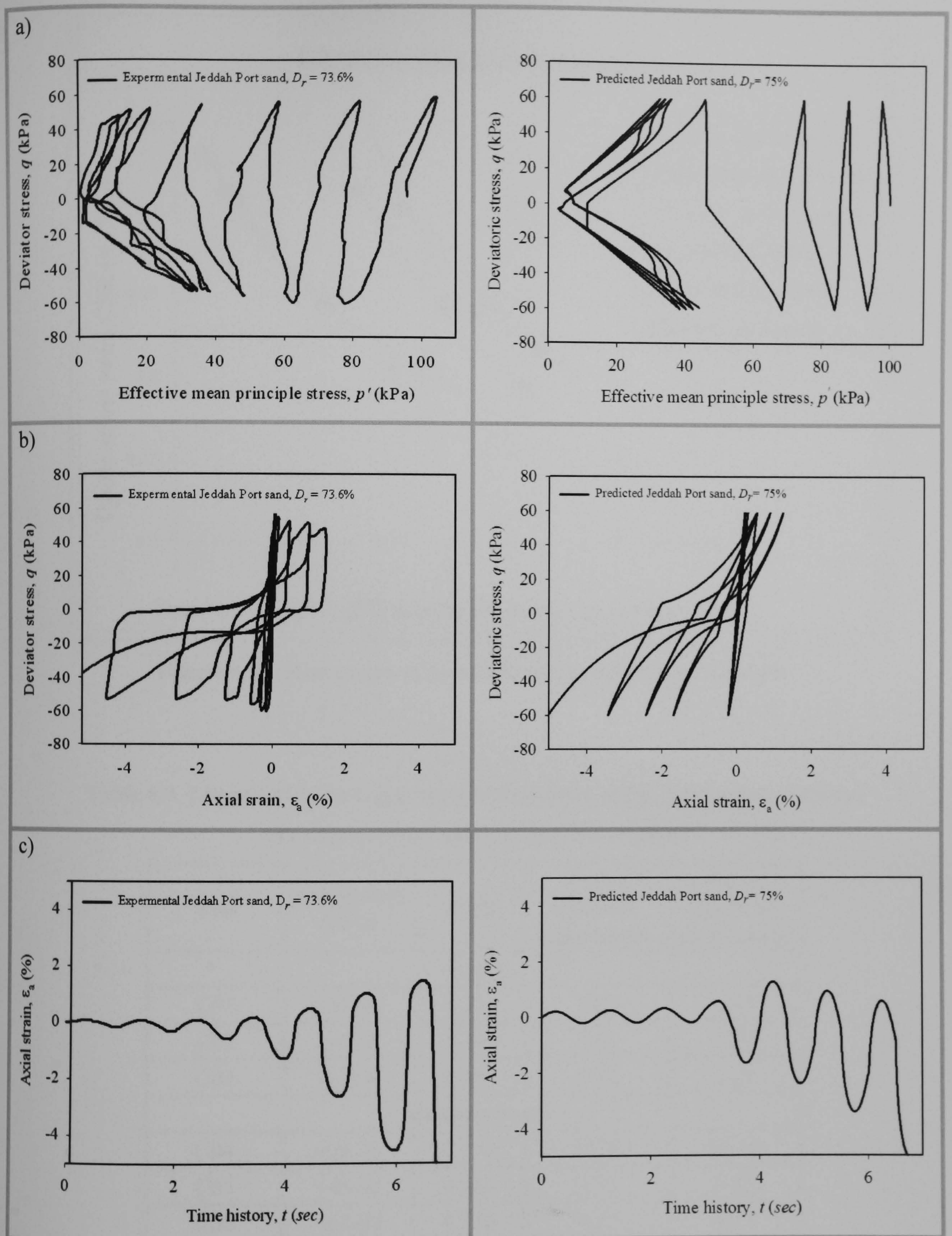

Figure 6.14. Simulation of experimental data of test C09, under cyclic undrained loading where the axial stress equals ±60 kPa: a) Stress path, b) Stress:strain relationship and c) Axial strain time history

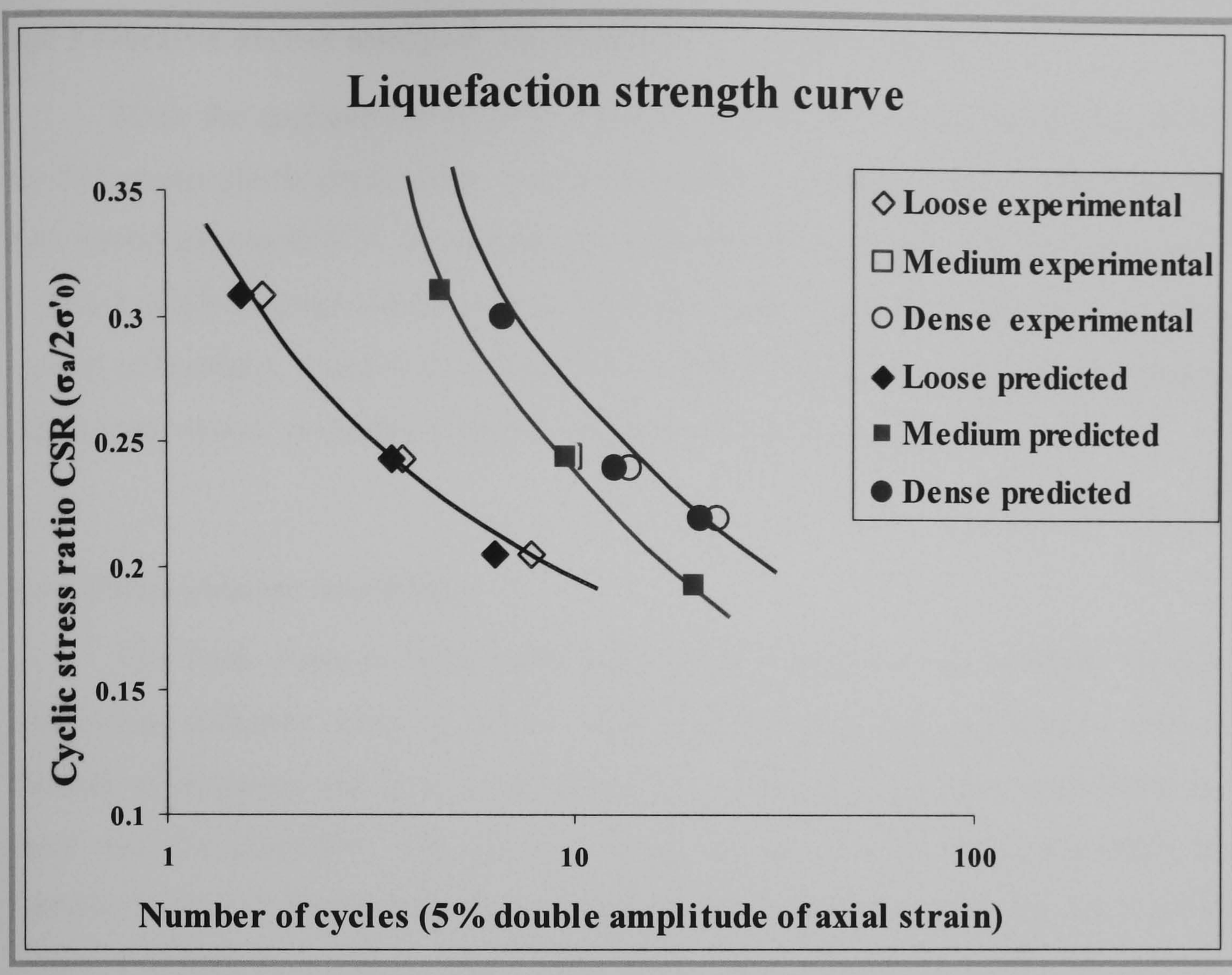

Figure 6.15. Simulation of liquefaction strength curve for (JPS)

Table 6.4. Liquefaction strength curves: Summary of the comparison between the experiments and simulations of (JPS)

Test	Amplitude (kPa)	CSR	No. of cycles in experiments	No. of cycles in predictions
Loose				
C01	±41.70	0.205	7.87	6.45
C02	±47.60	0.244	3.82	3.57
C03	±62.50	0.308	1.72	1.53
Medium dense				
C04	±38.70	0.193	19.76	19.75
C05	±48.80	0.244	9.76	9.62
C06	±62.00	0.310	4.72	4.75
Dense				
C07	±44.10	0.220	22.82	20.60
C08	±48.40	0.240	13.85	12.75
C09	±60.00	0.300	6.72	6.73

6.4 Effective stress analysis of Jeddah Port quay walls

Since the applicability of a two-dimensional effective stress analysis based on the P-Z elasto-plastic constitutive model (Pastor *et al.* 1990) has been validated on the Port Island quay-wall PC1 in Chapter 3, an additional numerical analysis using the P-Z model will be carried out for Jeddah Port quay walls. In the present study, the cross section of Berths 4, 5 and 6 of Jeddah Port as shown in Figure 6.3 will be analysed to predict the seismic resistance of these quay walls due to liquefaction.

6.4.1 Finite element modelling

The finite element mesh under plane strain conditions was carefully formed, considering different material zones. Each material zone was constructed using a number of elements and then those elements in each material zone were given the same material properties. The material zones and the corresponding properties are listed in Table 6.2. Figure 6.16 shows the geometry (in natural scale) with the material zones of Jeddah Port Berth 4 quay wall. These zones consist of: zone 1 is saturated backfill soil, zone 2 is submerged backfill and foundation soil, zone 3 saturated backfill rubble, zone 4 submerged backfill and foundation rubble, zone 5 is the dry wall, zone 6 is the submerged wall and zone 7 is the interface element. It should be noted that the same technique that was used for PC1 (see Section 3.5.2) to split the layers over the ground water table level and the layers under the ground water table level has also been used in the analysis of Berth 4. As recommended by the analysis in Section 4.2, low water level has been assumed. Therefore, the backfill layer is divided into two layers; the top layer is saturated soil with unit weight γ =1.875 Mg/m^3 and 3 m thickness, the submerged soil is measured under the water level with a submerged unit weight of γ =1.03 Mg/m^3 (see Table 6.2). Since, the top layer is not submerged and has low susceptibility to liquefy, the total stress analysis was considered instead of effective stress analysis. To ensure the stability of the numerical procedure, the damping coefficients (α = 0.1714 and β = 0.00174) were used. In addition, the horizontal and vertical permeability coefficients used for soil material were chosen to be 2.3x10^{-3} m/s in both directions (see Table 5.3).

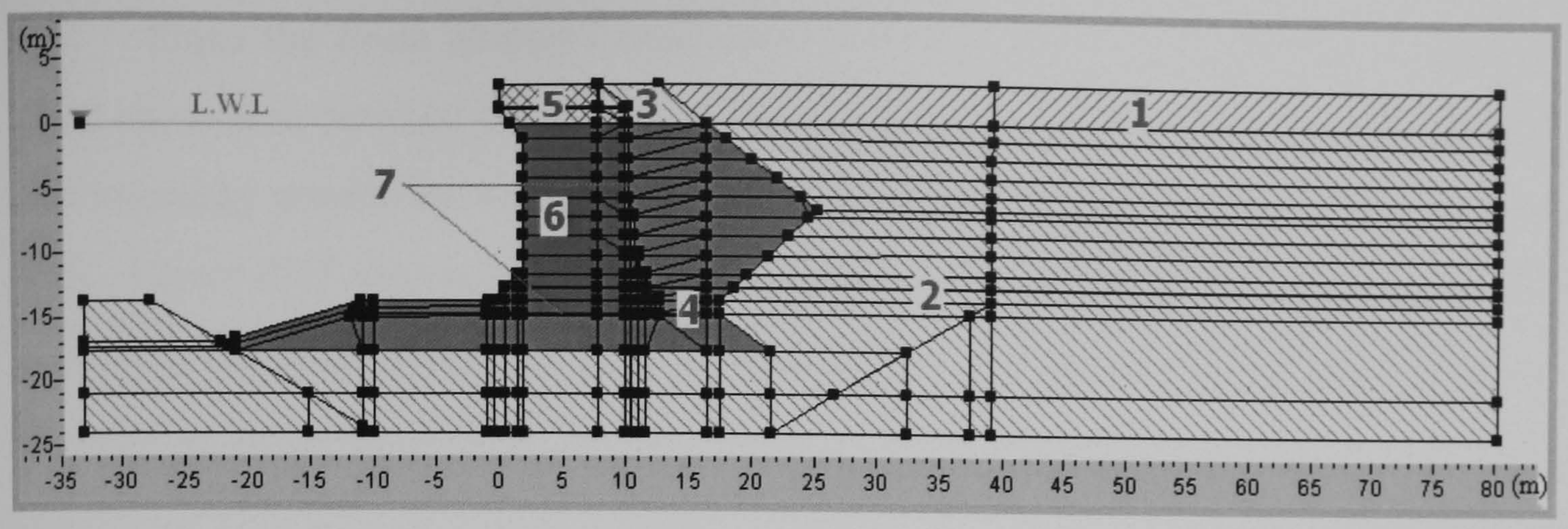

Figure 6.16. Geometry (in natural scale) and material zones of the Jeddah Port Berth 4 quay wall; zone 1 is saturated backfill soil, zone 2 is submerged backfill and foundation soil, zones 3 saturated backfill rubble, zones 4 submerged backfill and foundation rubble, zone 5 is the dry wall, zone 6 is the submerged wall and zone 7 is the interface

Different types of constitutive relations have been assigned to the different material zones. A simple elastic constitutive law was used to model the quay wall. The concrete wall which is considered to be acting as a rigid body block, has an elastic stiffness of $E = 20\text{x}10^6$ kN/m^2 and Poisson's ratio of $v = 0.25$. As the used software has no slip or gap element built in, a thin layer with interface properties described by an elastic-perfectly plastic model has been placed underneath and behind the wall. The interface material properties are listed in Table 6.5. It can be noticed that the layer was given a much reduced angle of friction (13.3 degrees) to simulate sliding or separation. In order to capture the non-linearity and hysteretic behaviour of the remaining soil layer, the advanced P-Z sand model described in Section 3.3, has been considered. The material parameters of this model were estimated from the triaxial experiments as explained in Section 6.3 and are given in Table 6.3.

Table 6.5. Elastic-perfectly plastic model parameters for interfaces parts

ϕ	ψ	E	v	C
Friction angle (degree)	Dilation angle (degrees)	Young's Modulus (kN/m^2)	Poisson's ratio	Cohesion (kN/m^2)
13.3	0	$208\text{x}10^3$	0.3	1

Since the finite element mesh used to analyse PC1 (see Chapter 3) showed good agreement between the observation and numerical results, similar mesh density and boundary conditions were considered in the analysis of Jeddah Port Berth 4 quay wall. Figure 6.17 shows the finite element mesh with a total of 2,073 nodes and 712 elements. The finite element model covered a cross sectional area of about 113 m by 27 m in the horizontal and vertical directions, respectively.

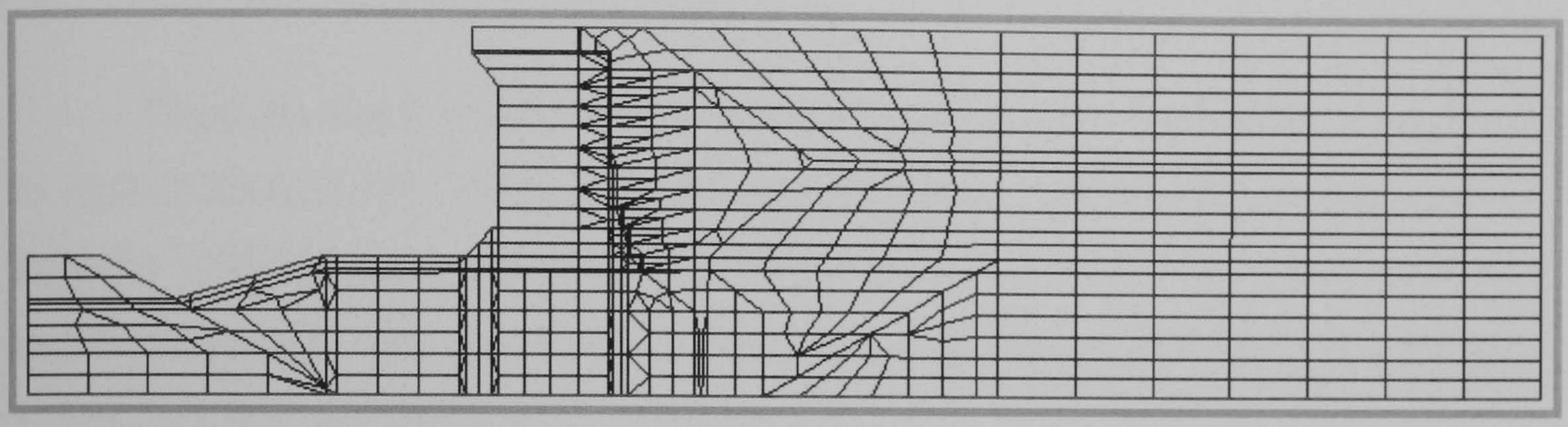

Figure 6.17. Geometry mesh of the Port Island PC1 quay wall.

6.4.2 Input motion for dynamic analysis

From the parametric studies carried out in Section 4.6, it has been concluded that it is sufficient to take into account the horizontal component of acceleration record only in analysing the response of quay walls under earthquake loading. Therefore, horizontal acceleration has been considered in the analysis of the Berth 4 model.

In this study two levels of earthauake intensity are considered. Theses should correspond to a return period of 75 years and 475 years as discussed in Section 2.3.3.

The only earthquake magnitude recorded so far in the study area was M_s=6.7. The recommended magnitude for design is 7.0 M_s, as discussed in Section 6.2.1. The type of fault causing the recorded earthquake was classified as strike/slip. In addition, the seismic motion at bed rock has never been measured due to the lack of accelerometers in the study area. Therefore, Al-Haddad *et al.* (1994) developed the 50-year iso-acceleration map indicating that the peak ground acceleration (PGA) in the study area is 0.15g = 1.5 m/s^2.

Since the seismic motion at the bedrock is required for dynamic analysis of soil-structure interaction and this data is not available, three different seismic motions at the bedrock that have been recorded in three different regions were implemented as Level 1 earthquake motions. These regions have conditions similar to the study area, i.e. earthquake magnitude (6.7~7 Ms), PGA (1~1.5 m/s^2), fault class (strike/slip), the distance between the hypocentre and the site where the earthquake is felt (40 km) and instrument foundation (soft soil).

Then, the worst deformation of the quay wall systems was taken, as required by EUROCODE (CEN, 1994). The chosen three seismic motions occurred in Aqaba-Egypt in 1995, Capono Lucano-Italy in 1980, and Tabas-Iran in 1978, where the PGA and the magnitude were (a_{max}=1.001 m/s^2 and 7.1 M_s), (a_{max}=1.363 m/s^2 and 6.87 M_s) and (a_{max}=1.004 m/s^2 and 7.33 M_s), respectively.

The results of the effective stress analysis will be discussed in more detail in the following section. The summary of these earthquake parameter details considered in the analysis for the Berth 4 model is given in Table 6.6 and their recorded motions are shown in Figure 6.18.

It is much more difficult to reliablely obtain an earthquake record that has a return period of 475 years, as records for these rare events are sparse. Therefore for Level 2 earthquake intensity, the Port Island bedrock incident waves (PI-79EW Base), which were recorded during the Hyogoken-Nanbu earthquake in 1995 in Japan as recommended by Japanese standard (OCDI, 2002).

Table 6.6. Earthquake details used in the analysis for Berth 4 model as Level 1

Earthquake	Aqaba (Egypt)	Capono Lucano (Italy)	Tabas (Iran)
Date	22/11/1995	23/11/1980	16/09/1978
Station	Eilat	Mercato San Severino	Boshroyeh
Location	---	40.789°, 14.763°	33.86°, 57.42°
Direction	Horizontal (N-S)	Horizontal (E-W)	Horizontal (N-S)
Fault type	Strike/Slip	Strike/Slip	Strike/Slip
Fault distance (km)	93.8	33	34
Foundation type	Soft soil	Soft soil	Soft soil
Magnitude	M_w=7.1	M_s=6.87	M_s=7.33
PGA (m/s^2)	1.001	1.363	1.004
Duration (sec.)	60	79.81	34.96
Reference	PEER (2000)	Ambraseys *et al.* (2000)	Ambraseys *et al.* (2000)

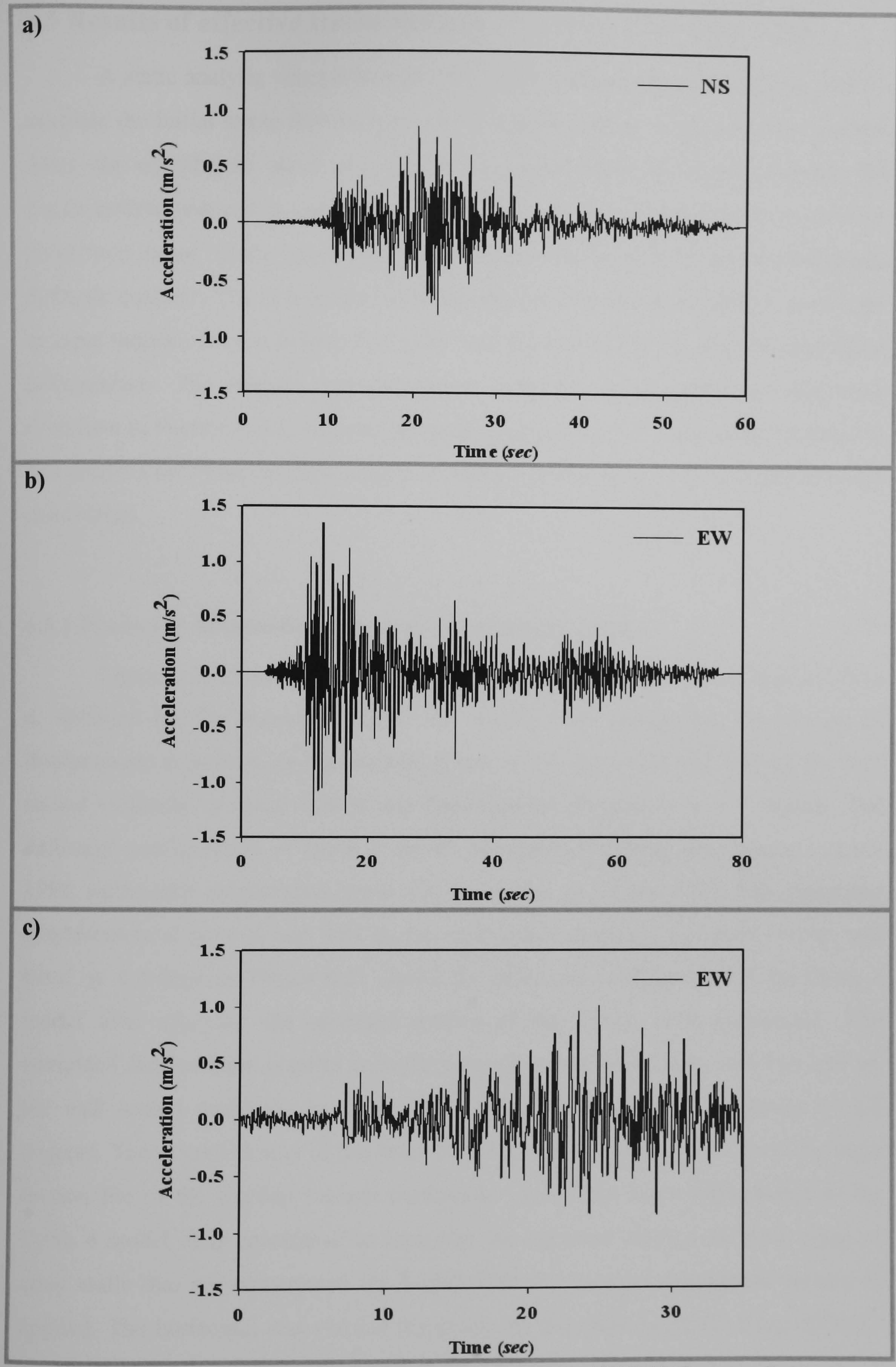

Figure 6.18. Recorded motions; a) Aqaba (Egypt) 1995, b) Capono Lucano (Italy) 1980, and c) Tabas (Iran) 1978

6.5 Results of effective stress analysis of Jeddah Port quay walls

A static analysis was performed before the dynamic response analysis, both to simulate the initial stress distributions and to take the effect of gravity into account. After the equilibrium state was reached by performing the static analysis, the displacements induced by gravity were reset to zero and the stresses at each Gauss point were saved. These values were then used as the initial state for the subsequent dynamic analysis. The two levels of earthquake motion introduced earlier were used as input motions for the Jeddah Port quay wall Berth 4 Model to obtain the predicted deformations. The analysis was performed using the model parameters that were described in Section 6.4.1, whereas the parameters of the P-Z sand model adopted in this analysis are those corresponding to a relative density of $D_r = 35\%$ (equal to *in situ* conditions).

6.5.1 Predicted deformation for Level 1 earthquake motion

Figure 6.19 shows the deformed shape of a typical quay wall section of Berth 4, obtained for the excitation file of the Aqaba 1995 earthquake. The computed displacement at point A on the seaward corner of the quay wall was 3.40 m, the wall settled vertically by about 1.08 m and tilted into the foundation by 4.3 degrees. The deformed configuration of Berth 4 model, obtained after using the Capono Lucano 1980 earthquake acceleration input file, is shown in Figure 6.20. The computed displacement at point A was 3.54 m, the wall settled vertically by about 1.03 m, and tilted by 4.4 degrees. Figure 6.21 shows the deformed configuration of the Berth 4 model after applying the recorded motion of the Tabas 1978 earthquake. The computed displacement at point A on the seaward corner of the quay wall was 2.67 m, the wall settled vertically by about 0.87 m and tilted into the foundation by 3.9 degrees. The overall results of the three cases are listed in Table 6.7. Since the input motion file of the Capono Lucano earthquake caused the worst deformation to the Berth 4 model, it is considered to represent the expected damage to those types of quay walls that are constructed on Jeddah Port if a Level 1 earthquake motion is applied. The horizontal and vertical displacement time history of the three different input accelerations are shown in Figure 6.22. The quay wall deformation at the end of each earthquake is considered in this work as the final deformation.

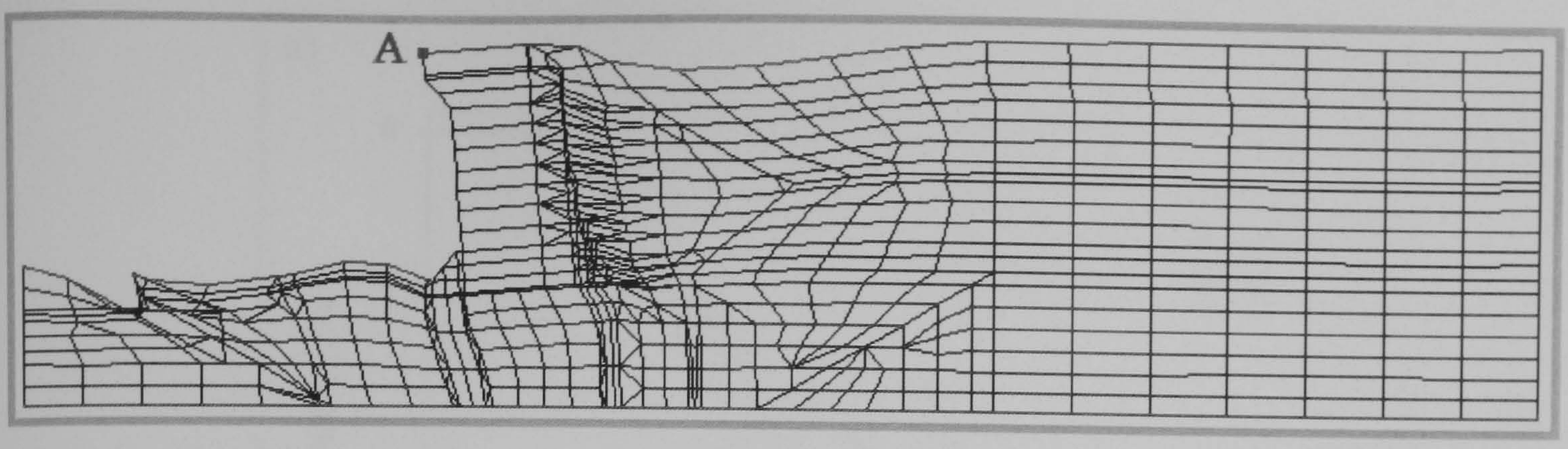

Figure 6.19. Computed deformation at the end of Aqaba earthquake ($t = 60\,\text{sec}$) of a typical quay wall section of Berth 4 in Jeddah Port

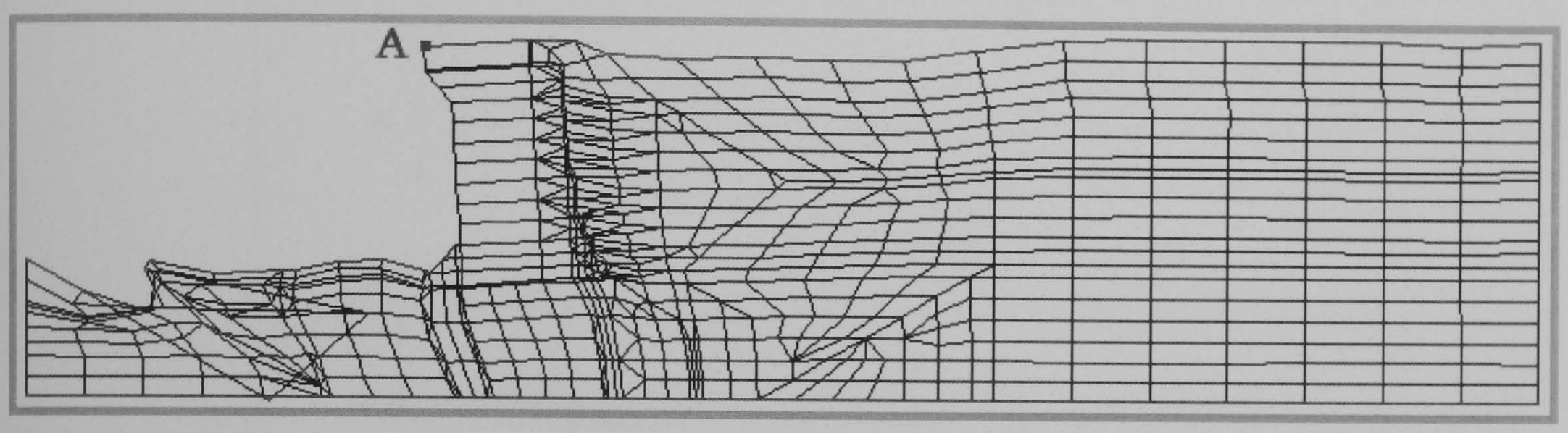

Figure 6.20. Computed deformation at the end of Capono Lucano earthquake ($t = 79.81\,\text{sec}$) of a typical quay wall section of Berth 4 in Jeddah Port

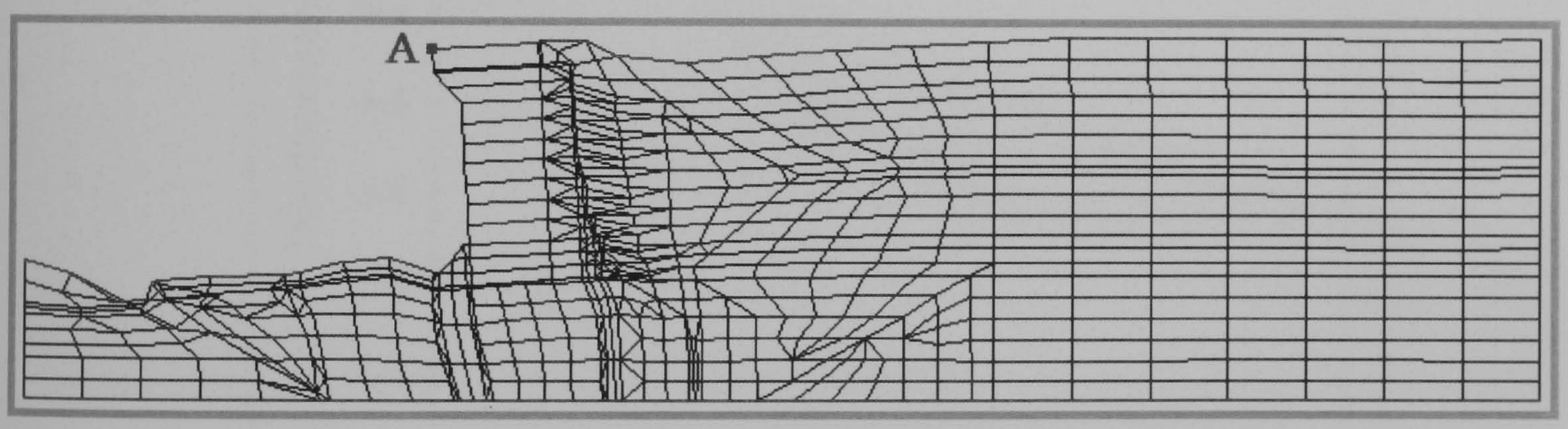

Figure 6.21. Computed deformation at the end of Tabas earthquake ($t = 34.96\ sec$) of a typical quay wall section of Berth 4 in Jeddah Port

Table 6.7. Computed deformation of Jeddah quay wall at the end of shaking (Level 1)

Earthquake	Deformation		
	Horizontal (m)	Vertical (m)	Tilting (deg.)
Aqaba	3.40	1.08	4.3
Capono	3.54	1.03	4.4
Tabas	2.67	0.87	3.9

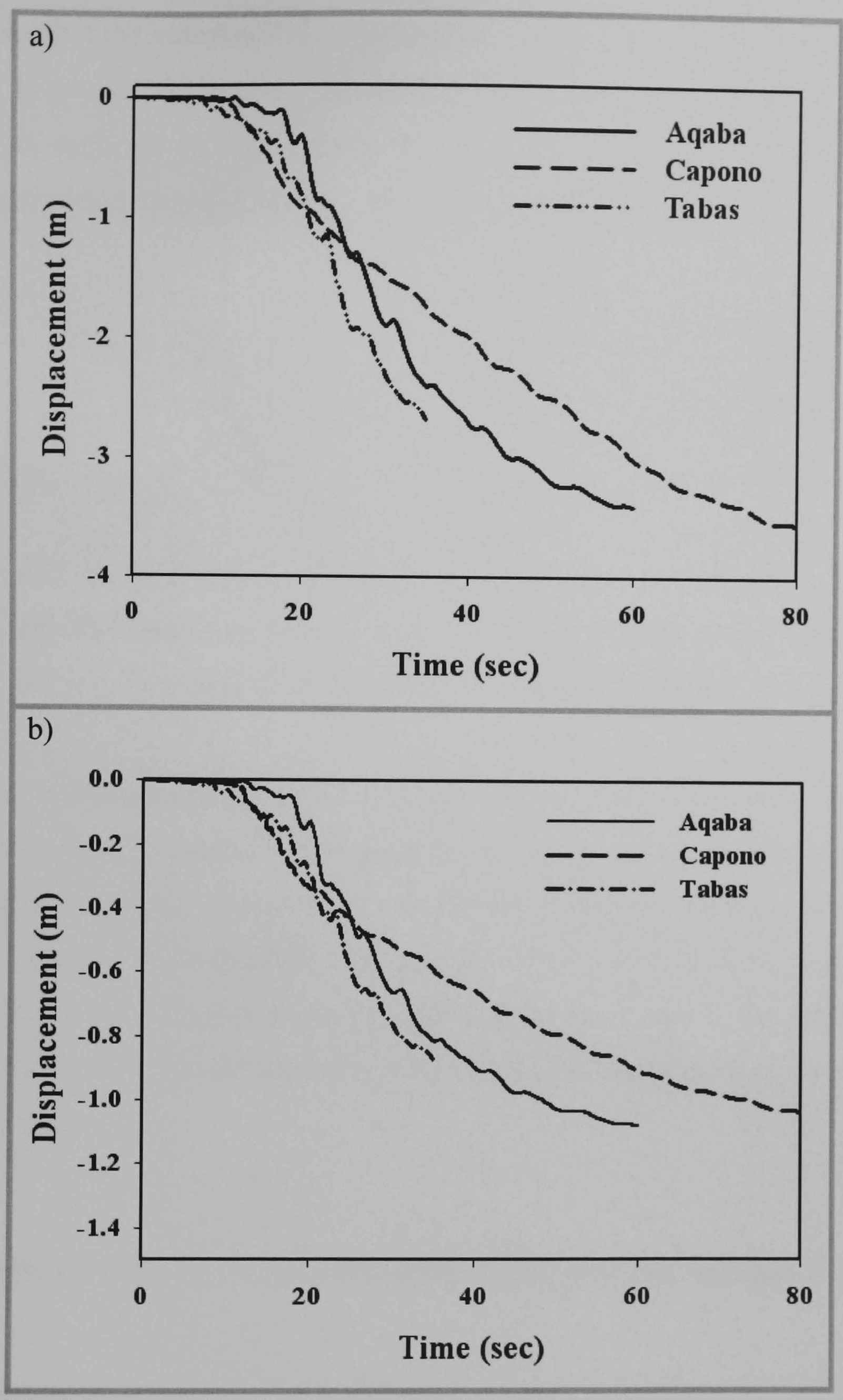

Figure 6.22. Computed displacement time histories at the upper seaward corner of Berth 4 Model (point A): a) Horizontal direction and b) Vertical direction

6.5.2 Predicted deformation for Level 2 earthquake motion

The Port Island bedrock incident waves (PI-79EW Base), recorded during the Hyogoken-Nanbu earthquake in 1995 in Japan (see Section 3.5.4) was applied to the model as Level 2 earthquake motion The deformed configuration of the Berth 4 model, obtained after 30 seconds of the Kobe earthquake, is shown in Figure 6.23. It

can be seen that the computed displacement at point A was 11.40 m, the wall settled vertically by about 2.99 m and tilted by 13 degrees. As it can be noticed, an extreme deformation occurred at the backfill. This is due to combined effects of the strong motion applied in the model and the loose state of the backfill soil.

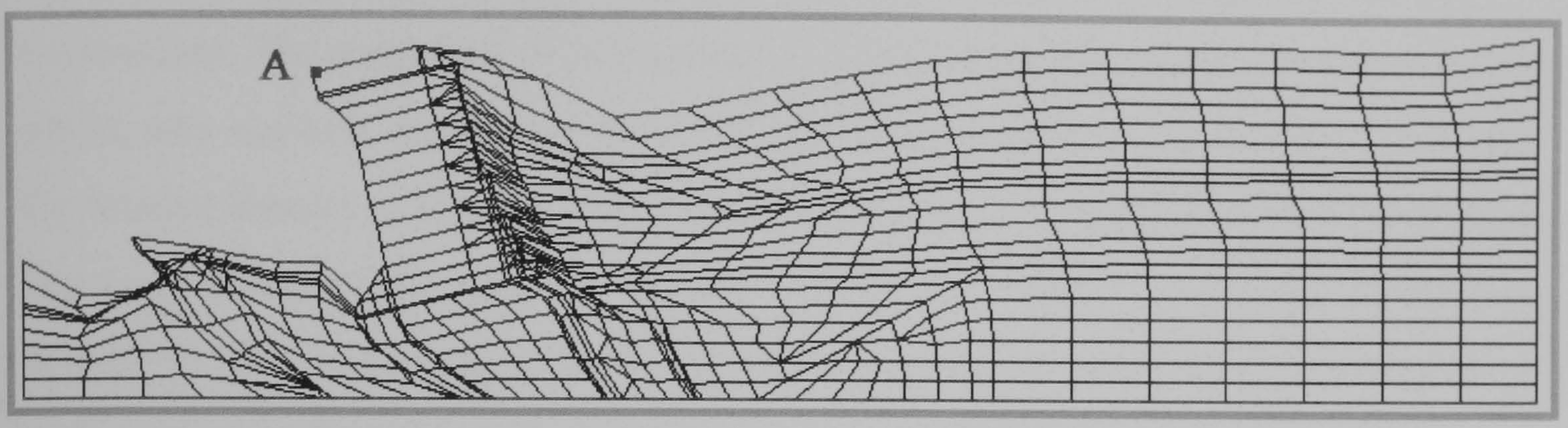

Figure 6.23. Computed deformation at the end of Kobe 1995 earthquake ($t = 30$ sec) of Jeddah Port quay wall Berth 4

The deformations caused by both the Capono Lucano and Kobe earthquakes exceed the allowable displacements specified by the Japanese standards (OCDI, 2002) and tabulated Table 2.1. Therefore, the deformation should be reduced by improving the relative density of the backfill. This technique has been intensively investigated in Section 4.4 and has been found to be a suitable method to enhance the performance of the quay wall. The results of improving backfill will be discussed in more detail in the following section.

6.6 Results of effective stress analysis of improving Jeddah Port quay walls

In order to reduce the deformation of model 4 caused by the applied Level 1 earthquake motion represented by the Capono Lucano 1980 earthquake and to satisfy the allowable displacements specified by the Japanese standards (OCDI, 2002), the parameters of the P-Z sand model, which were identified in Section 6.3 for $D_r = 55\%$ and 75%, are used in the following analysis.

6.6.1 Predicted deformation for Level 1 earthquake motion

For the quay wall with P-Z sand model parameters for $D_r = 55\%$, the results of the computed displacement at point A are reduced from 3.54 m to 0.21 m in the horizontal and from 1.03 m to 0.08 m in the vertical directions. The Berth 4 model analysed using the parameters for $D_r = 75\%$ remained stable with no significant movements. The computed deformations of different backfill relative densities for all earthquake motions considered in Level 1 are summarised in Table 6.8. The results for relative density ≥ 55% are within the range of allowable displacement for normal use as specified by the Japanese standard. Therefore, improving the backfill relative density to 55% is enough to safeguard the Jeddah quay walls, such as the Berth 4 wall, against earthquakes with Level 1 earthquake motions.

Table 6.8. Computed displacements of Jeddah quay wall at the end of shaking (Level 1) for different relative densities

Earthquake	Case 1 ($D_r = 35\%$)		Case 2 ($D_r = 55\%$)		Case 3 ($D_r = 75\%$)	
	Horizontal (m)	Vertical (m)	Horizontal (m)	Vertical (m)	Horizontal (m)	Vertical (m)
Capono	3.54	1.03	0.21	0.04	-0.02	-0.01

The computed distribution of excess pore water pressure ratio r_u for the quay wall for different relative densities of $D_r = 35\%$, 55% and 75%, at the end of Level 1 earthquake motion (Capono Lucano 1980 earthquake) are shown in Figure 6.24. In this figure, the red colour represents 100% liquefaction when r_u reached to 1. It can be clearly seen that susceptibility of liquefaction increases as the relative density of surrounding fill material reduces.

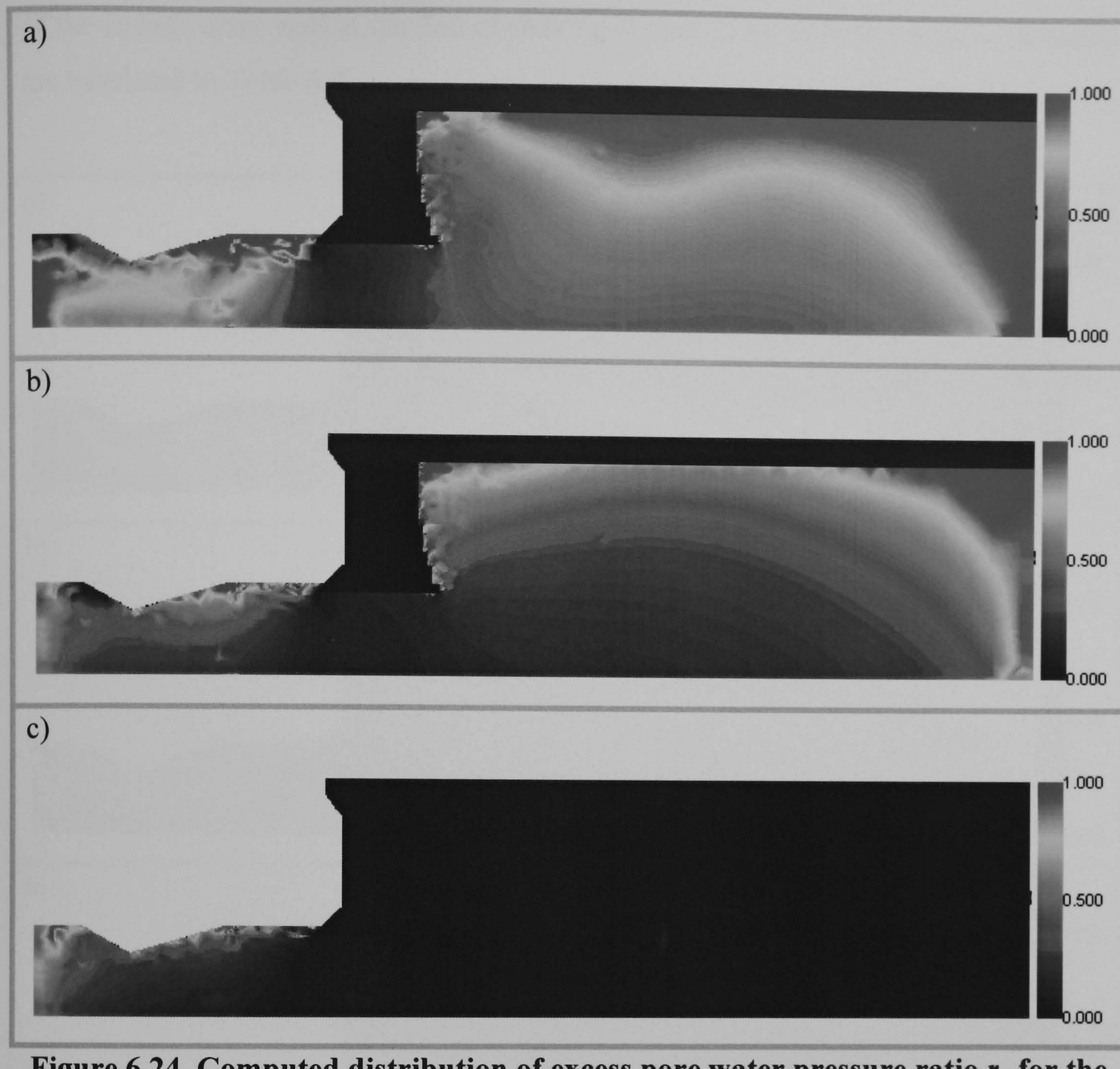

Figure 6.24. Computed distribution of excess pore water pressure ratio r_u for the quay wall for different relative densities: a) D_r = 35%, b) D_r = 55% and c) D_r = 75%, at the end of Level 1 earthquake motion (Capono Lucano 1980 earthquake)

6.6.2 Predicted deformation for Level 2 earthquake motion

Figure 6.25 shows the computed distribution of excess pore water pressure ratio r_u of the model for different relative densities of D_r = 35%, D_r = 55% and D_r = 75%, at the end of Level 2 earthquake motion (Kobe 1995 earthquake). For comparison, the liquefied area behind the wall in Figure 6.25 is greater than that of Figure 6.24 due to the earthquake motion levels. Since the computed deformation of the wall with D_r = 55% (0.32 m) is close to the range of restricted use from the viewpoint of the Japanese standard (0.3 m), a relative density greater than 55% should be applied to achieve the required performance for Level 2 earthquake motions. The computed displacements

of the Jeddah quay wall at the end of shaking (Level 2) for different relative densities are tabulated in Table 6.9.

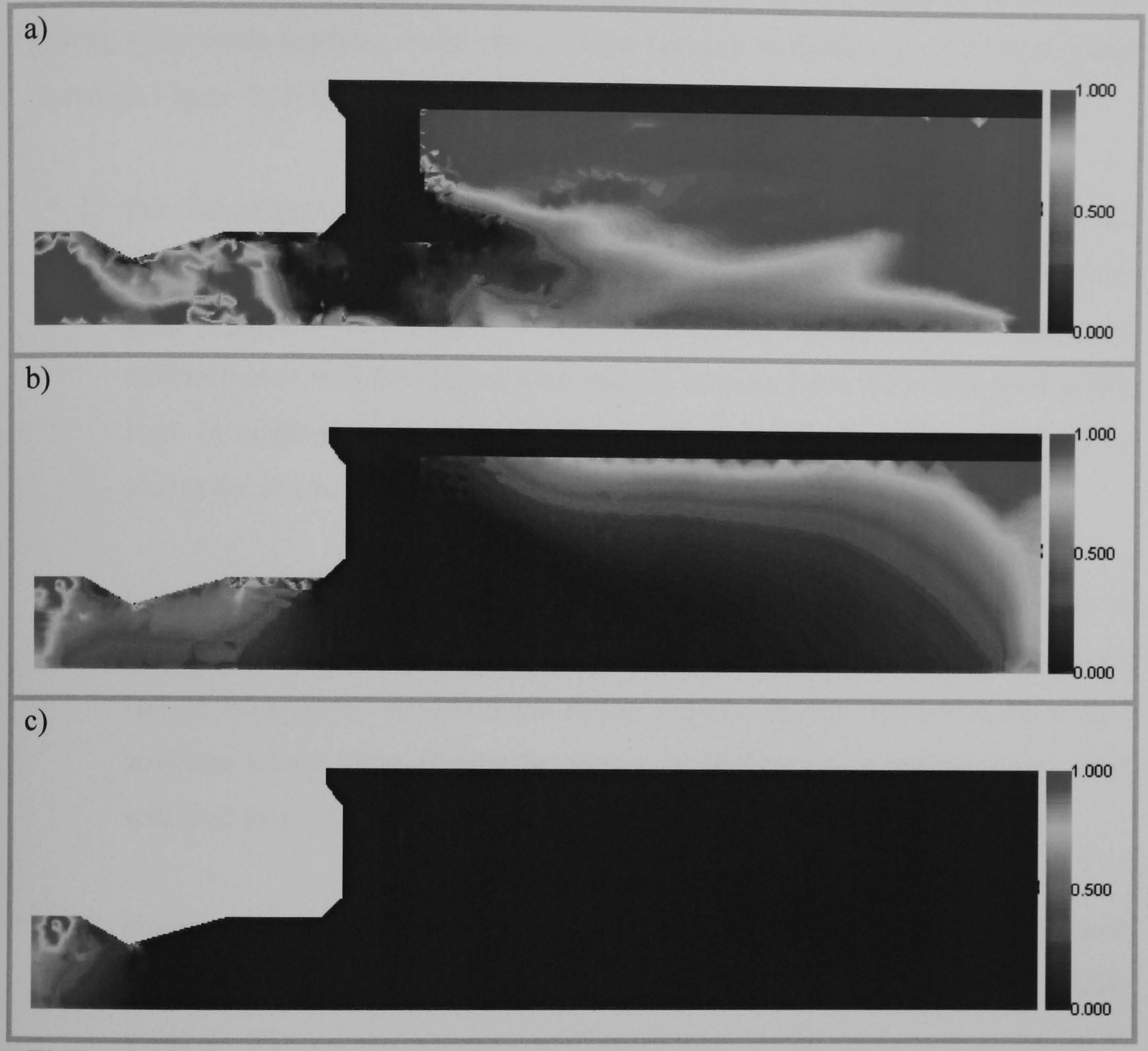

Figure 6.25. Computed distribution of excess pore water pressure ratio r_u for the quay wall for different relative densities: a) D_r = 35%, b) D_r = 55% and c) D_r = 75%, at the end of Level 2 earthquake motion (Kobe 1995 earthquake)

Table 6.9. Computed displacements of Jeddah quay wall at the end of shaking (Level 2) for different relative densities

Earthquake	Case 1 (D_r = 35%)		Case 2 (D_r = 55%)		Case 3 (D_r = 75%)	
	Horizontal (m)	Vertical (m)	Horizontal (m)	Vertical (m)	Horizontal (m)	Vertical (m)
Kobe	11.40	2.99	0.32	0.10	0.12	0.06

6.7 Proposed design procedure for gravity quay walls

As a conclusion of previous experimental and numerical methods which has been developed in this study, a flowchart illustrating a seismic design procedure for gravity quay walls applying Performance-based design methodology is proposed and shown in Figure 6.26 Relevant issues in this flowchart are discussed below.

1) Site investigations: These are divided into two categories: the first concern new quay walls and the second concern an existing quay wall. In case of new quay wall, a natural sample is required from the chosen fill soil. In case of existing quay wall the natural sand sample is taken from the *in situ* sand of the Port. In addition, a Standard Penetration Test (SPT) should be conducted to obtain the *in situ* relative density of backfill soil for existing quay walls.

2) Laboratory tests: monotonic and cyclic triaxial tests should be performed to obtain the susceptibility of the soil to liquefy. Samples for existing structures should be prepared to reflect the *in situ* relative density. However, for a new structure a low value of relative density is preferred as a starting value as it will lead to a more economic design.

3) Numerical analysis: after the experiments are conducted, the soil sand parameters should be identified. For example, a P-Z sand constitutive model could be adopted and the parameters estimated by the procedure described in Section 6.3. Once the soil constitutive model has been specified, a finite element mesh based on the geometry of the quay wall should be created. Then, the expected earthquake motion (Level 1 or Level 2) should be defined. The Level 1 is where the earthquake motion is expected to have a return period of 75 years, whereas the Level 2 is the earthquake motion expected to have a return period of 475 years.

4) Evaluation of the deformed geometry: The computed deformation after the earthquake is compared to the allowable horizontal displacements (0~0.3 m) for normal use and (0.3 m~1.0 m) for restricted use. If the deformation criteria are satisfied, the design is finished; otherwise, enhancement of the

performance of the quay wall is required. This can be achieved either by improving the fill soil or modifying the structure. For existing quay wall, any mitigation strategy will be both difficult and expensive to implement and further work needs to be done in this area.

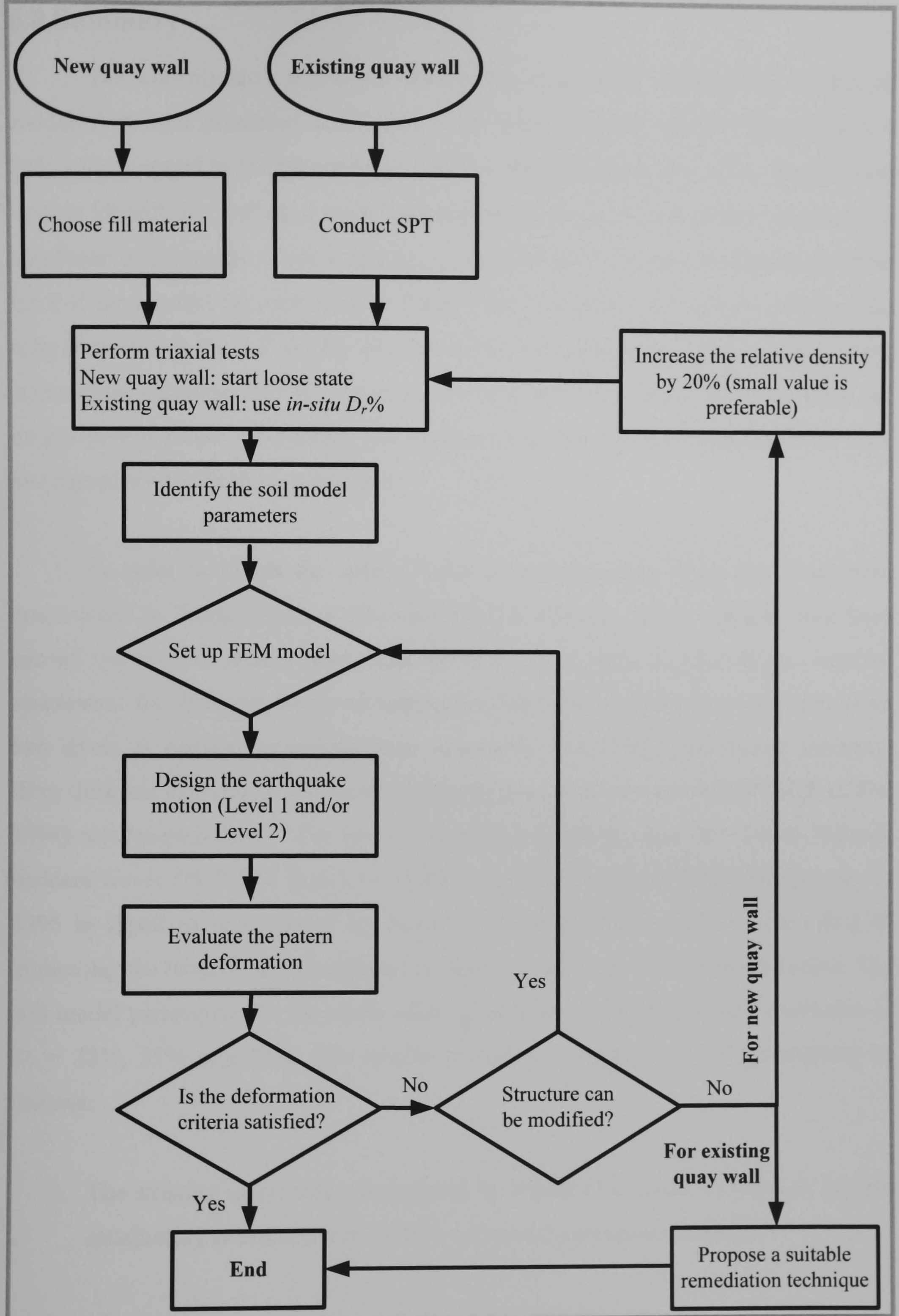

Figure 6.26. Flowchart illustrating the proposed seismic design procedure for gravity quay walls

6.8 Summary

The consolidated undrained monotonic and cyclic triaxial test results of Jeddah Port sand presented in Chapter 5 for three different relative densities (D_r = 35% - loose, equal to *in situ* conditions, 55% - medium dense and 75% - dense) were used to identify the P-Z sand model parameters. It should be noted that, although the amplitude of deviatoric stress varied in each cyclic test, a single set of parameters for the P-Z sand model for each relative density were estimated. The results of the cyclic tests showed that the P-Z model was successful in matching the general shape of the stress:strain response and the decrease in mean effective stress resulting from the excess pore pressure generation. The number of cycles to reach liquefaction in each test agreed well with those measured.

In order to assess the safety levels of existing quay walls that have been constructed in Jeddah Port, a two-dimensional effective stress analysis has been carried out for the Jeddah quay wall Berth 4. As modern seismic design requires assessment for different levels of earthquake intensity, deformatiosn resulting from two levels of earthquake motion were calculated. For level 1 of seismic intensity, three different earthquake acceleration records were used (as per EUROCODE (CEN, 1994) recommendations). For level 2 of seismic intensity, The Port Island bedrock incident waves (PI-79EW Base), recorded during the Hyogoken-Nanbu earthquake in 1995 in Japan as recomanded by Japanees standard (OCDI, 2002). The effect of improving the backfill and foundation on the final deformation was investigated. The soil model parameters for the sands used in the case studies had relative densities of D_r = 35%, 55% and 75%. The results of the case studies can be summarised as follows:

1. The existing quay walls constructed in Jeddah Port, such as Berth 4, are not satisfactory to resist either Level 1 or Level 2 earthquake motions.

2. Improving the backfill and foundation soil's density has a major effect on enhancing the seismic performance of these quay walls. As a result, backfill and foundation with relative density of 55% is enough to protect the Jeddah quay walls, such as the Berth 4 wall, against an earthquake similar to Level 1

earthquake motion. A relative density greater than 55% should be applied to achieve the required performance for Level 2 earthquake motion.

A flowchart illustrating a proposed seismic design procedure for gravity quay walls was suggested. The proposed seismic design method can be applied to either existing or new gravity quay walls.

CHAPTER SEVEN

7. SUMMARY, CONCLUSIONS AND RECOMMENDATIONS

7.1 Introduction

This thesis developed a methodology for implementing seismic design for gravity quay walls. This method adopted a performance based design approach which was made possible by the use of inelastic dynamic finite element anaylsis. The method was applied to existing gravity quay walls constructed in Jeddah Port, Saudi Arabia. The analysis showed that these walls are likely to have insufficient seismic capacity for the levels of earthquake intensity that may be experienced at Jeddah Port. Remediation strategies were also investigated and possible solutions for both existing and future quay walls have been proposed.

7.2 Summary and conclusions

In Chapter 2, previous studies on seismic behaviour of gravity quay walls were reviewed and the validity of simplified methods examined. The results showed that that there is a limitation to the applicability of these practical methods of design based on the pseudo-static approach.

In addition, nine case histories of damage to gravity retaining walls during the period 1964–1999, have been presented. These case histories suggest that the damage to gravity quay walls is often associated with significant deformation of liquefiable soil deposits. Better seismic performance can be attained by using more sophisticated design methods such as performance-based design. These approaches require accurate modelling of seismic behaviour of soil and therefore better soil models that can simulate liquefaction should be adopted.

The liquefaction phenomena and the procedure to determine the soil properties relevant to liquefaction potential were reviewed. The available constitutive soil models, which are able to describe the soil behaviour under earthquake loading, were also reviewed. The P-Z sand model was considered to be the most suitable for

use within this study because it satisfies all the essential requirements for a constitutive model.

In Chapter 3, a two-dimensional, effective-stress finite element procedure in conjunction with a generalised elasto-plastic constitutive model of Pastor *et al.* (1990), with slight modifications has been conducted. The model was first validated by simulating published monotonic and cyclic test results. The results of the monotonic tests showed excellent agreement between the experiment results and numerical simulations with successful prediction of the dilative and contractive behaviour of sand. For the cyclic tests, the model was successful in matching the general shape of the stress:strain response and the decrease in mean effective stress resulting from the excess pore pressure generation. The number of cycles to reach liquefaction in each test then agreed well with those measured.

To demonstrate the validity of the finite element procedure, a model of Port Island quay walls was then developed using a finite element package UWLC. Both vertical and horizontal accelerations were applied to the model and the results were compared to the observed field measurements. The computed residual deformation results were consistent with field observations.

Major conclusions obtained in this chapter are as follows:

1. Computed overall displacements and rotations of the caisson wall were similar to those observed in the field. The computed displacement at point A on the seaward corner of the quay wall was 3.28 m (2.3 m to 3.13 m measured), the wall settled vertically by about 0.73 m (0.79 m to 1.40 m measured) and tilted into the foundation by 4.2 degrees (3 degrees measured).

2. The computed excess pore water pressure ratios were consistent with observed evidence of the liquefaction phenomenon.

In Chapter 4, computer simulations investigated the effects of various soil parameters, wall geometry and seismic excitation on the seismic performance of gravity quay walls. Twenty-six cases of effective stress analysis with variation of tidal range, soil permeability, soil relative densities, wall width size and level of seismic excitation were performed.

Major conclusions obtained in this chapter are as follows:

1. Two cases involving different scenarios of tidal range, one at low water level and the other at high water level, were performed. The results indicate that the low water level case is the worst case that this case should be considered by practicing engineers.

2. Three different values of permeability were analysed to investigate the influence of permeability on the development of pore pressure behind the wall. The results show that when permeability increases the accumulation of pore pressure is reduced. Furthermore, if the permeability is low enough, the pore water pressure will not readily dissipate.

3. Improving the backfill and the foundation soils of caissons reduces the vertical settlement at the toe of the wall by over 73%, while the horizontal displacement is reduced by over 77%.

4. Improving the foundation while keeping the backfill loose as represented by Case 2 caused a lower residual deformation of the caisson than when both the foundation and backfill were improved.

5. The weight of the wall acting on the foundation leads to increased confining pressure beneath the wall, which reduces the susceptibility of liquefaction.

6. Increasing the width of the wall also reduced the horizontal displacement of the wall; however, the relative reduction in displacements is less than the relative increase in the wall width. Increasing the width of the wall also increases the vertical settlement slightly.

7. It is sufficient to analyse the finite element meshes using an acceleration record in one direction only (i.e. the horizontal component, instead of horizontal and vertical).

Chapter 5 described the mechanical properties of Jeddah port soil. These properties were measured using both monotonic and cyclic tests. To ensure that the tests were representative of the *in situ* conditions, SPT tests were conducted at Jeddah Port and the results compared to other tests conducted by the Saudi Port Authority (Saudi Ports Authority, 2006). The tests showed good consistency and were used to determine the relative density of the *in situ* soil.

Index and classification tests for samples that were obtained from the North Container Terminal at Jeddah Port have also been conducted. The results include particle size distribution, Atterberg limits, particle density, maximum and minimum density as well as consolidation derived coefficients. These results showed that Jeddah Port sand used in this investigation consists of 82% sand and 18% silts. Also the sand is angular in nature and fines are non plastic, making Jeddah Port sand susceptible to liquefaction. In addition, Samples with this density were prepared in the lab and a series of undrained triaxial tests were conducted for three different relative densities; D_r = 35%, 55% and 75%. These represent loose (equal to *in situ* conditions), medium dense and dense, respectively.

Major conclusions obtained in this chapter are as follows:

1. The relative density of reclaimed soil retained by Jeddah Port quay walls is approximately 35%.

2. Physical and engineering proprieties of Jeddah Port sand are presented in Table 5.4.

3. It was found that loose samples failed due to cyclic liquefaction, whereas medium dense and dense samples failed as a result of cyclic mobility. This proves that Jeddah Port sand is susceptible to liquefaction.

4. Liquefaction strength curves were determined using cyclic triaxial tests and are presented in Figure 5.20.

In Chapter 6, the consolidated undrained monotonic and cyclic triaxial test results of Jeddah Port sand presented in Chapter 5 for three different relative densities (D_r = 35% - loose, equal to *in situ* conditions, 55% - medium dense and 75% - dense) were used to identify the P-Z sand model parameters. It should be noted that, although the amplitude of deviatoric stress varied in each cyclic test, a single set of parameters for the P-Z sand model for each relative density were estimated. The results of the cyclic tests showed that the P-Z model was successful in matching the general shape of the stress:strain response and the decrease in mean effective stress resulting from the excess pore pressure generation. The number of cycles to reach liquefaction in each test agreed well with those measured

In order to assess the safety levels of existing quay walls that have been constructed in Jeddah Port, a two-dimensional effective stress analysis has been carried out for the Jeddah quay wall Berth 4. As modern seismic design requires assessment for different levels of earthquake intensity, deformations resulting from two levels of earthquake motion were calculated. For level 1 of seismic intensity, three different earthquake acceleration records were used (as per EUROCODE (CEN, 1994) recommendations). For level 2 of seismic intensity, The Port Island bedrock incident waves (PI-79EW Base), recorded during the Hyogoken-Nanbu earthquake in 1995 in Japan as recommanded by Japanees standard (OCDI, 2002). The effect of improving the backfill and foundation on the final deformation was investigated. The soil model parameters for the sands used in the case studies had relative densities of D_r = 35%, 55% and 75%. Finally, a flowchart illustrating a proposed seismic design procedure for gravity quay walls was suggested. The proposed seismic design stages can be applied to both existing and new gravity quay walls.

Major conclusions obtained in this chapter are as follows:

1. The soils parameters for the P-Z sand model for Jeddah Port sand for different densities were calibrated and are presented in Table 6.3.

2. The existing quay walls constructed in Jeddah Port, such as at Berth 4, are not satisfactory to resist either Level 1 or Level 2 earthquake motions.

3. Improving the backfill and foundation soil's density has a major effect on enhancing the seismic performance of these quay walls. As a result, backfill and foundation with a relative density of 55% is enough to protect the Jeddah quay walls, such as the Berth 4 wall, against an earthquake with Level 1 intensity. A greater relative density than 55% should be applied to achieve the required performance for Level 2 earthquake motion.

4. A flowchart illustrating a proposed seismic design procedure for gravity quay walls was suggested. These proposed seismic design stages can be applied for both existing and new gravity quay walls.

Finally it is concluded that both soil models and numerical analysis have progressed to the point where it is now possible to implement performance based design for geotechnical problems. This approach has great benefits over the traditional pseudo-static methods currently used by most practising engineers. It is therefore recommended that the design methodology developed as part of this thesis be adopted for the seismic design of gravity quay walls.

As modern seismic codes and guidelines now allow time-history analysis to be applied in the design of seismic resistant structures, the approach developed in this research could be used to by practicing engineers and it is therefore recommended that practicing engineers designing gravity quay walls in seismic regions, use the methodology outlined in Section 6.7.

7.3 Recommendations for future research

The following recommendations are made

1. One of the most important seismic design criteria for gravity quay walls is ensuring that the backfill and foundation soils do not liquefy. The pseudo-static limit equilibrium method cannot consider the occurrence of this and it is

therefore recommended that a finite element effective stress analysis with a soil model that can consider liquefaction be adopted. In addition to this, because of the economic importance of port structures, it is essential that they remain functional and yet still be designed economically. This can only be achieved if the analysis considers different performance levels for events with different probabilities of occurrence and therefore different magnitudes. It is therefore recommended that the a finite element effective stress analysis is implemented in a performance-based design framework

2. This work is focused on the seismic behaviour of gravity quay walls on saturated soil only. However, it has been observed that liquefaction can even occur in unsaturated soil. Therefore, further investigation for partially saturated soil is needed.

3. The relation between the residual deformation and the increase in relative density is a hot topic for future detailed investigations. Future work should focus on how to identify the correct values of the desired relative densities and their corresponding residual deformations.

4. The results of parametric study show that when permeability of backfill and foundation material increases the accumulation of pore pressure is reduced. Furthermore, if the permeability is low enough the pore water pressure will not readily dissipate; however, the residual deformation of the quay wall increased with increasing permeability, which is counterintuitive and could not be explained. This needs further investigation.

5. In the case of existing quay walls, mitigation strategies are either costly, or impractical. There are existing materials, such as geotextiles, which may be used to mitigate the backfill layer against liquefaction. Therefore, constitutive models for those materials need to developed and incorporated in finite element tools.

References

Alarcon-Guzman, A., Leonards, G.A. & Chameau, J.L., (1988). "Undrained monotonic and cyclic strength of sands". *Journal of Geotechnical Engineering*, Vol. 114, pp. 1089–1109.

Alyami, M., (2003). "Static and seismic design of gravity quay walls". MSc. *Alexandria Unvirsity,* Alexandria. Egypt, 90pp.

Al-Haddad, M., Eeri, M., Siddiqi, G.H., Al-Zaid, R., Arafah, A., Necioglu, A., & Turkelli, N., (1994). "A basis for evaluation of seismic hazard and design criteria for Saudi Arabia." *Earthquake Spectra*, pp. 231–258.

Al-Amri, A.M., (2004). "Seismic Zones in the Arabian Peninsula", *King Saud University*, Riyadh, Saudi Arabia, 164pp.

Ambraseys N., Smit, P., Berardi, R., Rinaldis, D., Cotton, F. and BERGE, C., (2000). "Dissemination of European Strong-Motion Data". CD-ROM collection. *Council of European Communities. Environment and Climate Programme*. ENV4-CT97-0397. Bruxelles. Belgium 146.

ASTM Designation: D 5311-92, (1996). "Standard test method for load controlled cyclic Triaxial strength of soil", *Annual Book of ASTM standards*, ASTM International, West Conshohocken, PA, 1996.

Biot, M.A., (1956). "Theory of propagation of elastic waves in a fluid saturated porous solid, Part I: Low frequency rang, Part II: High frequency range". *Journal of Acoustic Soc. Of Am.*, Vol.28, pp 168–199.

Bishop, A. & Henkel, D., (1962). "The measurement of Soil Properties in the Triaxial Test". (2nd Edition), Edward Arnold, London.

British Standard Institution, (1990). "Methods of test for soils for civil engineering purposes". *BS 1377*, London.

British Standard Institution, (1999). "Code of practice for site investigations". *BS 5930*, London.

Castro, G. (1969). "Liquefaction of sands". PhD thesis, Harvard University, Cambridge, Massachusetts.

Castro, G. (1975). "Liquefaction and cyclic mobility of saturated sands". *Journal of the Geotechnical Engineering Division*, ASCE. Vol. 101, pp. 551–569.

Castro, G. (1987). "On the behavior of soils during earthquakes-liquefaction". *Journal of Soil Dynamics and liquefaction*, pp. 169–204.

Castro, G. & Poulos, S.J. (1977). "Factors affecting liquefaction and cyclic mobility". American Society of Civil Engineers, *Journal of the Geotechnical Engineering Division,* ASCE. Vol. 103, pp. 501–516.

CEN (1994). Eurocode 8: Design Provisions for Earthquake Resistance of Structures E. C. f. Standardization.

Chan, A.H.C. (1988). "A unified finite element solution to static and dynamic geomechanics problems". PhD. *University College of Swansea*, Wales.

Chan, A.H.C., (1989). "User manual for DIANA SWANDYNE-II". Department of Civil Engineering, *University of Glasgow*, U.K.

Chen, C. & Hwang, G. (1999). "Preliminary Analysis for Quay wall Movement in Taichung Harbour During The September 21, 1999, Chi-Chi Earthquake". *Journal of Earthquake Engineering and Engineering Seismology*. Vol. 2, pp. 43–54.

Cubrinovski, M., & Ishihara, K. (2001). "Correlation between penetration resistance and relative density of sandy soil." *15th International conference on soil mechanics and geotechnical engineering,* Istanbul, Turkey, pp. 393–396.

Cuellar, V., Bazant, Z.P., Krizek, R.J. and Silver, M.L., (1977). "Densification andhysteresis of sand under cyclic shear", J *Geotechnique*. Vol. 103, pp 918.

CUR, (2005). "Quay Walls". *Centre for Civil Engineering Research and Codes*, Gouda, The Netherlands.

Dafalias, Y.F., & Herrmann, L.R., (1982). "A bounding surface soil plasticity model". *Proceeding of international symposium on soil under cyclic and transient loading,* Vol. 1, pp. 335–346, Eds. by G. N. Pande and O. C. Zienkiewicz, A. A Balkema, Rottedam.

Dakoulas, P. & Gazetas, G. (2005). "Seismic effective-stress analysis of caisson quay walls: application to Kobe", *Journal of Soils and Foundations*, Vol. 45(4), pp.133–147.

Ebeling, R.M. & Morrison, E.E. (1993). "The seismic design of waterfront retaining structures". Technical Report ITL-92-11/NCEL. US Army Corps of Engineers. Washington, DC . USA, pp. 256.

Elgamal, A., Yang, Z., Parra, E. & Rageb, E., (2003). "Modelling of cyclic mobility in saturated cohesionless soils". *Journal of Plasticity*. Vol. 19, pp. 883–905.

Elsharnoby, B., Elkamhawy, H., Elnaggar, E. & Alyami, M., (2004). "Enhancing load capacity performance of Harbour berths". *In: The 20th International Port Conference*, Alexandria, Egypt, No. 4, pp. 1–11.

Feng, Z., Lin, J., Chi, S. & Chern, J., (2003). "Numerical simulation for liquefiable sands". *Proceeding of the 10th Conference on current researches in Geotechnical Engineering* in Taiwan, Taiwan.

Finn, W.D.L., Lee, K.W. & Martin, G R., (1977). "An effective stress model for liquefaction" *Journal of Geotechnical Engineering*, Vol. 103, pp. 513–533.

FORUM8, (2006). "Dynamic effective stress analysis for ground (UWLC)". *Instruction manual for version. 1.00.00.*

Franklin, A.G. & Chang, F.K., (1977). "Earthquake resistance of earthen and rockfill dams". Report 5: Permanent displacements of earth dams by Newmark analysis, US Army Corps of Engineers, Waterways Experiment Station, Miscellaneous Paper 2-71-17.

Ghaboussi, J. & Momer, H., (1982). "Modelling and analysis of cyclic behaviour of sands". *Soil Mechanics-Transient and Cyclic Loads*, pp. 313–342.

Ghalandarzadeh, A., Towhata, I., Orita, T. & Yun, F., (1998). "Shaking table tests on seismic behaviour of quay walls subjected to backfill liquefaction" Geotechnical Special Publication, No. 75, *Geotechnical Earthquake Engineering and Soil Dynamics II*, Vol. 2, pp. 1045–1056.

Ghionna, V.N. & Porcino, D., (2006). "Liquefaction Resistance of Undisturbed and Reconstituted Samples of a Natural Coarse Sand from Undrained Cyclic Triaxial Tests". *Journal of the Geotechnical Engineering Division*, ASCE, Vol. 132 No. 2, pp. 194–202.

Ghosh, B. & Madabhushi, S.P.G., (2003). "A numerical investigation into effects of single and multiple frequency earthquake motions". *Soil Dynamics and Earthquake Engineering,* Vol. 23, No. 8, pp 691–704.

GDS, (2005). "The GDS Pneumatic Cyclic Triaxial Testing System Hardware Handbook", GDS Instruments Ltd, Hook, Hampshire, UK.

Halcrow, W. & Partners, (1982). "Jeddah Port" Sir William Halcrow & Partners Consulting Engineering, Technical report, London.

Hardin, B.O. & Drnevich, V.P., (1972). "Shear modulus and damping in soils: design equations and curves". *Journal of Soil Mechanics and Foundations Division*, ASCE, 98, pp. 603–624.

Hayashi, S., Kubo, K. & Nakase, A., (1966). "Damage to harbour structures by the Nigata earthquake". *Journal of Soils and Foundations*, Vol. 6, pp. 89–111.

Hirai, H., (1987). "An elastoplastic constitutive model for cyclic behaviour of sands, *International Journal for Numerical and Analytical Methods in Geomechanics*, Vol. 11, pp. 503–520."

Huang, Y.-T., Huang, A.-B., Kuo, Y.-C. & Tsai, M.-D., (2004). "A laboratory study on the undrained strength of a silty sand from Central Western Taiwan". *Soil Dynamics and Earthquake Engineering*, Vol. 24, pp. 733–743.

Hyodo, M., Hyde, A.F.L. & Aramaki, N., (1998). "Liquefaction of crushable soils". *Geotechnique*, Vol. 48, No. 4, pp. 527–543.

Iai, S., Matsunaga, Y. & Kameoka, T., (1992). "Strain space plasticity model for cyclic mobility". *Journal of Soil and Foundation*, Vol. 32 (2), pp. 1–15.

Iai, S., Kameoka, T. & Matsunaga, Y., (1993). "Numerical (Class A) prediction of model No 1". *Proceedings of Verification of Numerical Procedures for the Analysis of Soil Liquefaction Problems*, (VELACS), Vol. 1, pp. 109–127.

Iai, S., (1998), "Seismic analysis and performance of retaining structures" Proceedings of the 1998. *Conference on Geotechnical Earthquake Engineering and Soil Dynamics III,* Part 2 (of 2), ASCE, pp. 1020–1044.

Iai, S. & Ichii, K., (1998). "Performance based design for Port structures". Proceedings of the *30th Joint Meeting of U.S.-Japan Panel on Wind and Seismic Effects*, pp. 84–96.

Iai, S., Ichii, K., Liu, H. & Morita, T., (1998). "Effective stress analysis of Port Structures" *Special issue of Soils and Foundations*, pp. 97–114.

Iai, S., Ichii, K., Morita, T. & Miyata, M., (1997). "Seismic performance of caisson walls on loose saturated sand foundation". *Proceedings of 14th International Conference on Soil Mechanics and Foundation Engineering*, Hamburg, pp. 987–990.

Iai, S. & Sugano, T., (2000). "Shaking table testing on seismic performance of gravity quay walls". *In: 12th World Conference on Earthquake Engineering* (12 WCEE), Auckland, New Zealand, paper no. 2680.

Ichii, K., Iai, S. & Morita, T., (2000). "Performance of the quay wall with high seismic resistance". *Journal of Computing in Civil Engineering,* Vol. 17, No. 2, pp 163–174.

Ichii, K., (2003). "Optimization of design seismic coefficient based on total expected cost for gravity type quay walls". *Structural Engineering/Earthquake Engineering*, Vol. 20, pp.13–23.

Ichii, K., (2004). "Application of risk density analysis for seismic design: A gravity-type quay wall case". *In: Fourth International Conference on Computer Simulation in Risk Analysis and Hazard Mitigation*, RISK ANALYSIS IV, WIT Press, Southampton, United Kingdom, Rhodes, Greece. 9, pp. 41–50.

Ichii, K., (2006). Personal communication.

Idriss, I. & Seed, H., (1974). "Seismic response by variable damping finite elements" *Journal of the Geotechnical Earthquake Engineering Division,* ASCE, Vol. 100, No. GT1, pp. 1–13.

Ikuo, T., Ghalandarzadeh, A., Sundarraj, K. & Vargas-Monge, W., (1996). "Dynamic failures of subsoils observed in waterfront areas". *Special Issue of Soils and Foundations*, pp. 149–160.

Inagaki, H., Iai, S., Sugano, T., Yamazaki, H. & Inatomi, T., (1996). "Performance of caisson type quay walls at Kobe port". *Special issue of Soils and Foundations*, pp. 119–136.

Inoue, K., Miura, K., Otsuka, N., Yoshida, N. & Sasajima, T., (2003). "Numerical analysis of the earth pressure during earthquake on the gravity type quay wall". *Proceedings of the 13th International Offshore and Polar Engineering Conference*, Honolulu, United States. pp. 2095–2099.

Ishihara, K., Tatsuoka, F. & Yasuda, S., (1975). "Undrained deformation and liquefaction of sand under cyclic stresses". *Journal of Soil and Foundation*, Vol. 15, pp. 29–44.

Ishihara, K., (1985). "Stability of natural deposits during earthquakes". *In: 11th International Conference on Soil Mechanics and Foundation Engineering,* San Francisco. 1, pp. 321–376.

Ishihara, K., (1993). "Liquefaction and flow failure during earthquakes". *Geotechnique*, Vol. 43, pp. 351–415.

Ishihara, K., (1994). "Evaluation of residual strength of sandy soils". I*n: Proc. 11th Int. Conf. on Soil Mech Found. Engineering.*, New Delhi. 5, pp. 175–181.

Ishihara, K., Yasuda, S. & Nagase, H., (1996). "Soil characteristics and ground damage". *Special issue of soils and foundations*, pp. 109–118.

Ishihara, K., (1997). "Geotechnical aspects of the 1995 Kobe earthquake". *Proc. 14th ICSMEF*, Hamburg, No. 4, pp. 2047–2073.

Iwasaki, T. & Tai M., (1996). "Strong records at Kobe Port Island". *Special issue of soils and foundations,* pp. 29–40.

Japanese Ministry of Transport (1997), "Damage to port and port-related facilities by the 1995 Hyogoken-nanbu Earthquake". *The Port and Harbour Research Institute*, Japan, pp. 777–792.

Jeyatharan, K., (1991). "Partial liquefaction of sand fill in a mobile arctic caisson under ice loading". PhD thesis, King's College, *University of Cambridge*, UK.

Kohama, E., Ohtsuka, N., Miura, K., Yoshida, N., & Kurita, S. (1998). "Dynamic Behavior of Gravity Type Quay Wall-Backfill system During Earthquake with Regards to the Liquefaction of Backfill". *In: Proc. 8th Int. Offshore and Polar Engineering Conference*, Montreal, Canada, pp. 383–389.

Kramer, S.L. & Seed, H.B., (1988). "Initiation of Soil Liquefaction Under Static Loading Conditions". *Journal of the Geotechnical Engineering Division*, ASCE. Vol. 114 No. 4, pp. 412–430.

Kramer, S.L., (1996). "Geotechnical Earthquake Engineering". Prentice Hall, London.

Krieg, R.D., (1975). "A practical two-surface plasticity theory". *J. Appl. Mech., Trans.* ASME, E42, pp. 641–646.

Lee, C.J., (2005). "Centrifuge modeling of the behavior of caisson-type quay walls during earthquakes". *Journal of Soil Dynamics and Earthquake Engineering*, 25, pp. 117–131.

Liu, H. and Ling, H. I., (2002). "A sand model based on generlized plasticity". *Proceeding of 15th ASCE Engineering Mechanics Conference*, Columbia University, New York.

Madabhushi, S.P.G. & Zeng, X. (1998). "Seismic response of gravity quay walls". II: Numerical modeling. *Journal of Geotechnical and Geoenvironmental Engineering*, 124, pp. 418–427.

Manazari, M.T. & Dafalias, Y.F. (1997). "A critical state two surface plasticity model for sands". *Geotechnique*. Vol. 47 (2), pp. 255–272.

Martin, G.R., Finn, W.D.L. & Seed, H.B., (1975). "Fundamentals of liquefaction under cyclic loading". *Geotechnique.* Vol. 101, pp. 423–438.

Matsuzawa, H., Ishibashi, I. & Kawamura, M., (1985). "Dynamic soil and water pressure of submeged soil". *Journal of Geotechnical Engineering,* Vol. 111, pp. 1161–1176.

Miyata, M. & Sugano, T., (2000). "Experimental and analytical study on the effect of input motion on the behaviour of a caisson quay wall". *In: 12th World Conference on Earthquake Engineering (12 WCEE)*, Auckland, New Zealand. Paper No. 0895.

Miura, K., Kohama, E., Kurita, S., Ohtsuka, N. & Yoshida, N., (1997). "Behavior of gravity type quay wall during earthquake observed in model shaking table test". *In: Proceedings of the 7th International Offshore and Polar Engineering Conference.* Part 1 (of 4), Honolulu, HI, USA. 1, pp. 683–688.

Mohajeri, M., Ichii, K., & Tamura, T., (2002). "Modification of the sliding block concept for caisson walls". *The Earthquake Engineering Symposium Proceedinges*. Vol. 11, pp. 1015–1020.

Mohajeri, M. & Towhata, I., (2003). "Shake table tests on residual deformation of sandy slopes due to cyclic loading". *Journal of Soils and Foundations*, Vol. 43, pp. 91–106.

Mononobe, N. & Matsuo, H., (1929). "On the determination of earth pressure during earthquake". *Proceedings, World Engineering Congress*, Vol. 9.

Mroz, Z., (1967). "On the description of anisotropic work-hardening". *J. Mech. Phys. Solids*, Vol. 15, pp 163–175.

Mroz, Z., Norris, V.A. & Zienkiewicz, O. C., (1981). "An anisotropic critical state model for soils subject to cyclic loading", *Geotecnique*, Vol. 31(3), pp. 451–469.

Nadim, F. & Whitman, R.V., (1983). "Seismically induced movement of retaining walls". *Journal of Geotichnical Engineering*, Vol. 109, No. 7, pp. 915–931.

Nakahara, T., Sugano, T., Oikawa, K. & Mito, M., (2000). "An expermental study on pier damaged by 1995 Hyogoken-Nanbu earthquake". *In: 12th World Conference on Earthquake Engineering (12 WCEE)*, Auckland, New Zealand. Paper No. 1923.

Newmark, N.M., (1965). "Effects of earthquakes on dams and embankment, 5th Rankine lecture". *Geotechnique*, Vol. 15, pp. 139–160.

Nova, R. & Wood, D.M., (1982). "A consititutive model for soil under monotonic and cyclic loading". In: John Wiley & Sons, I. (ed.) *Soil mechanics-transient and cyclic loads*, G. N. Pande and O. C. Zienkiewicz, New York, N.Y.

Nova, R., & Wood, D. M., (1979). "A constitutive model for sand in triaxial compression". *International Journal for Numerical and Analytical Methods in Geomechanics*, Vol. 3, pp. 255–278.

Nozu, A., Ichii, K. & Sugano, T., (2004). "Seismic design of Port structures". *Journal of Japan Association for Earthquake Engineering*, Vol.4, No. 3 (special issue), pp 195–208.

OCDI, (2002). "Technical Standards and Commentaries for Port and Harbour Facilities in Japan", *Overseas Costal Area Development Institute of Japan.*

Okabe, N., (1924). "General theory on earth pressure and seismic stability of retaining wall and dam". *Journal of Japan Society of Civil Engineers*, Vol. 10, No. 6, pp. 1277–1323.

Okamura M., Ishihara M., Tamura K., 2006, Degree of saturation and liquefaction resistances of sand improved with sand compaction pile, Journal of geotechnical and Geoenvironmental engineering, ASCE, Vol. 132, No. 2, pp. 258-264.

Pastor, M., Zienkiewicz, O.C. & Leung, K.H., (1985). "Simple model for transient soil loading in earthquake analsis.II. non-assocative models for sands". *International Journal for Numerical and Analytical Methods in Geomechanics*, Vol. 9, pp. 477–498.

Pastor, M. & Zienkiewicz, O. C. (1986)., "A generalized plasticity, hierarchical model for sand under monotonic and cyclic loading". *Proceeding of 2nd International Symposium on Numerical Models in Geomechanics*, Ghent, pp. 131–150.

Pastor, M., Zienkiewicz, O. & Chan, A.H.C., (1990). "Generalized Plasticity and the modelling of soil behaviour". *International Journal for Numerical and Analytical Methods in Geomechanics,* Vol. 14, pp. 151–190.

PEER., (2000). Strong Motion Database, http://www.Peer.berkeley.edu/smcat. Data accessed 05/09/2007

PIANC., (2001). "Seismic design guielines for port structures". *International Navigation Association,* Balkema, 474p.

Pitilakis, K. & Moutsakis, A., (1989). "Seismic analysis and behaviour of gravity retaining walls-the case of Kalamata harbour quay wall" Soils and Foundations, Vol. 29(1), pp. 1–17.

Poulos, S.J., (1971). "The Stress-Strain Curves of Soils" Geotechnical Engineering Inc., Winchester, Mass., Jan., pp.1–180.

Poulos, S.J., (1981). "Steady state of deformation". American Society of Civil Engineers, *Journal of the Geotechnical Engineering Division,* Vol. 107, pp. 553–562.

Poulos, S.J. Castro, G. & France, J.W., (1985). "Liquefaction evaluation procedure". *Journal of Geotechnical Engineering*, Vol. 111, pp. 772–792.

Prevost, J. H., (1977). "Mathematical modelling of monotonic and cyclic undrained clay behaviour". I*nt. J. Num. anal. Meth. Geomech.*, Vol. 1, pp195–216.

Prevost, J. H., (1985). "A simple plasticity theory for frictional cohesionless soils". *Soil dynamic Earthquake Engineering*. Vol. 4 (1), pp. 9–17.

Rauch, A.F., (1996). "EPOLLS: An Empirical Method for Prediciting Surface Displacements Due to Liquefaction-Induced Lateral Spreading in Earthquakes". PhD. *Virginia Polytechnic Institute and State University* (Virginia Tech), 245 pp.

Richards, R. & Elms, D., (1979). "Seismic behaviour of gravity retaining walls". *Journal of Geotechnical Engineering Division*, ASCE 105(GT4), pp.449–464.

Richart, F., Hall, J. & Wood, R., (1970). "Vibrations of soils and foundations". Prentice-Hall Inc., Englewood Cliffs (New Jersey).

Robertson, P.K., (1994). "Design considrations for liquefaction". I*n: Proc., 13th Int. Conf. Soil Mech. Found. Eng.*, New Delhi. Vol. 5, pp. 185–188

Rouainia M. & Muir Wood, D., (2001) "Numerical integration fo a kinamatic hardening soil plasticity model". *International Journal of Numerical Analytical Methods in Gemechanics.* Vol. 25, pp. 1305–1325.

Sagaseta, C., Cuellar, V. & Pastor, M., (1991). "Modelling stress-strain-time behaviour of natural soils-cyclic loading". *In: Proc. 10th European Conference on Soil Mechanics and Foundation Engineering,* Florence (Italy). 3, pp. 981–999.

Sasajima, T., Sakikawa, M., Miura, K. & Otsuka, N., (2003). "In-situ observation system for seismic behavior of gravity type quay wall". *In: Proceedings of the 13th International Offshore and Polar Engineering Conference*, Honolulu, HI, United States. pp. 2087–2094.

Saudi Ports Authority, (2006). "Northwest berths extension detail." Jeddah Port, Jeddah, Saudi Arabia edition.

Sawada S., Tsukamoto Y., Ishihara K., (2006). "Residual deformation characteristics of partially saturated sandy soils subjected to seismic excitation". *Soil dynamics and earthquake engineering*, Vol. 26, pp. 175-182.

Schofield, A.N., & Worth, CP., (1968). "Critical state soil mechanics", McGraw Hill, London.

Seed, H.B., (1979). “Soil liquefaction and cyclic mobility evaluation for level ground during earthquakes”. *Journal of the Geotechnical Engineering Division*, ASCE. Vol. 105, No. 2, pp 201–255.

Seed, H.B. & Lee, K.L., (1966). "Liquefaction of Saturated Sands during Cyclic Loading". *Journal of Soil Mechanics and Foundation Division*, ASCE, Vol. 92, pp. 105–134.

Seed, H.B. & Idriss, I.M., (1967). "Analysis of soil liquefaction: Niigata earthquake". *Journal of the Soil Mechanics and Foundation Division*, ASCE. Vol. 93, pp. 83–110.

Seed, H.B. & Whitman, R.V., (1970). "Design of earth retaining structures for dynamic loads. ASCE, *Specialty Conference on Lateral Stresses in Ground and Design of Earth-Retaining Structures,* pp. 103–147.

Seed, H.B. & Idriss, I.M., (1971). "Simplified procedure for evaluating soil liquefaction potential". *Journal of the Soil Mechanics and Foundation Division*, Vol. 97, pp. 1249–1273.

Sugano, T., Morita, T., Mito, M., Sasaki, T. & Ingaki, H., (1996). “Case studies of caisson type quay wall damage by 1995 Hyogoken-Nanbu earthquake”. *Eleventh World Conference on Earthquake Engineering*, paper no. 765.

Sumer, B.M., Kaya, A. & Hansen, N.-E.O., (2002). "Impact of liquefaction on coastal structures in the 1999 Kocaeli, Turkey earthquake". *In: Proceedings of the Twelfth (2002) International Offshore and Polar Engineering Conference,* Kitakyushu, Japan. Vol. 12, pp.504–511.

Taylor, D.W., (1984). “Fundamentals of soil mechanics”. Wiley.

Toyota, H., Iai, S. & Kazama, M., (1996). “Characteristics Performance of sandy soils in triaxial tests”. *Special Issue of Soils and Foundations*, pp 119–136.

Toyota, H., Nakamura, K., & Kazama, M., (2004). "Shear and Liquefaction Characteristics of Sandy Soils in Triaxial Tests", *Journal of Soils and Foundations*, Vol. 44, (2), pp. 117–126.

Towhata, I., Ghalandarzadeh, A., Sundarraj, K.P. & Vargas-Monge, W., (1996). "Dynamic failures of subsoils observed in waterfront areas". *Special issue of soils and foundations*, pp 149–160.

Vaid, Y.P. & Sivathayalan, S., (2000). "Fundamental factors affecting liquefaction susceptibility of sands". *Canadian Geotechnical Journal.* Vol. 37 (3), pp. 592–606.

Waerner, S. D., (1998). "Seismic guidlines for ports,technical council on live line earthquake engineering". ASCE. *Technical Council on Lifeline Earthquake Engineering* No. 12.

Wang, W., (1979). "Some findings in soil liquefaction", *Water Conservancy and Hydroelectric Power Scientific Research Institute,* Beijing, China.

Wood, D.M., (2004). "Geotechnical modelling ". Spon Press, New York.

Xenaki, V.C. & Athanasopoulos, G.A., (2003). "Liquefaction resistance of sand-silt mixtures: an experimental investigation of the effect of fines". *Soil Dynamics and Earthquake Engineering,* Vol. 23, pp. 1–12.

Yang, Z., Elgamal, A., Abdoun, T. and Lee, C., (2001). "A numerical study of lateral spreading behind a caisson-type quay wall", *Proceedings of the 4th International Conference on Recent Advances in Geotechnical Earthquake Engineering and Soil Dynamics*, San Diego, California, Paper No. 7.06.

Yilmaz, M.T., Pekcan, O. & Bakir, B.S., (2004). "Undrained cyclic shear and deformation behavior of silt-clay mixtures of Adapazari, Turkey", *Soil Dynamics and Earthquake Engineering,* Vol. 24, pp. 497–507.

Yoshimi Y., Tanaka K., Tokimatsu K., (1989), "Liquefaction resistance of a partially saturated sand". *Journal of Soils and foundations.* Vol. 29, No. 3, pp. 157-162.

Yoshimi, Y., Tokimatsu, K. & Hosaka, Y., (1989). "Evaluation of Liquefaction Resistance of Clean Sands Based on High-Quality Undisturbed Samples", *Journal of Soils and Foundations*, Vol. 29, No. 11, pp. 93–104.

Youd, T.L. & Idriss, I.M., (2001). "Liquefaction resistance of soils: Summary report from the 1996 NCEER and 1998 NCEER/NSF workshops on evaluation of liquefaction resistance of soils". *Journal of Geotechnical and Geoenvironmental Engineering,* Vol. 127, pp. 297–313.

Zhang, J. M., Shamoto, Y. & Tokimatsu, K., (1998). "Earth pressures on rigid walls during earthquakes", *Geotechnical Special publication No. 75, Geotechnical Earthquake Engineering and Soil Dynamics II, Vol. 2, Proceedings of a Specialty Conference*, pp 1057–1070.

Zeng, X., (1992). "The Seismic Response of Gravity Type Quay Wall. Department of Engineering", *Cambridge University*, Cambridge, 20pp.

Zeng, X., (1998). "Seismic response of gravity quay walls. I: Centrifuge modeling". J*ournal of Geotechnical and Geoenvironmental Engineering*, Vol. 124, pp. 406–416.

Zeng, X. & Steedman, R.S., (2000). "Rotating block method for seismic displacement of gravity walls". J*ournal of Geotechnical and Geoenvironmental Engineering*, Vol. 126, pp. 709–719.

Zienkiewicz, O.C., Chan, A.H.C., Pastor, M., Schrefler, B. A. & Shiomi, T., (2001). "Computational geomechanics with special reference to earthquake engineering". John Wiley & Sons Ltd., West Sussex, England.

Zienkiewicz, O.C., Taylor, R.L. & Zhu, J.Z., (2005). "The finite element method". Elsevier Butterworth-Heinemann, Amsterdam, London.

Zienkiewicz, O.C., Chang, C. T. & Henton, E., (1978). "Non-linear seismic response and liquefaction". *International Journal for Numerical and Analytical Methods in Geomechanics,* Vol. 2, pp 381–404.

Zienkiewicz, O.C., Leung, K.H. & Pastor, M., (1985). "Simple model for transient soil loading in earthquake analysis. I. basic model and its application". *International Journal for Numerical and Analytical Methods in Geomechanics,* Vol. 9, pp 453–476.

APPENDIX A

MODEL RESOLUTION AND CONVERGENCE VERIFICATION

In order to examine whether the results of the finite element model have converged, four models of PC-1 with different meshes resolutions were analysed. Table A.1 shows the total number of elements in each analysis and both the horizontal and vertical deflection of point A (as shown in Figure 3.10). These results are also plotted in Figure A.1 and Figure A.2. From the table and figures, It can be seen that the results are similar for all cases and therefore have converged. In this study mesh size three was adopted (i.e. 644 elements).

Table A.1 Summary of Convergence results

Model	Elements number	Deflection in x axis	Deflection in y axis
1	325	3.15	0.69
2	427	3.16	0.71
3	644	3.28	0.73
4	1048	3.2	0.70

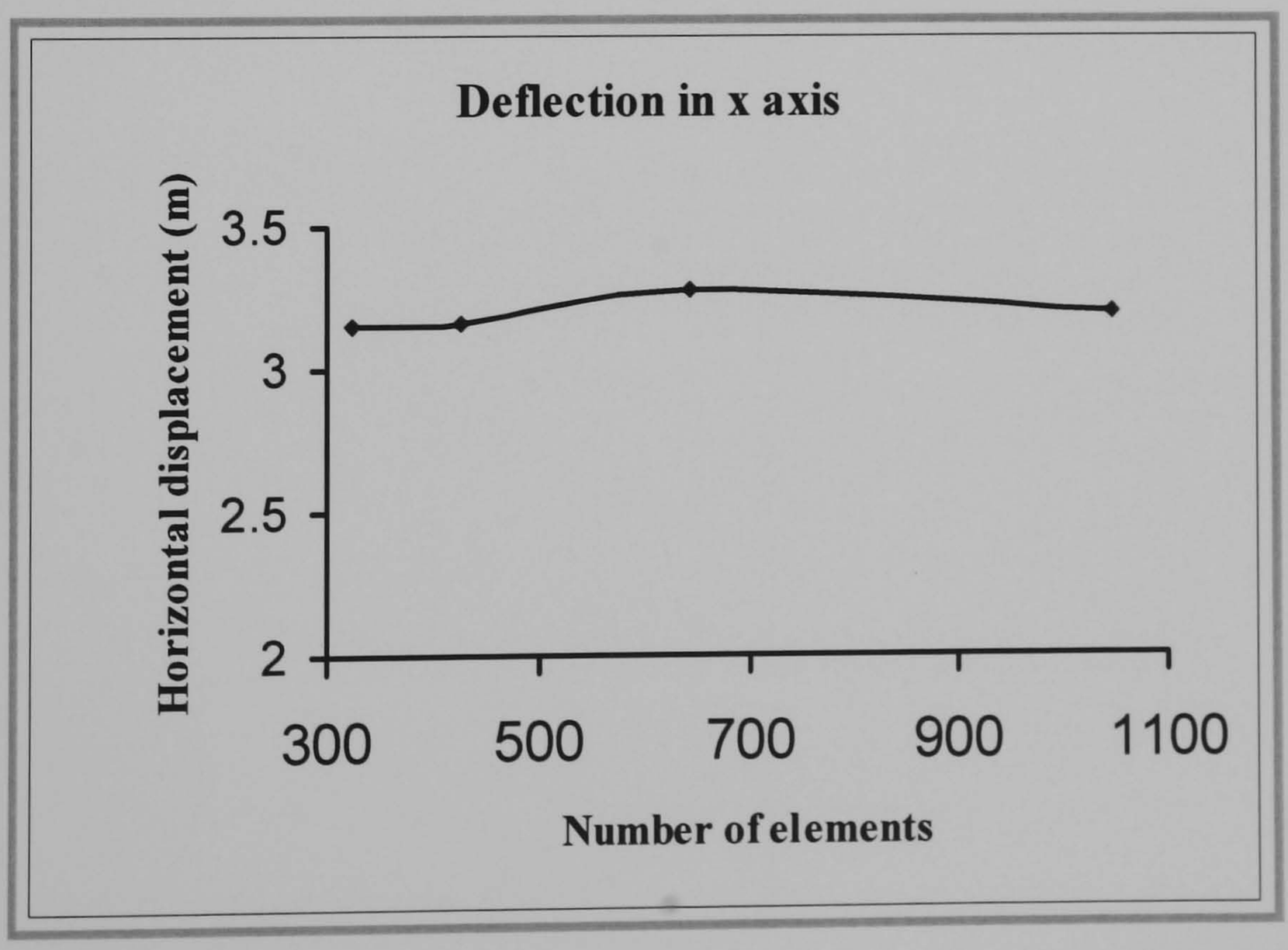

Figure A.1 Horizontal deflection results at point A of PC-1 model for different number of elements

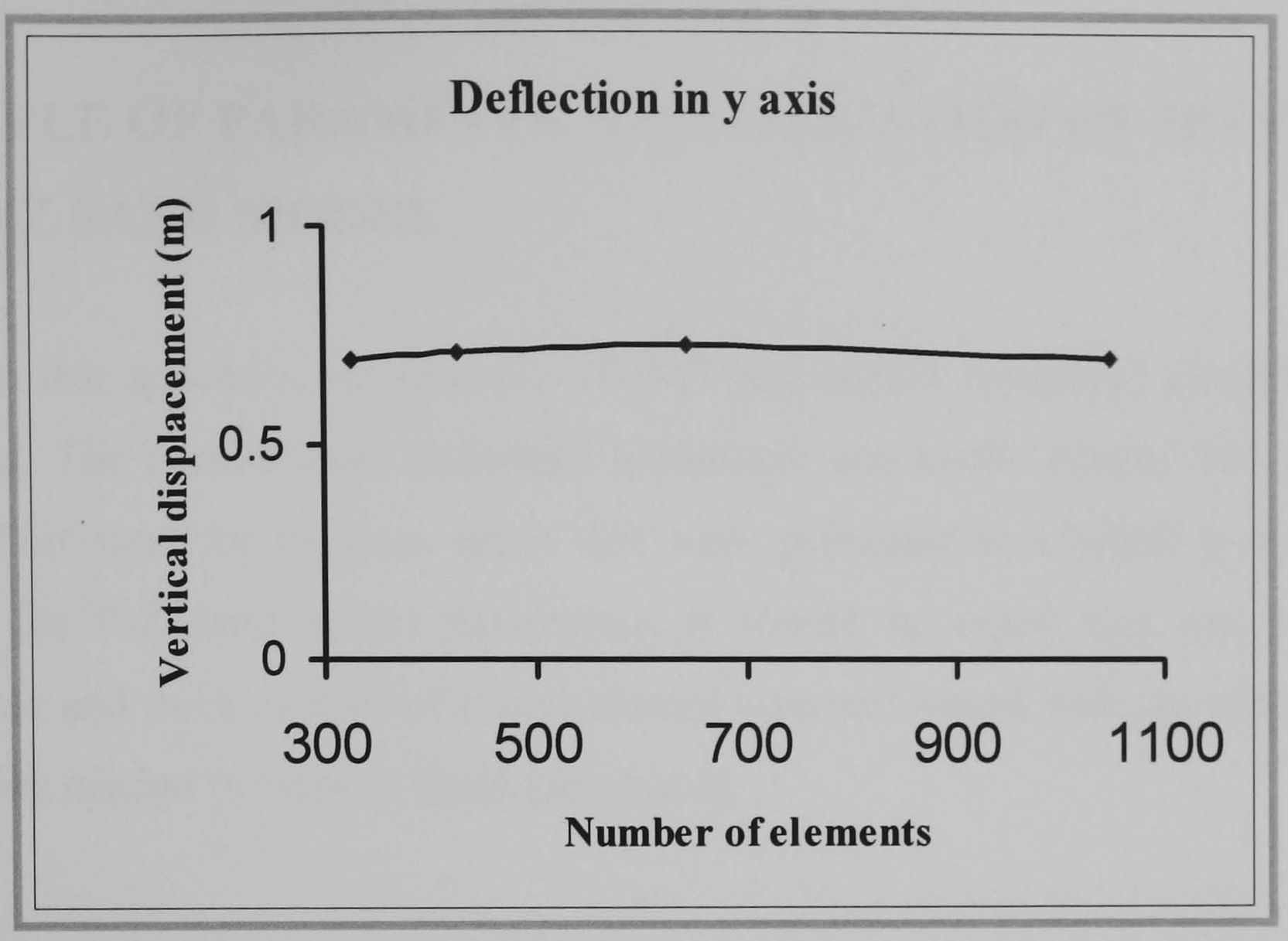

Figure A.2 Vertical deflection results at point A of PC-1 model for different number of elements

APPENDIX B

EXAMPLE OF PARAMETER IDENTIFICATION OF JPS FOR THE P-Z SAND MODEL

In this appendix, an example of P-Z sand model parameter identification is described. The consolidated undrained monotonic and cyclic triaxial test results of Jeddah Port sand for medium dense that were presented in Chapter 5 are used to identify the P-Z sand model parameters. It should be noted that, one undrained monotonic and three undrained cyclic triaxial tests performed with the same relative density are needed to identify those parameters.

B.1 Consolidated undrained monotonic triaxial test

B.1.1 Experimental conditions

Material: Jeddah Port sand

Relative density: D_r =55.4%

Initial effective confining pressure: 100kPa

Maximum axial strain: 15%

B.1.2 Experimental Results

The consolidated undrained monotonic triaxial test results of Jeddah Port sand for medium dense are shown in Figure B.1.

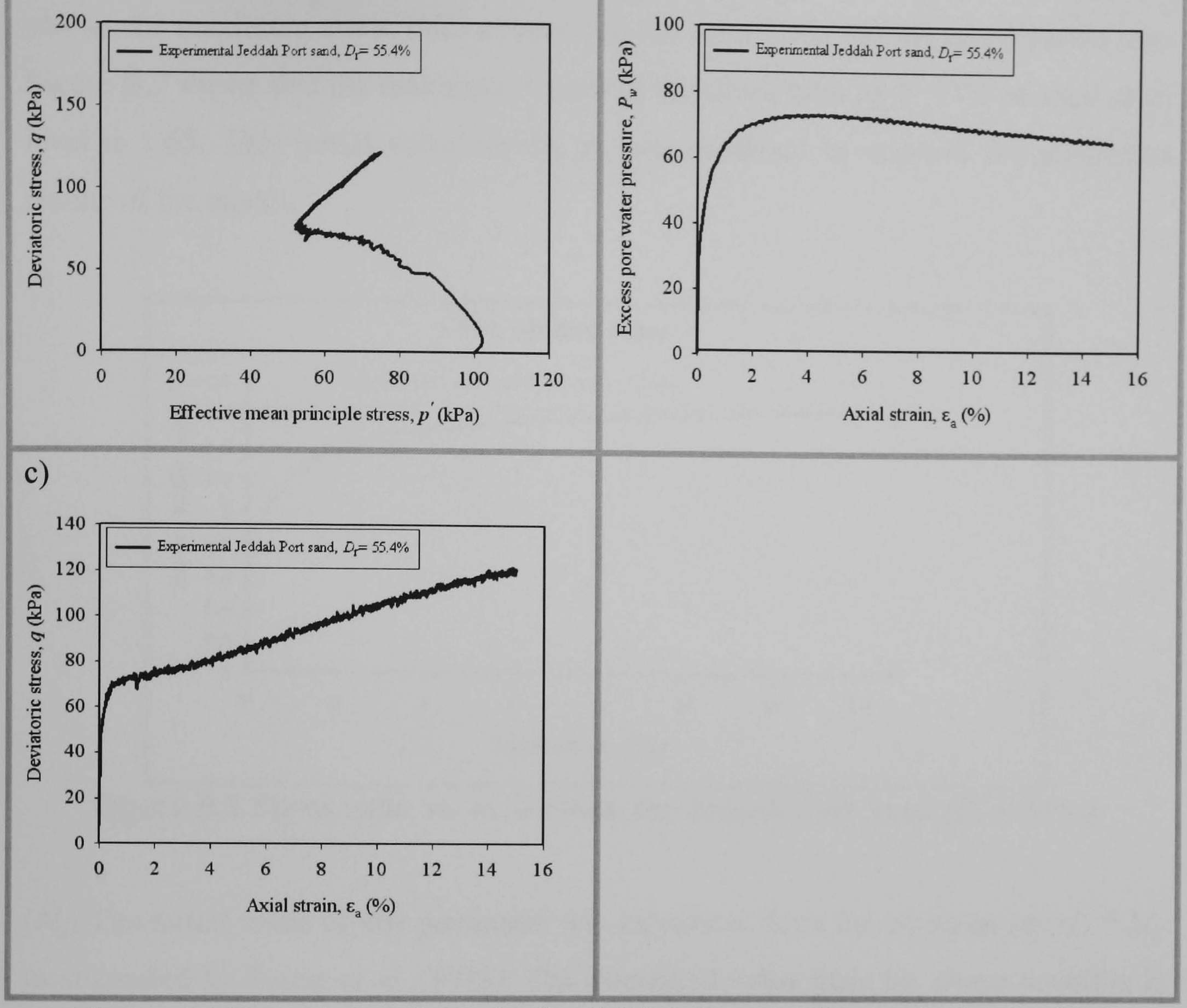

Figure B.1 Experimental results for Jeddah Port sand in undrained trixial compression tests: a) stress path, b) excess pore pressure: axial strain and c) stress:strain relationship

B.1.3 Parameter identification

The twelve P-Z sand model parameters (M_g, M_f, C, α_g, α_f, K_{ev0}, G_{es0}, m_v, m_s, β_0, β_1, H_0), and two additional state parameters (p'_0 and OCR) are firstly assigned by matching monotonic triaxial compression tests with simulated results. However, before any simulations can be performed, initial values of these parameters must be estimated. Wherever possible, initial values were chosen from the recommendations in the literature and these are discussed in detail later. The remaining three parameters (H_{Uo}, γ, γ_U) are assigned values of 0.0, as they are not relevant for monotonic tests and are later identified from the cyclic triaxial tests.

(M_g) The initial value of this parameter was estimated from the stress ratio:axial strain plot as the maximum stress ratio obtained in the monotonic triaxial compression test. Figure B.2 shows that the maximum values of the stress ratio up to 15% of axial stain level is 1.65. This initial value for M_g is later modified to improve the prediction results of the model.

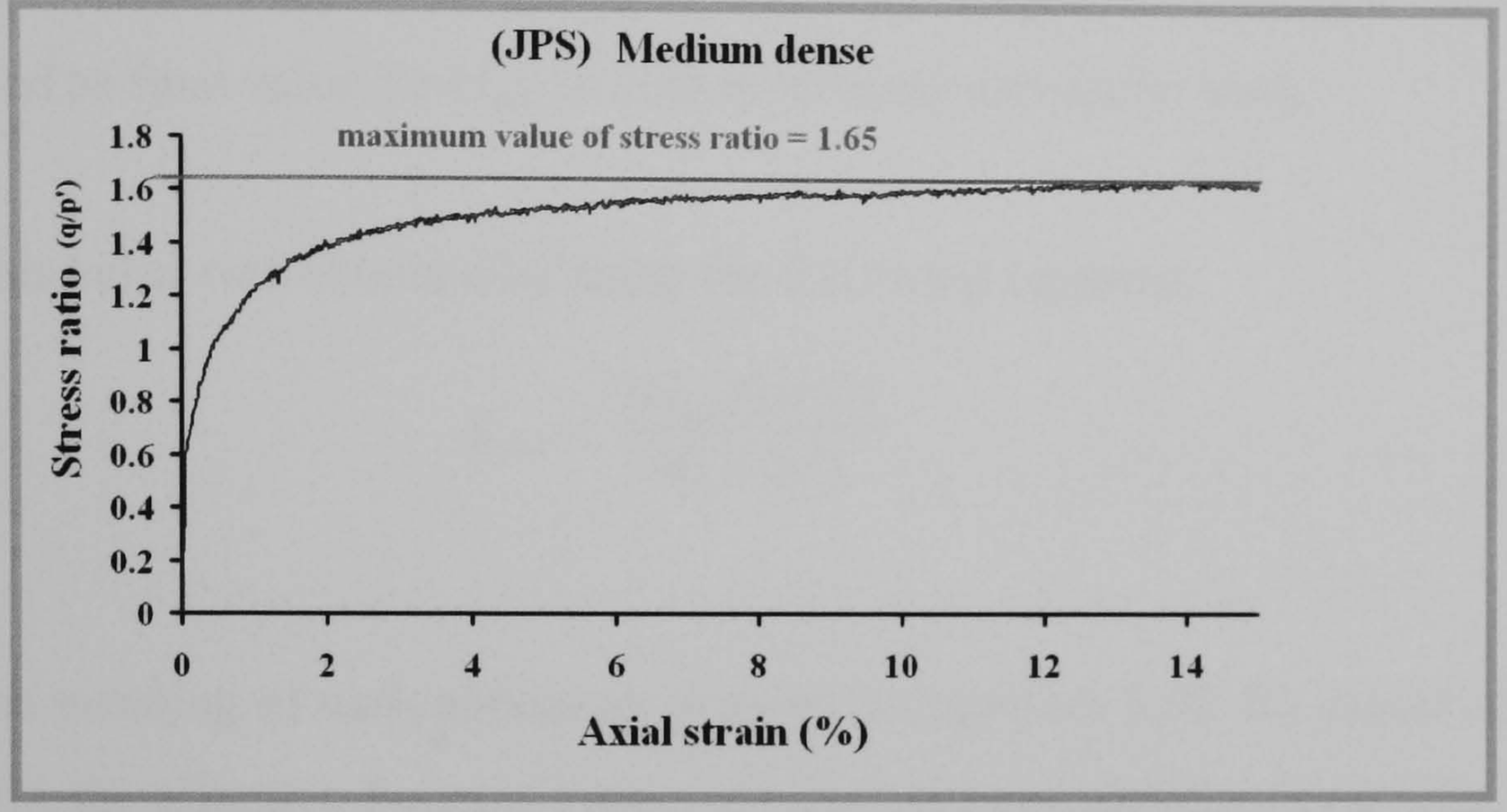

Figure B.2 Stress ratio vs. axial strain for Jeddah Port Sand (D_r = 55%)

(M_f) The initial value of this parameter was calculated from the equation $M_f = D_r * M_g$ as suggested by Pastor *et al.* (1985). The calculated value from the above equation is 0.91.

(C) This value is usually taken as 0.80 as explained in Section 3.3.2.

(α_g) This value is usually taken as 0.45 as suggested by Pastor *et al.* (1985).

(α_f) This value is usually taken to be equal to (α_g) as suggested by Pastor *et al.* (1985).

(m_s) This value is usually taken as 0.5 as explained in Section 3.3.2.

(m_s) This value is usually taken as 0.5 as explained in Section 3.3.2.

(G_{es0}) This value was obtained by using the following equation:

$$G_{es0} = \frac{3E_i}{2(1+v)p_a(p'_0/p_a)^{m_s}} \qquad \text{(B.1)}$$

where the meaning of each parameter is given in Equation 3.37. By assuming an undrained Poisson's ratio $v = 0.5$, the Young's Modulus E_i was obtained by matching the initial slope of the stress:strain relationship curve (see Figure B.1(b)), which is equal to 28 000 kPa. The atmospheric pressure p_a is usually taken as 100 kPa. The calculated value of G_{es0} from the above equation is equal to 280. This value will be considered as final value for G_{es0} in both monotonic and cyclic tests.

(K_{ev0}) This value was obtained by using the following equation:

$$K_{ev0} = \frac{2G_{es0}(1+v')}{9(1-2v')} \qquad \text{(B.2)}$$

where the meaning of each parameter is given in Equation 3.39. By assuming a value of 0.25 for the effective Poisson's ratio, $v' = 0.25$, the calculated value of K_{ev0} from the above equation is equal to 155. This value will be considered as final value for K_{ev0} in both monotonic and cyclic tests.

(β_0) Pastor *et al.* (1985) suggested a value of 4.2 as an initial estimate. This was used in the first set of simulations that were conducted to obtain the value of M_g. Once this parameter was fixed, other simulations were conducted to further improve the fit by adjusting β_0.

(β_1) This was suggested by Pastor *et al.* (1985) to be 0.2 as an initial estimate. A similar procedure to that used for β_0 was used to obtain β_1.

(H_0) This value was taken from Table 3.2; for medium dense sand it is recommended to start with 400. Slight adjustments are needed to improve the simulation results.

(p'_0) The value of preconsolidation stress was calculated as follows:

$$p'_0 = \frac{\sigma_1 + \sigma_2 + \sigma_3}{3} = \frac{100 + 100 + 100}{3} = 100 \text{ kPa}$$

(*OCR*) The samples tested are normally consolidated; thus this value was taken to be 1.0.

The initial model parameters are tabulated in Table B.1.

Table B.1 Initial model parameters for the undrained monotonic test (D_r=55%)

M_f	M_g	C	α_f	α_g	K_{ev0}	G_{es0}	m_v	m_s	β_0	β_1	H_0	H_{U0}	γ	γ_U	p'_0
0.91	1.65	0.8	0.45	0.45	155	280	0.5	0.5	4.2	0.2	400	0	0	0	100

B.1.4 Simulation results and parameter adjustments

Figure B.3 shows the simulation results of the initial model parameters which have been obtained in the previous section.

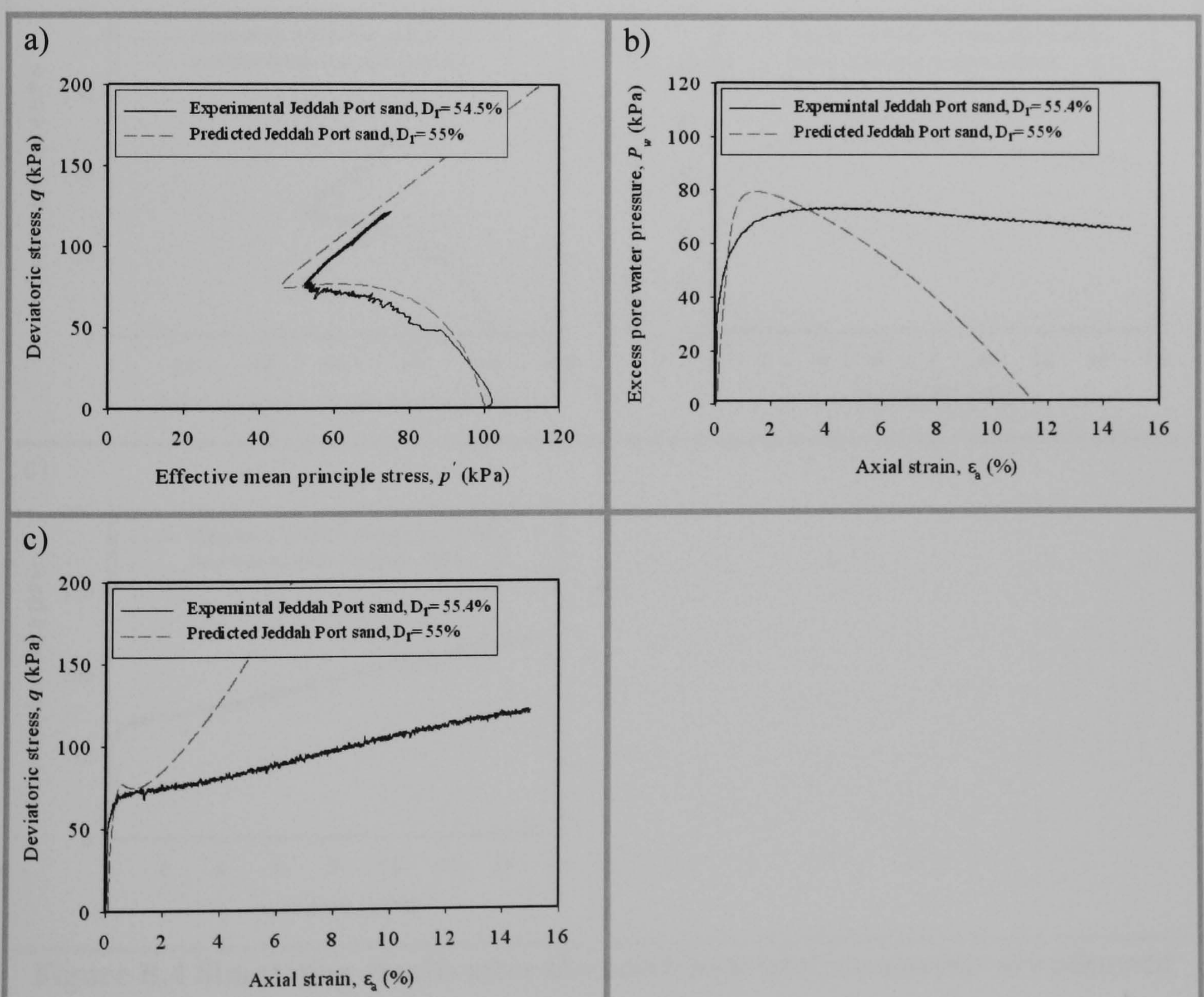

Figure B.3 Simulation results of the initial model parameters for Jeddah Port Sand: a) stress path, b) excess pore pressure: axial strain and c) stress:strain relationship

As shown in the Figure B.3 it is clear that the deviatoric stress is overestimated and the pore water pressure is underestimated. Therefore, some parameters are needed to be adjusted and the simulation should be repeated to improve the results by adjusting the following parameters:

$M_g = 1.65 \rightarrow 1.4$

$\beta_0 = 4.2 \rightarrow 1$

$\beta_1 = 0.2 \rightarrow 0.1$

$H_0 = 400 \rightarrow 450$

Figure B.4 shows the simulation results after the initial model parameters have been adjusted.

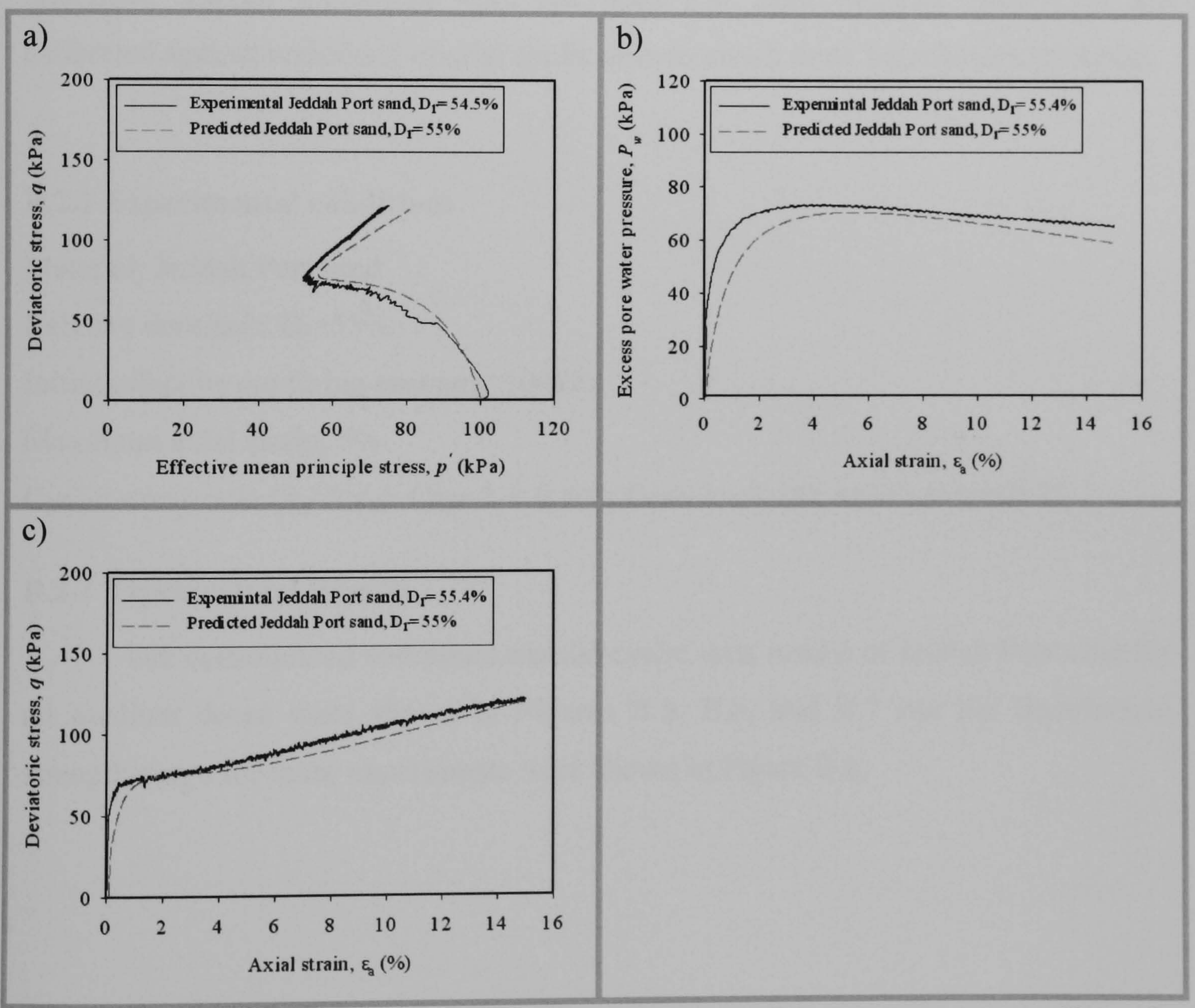

Figure B.4 Simulation results after the previous model parameters are adjusted for Jeddah Port Sand: a) stress path, b) excess pore pressure: axial strain and c) stress:strain relationship

From Figure B.4 it is clear that the simulation and the experimental results agree quite well. The final model parameters are listed in Table B.2.

Table B.2 Final model parameters obtained from the undrained monotonic test (D_r=55%)

M_f	M_g	C	α_f	α_g	K_{ev0}	G_{es0}	m_v	m_s	β_0	β_1	H_0	H_{U0}	γ	γ_U	p'_0
0.91	1.40	0.8	0.45	0.45	155	280	0.5	0.5	1.0	0.1	450	0	0	0	100

B.2 Consolidated undrained cyclic triaxial tests

Starting from the previous parameters which have been obtained from the undrained triaxial monotonic test, the final P-Z sand material parameters are calibrated against undrained triaxial cyclic tests to match three liquefaction strengths.

B.2.1 Experimental conditions

Material: Jeddah Port sand

Relative densities: D_r=55%

Initial effective confining pressure: 100kPa

Maximum axial strain: 5%

Cyclic stress ratio (σ_a/ $2\sigma'_0$): Case 1 = 0.193, Case 2 = 0.244 and Case 3 = 0.31

B.2.2 Experimental Results

The consolidated undrained triaxial cyclic tests results of Jeddah Port sand for all medium dense ware shown in Figures B.5, B.6, and B.7 and the liquefaction strength curve for those experiments ware shown in Figure B.8.

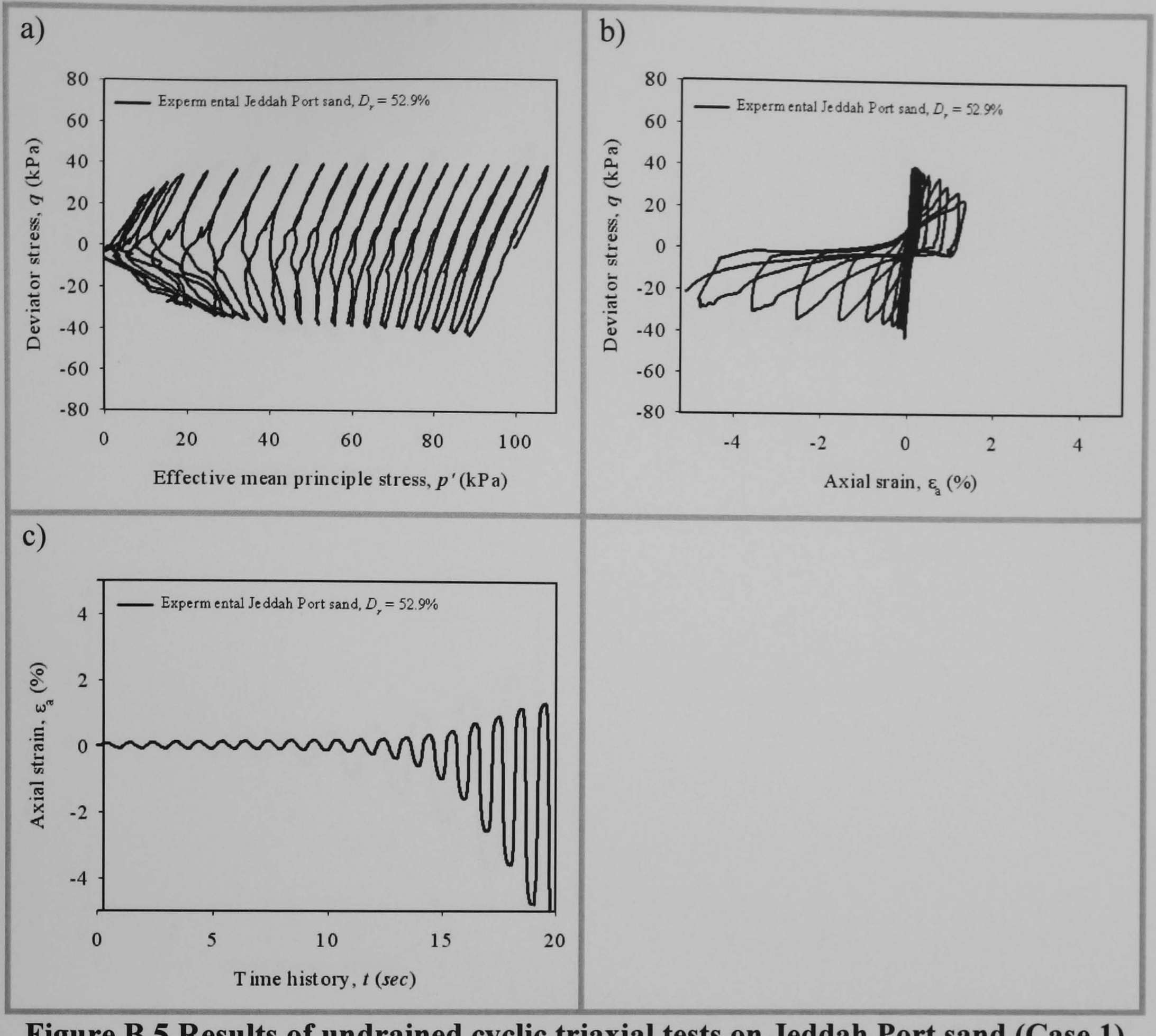

Figure B.5 Results of undrained cyclic triaxial tests on Jeddah Port sand (Case 1) (Relative density, D_r=52.9% & Peak Amplitude, q=38.7 kPa): a) stress path; b) stress:strain relationship; c) axial strain time history

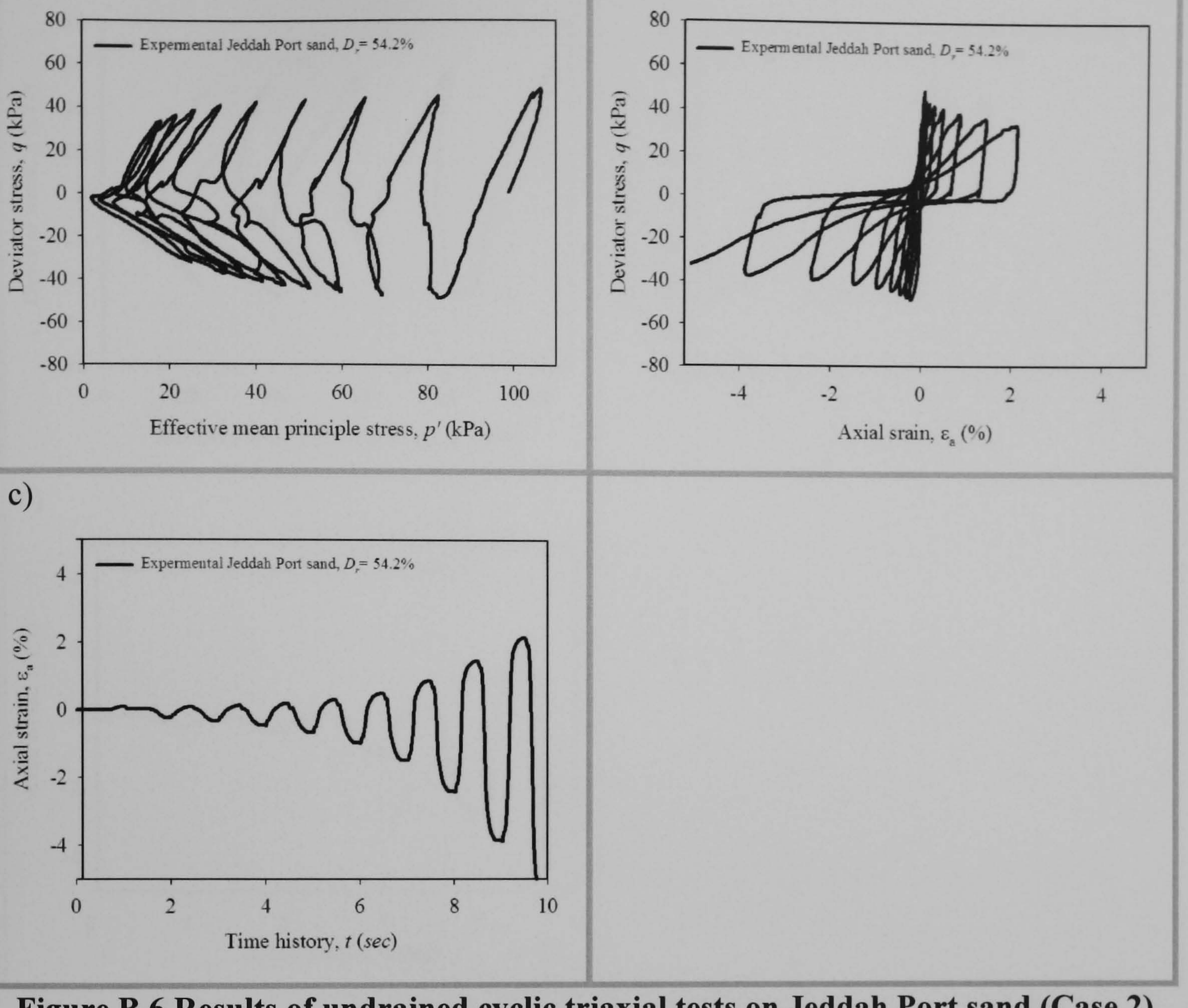

Figure B.6 Results of undrained cyclic triaxial tests on Jeddah Port sand (Case 2) (Relative density, D_r=54.2% & Peak Amplitude, q=48.8 kPa): a) stress path; b) stress:strain relationship; c) axial strain time history

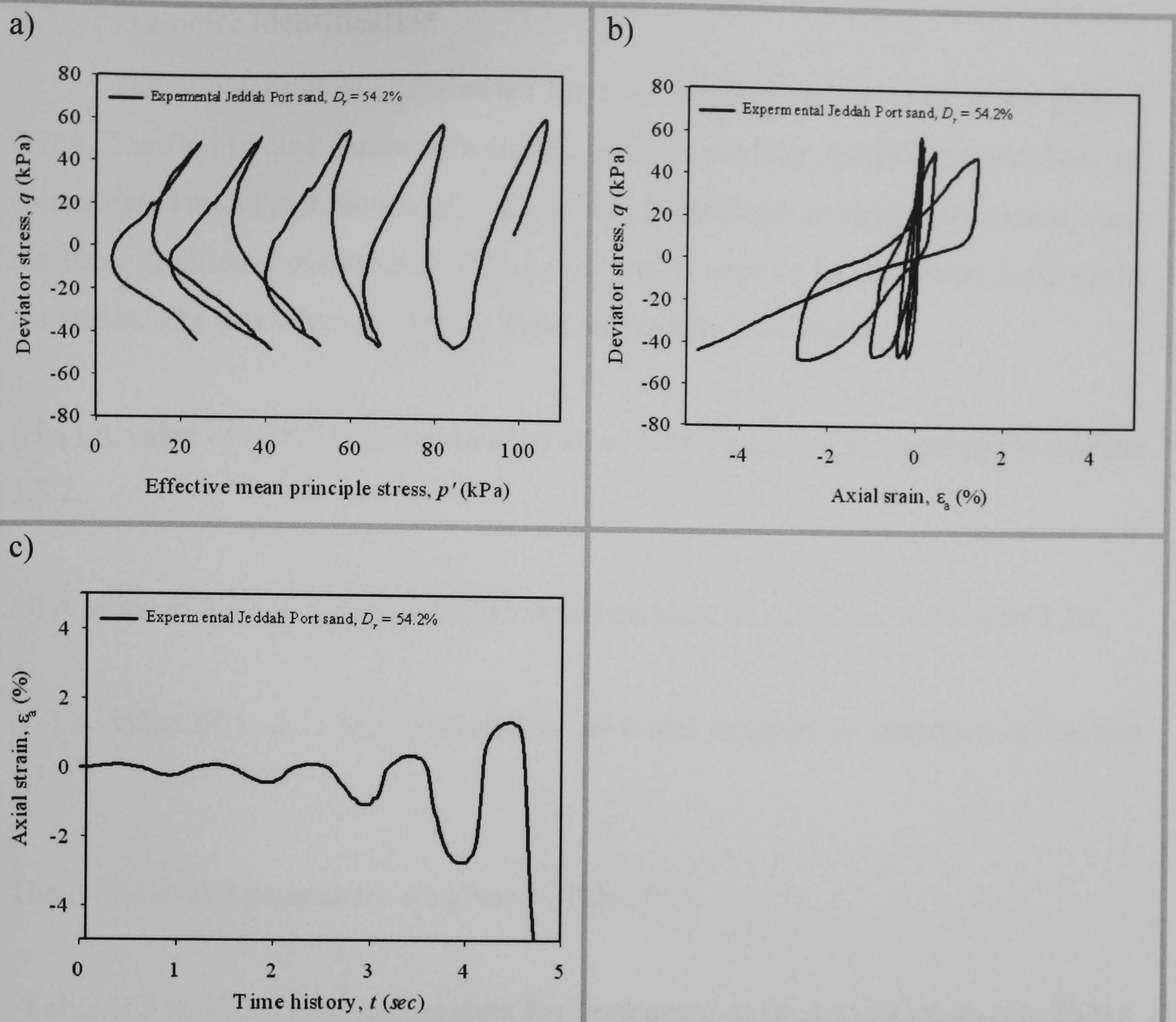

Figure B.7 Results of undrained cyclic triaxial tests on Jeddah Port sand (Case 3) (Relative density, D_r=54.2% & Peak Amplitude, q=62.0 kPa):

a) stress path; b) stress:strain relationship; c) axial strain time history

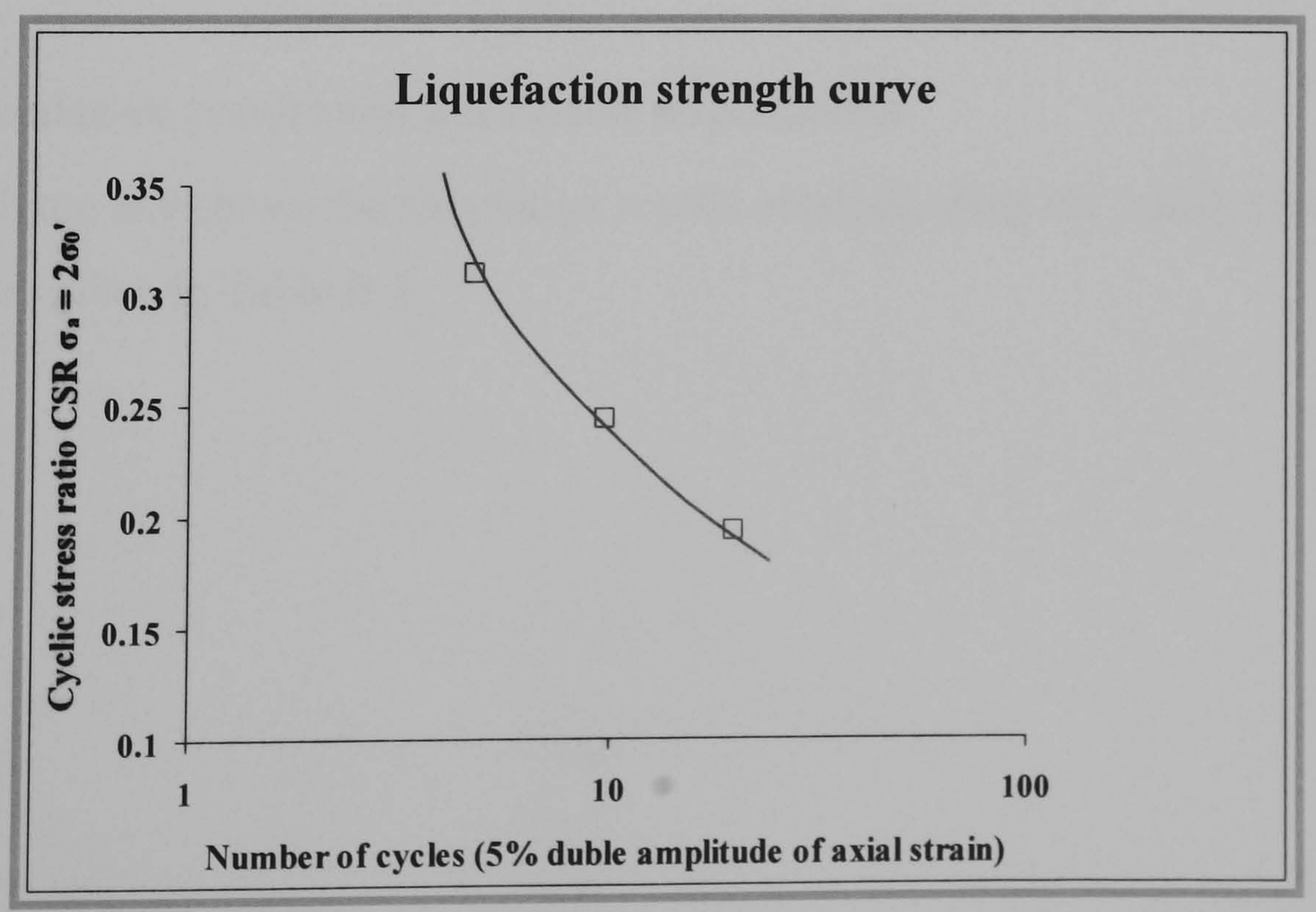

Figure B.8 Liquefaction strength curve for JPS

B.2.3 Parameter identification

The simulations are performed for case 2 which has a cyclic stress ratio of 0.244. The first twelve parameters are the same as the final results obtained from the consolidated undrained monotonic triaxial test. In addition, as mentioned earlier, there are three additional parameters (H_{Uo}, γ, γ_U) which need to be calibrated from cyclic responses. The procedure to identify these parameters is as follows:

(H_{Uo}) A value of 6 000 is recommended as an initial estimate as explained in Section 3.3.2.

(γ) A value of 8 is recommended as an initial estimate as explained in Section 3.3.2.

(γ_U) A value of γ -2 is recommended as an initial estimate as explained in Section 3.3.2.

The initial model parameters are given in Table B.3.

Table B.3 Initial model parameters for undrained cyclic triaxial tests (D_r=55%)

M_f	M_g	C	α_f	α_g	K_{ev0}	G_{es0}	m_v	m_s	β_0	β_1	H_0	H_{U0}	γ	γ_U	p'_0
0.91	1.4	0.8	0.45	0.45	155	280	0.5	0.5	1.0	0.1	450	6000	8	6	100

B.2.4 Simulation results and parameter adjustments

Figure B.9 shows the simulation results obtained using the initial model parameters given in Table B.3.

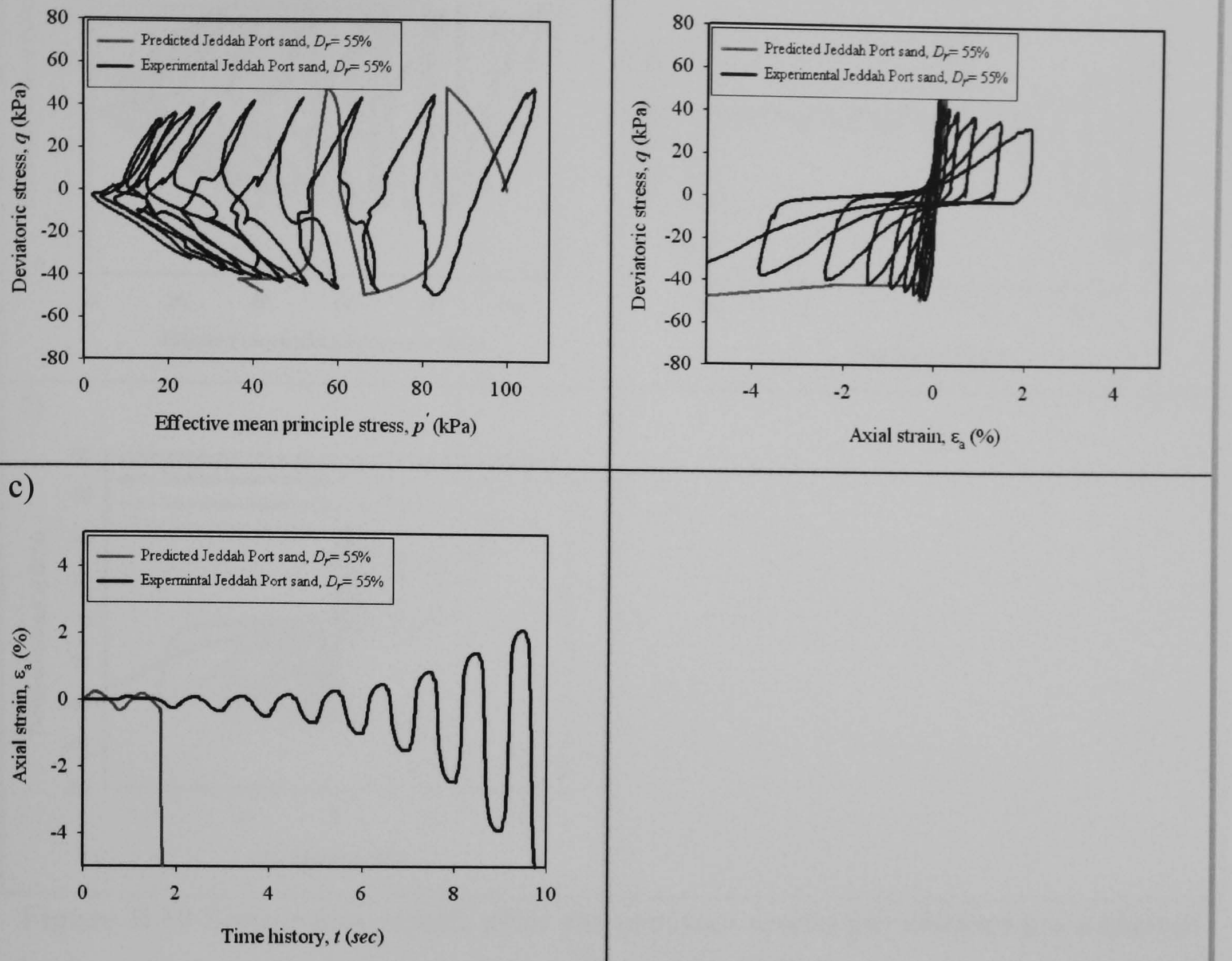

Figure B.9 Simulation results after the previous model parameters are adjusted

a) stress path ; b) stress:strain relationship; c) axial strain time history

From Figure B.9 it can be seen that the simulation results have reached 5% double amplitude of axial strain after 2 cycles compared to 10 cycles of the experiment. Therfore, the simulation should be repeated by adjusting the following parameters:

$\beta_0 = 1 \rightarrow 4.2$

$\beta_1 = 0.1 \rightarrow 0.5$

$\gamma = 8 \rightarrow 6$

$\gamma_U = 6 \rightarrow 5$

After adjusting the model parameters, the results of the simulations are shown in Figure B.10.

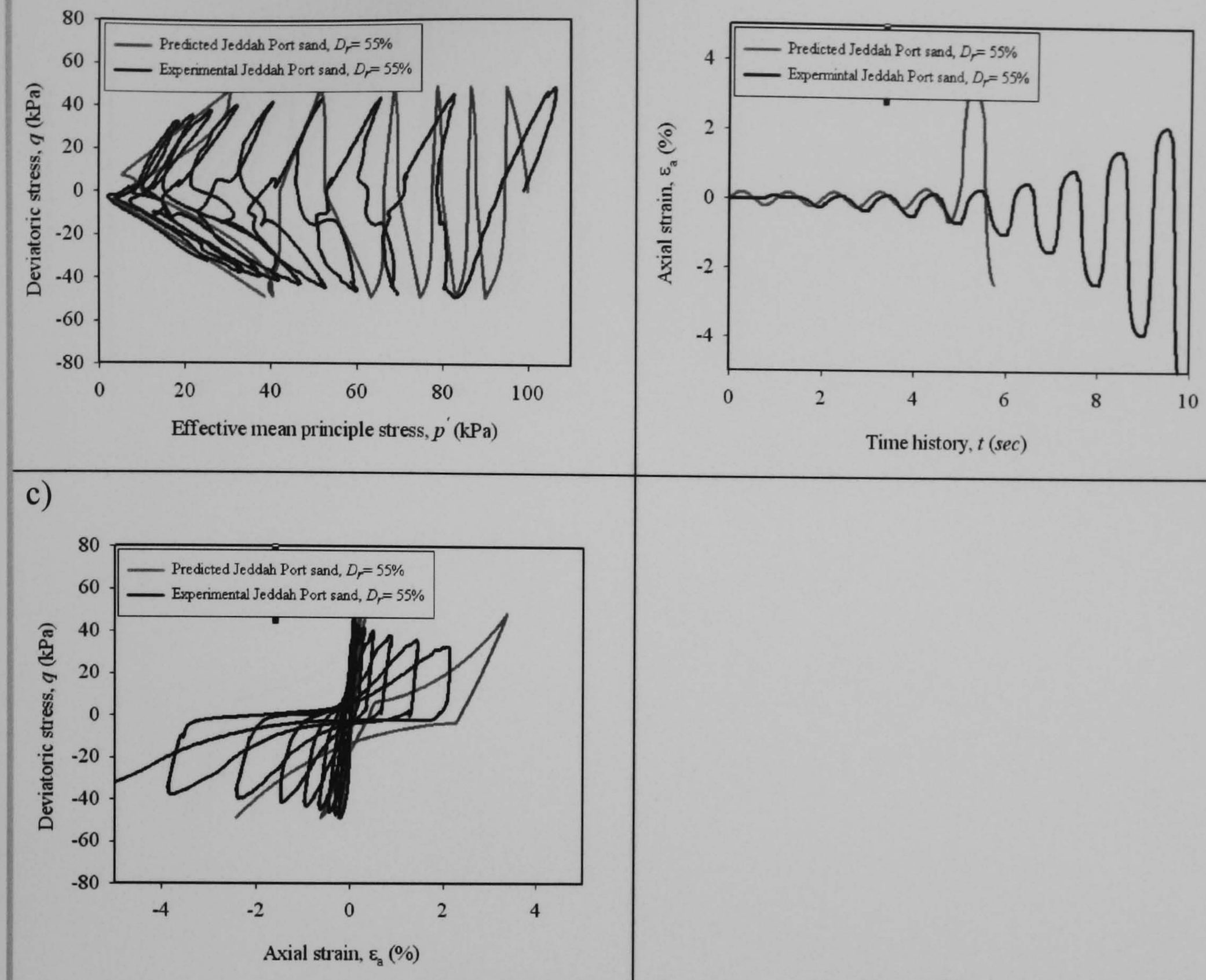

Figure B.10 Simulation results after the previous model parameters are adjusted a) stress path; b) stress:strain relationship; c) axial strain time history

It can be seen that the simulation results have reached 5% double amplitude of axial strain after 6 cycles compared to 10 cycles of the experiment. Therfore, the simulation should be repeated again by adjusting the following parameters:

$\beta_0 = 4.2 \rightarrow 6$

$\beta_1 = 0.5 \rightarrow 0.7$

Figure B.11 shows the final simulation results after the last model parameters adjustment.

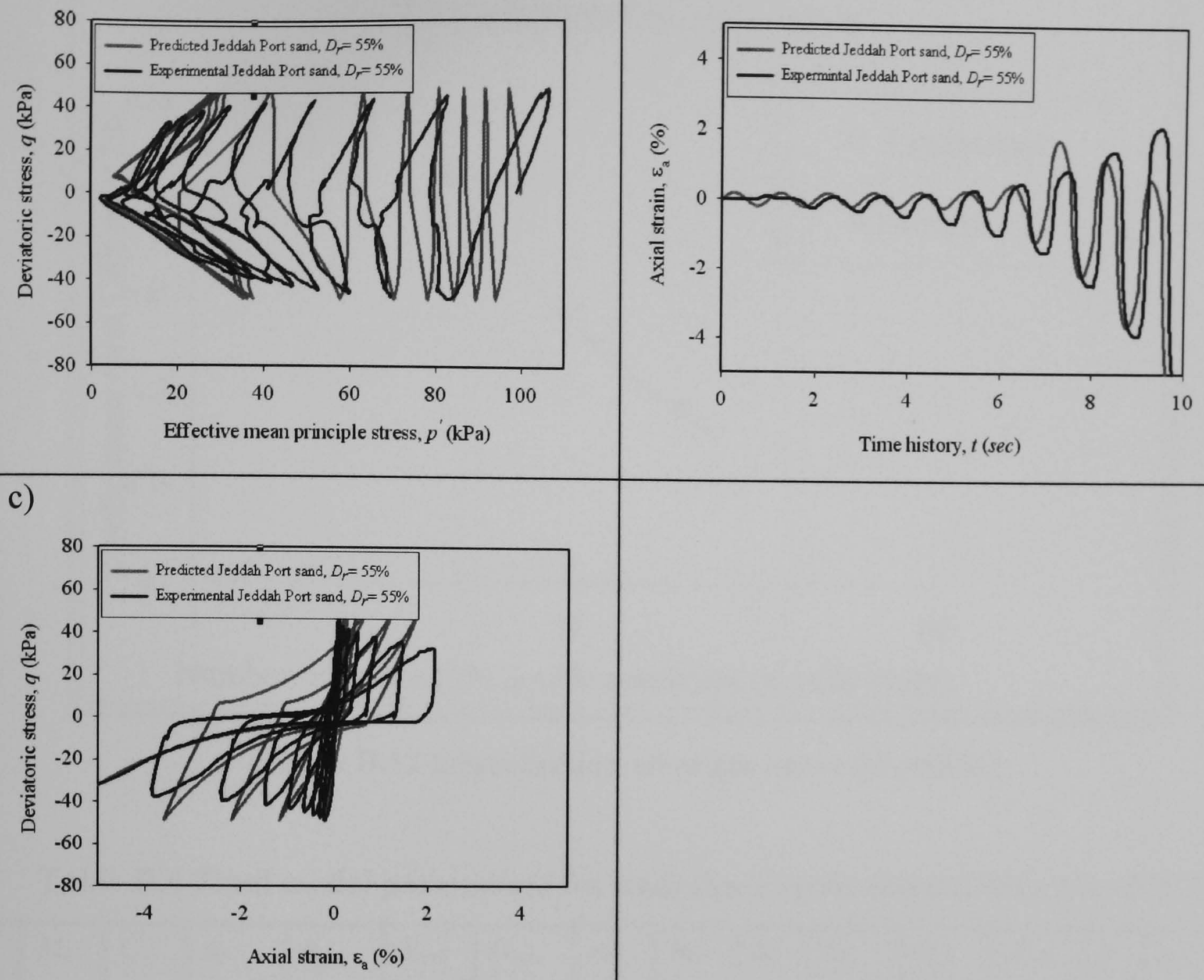

Figure B.11 Simulation results after the previous model parameters are adjusted a) stress path; b) stress:strain relationship; c) axial strain time history

It can be seen that the simulation results have reached 5% double amplitude of axial strain after 10 which is exactly the number of cycles produced in experiment. Therfore, the simulation should be terminated.

Using the final model parametres for Case 2, simulations for Cases 1 and 3 are performed with the same parameters and changing the load condition. The number of cycles needed to reach 5% double amplitude of axial strain for both Cases 1 and 3 are as following:

Case 1: 20 cycles in the simulation compared to 20 in the experiment.

Case 3: 5 cycles in the simulation compared to 5 in the experiment.

The deduced liquefaction strength curve of Jeddah Port sand with D_r = 55% is shown in Figure B.12. The final model parameters are listed in Table B.4.

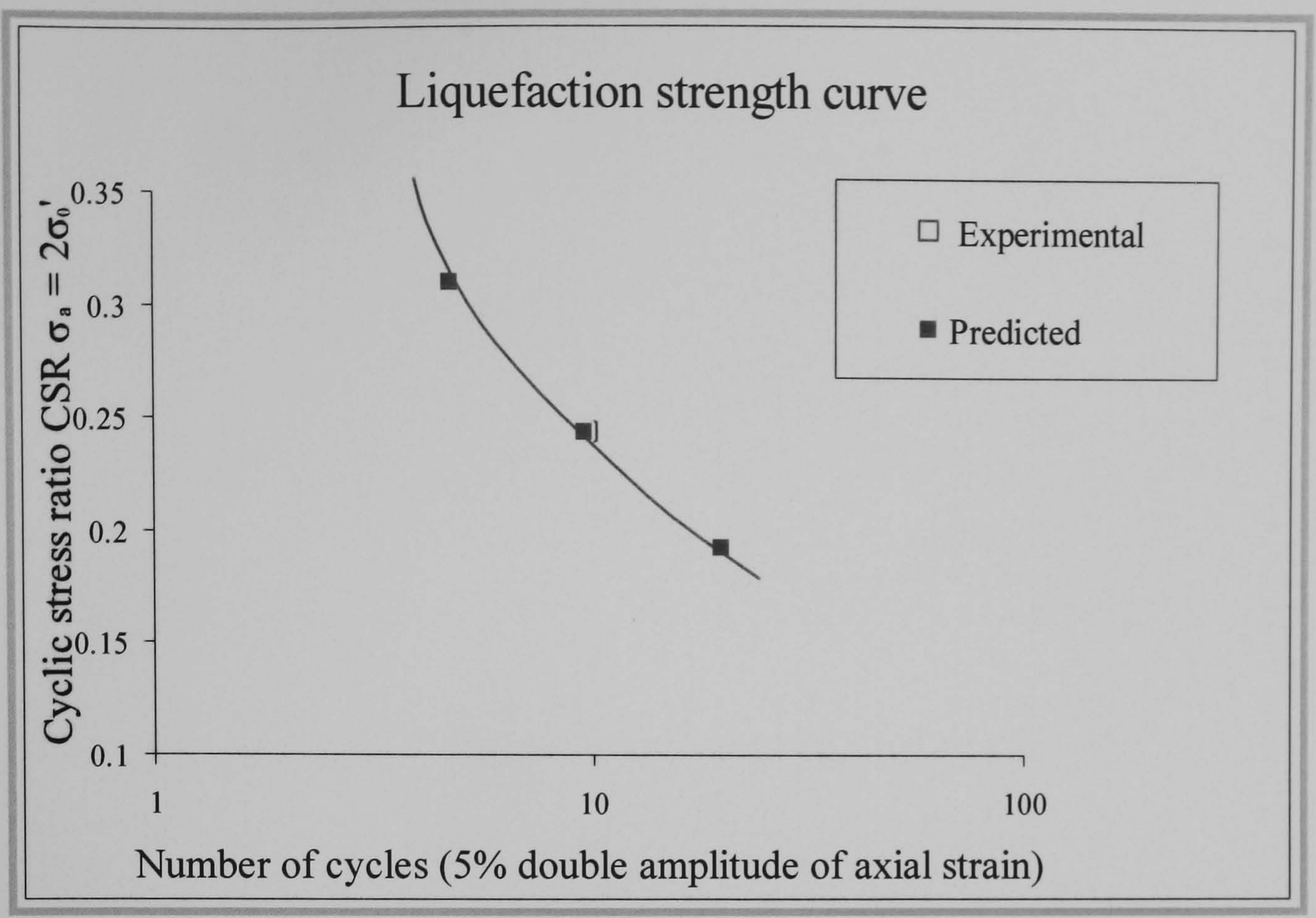

Figure B.12 Liquefaction strength curve (D_r=55%)

Table B.4 Final model parameters for undrained cyclic triaxial tests (D_r=55%)

M_f	M_g	C	α_f	α_g	K_{ev0}	G_{es0}	m_v	m_s	β_0	β_1	H_0	H_{U0}	γ	γ_U	p'_0
0.91	1.4	0.8	0.45	0.45	155	280	0.5	0.5	1.0	0.1	450	6000	8	6	100